

Sheffield Hallam University

Fatigue crack initiation and propagation in plain carbon-manganese steels.

FOX, Peter.

Available from the Sheffield Hallam University Research Archive (SHURA) at:

<http://shura.shu.ac.uk/19206/>

A Sheffield Hallam University thesis

This thesis is protected by copyright which belongs to the author.

The content must not be changed in any way or sold commercially in any format or medium without the formal permission of the author.

When referring to this work, full bibliographic details including the author, title, awarding institution and date of the thesis must be given.

Please visit <http://shura.shu.ac.uk/19206/> and <http://shura.shu.ac.uk/information.html> for further details about copyright and re-use permissions.

7904057018



**Sheffield City Polytechnic
Eric Mensforth Library**

REFERENCE ONLY

This book must not be taken from the Library

PL/26

R5193

ProQuest Number: 10694086

All rights reserved

INFORMATION TO ALL USERS

The quality of this reproduction is dependent upon the quality of the copy submitted.

In the unlikely event that the author did not send a complete manuscript and there are missing pages, these will be noted. Also, if material had to be removed, a note will indicate the deletion.



ProQuest 10694086

Published by ProQuest LLC (2017). Copyright of the Dissertation is held by the Author.

All rights reserved.

This work is protected against unauthorized copying under Title 17, United States Code
Microform Edition © ProQuest LLC.

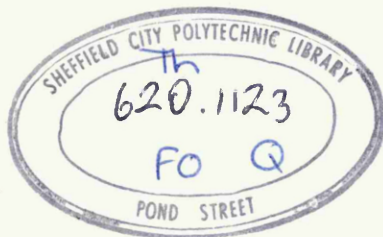
ProQuest LLC.
789 East Eisenhower Parkway
P.O. Box 1346
Ann Arbor, MI 48106 – 1346

FATIGUE CRACK INITIATION AND PROPAGATION
IN PLAIN CARBON-MANGANESE STEELS

by

PETER FOX, A.C.T.(Sheff.), A.I.M.

A research project carried out for the
degree of Master of Philosophy of the
Council for National Academic Awards



7904057-01

"..... it may appear equally conclusive that a bar of iron or any other material so loaded, would, under the least change either by increasing or diminishing the load, however minute, ultimately tend to destruction. I am aware of the great difference of opinion which exists on this subject. It is one which I conceive to be worthy of investigation"

W. Fairbairn, Esq. Report of the Commissioners appointed to inquire into the Application of Iron to Railway Structures, 1848, p.403.

CONTENTS

| | | |
|----------|--|----|
| 1. | INTRODUCTION | 1 |
| 2. | REVIEW OF PREVIOUS LITERATURE | 3 |
| 2.1 | FATIGUE DAMAGE AND CRACK INITIATION | 3 |
| 2.1.1. | INITIAL PHYSICAL MECHANICAL & STRUCTURAL CHANGES. | 3 |
| 2.1.2. | OBSERVATIONS OF FATIGUE DAMAGE | 4 |
| 2.1.2.1. | Slip During Cyclic Loading | 4 |
| 2.1.2.2. | Persistent Slip Bands | 5 |
| 2.1.2.3. | Extrusions and Intrusions | 6 |
| 2.1.2.4. | Importance of cross-slip | 7 |
| 2.1.2.5. | Pore Formation | 9 |
| 2.1.2.6. | Effect of Grain Boundaries | 10 |
| 2.1.2.7. | Fatigue Crack Initiation in Iron and Carbon Steels. | 11 |
| 2.1.2.8. | Effect of Strain Ageing | 14 |
| 2.1.3. | MECHANISMS OF CRACK INITIATION | 15 |
| 2.1.3.1. | General | 15 |
| 2.1.3.2. | Mechanism of Cottrell and Hull | 15 |
| 2.1.3.3. | Random Walk Theory | 16 |
| 2.1.3.4. | Theories Involving Cross-slip | 16 |
| 2.2 | FATIGUE CRACK PROPAGATION | 17 |
| 2.2.1. | MICROSCOPIC OBSERVATIONS | 17 |
| 2.2.1.1. | Fractography | 17 |
| 2.2.1.2. | Modes of Fatigue Crack Propagation | 17 |
| 2.2.1.3. | Stage I Crack Propagation | 18 |
| 2.2.1.4. | Stage II Crack Propagation | 19 |
| 2.2.2. | MECHANISMS OF CRACK PROPAGATION | 21 |
| 2.2.2.1. | Stage I Crack Propagation | 21 |
| 2.2.2.2. | Stage II Crack Propagation | 22 |

| | | |
|----------|---|----|
| 2.2.3. | ANALYSIS OF CRACK PROPAGATION MEASUREMENTS | 24 |
| 2.2.3.1. | Early Work | 24 |
| 2.2.3.2. | Fracture Mechanics Approach | 26 |
| 3. | EXPERIMENTAL METHODS AND MATERIALS USED | 28 |
| 3.1 | EXPERIMENTAL MATERIALS | 28 |
| 3.1.1. | CHEMICAL COMPOSITION | 28 |
| 3.1.2. | PREPARATION | 28 |
| 3.1.3. | MICROSTRUCTURE | 29 |
| 3.1.4. | TENSILE PROPERTIES | 30 |
| 3.2 | FATIGUE TESTING | 30 |
| 3.2.1. | SPECIMENS | 30 |
| 3.2.2. | TESTING PROCEDURE | 31 |
| 3.2.3. | CRACK PROPAGATION MEASUREMENTS | 31 |
| 3.3 | EXAMINATION OF SPECIMENS | 32 |
| 4. | EXPERIMENTAL WORK | 34 |
| 4.1 | PRELIMINARY WORK ON PURE IRON | 34 |
| 4.2 | EXPERIMENTAL WORK ON CARBON-MANGANESE STEEL PLAIN SPECIMENS | 35 |
| 4.2.1. | TEST RESULTS | 35 |
| 4.2.2. | THE DEVELOPMENT OF SURFACE FATIGUE DAMAGE | 36 |
| 4.2.3. | THE SPREAD OF PLASTICITY DURING FATIGUE | 37 |
| 4.2.4. | SLIP INTENSIFICATION AT GRAIN BOUNDARIES | 39 |
| 4.2.5. | CRACK INITIATION | 40 |
| 4.2.6. | SURFACE CRACK PROPAGATION | 41 |
| 4.2.7. | INITIATION OF MAIN CRACKS AND STAGE I CRACK PROPAGATION | 41 |
| 4.3 | EXPERIMENTAL WORK ON CARBON-MANGANESE STEEL NOTCHED SPECIMENS | 43 |
| 4.3.1. | TEST RESULTS | 43 |
| 4.3.2. | STAGE II CRACK PROPAGATION | 45 |

| | | |
|----------|---|----|
| 4.3.2.1. | General | 45 |
| 4.3.2.2. | Intergranular Fracture | 45 |
| 4.3.2.3. | Effect of Pearlite | 46 |
| 4.3.2.4. | Branch Cracks | 47 |
| 5. | DISCUSSION | 48 |
| 5.1 | THE DEVELOPMENT OF SURFACE FATIGUE DAMAGE | 48 |
| 5.2 | CRACK INITIATION | 50 |
| 5.3 | CRACK PROPAGATION | 51 |
| 6. | CONCLUSIONS | 55 |
| 7. | REFERENCES | 57 |
| 8. | STATEMENT OF ADVANCED COURSES OF STUDY ATTENDED | 62 |
| 9. | ACKNOWLEDGMENTS | 63 |

1. INTRODUCTION

The term "fatigue" is used to denote those processes which occur in a material when it is subjected to fluctuating stresses, which may lead to failure at stress levels well below those required to cause failure in static tension. Fatigue in plain unnotched specimens of metals and alloys usually begins with changes in the mechanical properties of the bulk material, followed by the occurrence of surface damage. Cracks then form from this surface damage and propagate through the bulk of the material. Eventually the crack becomes large enough to be unstable, and final fracture occurs, which can be brittle or ductile depending upon the properties of the material under tensile loading.

Wood⁽¹⁾ has classified the stress-endurance diagram into three sections (Fig.1). These are the "H" or high stress fatigue range, the "F" or fatigue range and the "S" or pseudo-safe range. Wood considers the "F" range to be absent in body-centred cubic metals. The present work on crack initiation is restricted to the study of low stress fatigue, i.e. the F and S ranges.

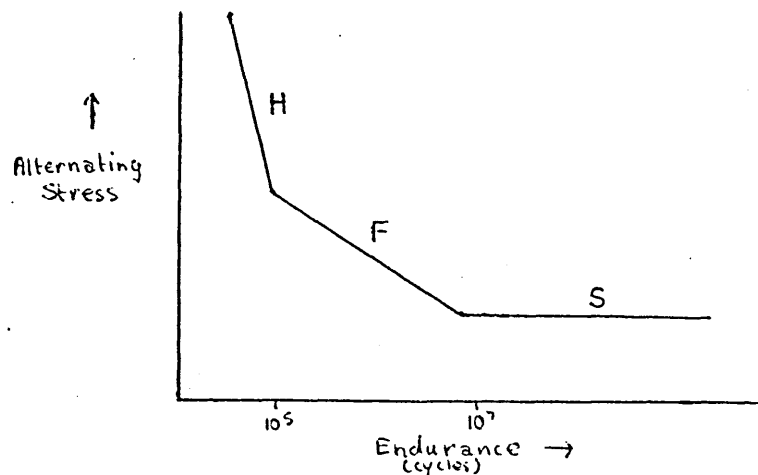


Fig.1 Schematic Representation of S-N diagram(after Wood⁽¹⁾).

Surface fatigue damage in face-centred cubic metals generally takes the form of wide slip bands from which cracks eventually develop. However, there is some conflict in the literature concerning fatigue crack initiation in iron and plain carbon steels, some workers observing persistent slip bands similar to those seen in FCC metals, whilst others have observed the formation of a cell structure with cracks originating in cell boundaries. Consequently, in the present work in order to resolve the question of initiation site three carbon steels have been studied, with carbon contents chosen to give no pearlite, a small percentage of pearlite and approximately 50% pearlite. These have been examined by optical microscopy, replica electron microscopy and scanning electron microscopy in an attempt to determine the type of fatigue damage which occurs, how cracks initiate, and the way in which microstructure affects this behaviour.

Fatigue crack propagation has in the past been studied by means of replica electron fractography. In the present work, scanning electron microscopy has been used. This enables fractures to be examined directly at magnifications ranging from x20 to x20,000, and therefore the fine fracture features can be related to the macroscopic fracture appearance. Also, artefacts due to replication technique are avoided. The majority of previous work has again been on non-ferrous materials, and in the present work, three carbon steels of similar compositions to the three used for crack initiation studies have been used to determine crack propagation rate data by direct microscopical observation, and to correlate this with the fractographic features.

2. REVIEW OF PREVIOUS LITERATURE

2.1. FATIGUE DAMAGE AND CRACK INITIATION

2.1.1. INITIAL PHYSICAL, MECHANICAL AND STRUCTURAL CHANGES

The first stage in the fatigue process consists of an initial rapid change in physical and mechanical properties, followed by a slowing down and then saturation⁽²⁾. Many workers have observed the change in mechanical properties with number of cycles, and methods used include the measurement of the peak stress required to produce a fixed strain amplitude or the strain resulting from a fixed stress amplitude, and the variation in the stress-strain curve or the indentation hardness. It has been found that whereas annealed metals show an initial increase in hardness, cold worked metals often show an initial decrease. In annealed pure metals, the saturation level of hardening generally occurs within 0.1-10% of the fatigue life, but alloys of low stacking fault energy may saturate much later in the test.

During the initial hardening stage, there is also an increase in electrical resistivity, which appears to be partly due to an increase in point defect concentration as well as to an increase in dislocation density, since some of the increase will anneal out at temperatures where only point defects are sufficiently mobile⁽³⁾.

It has been suggested by Backofen⁽⁴⁾ that the same mechanism is responsible both for work softening and the absence of hardening at saturation in fatigue. He suggests that a balance is eventually created between dislocation generation and annihilation, and that cross slip of screw

dislocations is an important feature of the mechanism. Edge dislocation annihilation could also be occurring by a process of internal void formation as suggested by Fujita⁽⁵⁾.

Avery & Backofen have shown that if a fatigue test is interrupted during the initial fatigue hardening stage, and annealing carried out, any damage present is removed and the fatigue life is prolonged, suggesting that no permanent damage (such as cracks or voids) exists⁽⁶⁾.

More detailed reviews of fatigue hardening are given in references 7, 8 & 9.

Thin foil electron microscopy has been used by many workers to determine the dislocation arrangements which produce the effects referred to above. At high strain amplitudes, a cell structure similar to that accompanying unidirectional deformation is produced. At low strain amplitudes, small dislocation loops and dipoles are formed. The dislocation distribution in the surface layer has been correlated with the shape of the persistent slip bands in copper by Lukás et al⁽¹⁰⁾. The persistent slip bands consist of zones of alternately high and low dislocation density, the high density zones linking together at a particular depth below the surface. The low density zones in between act as "channels in which dislocation motion is easy and extrusions occur on the surface of these zones". An extensive review⁸ of this subject appears in reference 11.

2.1.2. OBSERVATIONS OF FATIGUE DAMAGE

2.1.2.1. Slip during cyclic loading

Ewing and Humfrey carried out surface observations on Swedish iron, and found that slip lines appeared in certain

grains after a few cycles of stress⁽¹²⁾. As cycling continued, these lines became far more distinct and later broadened into wide bands with rather hazily defined edges. Eventually cracks appeared along the broadened slip bands. These were proved to be cracks by repolishing the surface. The density of bands was higher at higher stress levels, and cracks appeared earlier the higher the stress level. Gough showed that slip in fatigue occurs on the same slip systems as under static loading for various metals⁽¹³⁾. These were aluminium and silver (F.C.C. $\{111\} \langle 110 \rangle$), zinc (C.P.H. $\{0001\} \langle 10\bar{1}0 \rangle$) and iron (B.C.C. $\{110\}$, $\{112\}$ and $\{123\} \langle 111 \rangle$). He also showed that the same critical resolved shear stress law was followed, and that there was a stress below which slip could be observed without cracking occurring.

It has been shown by electron microscopy that the slip bands formed in F.C.C. metals in unidirectional deformation consist of parallel straight lines of varying heights⁽¹⁴⁾. The slip bands formed under cyclic loading, however are much less regular in appearance and appear to be curved⁽¹⁵⁻¹⁷⁾.

Plastic deformation is an essential process in fatigue failure. This has been confirmed by Eisner⁽¹⁸⁾ who carried out tests on copper whiskers and found that fatigue failure did not occur until plastic flow had occurred.

2.1.2.2. Persistent Slip Bands

Thompson et al carried out repolishing experiments during the fatigue of annealed copper, and found that many of the surface slip bands could be removed in this way⁽¹⁹⁾. A few persisted, however, and these were therefore named

"persistent slip bands". These were present after about 5% of the specimen life, and fatigue cracks grew from them. It was, therefore, suggested that the persistent slip bands were in fact incipient cracks, and that the majority of the test was spent propagating these cracks. If the specimens were repeatedly electropolished, the persistent slip bands were eventually removed. No new slip bands were ever discovered in this process showing that they only formed on the surface of the specimen, despite the uniform stress throughout its volume. If electropolishing was carried out long enough to remove the persistent slip bands and the specimen was refatigued, new slip bands formed in the same positions, showing that slip was still active on the same planes.

It has been shown that cracks in fatigue slip bands form as early as 1% of the total fatigue life, the rest of the time being spent propagating these cracks⁽²⁰⁾. In copper and α -brass, persistent slip bands can be revealed by etching after electropolishing⁽¹⁾.

2.1.2.3. Extrusions and Intrusions

Forsyth carried out surface observations on fatigued partially age hardened Al-4%Cu, and observed ribbons of material exuded from the slip bands⁽²¹⁾. He referred to these as "extrusions" and noted that they were of the order of $10\ \mu$ high and very thin. They had a metallic lustre and were sometimes continuous along the length of the slip band, although they were usually broken up into smaller lengths. Extrusion was almost negligible at -25°C and because of this and the fact that extrusions had not been

observed in pure aluminium, it was thought that the phenomenon was caused by localised overageing.

Forsyth and Stubbington showed that extrusions could occur in aluminium if it had previously been cold rolled⁽²²⁾. It was thought that this could be due to local softening of the work hardened material. However, extrusions have since been observed in many materials including annealed pure copper⁽¹⁹⁾, α -brass⁽²³⁾, iron⁽¹⁷⁾ and silicon iron⁽²⁴⁾.

The reverse process to extrusion formation, namely, the production of intrusions has also been shown to occur^(25,26). Hull found that extrusions and intrusions could be observed in copper at less than 1% of the fatigue life at temperatures as low as 4.2°K⁽²⁷⁾. It was, therefore, unlikely that thermally activated processes were necessary for the production of intrusions, and a mechanism involving cross-slip was proposed⁽²⁶⁾ (see section 2.1.3.2.). It has been demonstrated by Wever et al and Wood and Segall⁽²⁸⁾ that intrusions can grow into cracks.

2.1.2.4. Importance of Cross-Slip

The effect of cross-slip on the formation of extrusions has been demonstrated by Avery, Miller and Backofen⁽²⁹⁾ who fatigued two single crystals of high purity copper. The orientations of these crystals were such that the Schmid resolved shear stress factors for the primary slip system were nearly alike, but those for the cross-slip system were different, one being³10 times the other. Both crystals were fatigued beyond saturation, and the extrusions produced on the surface were removed by electropolishing. After an additional 50 cycles, the crystal with the higher Schmid

factor on the cross-slip system showed much higher extrusions than the other crystal when examined by a taper sectioning technique. Also, the height of the extrusions was greater than could be accounted for by a mechanism involving steady extrusion development.

It has also been shown that fatigue failure is extremely difficult to produce in materials which have a high resistance to cross-slip, e.g. zinc single crystals fatigued at -196°C ⁽³⁰⁾, lithium fluoride⁽³¹⁾ and magnesium oxide⁽³²⁾. Alden⁽³³⁾ has compared dynamic recovery in zinc and cadmium at low temperatures and found that cadmium easily saturates at about 200lb/sq.in., whereas the fatigue hardening curve for zinc is essentially linear up to 3000lb/sq.in. Both metals are CPH and have a primary slip system of (0001) $[\bar{1}\bar{2}10]$, but cadmium cross slips on (10 $\bar{1}$ 1) $[\bar{1}\bar{2}10]$ whereas zinc does not. However, it is possible to produce fatigue failure in zinc at low temperature (see section 2.1.3.3.).

It seems, therefore, that the ability to cross-slip is extremely important in allowing saturation, and hence fatigue failure to occur, since it has been mentioned previously that fatigue cracks do not form in fatigue slip bands until saturation has occurred. The fact that cross-slip can be important in the development of a surface notch peak topography also lends support to the view that cross-slip plays an essential part in the fatigue failure mechanism of most metals.

The effect of reducing stacking fault energy, and hence inhibiting cross-slip has been demonstrated by McGrath

and Thurston⁽³⁴⁾ who compared Cu, Cu-15%Zn and Cu-35%Zn fatigued at the same stress level. They found that slip bands became thinner and fatigue life increased greatly as the concentration of zinc (and the resistance to cross-slip) was increased. However, when zinc is added to copper, mechanical properties, e.g. yield stress and U.T.S. are also altered. Later work⁽³⁵⁾ has compared Cu-Al and Cu-Ni alloys. Aluminium and nickel additions have similar effects on the mechanical properties of copper but aluminium produces a greater reduction in stacking fault energy, and was shown to produce the better fatigue properties.

2.1.2.5. Pore Formation

Wood, Cousland and Sargent⁽³⁶⁾ used a taper sectioning technique on copper and 70/30 brass, and observed pore formation on slip planes. Later during the tests, these pores linked up to form fissures which were the embryo fatigue cracks. In another paper⁽¹⁾ blocks of metal were seen to be loosened from the surface. Intrusions and extrusions were considered to be side effects which could not account for the primary source of damage, even though slip band cracks often seemed to be associated with surface extrusions.

Dover and Jones⁽³⁷⁾ used a technique of successive sectioning to build up a three-dimensional picture of the features near the surface in fatigued copper. The major conclusion of their work was that as successive surface layers were polished away, no new pores or cracks appeared below the surface. It was considered that the "pores" observed by Wood et al were in fact intrusions, which appeared to be pores because of Wood's taper sectioning

technique. Irregular microcracks were seen linking up the slip band cracks below the surface. The slip band cracks had an irregular crack front, and split up into a series of tubular holes before disappearing.

2.1.2.6. Effect of Grain Boundaries

Predominantly grain boundary fatigue cracking has usually been considered to occur at high temperatures, but a number of workers have reported such cracking at lower temperatures. Lead and tin fail by grain boundary fracture when fatigued at room temperature⁽³⁸⁻⁴⁰⁾, but these are low melting point metals, and this can be classed as high temperature fracture. Snowden⁽⁴⁰⁾ has observed extrusions at grain boundaries in lead fatigued at room temperature in vacuo. These were of two types, whisker-like extrusions up to 50μ long with a diameter of approximately 1μ , and more continuous extrusions which were much smaller. Some boundaries showed localised slip patterns which were parallel to slip traces in other parts of the same grain, on one or both sides of the boundaries.

Golland and James⁽⁴¹⁾ have also observed grain boundary exudation in iron with a high oxygen content. They observed slip intensification near grain boundaries, and the whole of the fatigue fracture was intergranular. They attributed this to grain boundary embrittlement due to the high oxygen content of the material.

Grain boundary fatigue cracking has, however, been observed at room temperature in metals with high melting points in which there is no obvious grain boundary embrittlement. Hoepfner and Vitovec⁽⁴²⁾ tested tricrystals

of 99.988% copper with grain boundaries orientated at various angles to the stress axis. The fractures were part intergranular and part transgranular. They showed that the probability of initiation of grain boundary cracks increases with decreasing angular misorientation of neighbouring grains.

Smith⁽⁴³⁾ has shown that the tendency for grain boundary fatigue cracking is a function of temperature. In high purity aluminium, grain boundary cracking was most marked at 300°C, but was still visible at -73°C. It was absent at -180°C.

Local concentration of slip bands at grain boundaries has been observed in copper⁽⁴⁴⁾. Valleys occur in high stress specimens at grain boundaries, and it has been shown that intergranular fracture is favoured by high stress⁽⁴⁵⁾. Cracking also frequently occurs at twin boundaries in copper which are parallel to slip planes, and it has been proposed that the twin boundaries and grain boundaries act as dislocation sources, resulting in increased plastic deformation adjacent to them⁽⁴⁶⁾.

Grain boundary crack initiation has also been observed in β -brass, which has an ordered body-centred-cubic structure at room temperature⁽⁴⁷⁾. This has been attributed to the high elastic anisotropy of the material ($E_{111}/E_{100} = 8.94$) which would result in a high stress concentration at grain boundaries.

2.1.2.7. Fatigue Crack Initiation in Iron and Carbon Steels

In contrast to the large amount of work done in the past on fatigue crack initiation in F.C.C. materials, comparatively little work has been carried out on ferrous materials. The most exhaustive treatment is that of Hempel

and his co-workers⁽⁴⁸⁻⁵⁰⁾. They showed that in an 0.09% carbon steel, slip bands begin to occur in the first 1% of the life. The number and extent of the slip bands increase as the test progresses, and slip bands occur both above and below the fatigue limit, but are completely absent at a stress amplitude which is 22% below the fatigue limit. Repolishing after fatigue shows that many of the slip bands contain fine microcracks. Persistent slip bands in mild steel which develop into cracks have also been observed by Modlen and Smith⁽⁵¹⁾.

Electron microscopy of plastic replicas shows that the slip bands have a pitted surface showing numerous fine dark lines and some crevice-like grooves and splits. Hempel et al propose that these fissures join together to produce microcracks which can then propagate.

Single crystal work on Armco iron shows that fatigue slip bands are either straight or wavy, depending on whether their orientation is such that single or multiple slip occurs. The wavy course of the slip bands produced in specimens oriented for multiple slip appears to result from an accumulation of several slip lamellae which "arch out from the ferrite to different extents".

Tests on bi- and tri-crystals showed that when a grain boundary is favourably orientated at right angles to the direction of the bending stress, slip bands are concentrated into a narrow zone alongside the grain boundary. The fatigue failure starts from this boundary, which is heavily deformed because of the anisotropic behaviour of the adjoining crystals.

Wood et al⁽⁵²⁾ studied the microstructural changes

produced in pure iron and Armco iron subjected to alternating torsion at amplitudes above and below the knee of the S-N curve to identify the basic mechanisms of fatigue and to find why they should give rise to a sharp S-N knee in contrast to the smooth S-N curve shown by face centred cubic metals.

Above the knee of the S-N curve they found that an unusually pronounced cell structure appeared in the grains. They suggested that this was due to internal disorientation or rumpling of the grains. This rumpling was accompanied by so much local distortion as to be almost of the nature of a structural fault, and the cell boundaries were zones of very high dislocation density. Eventually pores appeared at these cell boundaries, which then multiplied into boundary microcracks. These microcracks then became cross-linked with other cell boundary cracks to give macroscopic crack formations. These observations are similar to those of Holden⁽⁵³⁾.

Below the knee of the S-N curve they found dense "clouds" of short faint slip markings. A "cloud" would start in one region of a grain and eventually spread over the grain in a dense mass too fine to resolve optically. Pores formed from these slip bands, but these were so dispersed as to preclude their linking up to form microcracks, although odd cracks were noticed at grain boundaries.

Reimann⁽⁵⁴⁾ considered that the apparent discrepancies between Wood's work and that of Hempel was due to the initial condition of the test specimens. He therefore carried out tests on Armco iron in alternating torsion on

specimens that had been subjected to preliminary cycling at high strain amplitudes and compared these with specimens subjected to low strain amplitude cycling only. It was found that specimens with preliminary large amplitude cycling showed slip in concentrated zones similar to Hempel's observations.

2.1.2.8. Effect of Strain Ageing

It has been shown that strain ageing plays an important part in determining the fatigue limit in carbon steels^(7,55). Two types of strain ageing are thought to be responsible for the effect. Oates and Wilson⁽⁵⁵⁾ have shown that a fatigue limit exists in fine grained annealed low carbon steel which is considerably reduced by pre-straining just above the yield point. Thus initial dislocation locking or "static strain ageing" is probably a prime cause of the fatigue limit in steels where the fatigue limit is at or below the yield point. Coarse grained mild steel, on the other hand, has a fatigue limit above its yield point. Pre-straining this before fatigue led to the fatigue limit being raised, this being consistent with a "dynamic strain ageing" mechanism, i.e. strain ageing during fatigue.

It was stated in section 2.1.2.1. that fatigue slip bands can still be seen below the fatigue limit, thus leading to the conclusion that the fatigue limit does not depend on micro-yielding behaviour. It has been proposed, however, that the spread of plasticity across grain boundaries rather than the initiation of plasticity is the limiting factor⁽⁵⁶⁾. Above the fatigue limit, fatigue slip bands gradually grow in width during a test, so that the

possibility of a dislocation source in an adjacent grain coming within the range of a high stress concentration will increase with time. The fatigue limit is the critical stress for this spread of plasticity to occur.

2.1.3. MECHANISMS OF CRACK INITIATION

2.1.3.1. General

The first theories of fatigue assumed that each cycle of stress work hardened the material by a small increment, until eventually a critical stress was exceeded and the material fractured. There is no evidence for either progressive work hardening, or such a critical fracture stress. More recently, it has been suggested that condensation of vacancies in a slip band could form voids which would nucleate a crack⁽⁵⁷⁾. These could be produced either by the non-conservative motion of a jogged screw dislocation or by dislocation pile ups of opposite sign on adjacent slip planes joining together to form a crack⁽⁵⁾. None of these proposals involves the nucleation of cracks at free surfaces, which are almost universally accepted to be the sites of fatigue crack initiation except in special circumstances. The only work in which this view is not accepted is that of Wood and his co-workers, in which crack initiation is said to be due to the accumulation of sub-surface "pores".

2.1.3.2. Mechanism of Cottrell and Hull⁽²⁶⁾

This involves slip on two intersecting slip systems. During the tensile half-cycle, a dislocation source S_1 produces a slip step on the surface. At a slightly higher stress in the same half cycle, source S_2 on an intersecting slip plane produces a second step. During the compression

half-cycle, the source S_1 produces a step of opposite sign which is in a different but parallel plane to the first slip step produced by this source, and an intrusion is formed. Similarly, S_2 produces an extrusion. If this mechanism were to occur, similar numbers of intrusions and extrusions would be observed, and the extrusions would be in a different slip band to the intrusions. These predictions are not always found to be true.

2.1.3.3. Random Walk Theory

May⁽⁵⁸⁾ has proposed that a notch-peak topography can develop by a process of random reversed slip, in metals where cross-slip is difficult. If slip occurs at random in each direction, and the distribution of slip at each half-cycle is independent of slip in previous cycles, the surface will be roughened. This roughening will concentrate the stress in the valleys, so that once valleys are formed, they will deepen. This mechanism could occur equally well in metals where cross slip is easy or difficult, and probably accounts for the fact mentioned earlier that fatigue can still occur in metals which do not cross-slip, e.g. zinc at low temperature⁽⁵⁹⁾.

2.1.3.4. Theories involving cross slip

Mott⁽⁶⁰⁾ has proposed that extrusions could form by the cyclic movement of a screw dislocation round a closed circuit, involving movement from the primary plane on to the cross-slip plane, returning via parallel primary and cross-slip planes. In the original mechanism, a pre-existing sub surface cavity was assumed to be present and it was proposed that this could form by the Fujita mechanism⁽⁵⁾.

This theory does not account for intrusion production, and requires a large number of cycles to produce one extrusion. However, extrusions have been observed in the first few cycles of fatigue testing⁽⁴⁾, and cavities beneath extrusions have not been observed in transparent crystals⁽⁶¹⁾.

McEvily and Machlin⁽³¹⁾ proposed that if two screw dislocations were to cross-slip simultaneously, material injected into the grain by intrusion could replace that lost underneath the extrusion. A number of other dislocation mechanisms involving cross-slip have been suggested, none of which is entirely satisfactory. Any successful mechanism must involve cross-slip and explain rapid intrusion - extrusion formation, the production of unequal numbers of extrusions and intrusions, and the appearance of intrusions and extrusions in the same slip band.

2.2. FATIGUE CRACK PROPAGATION

2.2.1. MICROSCOPIC OBSERVATIONS

2.2.1.1. Fractography

"Fractography" is a term coined by Zapffe and Worden⁽⁶²⁾ for the microscopical study of fracture surfaces. Originally optical microscopy was employed, but the majority of work has been carried out by electron microscopy, because of the superior resolution and depth of focus of this technique. Carbon replicas (both single stage and two stage) have been mainly employed for this work. Recently, the scanning electron microscope has become available but this instrument has only just begun to be employed for fractography.

2.2.1.2. Modes of Fatigue Crack Propagation

Forsyth⁽⁶³⁾ has distinguished two types of crack growth, which he calls Stage I and Stage II. Stage I growth is a

continuation of the crack initiation process, and occurs on slip planes orientated near to 45° to the direction of maximum tensile stress. This is also known as "shear mode crack growth". Stage II crack growth occurs after Stage I, and occurs at right angles to the direction of maximum tensile stress. Stage I crack growth is favoured by low stresses and slip on a single system, whereas Stage II growth is favoured by higher stresses and duplex slip.

2.2.1.3. Stage I Crack Propagation

Stage I crack propagation occurs on slip planes orientated near to the directions of maximum shear stress. Forsyth has suggested that the changeover from crack initiation to Stage I propagation is arbitrary and difficult to define and, therefore, he makes no distinction between these two stages. Stage I growth is favoured by low stresses, and in plain fatigue specimens may occupy the majority of the time of the test. Since the rate of crack propagation in Stage I is very small, normally only a small proportion of the fracture surface is taken up by this mode of propagation. Under certain circumstances, however, the whole of the final fracture may take place in Stage I. This has been shown to occur under corrosion fatigue conditions in aluminium alloys (64), and in a high strength nickel "superalloy" (65), where fatigue occurs at stresses well below the yield stress. Usually, the transition from Stage I to Stage II occurs at a grain boundary, but it can also occur within a grain. This was seen by Forsyth in Al-7.5%Zn - 2.5%Mg, and the changeover was not associated with any obvious metallurgical feature.

Stage I fracture surfaces in aluminium alloys often

show parallel lamellae running along the direction of crack growth. Flat and relatively featureless facets have also been observed, but this work was done by optical microscopy, and any fine detail would probably not have been resolved⁽⁶⁴⁾. Gell and Leverant⁽⁶⁵⁾ have also observed parallel lamellae running along the direction of crack growth in a high strength nickel alloy. They maintained that these were surface steps on highly reflective fracture facets. These facets were shown to be $\{111\}$ planes, and the cracks propagated in $\langle 110 \rangle$ directions. Replica electron microscopy showed a series of parallel narrow straight markings that make angles of approximately 60° to the steps. These markings correspond to traces of $\{111\}$ planes in the fracture facet and were attributed to slip occurring during the relaxation of the stress field at the crack front after the crack had passed.

2.2.1.4. Stage II Crack Propagation

This occurs at 90° to the maximum tensile stress and is of major engineering interest. In notched specimens, the time spent in Stage I is extremely small, and in the majority of engineering components failing by fatigue almost the whole of the fatigue process is spent in Stage II. The major feature of Stage II fracture surfaces is the existence of striations running perpendicular to the direction of crack propagation^(62,63). These striations occur on small plateaux, separated from one another by ridges. Forsyth and Ryder showed by programme loading experiments that each striation was produced by one cycle of stress⁽⁶⁶⁾. They also showed that the striation spacing increased as the stress increased. Two types of striations were distinguished in the work of Forsyth and his co-workers: ductile striations, in which the

spacing between the striations is narrow and there is no evidence of cleavage, and brittle striations in which cleavage fracture is thought to play an important part. These brittle striations show characteristic river markings running in the direction of crack propagation. This is discussed in section 2.2.2.2.

In high strain fatigue fine striations have been noted which run between and roughly parallel to the striations discussed above. It has been suggested that these are slip lines formed during plastic flow at the crack tip, and evidence has been presented to support this view⁽⁶⁷⁾.

There is little mention in the literature of the effect of grain boundaries and grain orientation on the direction of Stage II crack propagation. In most cases, it seems to be assumed that Stage II cracks propagate at 90° to the applied tensile stress, independently of grain orientation. Williams and Smith have, however, distinguished two types of Stage II crack propagation in β -brass⁽⁴⁷⁾. The initial mode of Stage II growth was described as "crystallographic". This was because the crack appeared to propagate along crystallographic planes, which were inclined at not more than 20° to the macroscopic crack propagation direction. River patterns similar to those observed on cleavage fracture were seen, and the plane of propagation changed direction at grain boundaries. Etch pitting showed that the fracture planes were either $\{100\}$ or $\{110\}$ planes, and x-ray diffraction showed that the surfaces were within 10° of the $\{110\}$ planes. Striations could be resolved towards the end of the "crystallographic" zone. When the rate of crack propagation increased

to $0.5 - 1\mu$ per cycle, the mode of crack propagation became "non-crystallographic" and the plane of fracture was normal to the applied tensile stress. The crack did not change direction at grain boundaries. It has recently been shown that α -titanium behaves in a similar manner⁽⁶⁸⁾.

2.2.2. MECHANISMS OF CRACK PROPAGATION

2.2.2.1. Stage I Crack Propagation

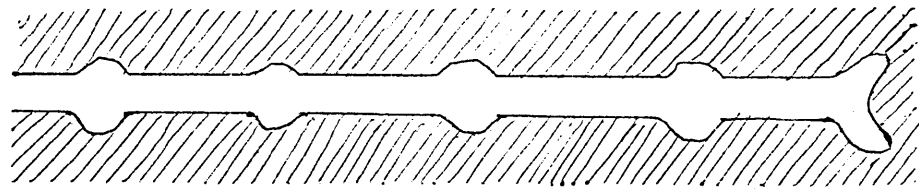
The majority of workers have considered Stage I crack propagation to occur by the same process as crack initiation. Any of the proposed initiation mechanisms could, therefore, be cited to account for this process. Kaplan and Laird have suggested two mechanisms by which Stage I crack propagation could occur⁽⁶⁹⁾. The first is a modification of Laird's "plastic blunting process" (see section 2.2.2.2.) in which slip occurs on one slip band only. The second is based on an unslipping process. During the tensile half-cycles shear occurs, and the distance from the specimen surface to the crack tip on one side of the crack increases. During the compression half-cycle, the original crack geometry is recovered, except that the crack has grown by a small increment.

Laird's evidence for the occurrence of the plastic blunting process in Stage I crack propagation⁽⁶⁷⁾ is that Williams and Smith observed striations towards the end of the "crystallographic" mode of crack growth in β -brass. However, this "crystallographic" crack propagation was in fact a type of Stage II propagation, and therefore, no real evidence of the occurrence of this process in Stage I propagation has yet been presented.

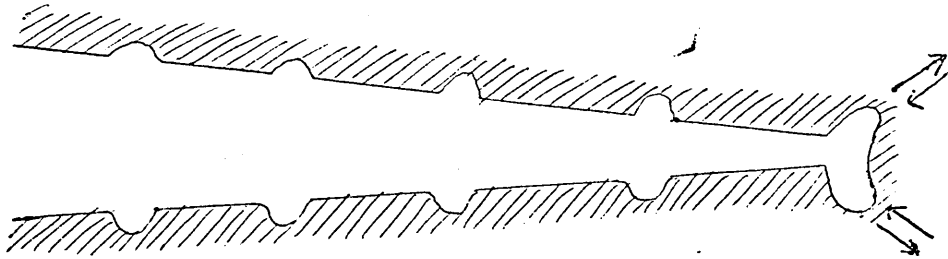
2.2.2.2. Stage II Crack Propagation

According to Forsyth⁽⁷⁰⁾ there are two mechanisms of Stage II crack propagation, depending on whether "ductile" or "brittle" striations are produced. For a ductile striation, the mechanism is as follows : at low stresses in the tensile half-cycle screw dislocations operate on a plane running lengthwise along the crack root, and the crack is extended by an unslipping process. As the stress rises, cross-slip occurs and rapid blunting of the crack tip occurs because slip operates on many parallel planes. For brittle striations, cleavage occurs along a (100) plane until crack tip blunting takes place by dislocation cross slip to accommodate the curvature of the crack front. A slight crack extension then occurs at 45° , but this is very insignificant compared to the large amount of cleavage fracture which takes place. Forsyth's mechanisms do not clearly account for the effect of stress reversal, except that he suggests the compression half-cycle will result in resharpenering of the crack tip, and a reversal of the residual stresses present there.

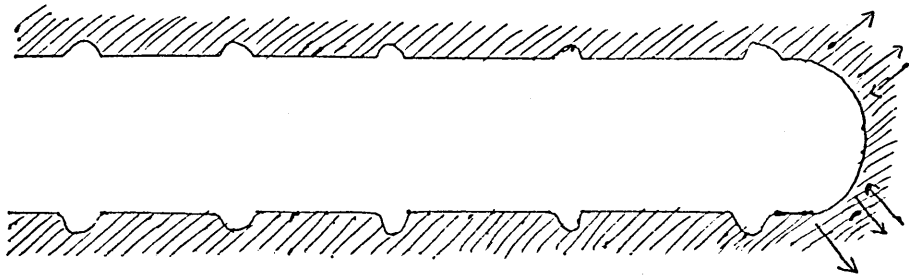
The most detailed treatment of Stage II crack propagation has been given by Laird, who has proposed a mechanism for fatigue crack propagation known as the "plastic blunting process"⁽⁶⁷⁾. This is shown schematically in Fig. 2. At zero load, the crack has the appearance shown in Fig. 2a. As the tensile load is applied, slip is concentrated in zones along planes at 45° to the direction of crack propagation (Fig. 2b). At the maximum tensile load, the crack tip blunts to the configuration shown in Fig. 2c. When compression occurs, the crack faces move together and



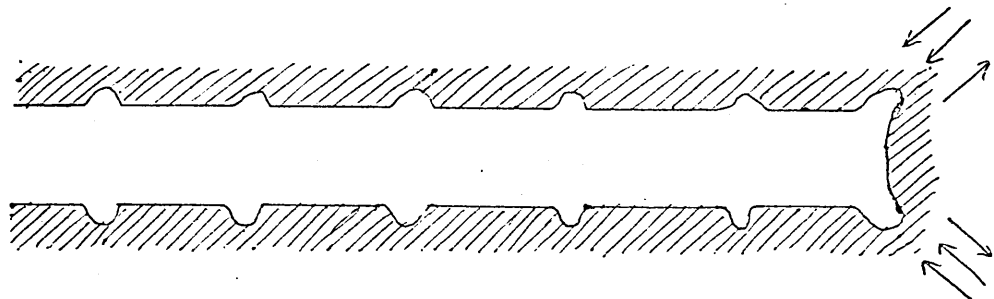
(a) zero load



(b) small tensile load



(c) maximum tensile load



(d) small compressive load

Fig. 2. The Plastic Blunting Process of Fatigue Crack Propagation (after Laird⁽⁶⁷⁾)

the new blunted crack tip surface created in tension is forced into the plane of the crack by buckling (Fig. 2d). At the maximum compressive load, the configuration shown in Fig. 2a reappears, and the cycle is then repeated.

Laird states that it is unlikely that cleavage plays a part in fatigue crack propagation, since the conditions under which cleavage striations have been observed do not produce cleavage fracture in unidirectional deformation. Also, when FCC metals fail by cleavage, (111) is the cleavage plane, and not (100). If crack propagation is by the plastic blunting mechanism, and slip occurs on (111) planes of an FCC metal, then the resultant plane of crack propagation would be (100).

Laird considers that the ridges which separate the plateaux on which the striations appear are caused by asymmetry of the residual notch left at a closed crack tip in compression. Along some lengths of the crack front, the part of the notch below the overall crack plane will be the more prominent, whereas the opposite will occur along the rest of the crack front. Plastic relaxation in the tension half-cycle will be concentrated in the most prominent of the two parts of the notch, and this will cause the crack plane to diverge onto different levels with a shear step in between.

The plastic blunting process predicts that peaks on one side of the crack should match up with peaks on the other side of the crack, and troughs should match up with troughs. This morphology has in fact commonly been noted. However, the opposite case, namely peaks matching up with troughs has also been reported, but in this case small cracks are

often seen undercutting the ridges on the fracture surface. This type of striation is formed when the orientation of the crystal with respect to the stress axis at the crack tip is such that the two parts of the notch remaining at the crack tip during the compression half-cycle are asymmetrical. During the tension half-cycle, the most advanced notch will propagate, and the other notch appears as an undercutting crack.

2.2.3. ANALYSIS OF CRACK PROPAGATION MEASUREMENTS

2.2.3.1. Early Work

Frost and his co-workers studied the behaviour of fatigue cracks by both mechanical and physical methods with the object of determining :

- (a) the critical alternating stress required to propagate a crack of given length, and
- (b) the laws governing the rate of growth of a growing crack.

For a wide variety of materials, Frost⁽⁷¹⁾ showed experimentally that :

$$\sigma^3 a = C \dots\dots\dots (1)$$

where σ = nominal alternating stress

a = crack length

C = a constant which varies from material to material.

If $\sigma^3 a > c$, the crack would grow, whereas if $\sigma^3 a < c$, the crack would remain dormant. If the stress concentration factor at the root of a notch was high, a crack would be initiated, but would not propagate.

It was also shown⁽⁷²⁾ that the rate of growth of a

propagating crack was given by :

$$\frac{da}{dN} = ka \dots\dots\dots (2)$$

where $\frac{da}{dN}$ = rate of crack growth

k = a constant

Also $k = A\sigma^3$

Hence $\frac{da}{dN} = A\sigma^3 a \dots\dots\dots (3)$

The constant A varies from material to material and bears no relationship to the static mechanical properties or plain fatigue strengths of the materials. For some materials the constant depends on mean stress.

The above relationship holds only when crack growth is continuous. Frost noticed experimentally that, even on a macroscopic scale, this is not the case, and while the crack length is small, it is possible for the rate of growth to decrease, sometimes to zero, for quite prolonged periods before continuing to grow again at the expected rate.

Other crack propagation laws have been formulated by a number of workers, e.g. Head's law : (73)

$$\frac{da}{dN} = \frac{C_1 \sigma^3 a^{\frac{3}{2}}}{(\sigma_y - \sigma) w_0^{\frac{1}{2}}} \dots\dots\dots (4)$$

where C_1 depends on the static mechanical properties of the material.

σ_y = the yield strength of the material.

w_0 = size of plastic zone near crack tip
(assumed to be constant)

Paris and Erdogan (74) have shown that if one plots the same crack propagation data on various axes, e.g. $\frac{1}{a^2} v.N$ for Head's law (integrating equation 4 gives $-\frac{2}{a^2} = DN+C$ where D&C are constants), or $\log a v.N$ for Frost's law,

straight lines can be drawn through portions of the data, but the slopes of these lines vary greatly with applied stress. According to the early method of verifying crack propagation laws, i.e. plotting data from single test specimens, the laws all accounted for observed data! It has since been suggested that to verify adequately a crack propagation law, a clear trend should be established using data from several specimens at different stresses plotted on the same graph.

2.2.3.2. Fracture Mechanics Approach

Irwin⁽⁷⁵⁾ suggested that the effect of the external load and the geometrical configuration on the intensity of the total stress field around a crack tip could be expressed as a "stress intensity factor", K . It was reasoned by Paris⁽⁷⁶⁾, that this factor should also control the rate of fatigue crack propagation, i.e. :

$$\frac{da}{dN} = f(\Delta K)$$

where K is the stress intensity range.

Many workers have proposed a simple power law, i.e. :

$$\frac{da}{dN} = A.(\Delta K)^n$$

where A and n are constants.

Since $\log \frac{da}{dN} = n \log K + \log A$.

then a plot of $\log \frac{da}{dN}$ v. $\log \Delta K$ should give a straight line of slope n . It has been shown that a straight line is indeed obtained by this method, even when data from tests at a number of stress levels are plotted on a single graph.

The stress intensity factor for a crack growing in a single edge notched specimen tested in tension is

$$K = \frac{Y.P. \sqrt{a}}{BW}$$

where P = applied force

B = breadth of specimen

W = width of specimen

a = crack length

where Y can either be determined experimentally or calculated from the relation of Gross et al⁽⁷⁷⁾

$$Y = 1.99 - 0.41\left(\frac{a}{W}\right) + 18.70\left(\frac{a}{W}\right)^2 - 38.48\left(\frac{a}{W}\right)^3 + 53.85\left(\frac{a}{W}\right)^4$$

Pulsating tension tests carried out on various carbon - manganese steels⁽⁷⁸⁾ showed that the rate of fatigue crack propagation was proportional to some function of the stress intensity range, but that the relationship consisted of two branches. For the upper branch, it was found that :

$$\frac{da}{dN} = c(\Delta K)^m$$

where c and m were functions of the yield stress

The lower branch of the $\log \frac{da}{dN}$ v. $\log \Delta K$ plot had a steeper gradient, and the position of the change in slope was stress dependant. No change in mechanism was noted at this position.

Broek⁽⁷⁹⁾ working on aluminium-zinc and aluminium-copper alloys showed a departure from linearity of the $\log da/dN$ v. $\log \Delta K$ curve at both low and high stress intensities, giving an S-shaped curve. He considered that at high stress intensities static tearing was taking place, and at low stress intensities the crack was "still in the initiation stage".

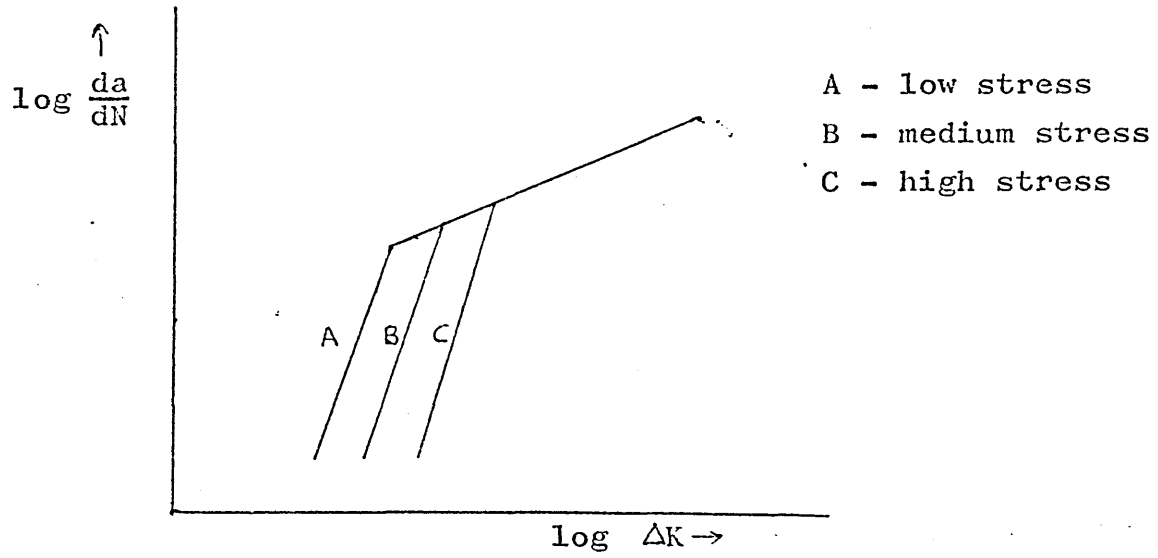


Fig. 3. Diagrammatic Representation of Results of Crack Propagation Measurements on Carbon-Manganese Steels (after Gurney (78)).

3. EXPERIMENTAL METHOD & MATERIALS USED

3.1 EXPERIMENTAL MATERIALS

3.1.1. CHEMICAL COMPOSITION

The materials used in the investigation consisted of a "pure" iron, and steels containing 0.01, 0.1 and 0.4% carbon (nominal). The compositions are shown in table I.

TABLE I. COMPOSITIONS OF EXPERIMENTAL MATERIALS

| MATERIAL | C | Si | Mn | S | P | Ni | Cr | Mo | Cu | O | N |
|----------|------|------|------|------|------|------|------|------|------|------|-------|
| A | .008 | .005 | .005 | .007 | .003 | .008 | .005 | .002 | .007 | .029 | - |
| B | .01 | <.01 | .42 | .022 | .032 | .10 | .018 | .030 | .09 | .012 | .004 |
| E | .11 | <.01 | .39 | .018 | .007 | .11 | .012 | .028 | .06 | .008 | .004 |
| F | .41 | <.01 | .40 | .018 | .008 | .11 | .015 | .025 | .07 | .003 | .003 |
| G | .011 | .012 | .51 | .016 | .025 | .12 | .02 | .02 | .10 | .009 | .003 |
| H | .125 | <.01 | .42 | .018 | .008 | .11 | .017 | .025 | .06 | .007 | .0035 |
| J | .40 | <.05 | .34 | .016 | .006 | .09 | <.03 | <.03 | .08 | .006 | .003 |

3.1.2. PREPARATION

Materials A, B, E, F, G and H were supplied by the British Iron and Steel Research Association, and were vacuum melted and rolled into strip of cross-section 3" x $\frac{3}{8}$ " (76 x 9.5mm). Material J was vacuum melted by G.I. Willan and Co. Ltd., and rolled into strip of cross section 3" x 1" (76 x 25mm) by BISRA.

After the fatigue specimens had been machined (section 3.2.1.) they were annealed for 30 minutes in a vacuum furnace. The furnace could be moved on rollers whilst the work tube remained stationary, to give a mean cooling rate of 33°C per minute from 900 to 600°C. The annealing temperatures are shown in Table II. The 0.41%C steels (F&J) were used without further heat treatment. The 0.01 and 0.11%C materials

(B, E, G and H) were subjected to a sub-critical anneal of 33½ hours at 200°C, in order to precipitate carbon from solution.

TABLE II. ANNEALING TEMPERATURES

| <u>MATERIAL</u> | <u>A</u> | <u>B</u> | <u>E</u> | <u>F</u> | <u>G</u> | <u>H</u> | <u>J</u> |
|-------------------------|----------|----------|----------|----------|----------|----------|----------|
| <u>TEMPERATURE (°C)</u> | 940 | 930 | 900 | 830 | 930 | 900 | 830 |

3.1.3. MICROSTRUCTURE

Fig. 4 shows photomicrographs of the materials used.

The iron (material 'A') consisted of ferrite grains, with numerous inclusions, which were probably iron oxide, both within the grains and at grain boundaries.

The 0.01% carbon steels ("B" & "G") consisted of ferrite grains, with small amounts of grain boundary cementite. There was also a cementite precipitate within the grains.

The 0.11 and 0.41% carbon steels consisted of ferrite and coarse pearlite. A certain amount of pearlite "banding" was present. It is extremely difficult to remove this by heat treatment, and it was decided to accept these materials in this form.

Table III shows the grain sizes and percentages of pearlite for the seven materials. The grain sizes were determined by lineal analysis, and the pearlite percentages by using a Metals Research "Quantimet" quantitative television microscope.

TABLE III. GRAIN SIZES AND PEARLITE PERCENTAGES

| <u>MATERIAL</u> | <u>FERRITE GRAIN SIZE (mm)</u> | <u>PERCENT PEARLITE</u> |
|-----------------|--------------------------------|-------------------------|
| A | .092 | - |
| B | .042 | - |
| E | .024 | 6 |
| F | .017 | 38 |
| G | .061 | - |
| H | .020 | 7 |
| J | .019 | 37 |

3.1.4. TENSILE PROPERTIES

Tensile tests were carried out in an Instron Universal Testing Machine using small specimens with a gauge length of 1" (25.4mm) and a cross-sectional area of .0625sq.in. (40.3mm²). The results are shown below :-

TABLE IV TENSILE PROPERTIES

| MATERIAL | YIELD STRESS tsi (MN/m ²) | | U.T.S. tsi (MN/m ²) | ELONGATION % | REDUCTION IN AREA % |
|----------|--|-------|------------------------------------|-----------------|---------------------------|
| B | 9.7 | (148) | 19.2 (297) | 75 | 80 |
| E | 14.6 | (225) | 22.1 (341) | 60 | 65 |
| F | 14.4 | (222) | 30.9 (477) | 40 | 45 |
| G | 10.4 | (161) | 19.8 (306) | 65 | 60 |
| H | 13.5 | (208) | 23.5 (363) | 55 | 50 |
| J | 14.7 | (227) | 29.9 (462) | 45 | 33 |

The yield stresses of materials F and J (0.41%C) were low when compared with the lower carbon materials. This is discussed in section 4.2.1.

The fracture surfaces of the tensile specimens were examined on the scanning electron microscope. All consisted entirely of ductile fracture. Equiaxed dimples were observed in all specimens (Fig. 5) and no intergranular failure was observed.

3.2. FATIGUE TESTING

3.2.1. SPECIMENS

Two types of specimen were used in the experiments, a plain one for crack initiation work, and a notched one for crack propagation work. The dimensions of these are shown in Fig. 6. The specimens were machined and rough ground

before heat treatment (see section 3.1.2.). After heat treatment all specimens were ground on successive grades of wet silicon carbide paper down to 600 grit. The specimens for initiation work were then electropolished in a bath of the following composition :

| | |
|-------------------------------------|-------|
| Glacial Acetic Acid 99.5 wt. % min. | 133ml |
| CrO ₃ | 25g |
| H ₂ O | 7ml |

Only the gauge length and the parts immediately beyond it were polished, the rest of the specimen being blanked off with "Lacomit". The electropolishing was carried out at a temperature of 20°C and at 20.5 volts. The time of polishing was half an hour, about .01mm being removed from the specimen surface. The test pieces for propagation work were not electropolished, but were finally mechanically polished with 6 micron and 1 micron diamond compound.

3.2.2. TESTING PROCEDURE

All fatigue tests were carried out in alternating tension and compression at zero mean stress on a 2 ton Amsler "Vibrophore". The frequency of testing was 185 cycles per second. During the test, the mean stress tended to show a slight drift into tension of about 0.25 t.s.i. (3.8MN/m²) but in the later propagation tests, an automatic mean load maintainer became available, so that zero mean stress could then be maintained through the test. This slight drift into tension is not thought to have significantly affected the results.

3.2.3. CRACK PROPAGATION MEASUREMENTS

Direct measurements of the progress of the propagating cracks in the notched specimens were made using two Vickers

travelling microscopes, one on each side of the specimen under test (Figs. 7 & 8). On the early work, only one set of measurements was taken, but since sloping crack fronts were sometimes obtained, it was thought desirable to record crack propagation on both surfaces. The interval between successive readings was determined by the observed rate of crack propagation, but was generally of the order of 5000 cycles.

3.3. EXAMINATION OF SPECIMENS

Observations of fatigue damage and crack initiation on the surfaces of the plain specimens were first made using the optical microscope. Replica electron microscopy was also carried out using two stage cellulose acetate - carbon replicas. Cellulose acetate sheet, .002" (.05mm) thick, was softened in acetone and applied to the specimen surface. When this had dried, it was stripped off, and then shadowed with platinum - carbon in a vacuum evaporating unit, at an angle of 30° to the specimen surface. Carbon was then evaporated on to this, and the cellulose acetate dissolved away in acetone. Considerable difficulty was experienced at this stage due to the expansion of the cellulose acetate causing the carbon film to break up. The two stage method was used so that the specimen surfaces could be preserved.

A "Stereoscan" scanning electron microscope became available later and this was also used for surface observations.

Taper sections were prepared for optical examination. The specimens were first nickel plated to preserve the specimen surface topography, and sections were prepared at an angle of $11\frac{1}{2}^{\circ}$ to the surface. This gave a taper

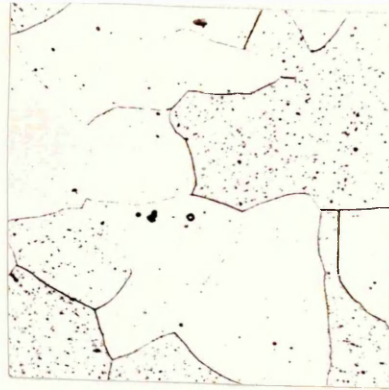
magnification of 5x. This magnification was chosen because it was thought that it would be high enough to give a clear picture of the phenomena occurring on the surface of the specimen, but would not be so high as to cause errors of interpretation to be made.

The fracture surfaces of the crack propagation specimens were examined by the naked eye, and by means of the scanning electron microscope. This information was supplemented by observation of cross-sections through the cracked specimens.

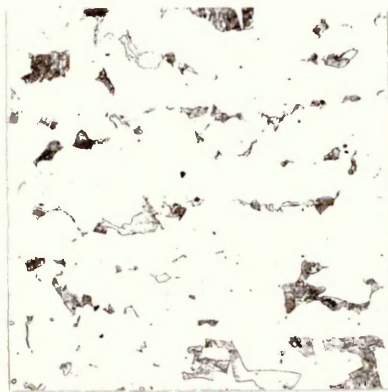
Note : arrows on photographs indicate the stress axis in the case of plain specimens, and the direction of crack propagation in the case of notched specimens.



0.01%C Material B



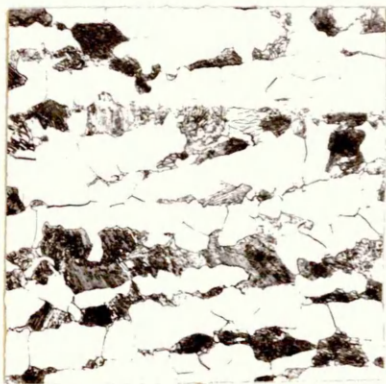
0.01%C Material G.



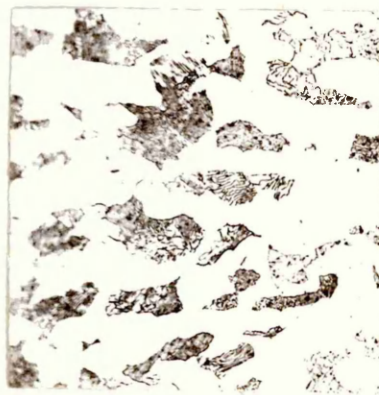
0.11%C Material E.



0.11%C Material H.

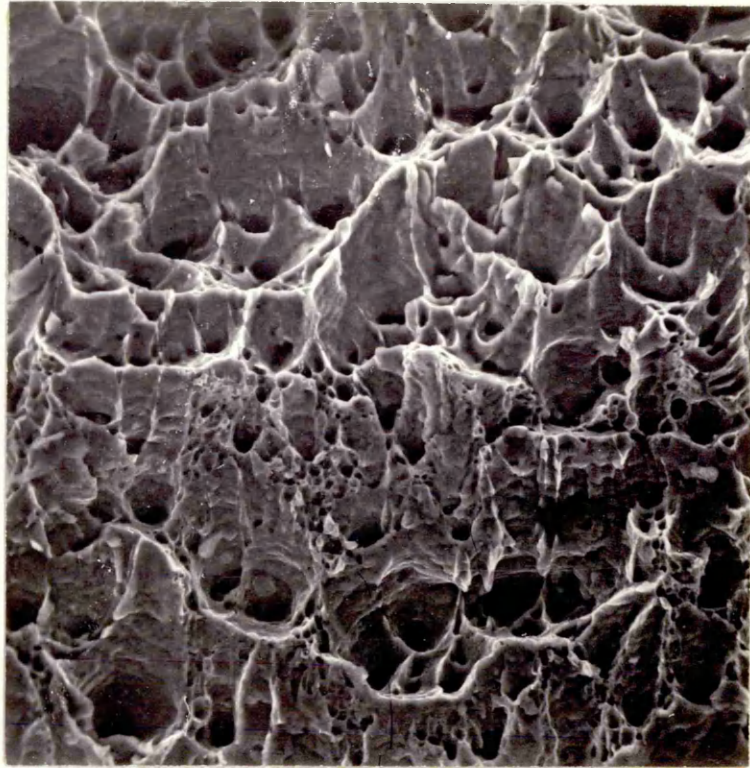


0.41%C Material J.



0.41%C Material F.

Fig. 4. Microstructure of Experimental Materials. X200



X 650

Fig. 5. Scanning Electron Micrograph of Fracture Surface of Tensile Specimen 0.01% Carbon Steel.

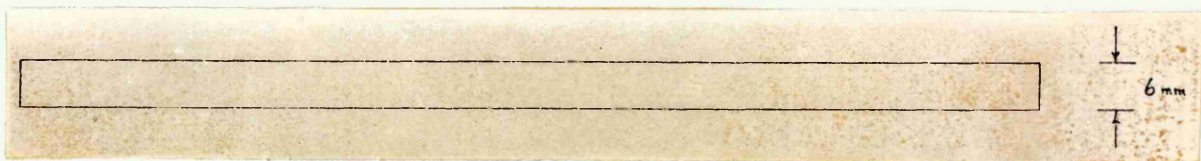
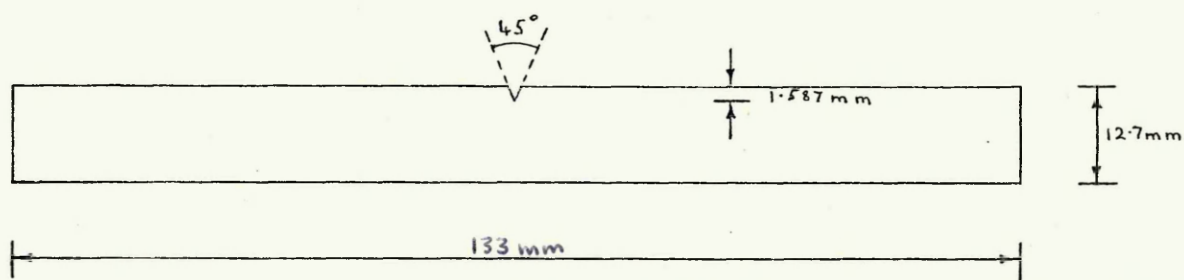
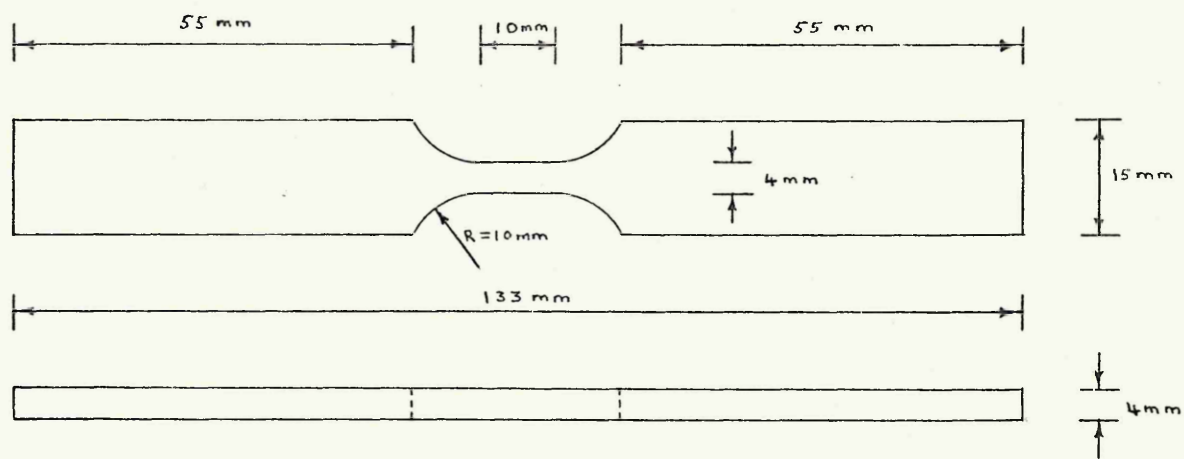


Fig. 6. Dimensions of Test Specimens.

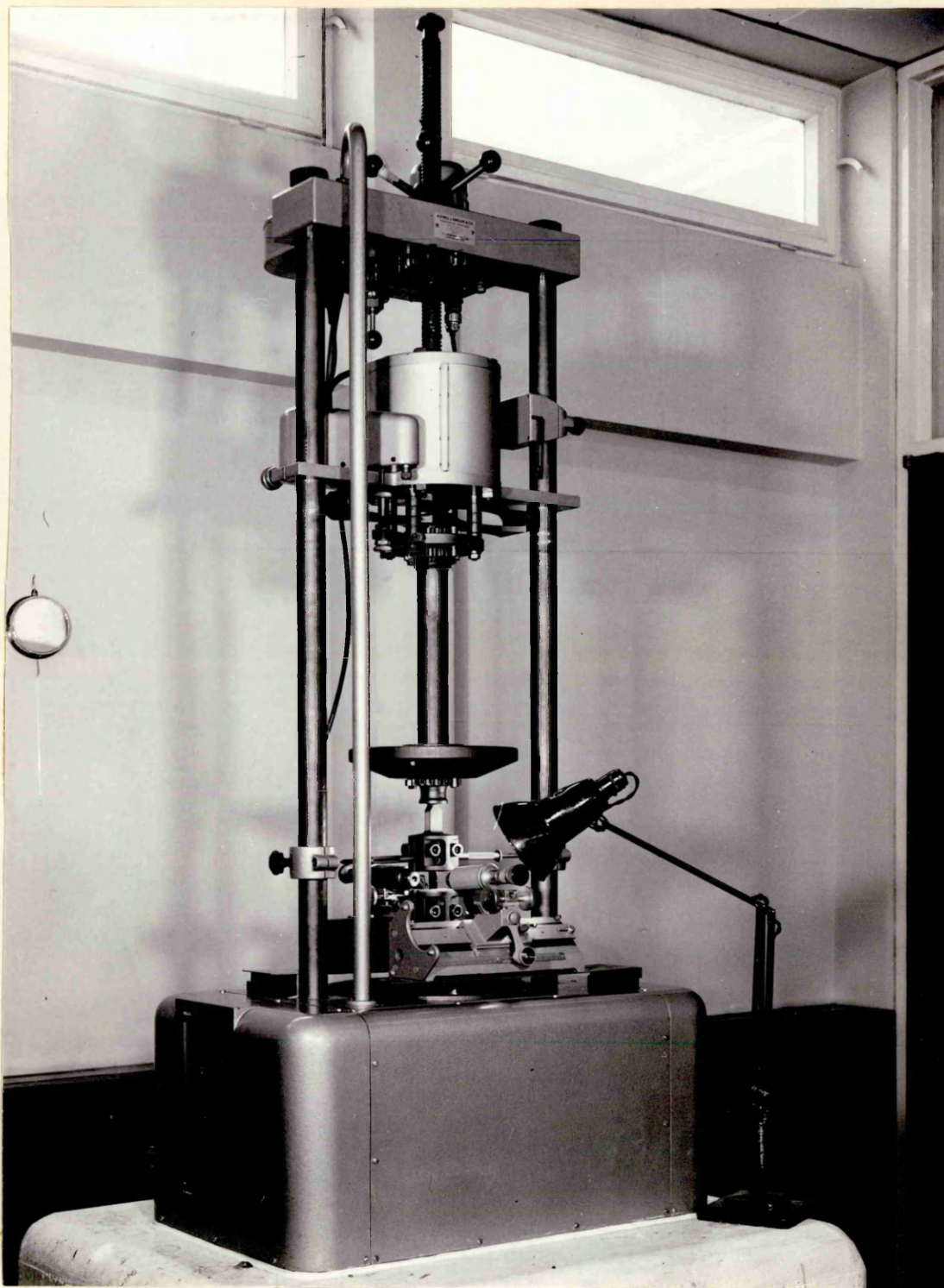


Fig. 7. Testing Arrangement Showing Amsler 2-ton Vibrophore.

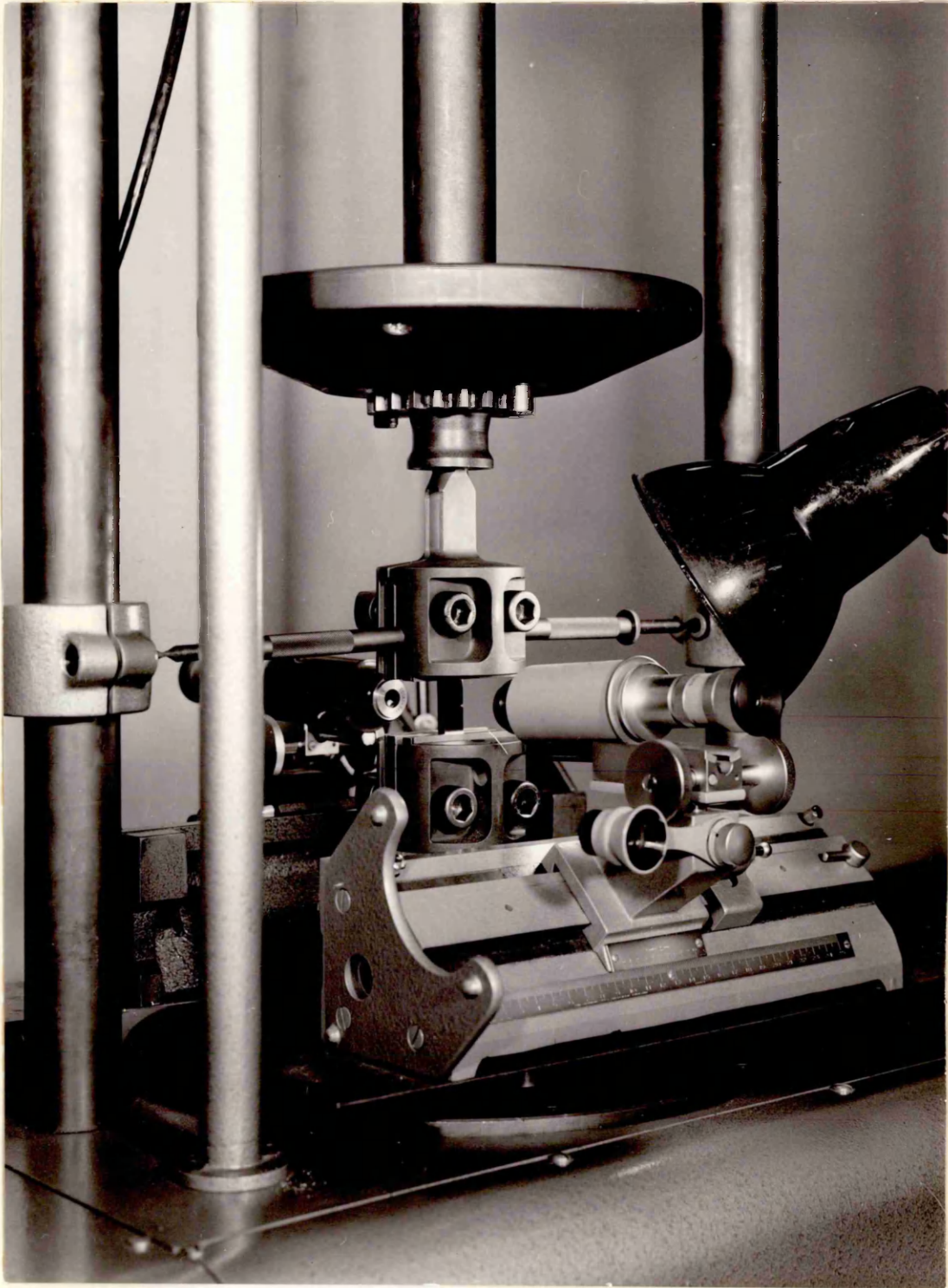
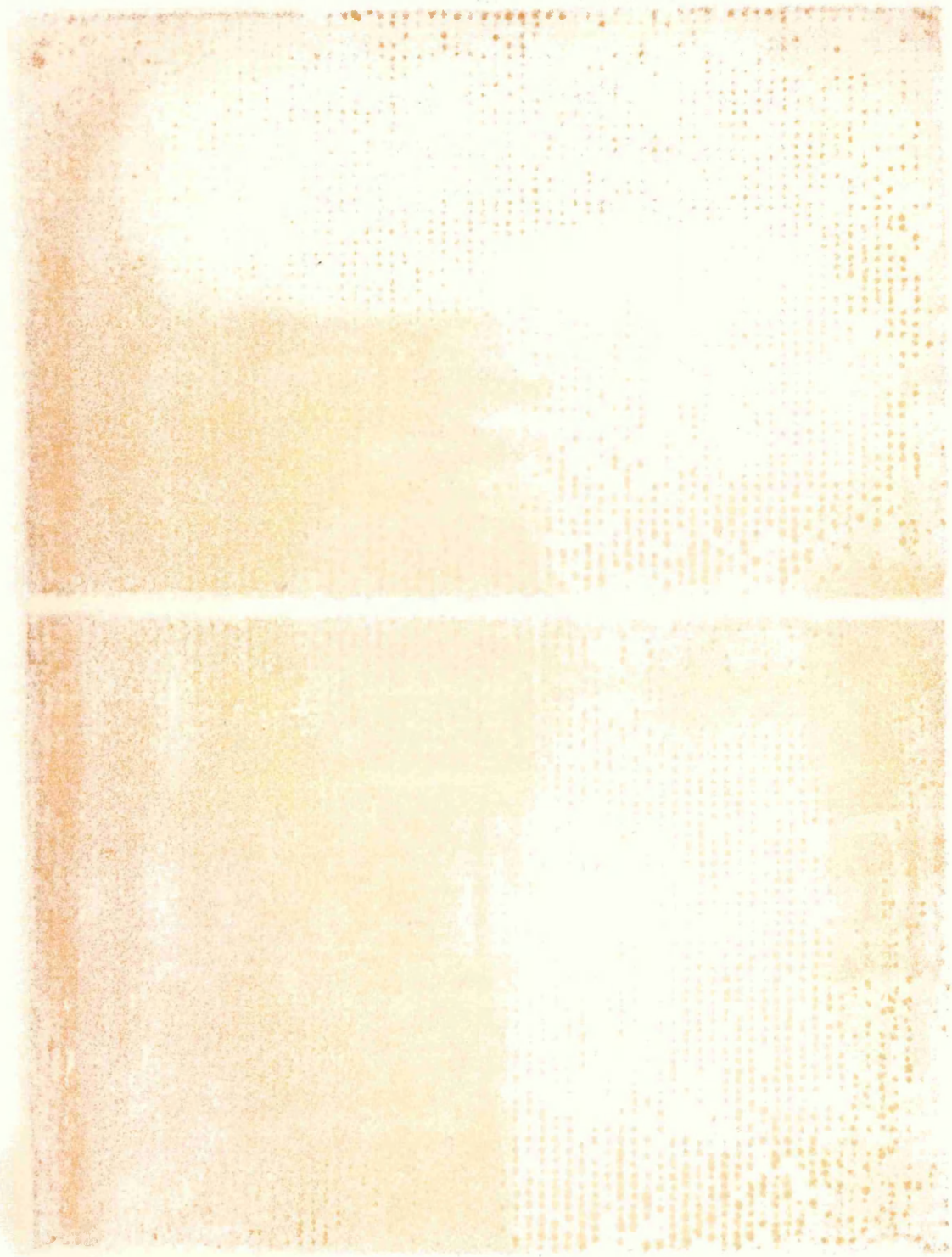


Fig. 8. Close-up of 2-ton Vibrophore Showing Notched Specimen and Travelling Microscopes.



4. EXPERIMENTAL WORK

4.1 PRELIMINARY WORK ON "PURE" IRON

Originally, it was intended to study the fatigue of pure iron, and then to proceed to the study of the plain carbon steels, in order to determine the effect of increasing amounts of pearlite on the fatigue process.

Tests were carried out in the as-rolled state, and after annealing at 940°C. In both cases, wavy slip bands which were very dark in appearance were noted, and crack propagation was intergranular. The appearance of the fatigue slip bands at low magnification, and the intergranular nature of the crack propagation is shown in Fig. 9. Fig. 10 is a higher magnification photograph and shows the diffuse appearance of the fatigue slip bands.

Rees, Hopkins & Tipler have shown that pure iron containing oxygen suffers from grain boundary embrittlement (80). It has also been shown by Tipler and Forrest that fatigue cracks in grain boundary embrittled iron are intergranular (81). The oxygen content of the pure iron used in this investigation was very high (.029%) and it was thought that this was probably the cause of the intergranular crack propagation. Because of the difficulty of obtaining a pure iron of lower oxygen content, it was decided not to continue the work on pure iron and to concentrate on the plain carbon steels. Work on intergranular cracking in iron has since been reported by Golland and James (41) and has confirmed the above results.

4.2 EXPERIMENTAL WORK ON CARBON-MANGANESE STEEL PLAIN SPECIMENS

4.2.1. TEST RESULTS

Semi-stress range - number of cycles to failure (S-N) curves for all uninterrupted fatigue tests carried out on the three materials used for the testing of plain specimens (F, G and H) are shown in Fig. 11. These curves were produced so that (a) estimates of percentage of life to failure could be made for specimens not taken to failure and (b) the approximate positions of the fatigue limits were known. The fatigue limits and fatigue ratios (fatigue limit/U.T.S.) for the three materials are as follows :

| MATERIAL | FATIGUE LIMIT TONS/SQ.IN. | (MN/m ²) | FATIGUE RATIO |
|------------|------------------------------|----------------------|---------------|
| F (0.41%C) | 10.6 | (164) | 0.34 |
| G (0.01%C) | 8.45 | (131) | 0.43 |
| H (0.11%C) | 10.35 | (160) | 0.44 |

It can be seen that there is a discrepancy in the fatigue ratio, as far as material "F" is concerned. Material "F" also has a low yield stress for its carbon content when compared with materials G and H. It is considered that the reason for this was the difference in heat treatments mentioned in section 3.1.2. A low temperature heat treatment causes carbide precipitation and will promote dislocation locking, which will in turn increase the yield stress. Oates and Wilson⁽⁵³⁾ have shown that this initial dislocation locking raises the fatigue limit of low carbon steels which have fatigue limits below the yield stress,

thus explaining the effect observed in this work.

4.2.2. THE DEVELOPMENT OF SURFACE FATIGUE DAMAGE

Examination of the polished surfaces of the fatigued specimens showed that the general surface appearance consisted of dark irregularly shaped areas of fatigue deformation separated by damage - free areas. The areas of fatigue deformation often bore no relation to grain shape. Although they often stopped at grain boundaries, they also sometimes crossed grain boundaries. This type of deformation occurred on all specimens examined. There did not appear to be any marked difference in the type of fatigue damage formed in the three materials. The proportion of the surface on which fatigue damage occurred increased with increasing stress amplitude. This is shown in Fig. 12, which compares three specimens of 0.11% carbon steel fatigued to failure at different stress levels. Fig. 13 shows parts of the same areas of fatigue damage at higher magnification.

The darkening of the surface slip bands is thought to be due to a thin film of oxide on the surface. The oxide showed interference colours in the early stages of the tests, changing to a dark appearance as the test progressed. It is thought that this is due to oxidation of the active newly generated surfaces in the slip bands.

Examination of carbon replicas taken from the surface of fatigued 0.41% carbon steel specimens showed that the fatigue damage consisted of wavy slip bands, which were rather shallow and which did not appear to exhibit the very sharp notch-peak topography which is characteristic of many FCC metals. The type of surface damage observed is shown in

figs. 14 and 15. The surface in these regions of fatigue damage was of a rather undulating character.

Scanning electron microscopy of specimen surfaces confirmed the replica observations as far as the type of surface fatigue damage was concerned (Fig. 16). Fig. 16A also shows a grain boundary crack (section 4.2.4.).

Fatigue damage almost invariably occurred in the ferrite grains. Very occasionally, a small amount of damage could be seen in the ferrite of the pearlite, but this was rather exceptional. Examination of taper sections confirmed this. Fig. 17 shows a surface notch-peak topography in a ferrite grain, with the surfaces of the adjacent pearlite colonies remaining quite flat.

The taper sectioning showed clearly the phenomena occurring in the surface slip bands. To demonstrate the effect of stress amplitude, three specimens of the 0.11% carbon steel tested at different stresses were examined (Fig. 18). The specimen tested below the fatigue limit showed only short extrusions and intrusions. In contrast, the two specimens tested above the fatigue limit showed much larger notches and peaks in those grains where damage was being produced. The maximum height of these peaks was of the order of $1\frac{1}{2}\mu$.

4.2.3. THE SPREAD OF PLASTICITY DURING FATIGUE

Oates and Wilson⁽⁵⁵⁾ proposed that the spread of plasticity was the controlling factor in deciding whether a plain fatigue specimen would fail or not. If appreciable numbers of fatigue damage clusters beyond a certain size (extending over several grains) were not formed, the specimen

would not fail. To investigate the validity of this concept for a material with a greater pearlite content than Oates and Wilson's 0.1% carbon steel, two 0.41% carbon steel specimens were examined at regular intervals during fatigue testing, and counts were made of the proportion and size of areas of fatigue damage. The results are shown in Figs. 19 and 20, which show the variation in the number of surface grains containing fatigue damage with endurance. Different curves are shown for single grains, clusters of 2 or 3 grains, clusters containing 4 or more grains and the total number of damaged grains. It can be seen from the graphs that in the higher stress specimen (F12), the total number of damaged grains gradually increased as the test progressed, until at approximately 50% of the life 30% of all grains contained surface damage. At 11% of the life (10^5 cycles), the majority of the fatigue damage consisted of clusters of fewer than 4 grains. Above 11% of the life, the size and number of fatigue damage clusters gradually increased, until at 50% of the life the majority of these clusters contained 4 or more grains. At failure, about 40% of all grains contained surface damage. The lower stress specimen (F16) showed an initial amount of fatigue damage at 7% of the life, which had not apparently changed after 85% of the life. There was then a sudden increase and the specimen failed. Examination of the failed specimen showed that the area adjacent to the fracture contained a large number of grains containing fatigue damage, but the rest of the specimen showed no increase in the number or size of fatigue damage areas.

4.2.4. SLIP INTENSIFICATION AT GRAIN BOUNDARIES

In all specimens, a certain amount of slip intensification was noted at grain boundaries. Fig. 21 shows an example of this effect at various percentages of the life of a 0.01% C steel specimen. At 2% of the life, the appearance was certainly that of a crack with a small amount of slip in each adjacent grain. At 10% of the life, however, the slip bands at right angles to the grain boundary were more apparent, and grain boundary extrusions were visible. These had a metallic appearance. At failure, both the intensity of slip and the size of the extrusions had increased.

In observations using the optical microscope, grain boundary slip intensification was easily confused with grain boundary cracking, especially at low percentage lives. To resolve this phenomenon, an area which showed this black grain boundary appearance on the optical microscope was observed on the Stereoscan. This is shown in Fig. 22, which compares optical and stereoscan photographs of the same area of a 0.11% carbon steel specimen which had been fatigued for 10% of its expected life. Although a crack appears to be present under the optical microscope, the Stereoscan clearly shows this to be an area of intense slip. Deformation has occurred adjacent to the boundary in both grains, so that there is a depression in the left-hand grain, and a peak in the right-hand grain.

Grain boundary slip intensification is also shown in Fig. 25, section 4.2.5. In this case a "cliff edge" has been formed at the grain boundary.

Taper sectioning clearly showed that enhanced slip at

grain boundaries could lead to the formation of intrusion-extrusion pairs. This effect is shown in Fig. 23.

4.2.5. CRACK INITIATION

Two types of cracks could be distinguished on the surface of failed specimens, namely slip band cracks and grain boundary cracks.

It was very difficult to distinguish slip band cracks under the optical microscope, owing to the dark surface oxide film which covered most of the fatigue damage regions. Thin black lines could be observed in these areas (Fig. 24) but it was not possible to say whether these were cracks or not. However, examination of areas of fatigue damage under the scanning electron microscope showed clearly that slip band cracking did occur (Figs. 25 and 26). Slip band cracks were also observed in taper sections (Fig. 27).

Certain specimens tested above the fatigue limit showed grain boundary cracks. One of these is shown in Fig. 28. However, as mentioned earlier, it was quite possible that this could just have been another case of grain boundary slip intensification. However, when this specimen was repolished, although it was difficult to find the area depicted in Fig. 28 again, a clear case of grain boundary cracking was revealed (Fig. 29). These cracks were often seen near to the main crack, and it is possible that these might have been a consequence of the high stress in the region around the advancing crack front. A grain boundary crack in a taper section is shown in Fig. 30.

Fig. 31 shows a scanning electron micrograph of a grain boundary crack which was seen in an area near to the main crack. The crack separates a grain in which much surface

fatigue damage has occurred from one in which there has been little damage. This is similar to Fig. 16A.

4.2.6. SURFACE CRACK PROPAGATION

Examination of the surface fatigue cracks showed that propagation occurred in a mixed transgranular - intergranular manner. When transgranular propagation occurred, the microscopic direction of crack propagation was irregular, and not straight as in a cleavage crack. Grain boundary propagation occurred when the boundary was suitably orientated with respect to the stress axis.

On virtually all the specimens examined, only one large crack was present at failure and this usually initiated at one of the specimen corners. However, on one side of one of the 0.01% carbon steel specimens, a large secondary crack was present, the appearance of which is shown in Fig. 32. It would seem that the feature in the centre consisted of two slip band cracks. This specimen was repolished and etched to show up the shape of the crack in relation to the grain structure. It can be seen that these two cracks have occurred on parallel planes in a single grain. Forking of the main crack had occurred at both ends. In Fig. 32B it can be seen that the direction of forking at the left-hand side is away from the slip band cracks. Observation earlier in the repolishing process also showed that this was also the case on the right-hand side of these cracks. It is, therefore, reasonable to assume that this crack originated at these slip band cracks.

4.2.7. INITIATION OF MAIN CRACKS & STAGE I PROPAGATION

In order to determine whether the fatigue cracks which

led to final failure were initiated at slip bands or grain boundaries, certain specimens of all three materials were broken open, and the fracture surfaces examined to determine the point of origin. Stereoscan examination was then carried out at this point. None of these specimens had fractures which had obviously initiated at a grain boundary. Fig. 33 shows the corner of a specimen at which a fracture originated. A distinct stage I fatigue zone can be seen at this point. Fig. 34 shows this origin from a different angle, and Fig. 35 shows this at higher magnification. It is rather difficult to decide whether the edge at "A" in Fig. 35 is a grain boundary. The edge at "B" is, however, definitely transgranular. On Fig. 36, which is a series of photographs taken at the same angle as Fig. 32 but at higher magnifications, line markings can be seen radiating away from the edge which corresponds to "B" in Fig. 35. It has been mentioned earlier (section 2.2.1.3.) that these lines run parallel to the direction of local crack propagation. Thus edge "B" is the likely crack initiation zone.

The general appearance of the stage I fracture near to the surface consisted of parallel slip band cracks. These seemed to converge onto one level at about one third of the way down the stage I area. Stage I fracture was not planar as has previously been reported for aluminium alloys⁽⁶³⁾, but appeared most irregular at high magnifications (Fig. 36).

Another Stage I fracture, this time in a 0.41% carbon steel is shown in Fig. 37. On this occasion, fracture did not start from a corner, but from the centre of one face of the specimen. Again, the lines parallel to the direction of

crack propagation could be seen at the specimen surface, but these tended to become less evident further away from the surface. The wavy nature of the propagating crack is clearly evident, and in the later stages the whole of the crack front appeared to change direction periodically.

4.3. EXPERIMENTAL WORK ON CARBON-MANGANESE STEEL NOTCHED SPECIMENS

4.3.1. TEST RESULTS

Endurance data from the crack propagation tests is shown in Table V (S-N diagrams have not been drawn, because the number of tests carried out on each material is not considered sufficient for these to be useful). "Endurance" denotes the number of cycles after which the test was stopped. Tests were stopped when the crack growth rate became too fast to follow accurately.

At the same time, the load could not be maintained without greatly increasing the power input to the machine.

The measured results for crack length v. number of cycles for all the specimens except B2, J1 and J2 are shown graphically in the appendix, Fig. A1. Specimens B3, J1 and J2 developed cracks in the area below the notch root, but these did not propagate.

Values of the slope, $\frac{da}{dN}$ of these curves at various points were obtained graphically and plotted against the calculated stress intensity range at such points, ΔK , on log-log graph paper. The results are shown in the appendix, Figs. A2-A4 for each material, and a composite plot for all three materials is shown in Fig. A5. There was considerable scatter in these results, the scatter in the results for individual materials being so large as to mask any possible effect of material on

the relationship. The slopes of the curves varied from approximately $\frac{1}{2}$ to $\frac{1}{3}$, giving a relationship of the form $\frac{da}{dn} \propto \Delta K^n$ where $n = 2$ to 3 .

TABLE V ENDURANCE OF CRACK PROPAGATION SPECIMENS

| SPECIMEN | STRESS | | ENDURANCE (cycles) |
|---------------|----------|----------------------|--------------------|
| | (t.s.i.) | (MN/m ²) | |
| <u>0.01%C</u> | | | |
| B1 | 5.15 | (80) | 1.3×10^5 |
| B2 | 3.80 | (59) | 1.6×10^7 |
| B4 | 5.65 | (87) | 2.3×10^5 |
| B5 | 4.00 | (62) | 4.7×10^5 |
| B6 | 4.70 | (73) | 4.8×10^5 |
| B10 | 4.25 | (66) | 4.6×10^5 |
| <u>0.11%C</u> | | | |
| E1 | 4.25 | (66) | 7.1×10^5 |
| E3 | 5.65 | (87) | 2.0×10^5 |
| E5 | 4.50 | (69) | 3.5×10^5 |
| E6 | 5.15 | (80) | 2.8×10^5 |
| E8 | 3.80 | (59) | 2.6×10^6 |
| E10 | 4.70 | (73) | 4.9×10^5 |
| <u>0.41%C</u> | | | |
| J1 | 3.30 | (51) | 1.4×10^7 |
| J2 | 2.83 | (44) | 1.9×10^7 |
| J5 | 5.65 | (87) | 1.6×10^5 |
| J6 | 4.70 | (73) | 5.7×10^5 |
| J7 | 3.80 | (59) | 1.3×10^6 |
| J13 | 5.65 | (87) | 1.7×10^5 |

4.3.2. STAGE II CRACK PROPAGATION

4.3.2.1. General

Observation of fracture surfaces on the scanning electron microscope showed that in the earlier part of Stage II crack propagation in all three materials, both transgranular and intergranular propagation occurred (Fig. 38). In the later stages, however, wholly transgranular propagation occurred (Fig. 39). The transgranular areas consisted of plateaux with edges running parallel to the local direction of crack propagation (Fig. 40). Characteristic fatigue striations which ran perpendicular to the local direction of crack propagation could be seen on top of the plateaux, and in the valleys between the plateaux. The plateaux sometimes tended to run together, to form one wider plateaux. Sometimes the opposite would occur, i.e. one plateaux would split into a number of narrower plateaux. Examination of stereo pairs showed that what appeared on one photograph to be plateaux were, in fact, hills and valleys which presented a curved appearance (Fig. 41). The spacing between fatigue striations was remarkably constant throughout the Stage II region, being of the order of $1 - 2 \times 10^{-4}$ mm for all three materials. On a number of specimens, fretting had occurred on the fracture surface producing rub marks and debris (Fig. 42). There was no problem in distinguishing between rub marks and striations.

4.3.2.2. Intergranular Fracture

The intergranular fractures were relatively featureless, apart from markings which resembled the slip lines seen on the surface of ferritic steels which have been subjected to unidirectional deformation (Fig. 43). Counts were carried

out of percentage intergranular fracture v. crack length for one specimen of each of the three steels. The results are shown below :-

| | <u>% INTERGRANULAR FRACTURE AT (mm)</u> | | | | | | | |
|--------|---|-----|-----|-----|-----|-----|-----|-----|
| | 0.5 | 1.0 | 1.5 | 2.0 | 2.5 | 3.0 | 3.5 | 4.0 |
| 0.01%C | 20 | 40 | 65 | 40 | 35 | 18 | 0.5 | 0 |
| 0.11%C | 10 | 12 | 18 | 14 | 6 | 1 | 0 | 0 |
| 0.41%C | 4 | 7 | 9 | 3 | 0 | 0 | 0 | 0 |

The 0.01 and 0.11% carbon steels showed more intergranular fracture than the 0.41% carbon steel. The percentage intergranular fracture showed an initial increase, and then decreased until a point occurred when the fracture became wholly transgranular. This effect occurred at all nominal stress levels in all three materials. During the first part of the stage II fracture, i.e. the part which contained the intergranular fracture the crack propagation path seemed to be structure sensitive, sometimes changing direction at grain boundaries. The latter part of the stage II fracture was structure insensitive, i.e. no clear indication of grain boundaries could be observed on the fracture surface, unless etching was resorted to.

4.3.2.3. Effect of Pearlite

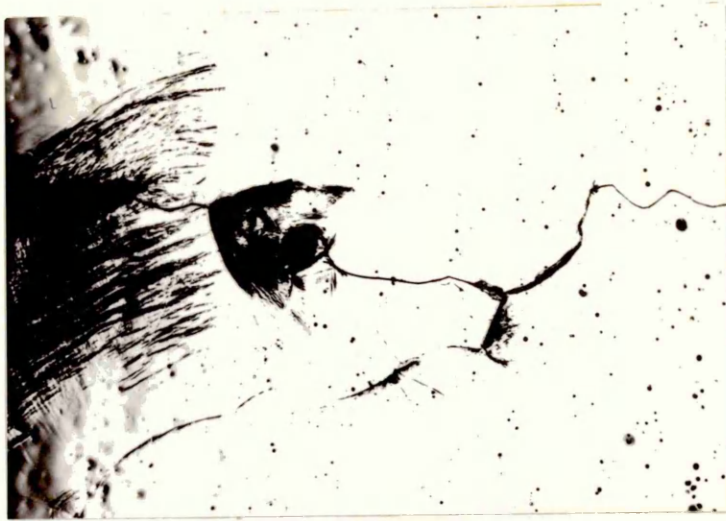
The effect of pearlite on the local direction of crack propagation was studied in both the 0.11 and 0.41% carbon steels by observation of cross-sections through the fracture (Figs. 44 and 45). Although, occasionally a crack would run down the interface between a pearlite colony and a ferrite grain, the crack usually cut through the pearlite colony. The actual mode of crack propagation through the pearlite

depended on the orientation of the cementite lamellae (Fig. 46). If this was approximately parallel to the direction of crack propagation, the crack propagated along the ferrite-cementite interface. If the orientation of the cementite was perpendicular to the crack propagation direction, the crack cut through both the ferrite and cementite as though no structure change was present. Some colonies showed a combination of these effects which gave rise to a step-like pattern. There was no tendency for the crack to avoid the pearlite colonies.

The appearance of both a fracture along a ferrite-pearlite interface and a fracture through a pearlite colony is shown in Fig. 47. This shows the fracture surface of a 0.41% carbon steel. Observation of stereo pairs showed that the crack had propagated along the ferrite-pearlite interface (A), and had then turned to propagate through the pearlite (B).

4.3.2.4. Branch Cracks

Direct observation of propagating cracks showed that a large amount of crack branching occurred in the later stages of crack propagation. This could be plainly seen on the scanning electron microscope (Fig. 48). Cross sections through the fractures, however, indicated that this crack branching also occurred early in the process, but that, as would be expected, the branch cracks were much larger and wider in the latter stages of Stage II crack propagation. An example of one of these cracks is shown in Fig. 49.



X 50

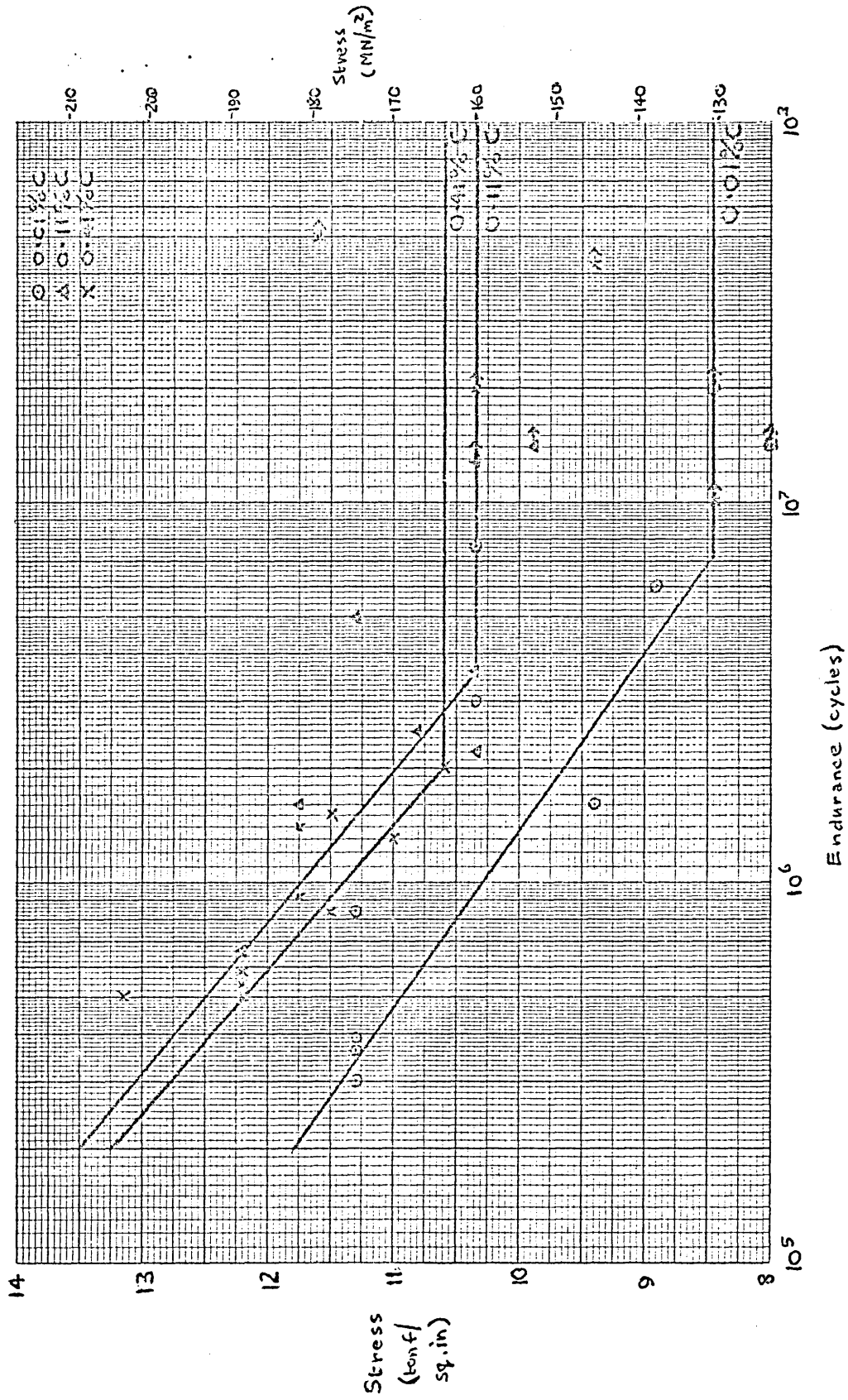
Fig. 9. Surface Damage and Intergranular Crack Propagation in Iron.



X200

Fig. 10. Surface Damage in Iron.

Fig. 11. S-N Curves for Plain specimens of 0.01, 0.11 & 0.41% Carbon Steels





Stress: 10.35 tons/sq.in.
(160 MN/m²)
Unbroken.

Stress: 10.8 tons/sq.in.
(167 MN/m²)
Endurance: 2.6 x 10⁶ cycles.



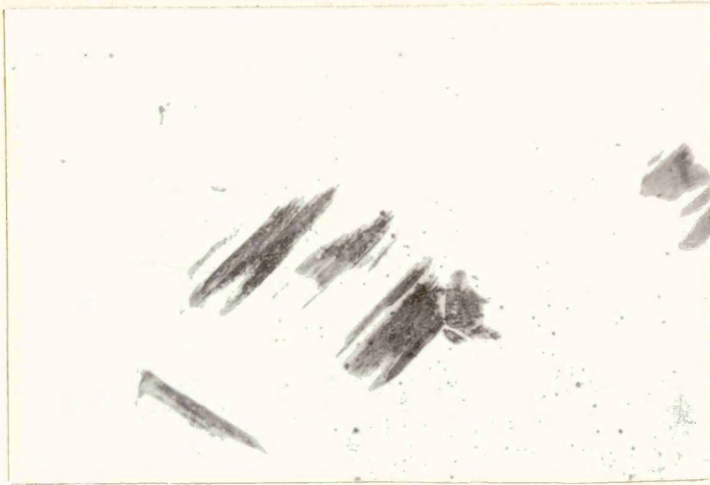
Stress: 11.75 tons/sq.in.
(181 MN/m²)
Endurance: 1.16 x 10⁶ cycles.

Fig. 12

x 200

Effect of Stress Amplitude on the Appearance of Surface Fatigue Damage in 0.11% Carbon Steel.

Stress: 10.35 tons/sq.in.
(160 MN/m²)
Unbroken.



Stress: 10.8 tons/sq.in.
(167 MN/m²)
Endurance: 2.6 x 10⁶ cycles.

Stress: 11.75 tons/sq.in.
(181 MN/m²)
Endurance: 1.16 x 10⁶ cycles.

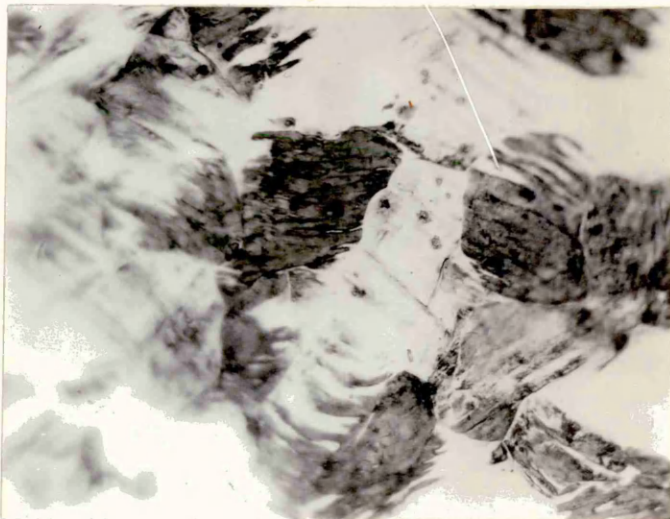


Fig. 13.

x 500

Effect of Stress Amplitude on the Appearance of Surface Fatigue
Damage in 0.11% Carbon Steel.



Fig. 1. Surface of a specimen
after 100 cycles
at a stress level of 0.11.

Fig. 2. Surface of a specimen
after 1000 cycles
at a stress level of 0.11.

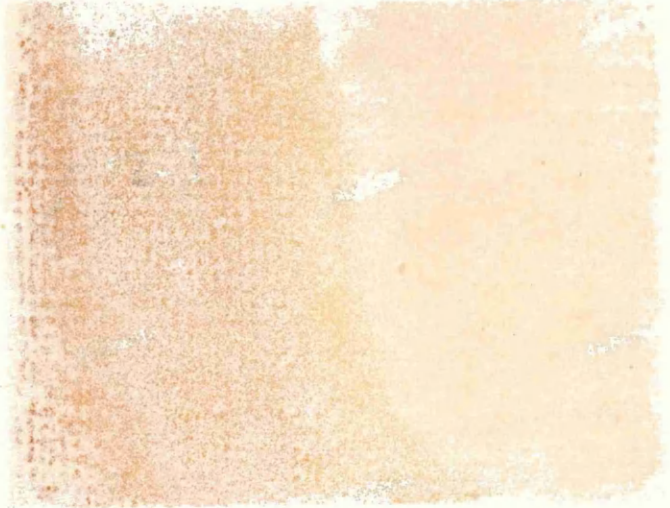
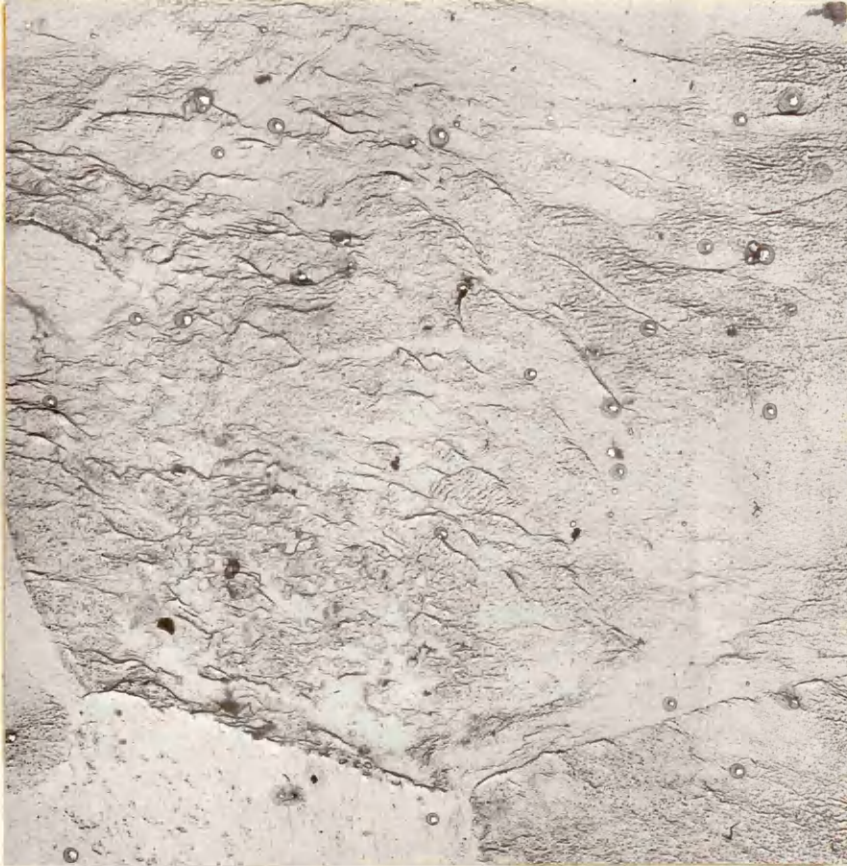
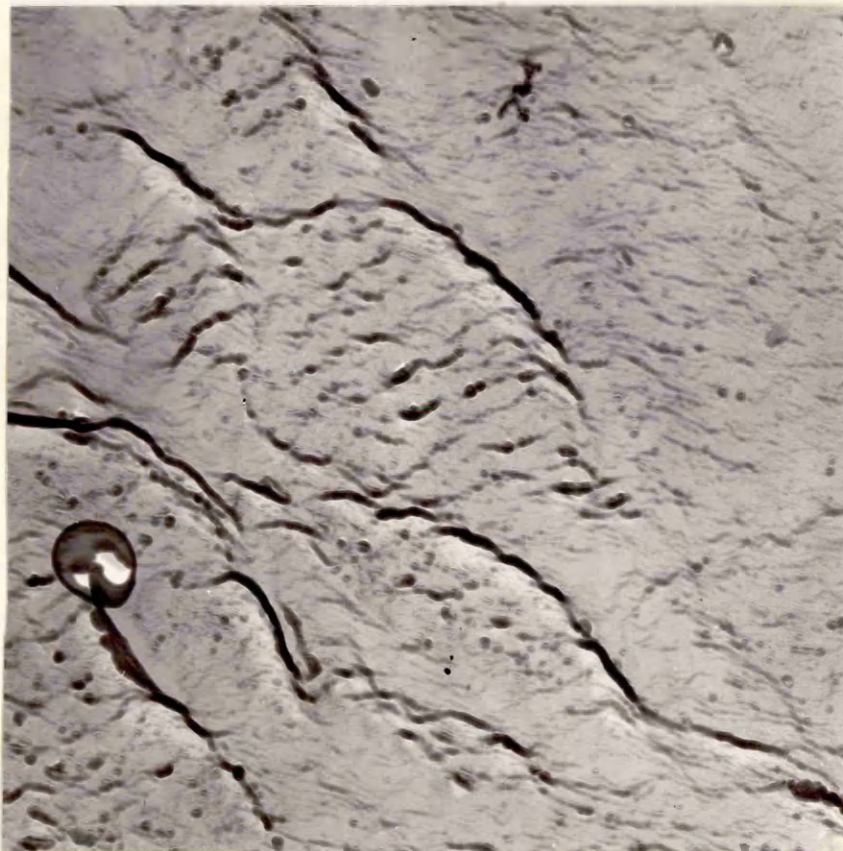


Fig. 3. Surface of a specimen
after 10000 cycles
at a stress level of 0.11.

Effect of Stress Amplitude on the Appearance of Surface Fatigue
Cracks in 0.11 Carbon Steel.



x 2000



x 21000

Fig. 14. Surface damage in a 0.41% Carbon Steel Specimen. Stress 12.2 tons/sq.in (188 MN/m^2) Endurance 5×10^5 cycles (Electron Micrographs of two stage platinum - carbon shadowed carbon replica).

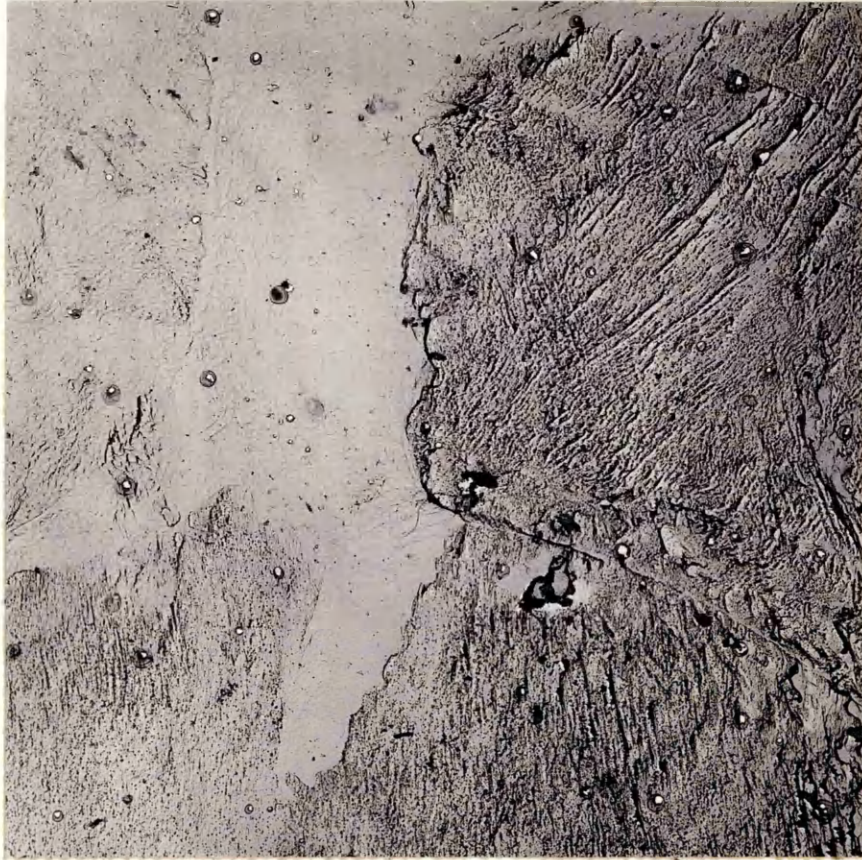
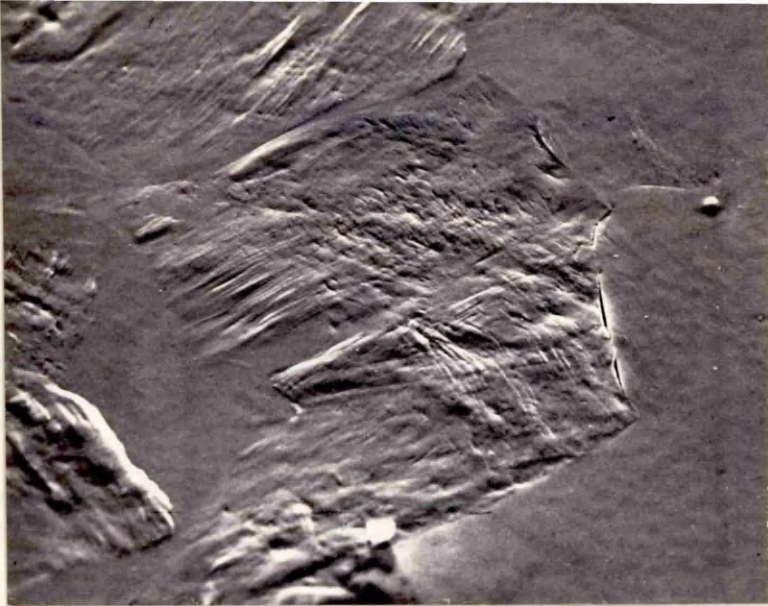


Fig. 15.

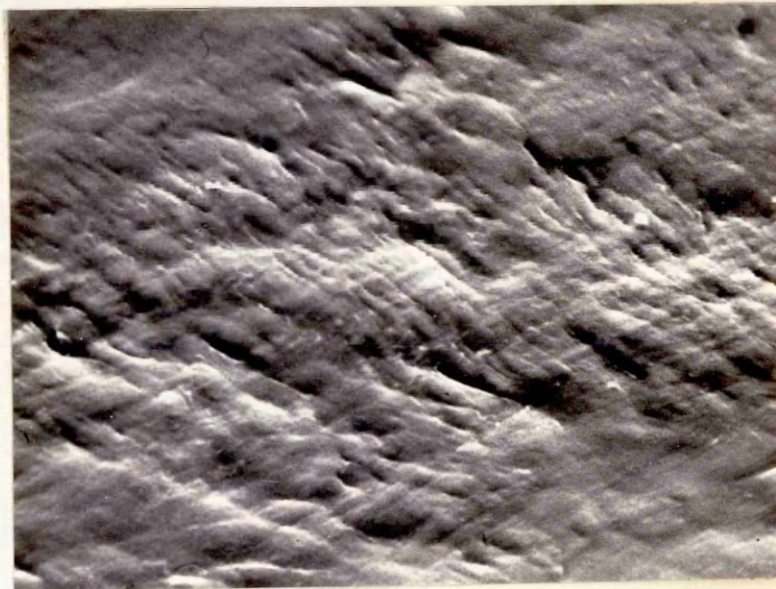
x 2000

Surface Damage on a specimen of 0.41% Carbon Steel, Stress 11.5 tons/sq.in. (177 MN/m^2). Endurance 7.33×10^5 cycles. (Electron micrograph. Two stage platinum-carbon shadowed carbon replica).

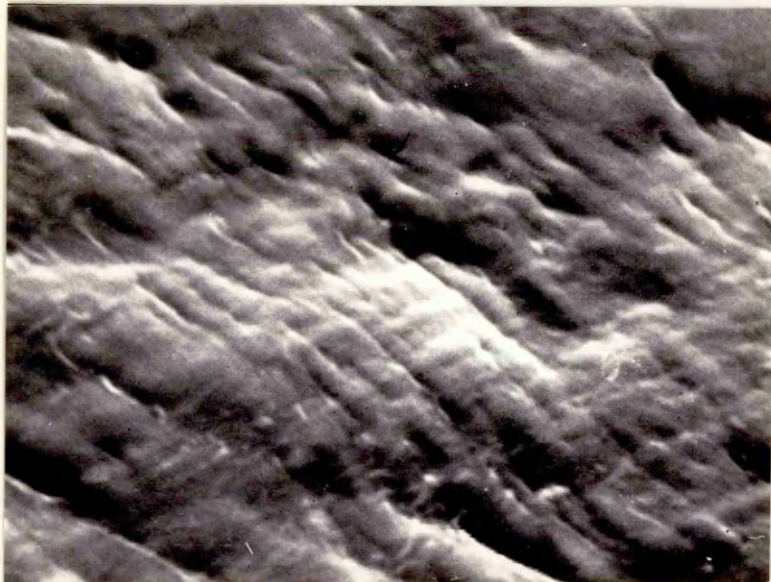


A.
x1150

A.



B.
x 5600



C.
x 11500

Fig. 16
Scanning Electron Micrographs of 0.41% Carbon Steel Specimen
Surface. Stress: 11.75 tons/sq.in (181 MN/m^2) Endurance:
 1.4×10^6 cycles.

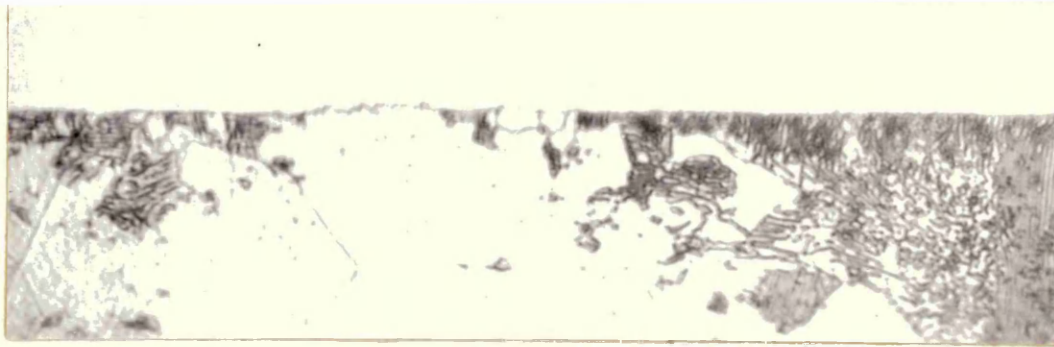
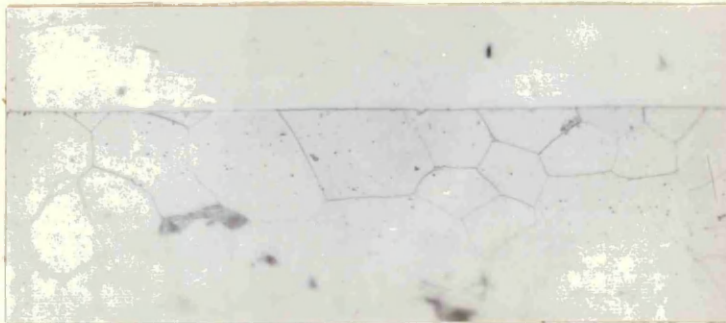
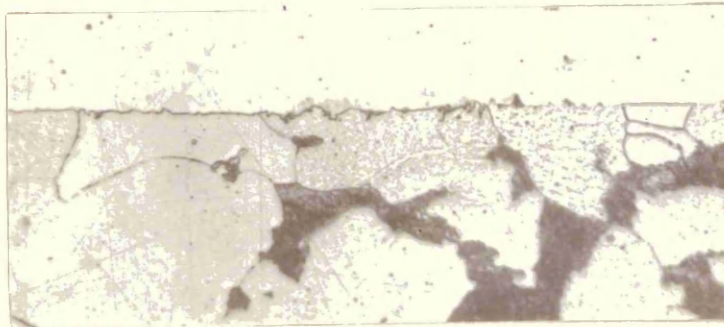
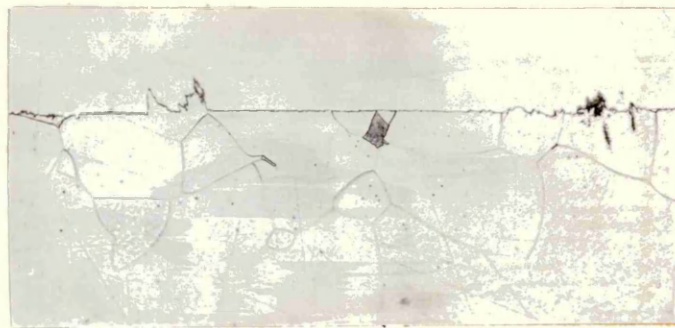


Fig. 17 x 1000
 Effect of Pearlite on the Development of Surface Fatigue
 Damage, 0.41% Carbon Steel. Stress: 11.75 tons/sq.in.
 (181 MN/m²) Endurance: 14 x 10⁶ cycles. Taper section.



Stress: 10.35 tons/sq.
 in. (160 MN/m²)
 Unbroken.

Stress: 10.8 tons/sq.in.
 (167 MN/m²)
 Endurance 2.6 x 10⁶ cycles.



Stress: 11.75 tons/sq.in.
 (181 MN/m²)
 Endurance 1.16 x 10⁶ cycles.

Fig. 18 x 500
 Effect of Stress Amplitude on Surface Fatigue Damage, 0.11%
 Carbon Steel. Taper Section.

Fig. 19. Variation in number of Grains containing fatigue damage with endurance. Specimen F12. Stress 12 tons/sq.in. (185 MN/m²) Endurance 9 x 10⁵ cycles.

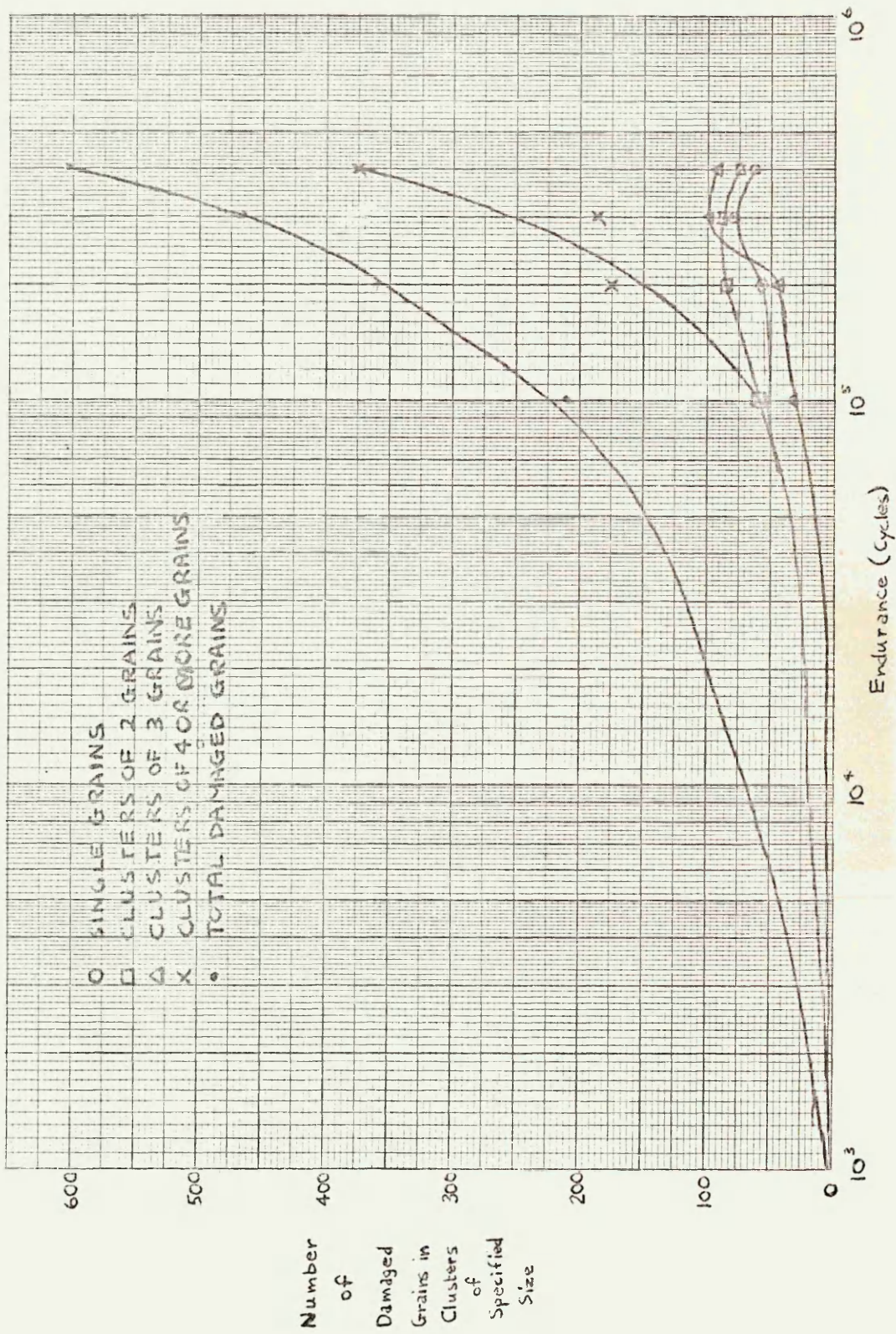
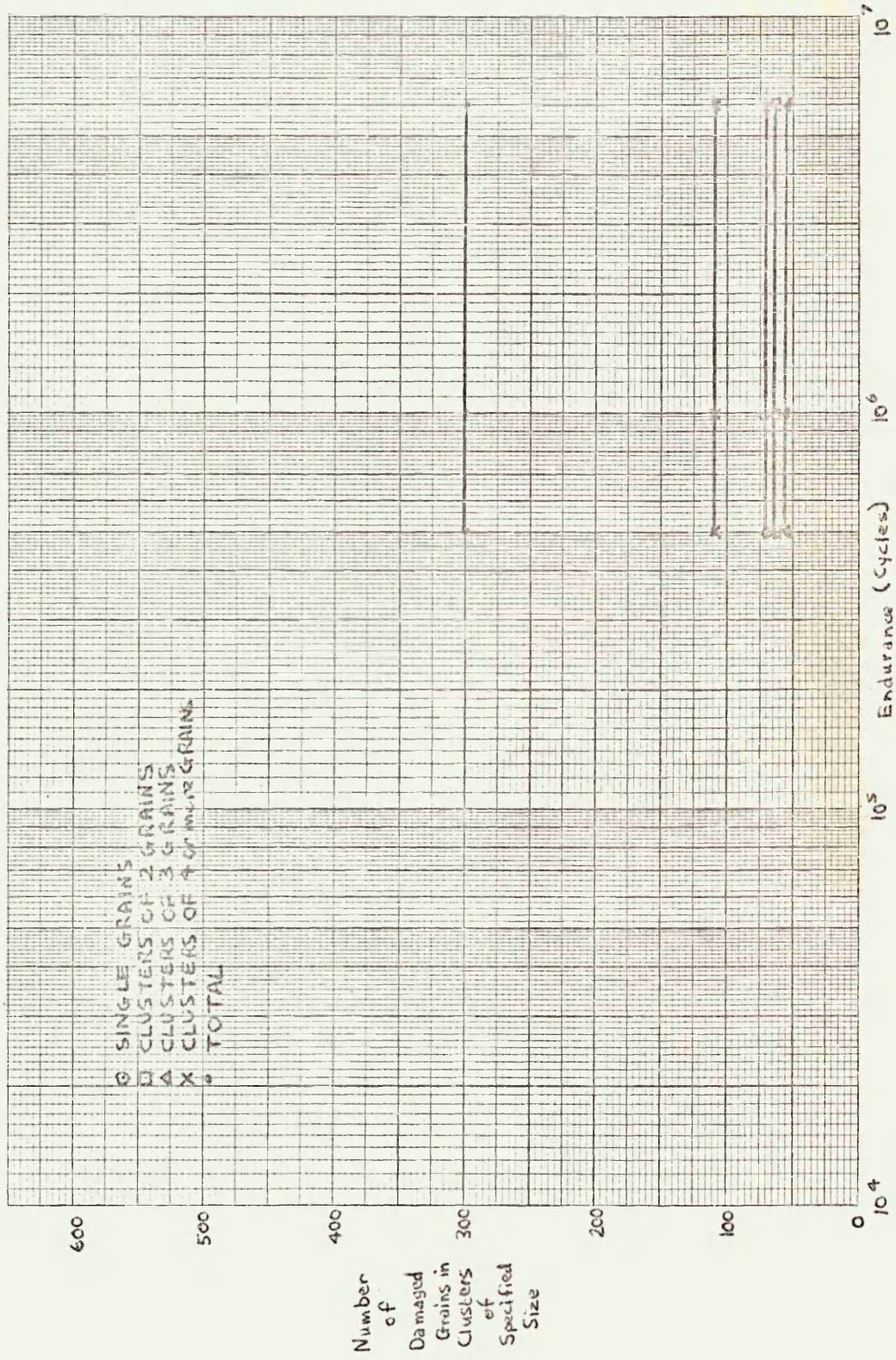


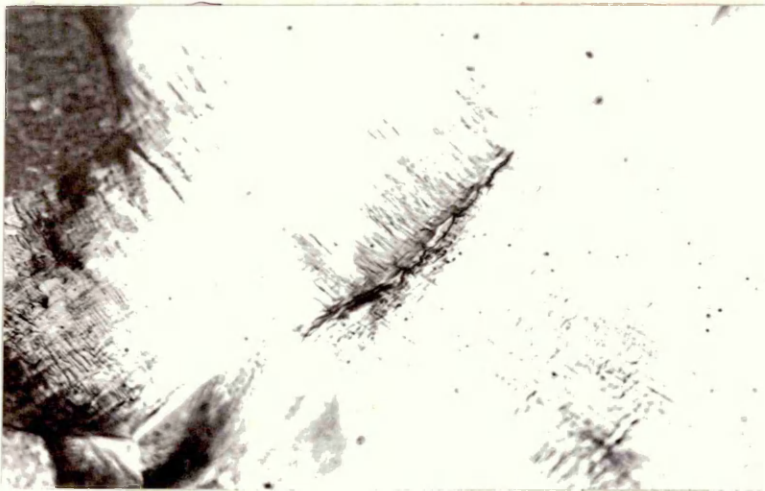
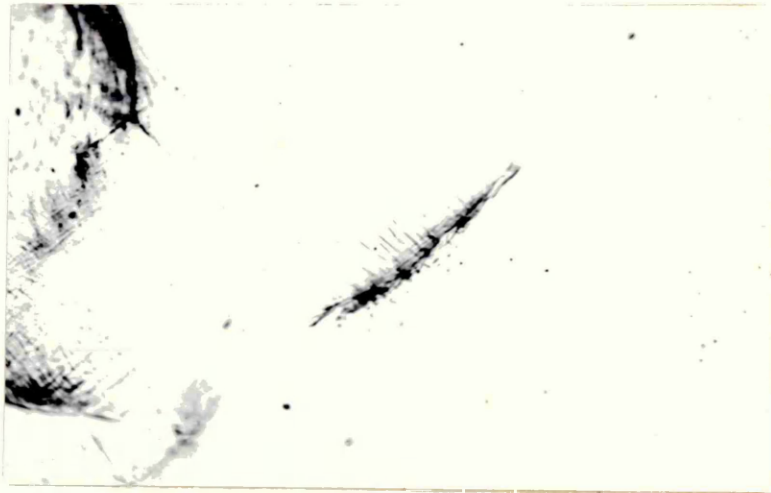
Fig. 20. Variation in Number of Grains Containing fatigue damage with endurance. Specimen F16. Stress 10.5 tons/sq.in. (162 MN/m²) Endurance 7 x 10⁶ cycles.





A. 2% of Life

B. 10% of Life



C. At Failure

Fig. 21

x 500

Slip Intensification at a Grain Boundary in 0.01% Carbon Steel. Stress: 11.3 tons/sq.in (175 MN/m^2). Endurance: 8.4×10^5 cycles.



A. Optical Micrograph X1000



B. Scanning Electron Micrograph
X2300



C. Scanning Electron Micrograph X5750

Fig. 22. Comparison of Optical and Scanning Electron Micrographs of Grain Boundary Slip Intensification in a 0.11% Carbon Steel. Stress: 10.35 tons/sq.in. (160 MN/m^2). Removed after 1.04×10^5 cycles.

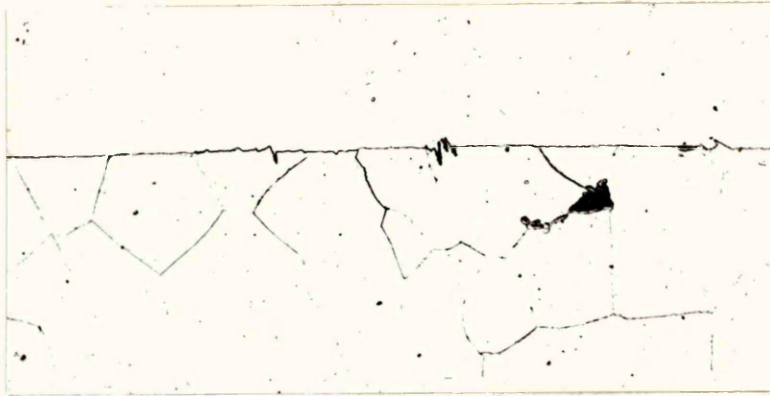


Fig. 23

X 500

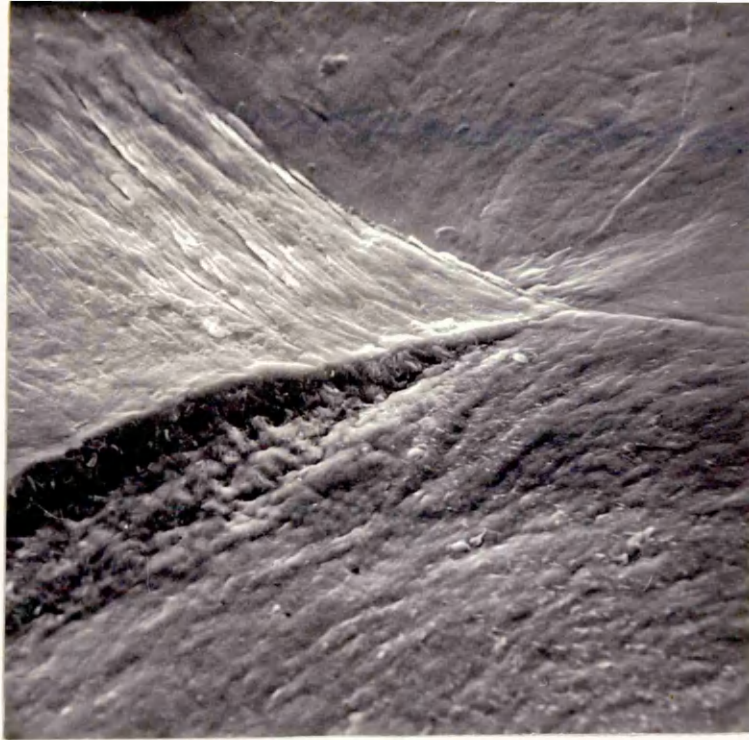
Formation of Intrusion-Extrusion Pairs near a Grain Boundary in 0.11% Carbon Steel Taper Section. Stress = 11.75 tons/sq. in. (181 MN/m^2). Endurance : 1.16×10^6 cycles.



Fig. 24

X 1000

Fatigue Damage on a 0.41% Carbon Steel Specimen Showing Dark Lines which could be Slip-band Cracks. Stress : 11 tons/sq. in. (170 MN/m^2). Endurance : 1.3×10^6 cycles.



A X 2000

B X 5000

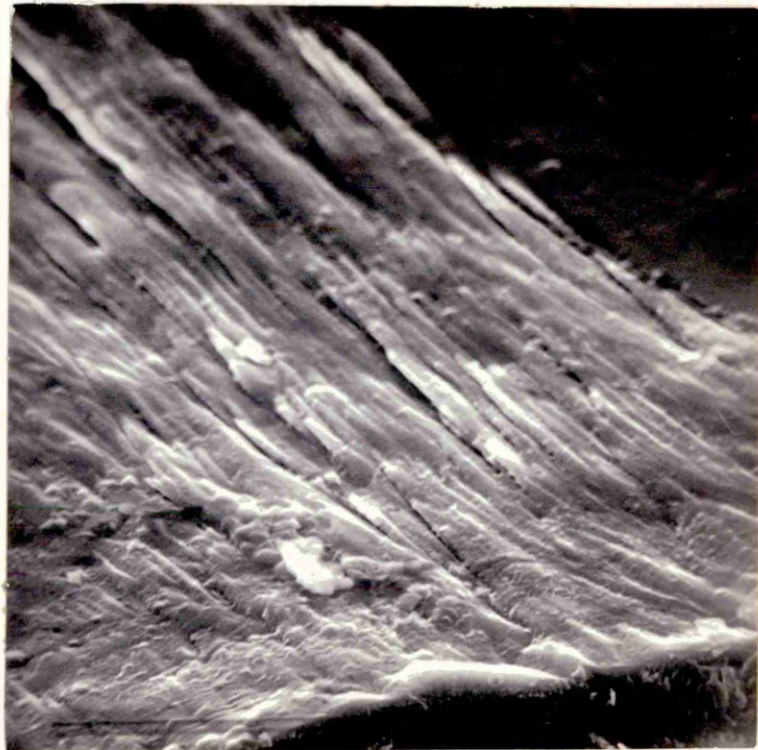
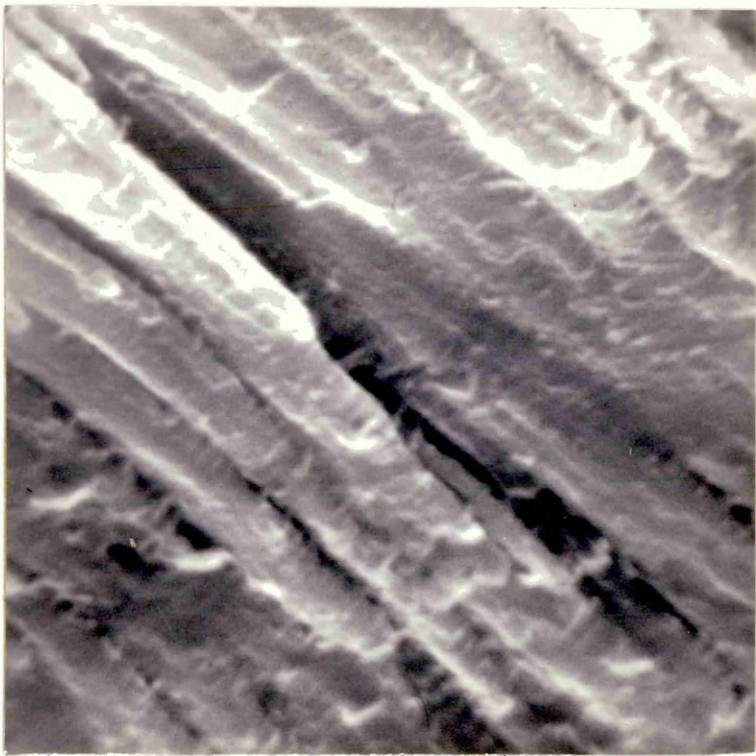


Fig. 25

Scanning Electron Micrographs of an 0.01% Carbon Steel Specimen Surface showing Slip Band Cracking. Fig. 25A also shows a ridge at the grain boundary separating a grain in which much slip has occurred from one in which little slip has occurred. Stress 11.3 tons/sq. in. (175 MN/m^2). Endurance 3×10^5 cycles.

C. X 10000



D X 20000

Fig. 25 cont.

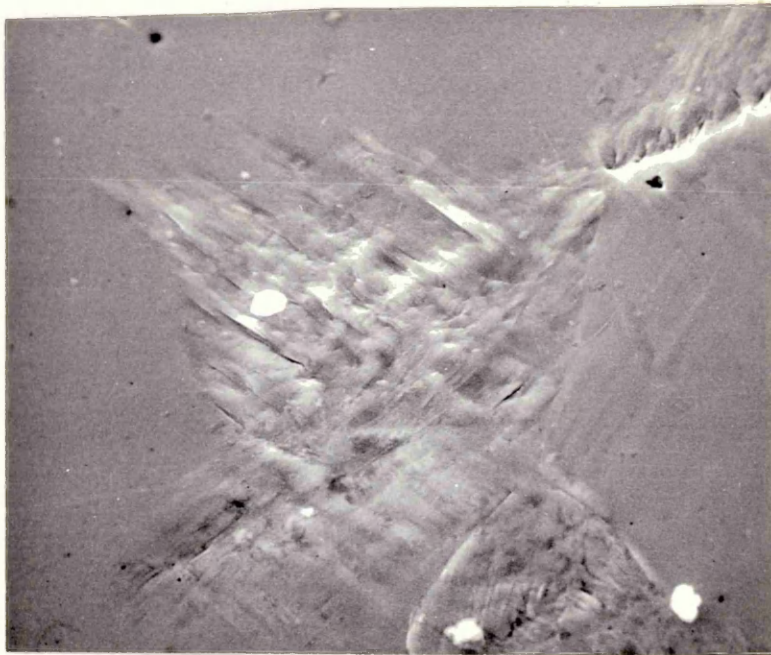


Fig. 26

x 1500

Slip Band Cracking in 0.01% Carbon Steel, Stress: 8.45 tons/sq.in. (130 MN/m^2). Endurance: 1.11×10^6 .



Fig. 27

X1500

Slip Band Cracking in 0.11% Carbon Steel. Taper Section. Stress: 11.75 tons/sq.in. (181 MN/m^2). Endurance 1.16×10^6 cycles.

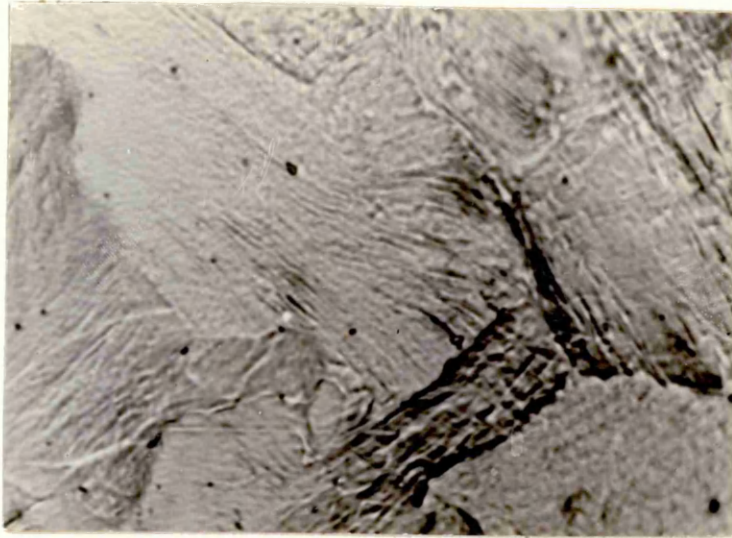


Fig. 28

x 2000

Grain Boundary Crack in 0.41% Carbon Steel. Stress: 11.5
tons/sq. in. (1.78 MN/m^2) Endurance: 1.5×10^6 .

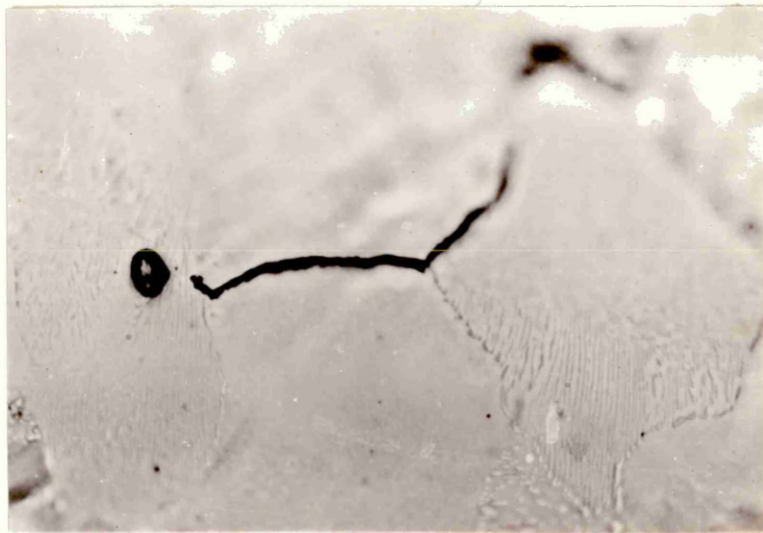


Fig. 29

x 1000

Same Specimen as Fig. 28 above, electropolished after fatigue,
showing Grain Boundary Crack.

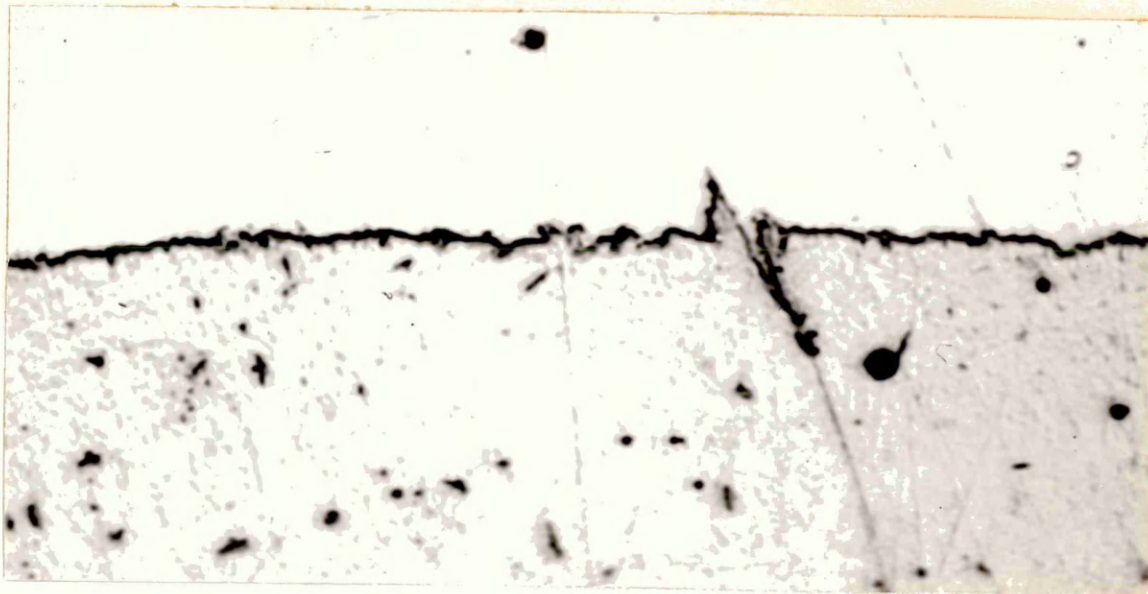


Fig. 30

x 2000

Grain Boundary Crack with Associated Extrusion in 0.01% Carbon Steel Taper Section. Stress: 11.3 tons/sq. in. (175 MN/m^2)
Endurance: 3.6×10^5 cycles.

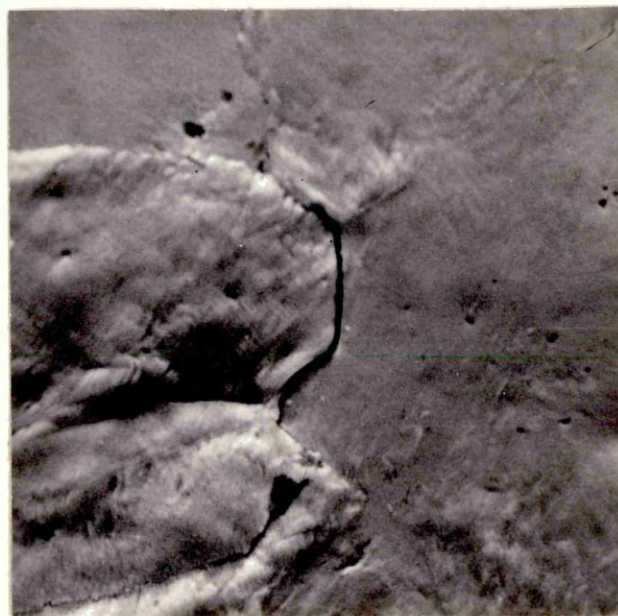


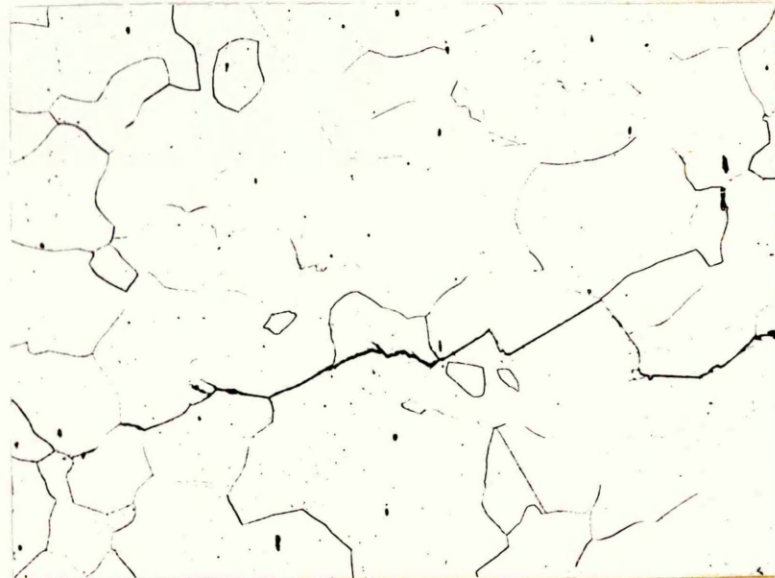
Fig. 31

x 3000

Scanning Electron Micrograph of 0.41% Carbon Steel Specimen showing Grain Boundary Microcrack. Stress: 10.6 tons/sq. in. (164 MN/m^2). Endurance: 5×10^5 cycles.



A. As fatigued



B. Repolished and Etched

Fig. 32

x160

Secondary Crack in a 0.01% Carbon Steel Specimen. Stress: 10.35 tons/sq.in (160 MN/m^2). Endurance: 3×10^6 cycles.



A. x 50

B. Diagrammatic Representation

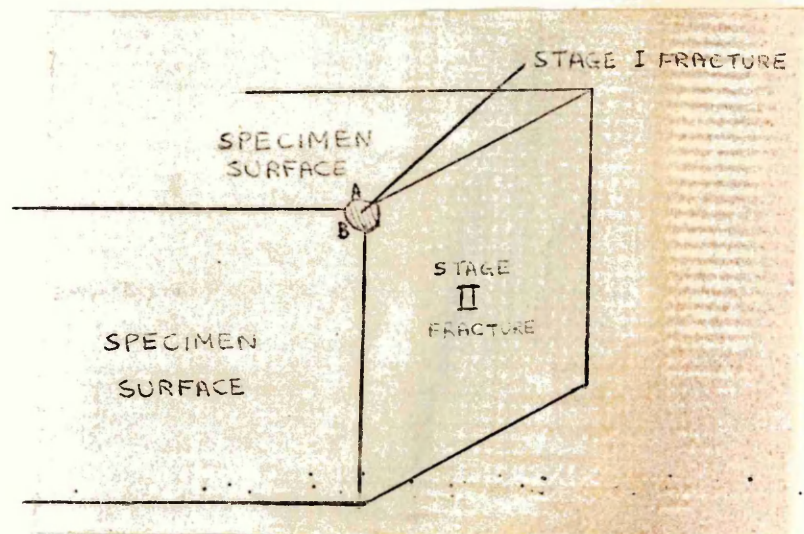


Fig. 33. Scanning Electron Micrograph of 0.01% Carbon Steel Specimen, showing Area of Stage II Crack Propagation. Stress: 11.3 tons/sq.in (175 MN/m²). Endurance: 3×10^5 cycles

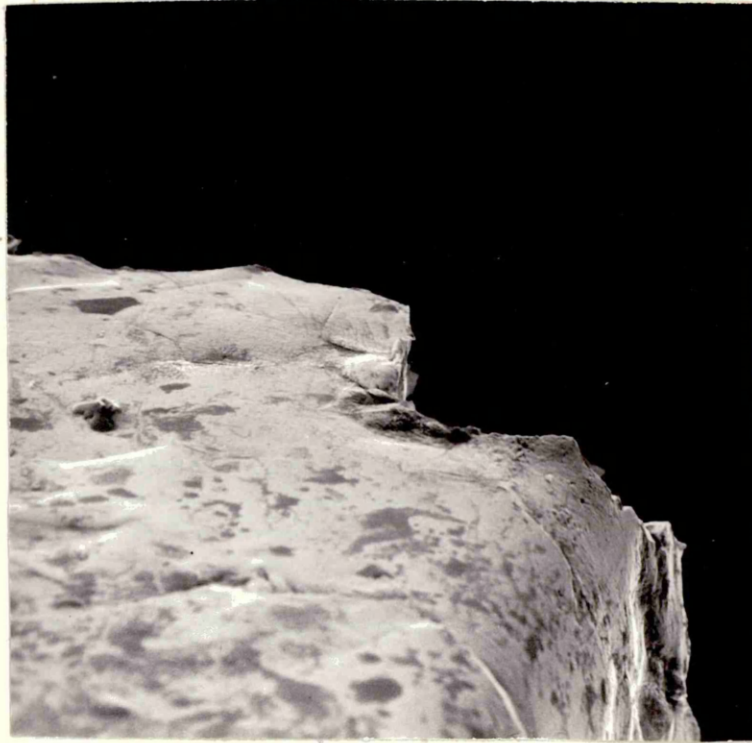


Fig. 34

x220

View of surface of specimen shown in Fig. 32 from an angle of 30° to the specimen surface showing the edge of the Stage I fracture.

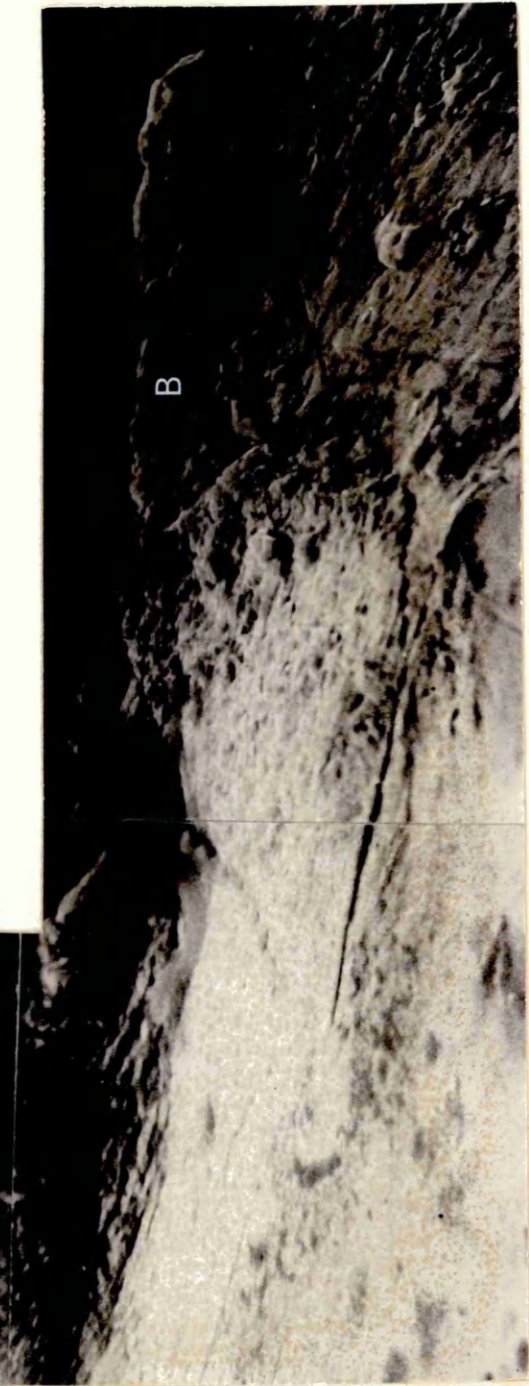
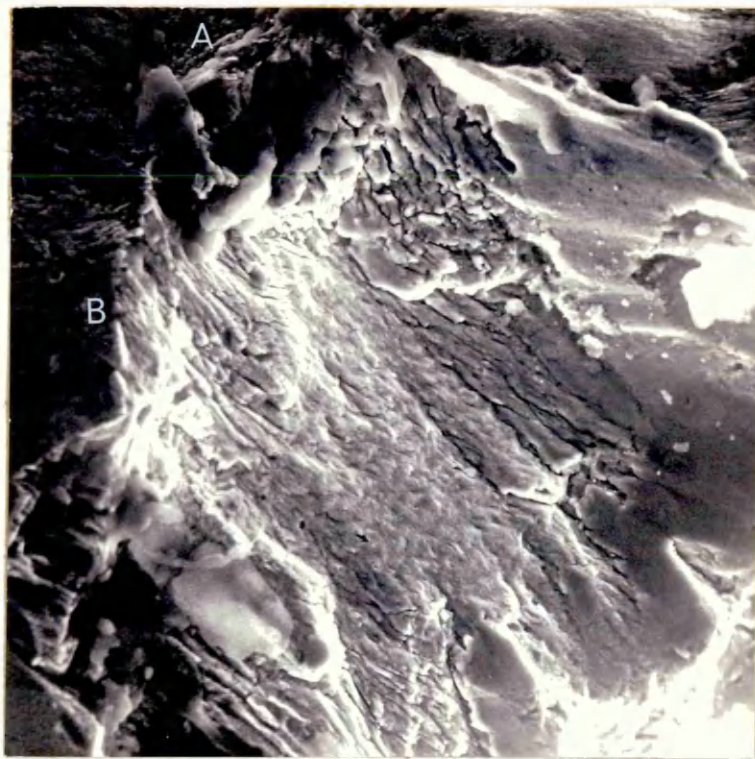
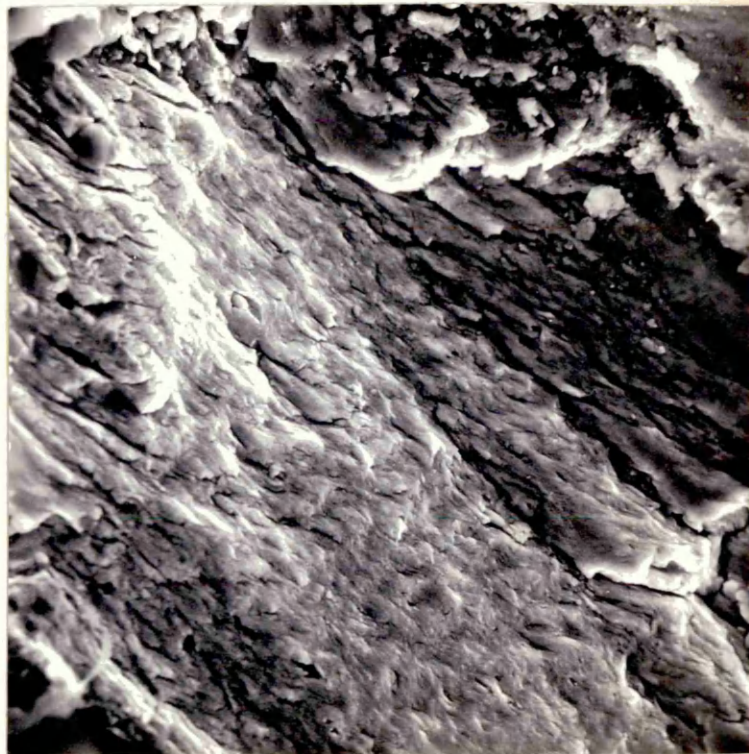


Fig. 35 High Magnification view of the edge of the Stage I fracture taken from the same angle as Fig. 34

x1100



A x 500

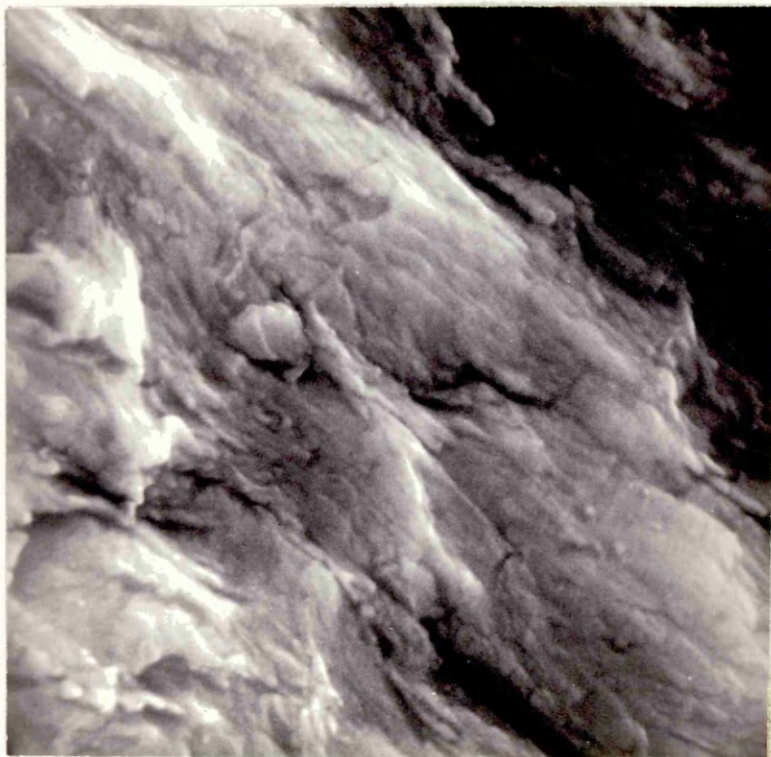
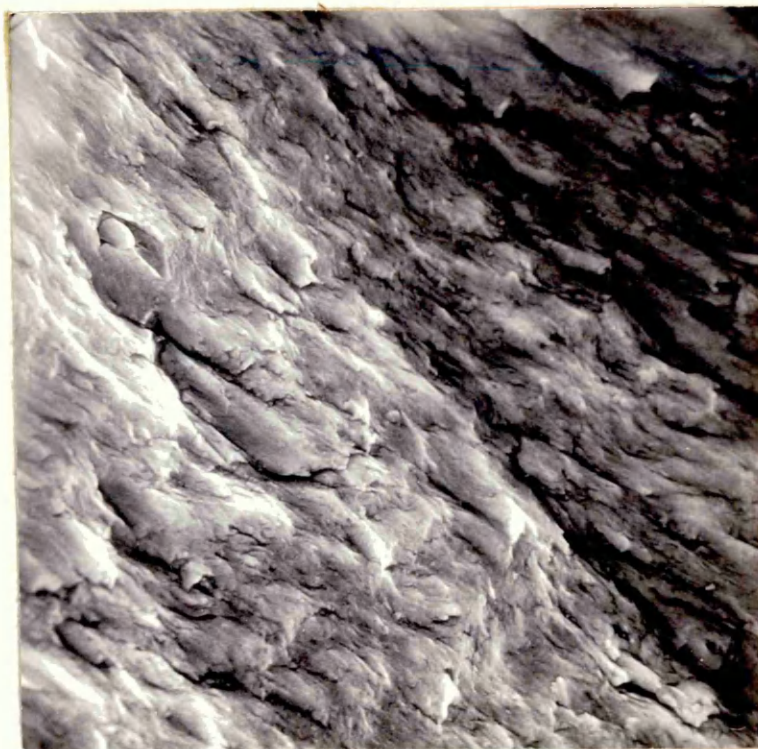


B x 1000

Fig. 36

Series of photographs of Stage I fracture in 0.01% Carbon Steel (same specimen as Figs. 32-35. Scanning Electron Micrographs.)

C X 2000



D X 10000

Fig 36 Cont.



A X 600



B X 2400

Fig. 37

Stage I Crack Propagation in 0.41% Carbon Steel. Scanning Electron Micrographs. Stress: 9.85 tons/sq. in. (152 MN/m^2)
Endurance : 4.7×10^6 cycles.



Fig. 37 (Cont.)

C X 6000



X 130

Fig. 38
Early form of Stage II fracture in 0.01% Carbon Steel showing mixed transgranular and intergranular propagation 1 mm from root of notch. Scanning electron micrograph.



X 130

Fig. 39
Later form of Stage II fracture in 0.01% Carbon Steel showing Wholly Transgranular Crack Propagation. $3\frac{1}{2}$ mm from root of notch. Scanning Electron Micrograph.

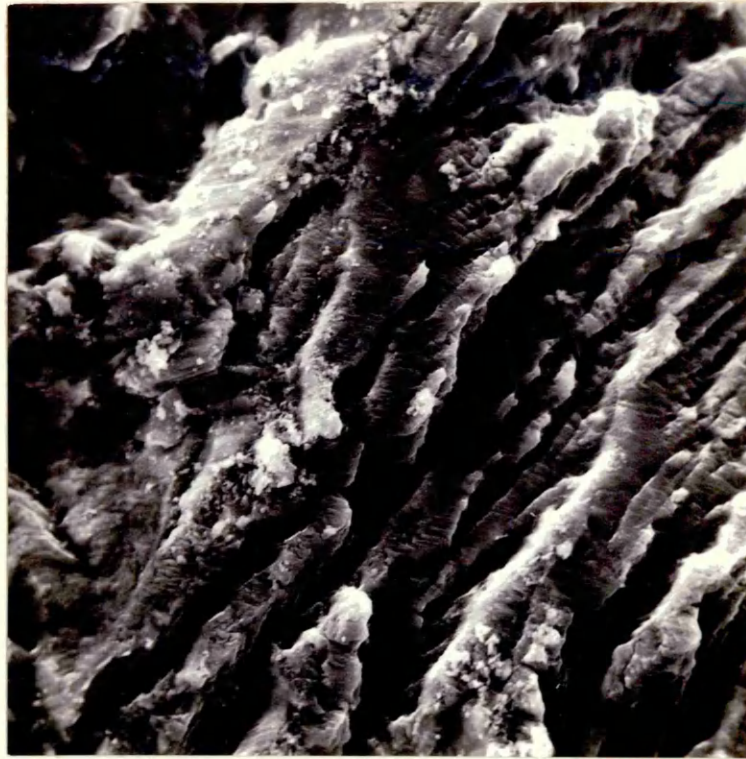


Fig. 40

X 2400

Stage II fracture surface of 0.01% Carbon Steel Specimen showing hills and valleys on which the Characteristic Fatigue Striations can be observed. Scanning electron micrograph.

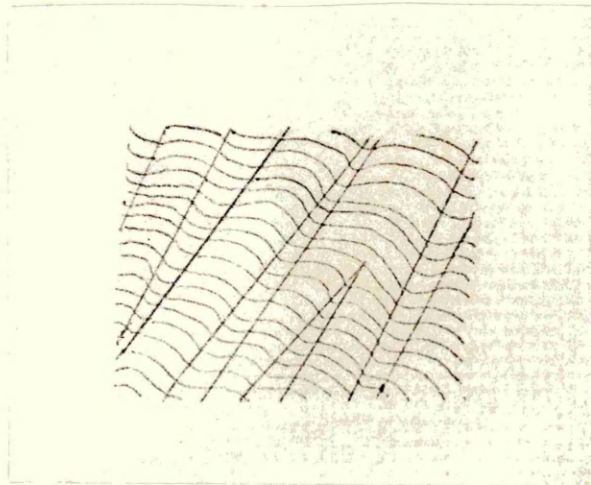


Fig. 41

Diagrammatic Representation of Fatigue Striations on Hills and Valleys on a Stage II Fatigue Fracture Surface.



Fig. 42

X 2350

Fretting on Stage II fracture surface producing rub marks and debris. Scanning Electron Micrograph.

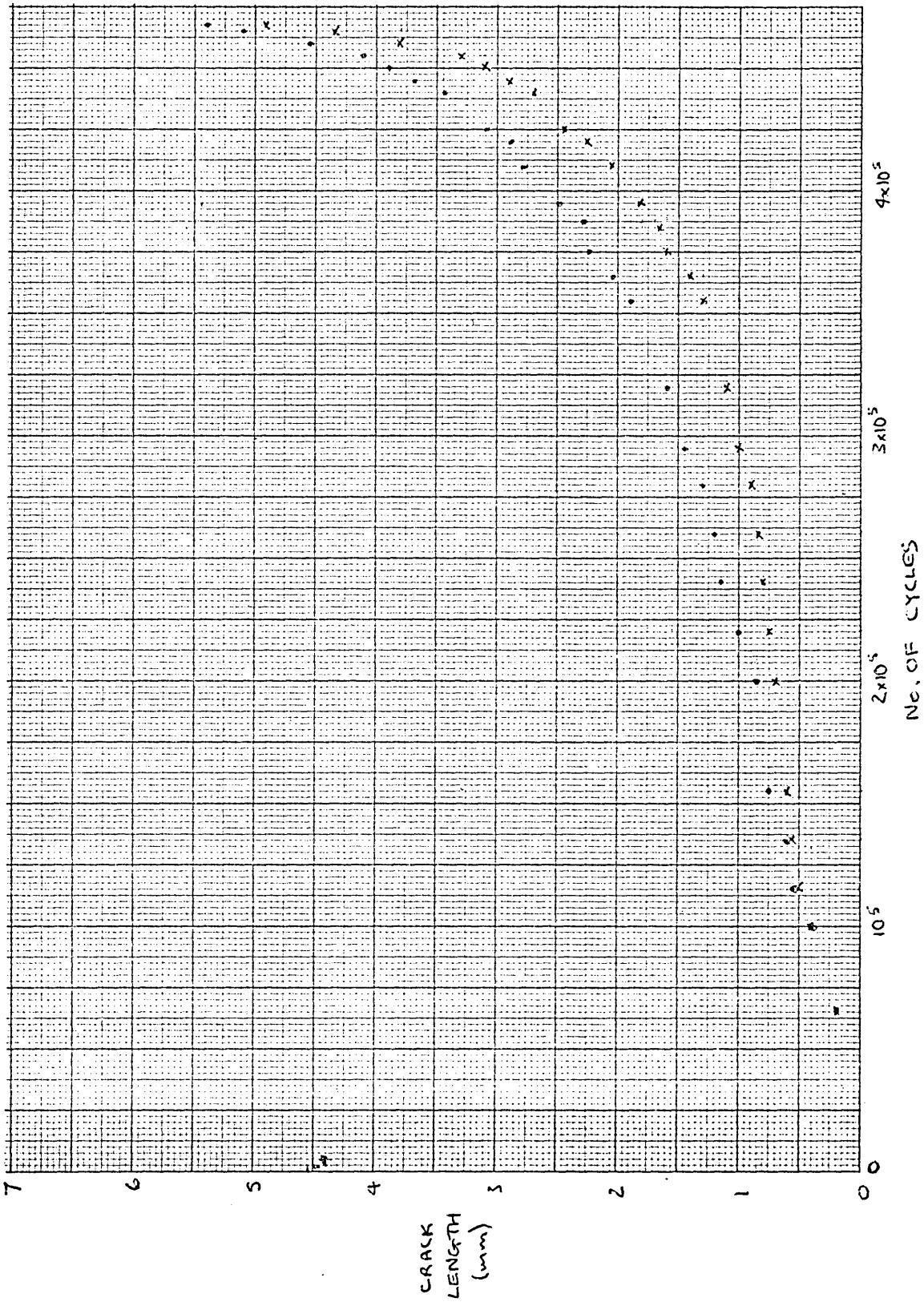


Fig. 43

X 12000

Intergranular Stage II Fatigue Surface in 0.01% Carbon Steel, showing slip lines.

Fig A1/3. Specimen B5. Stress $4\frac{1}{2}$ tons/sq. in. (66 MN/m^2). Endurance 4.67×10^5 cycles



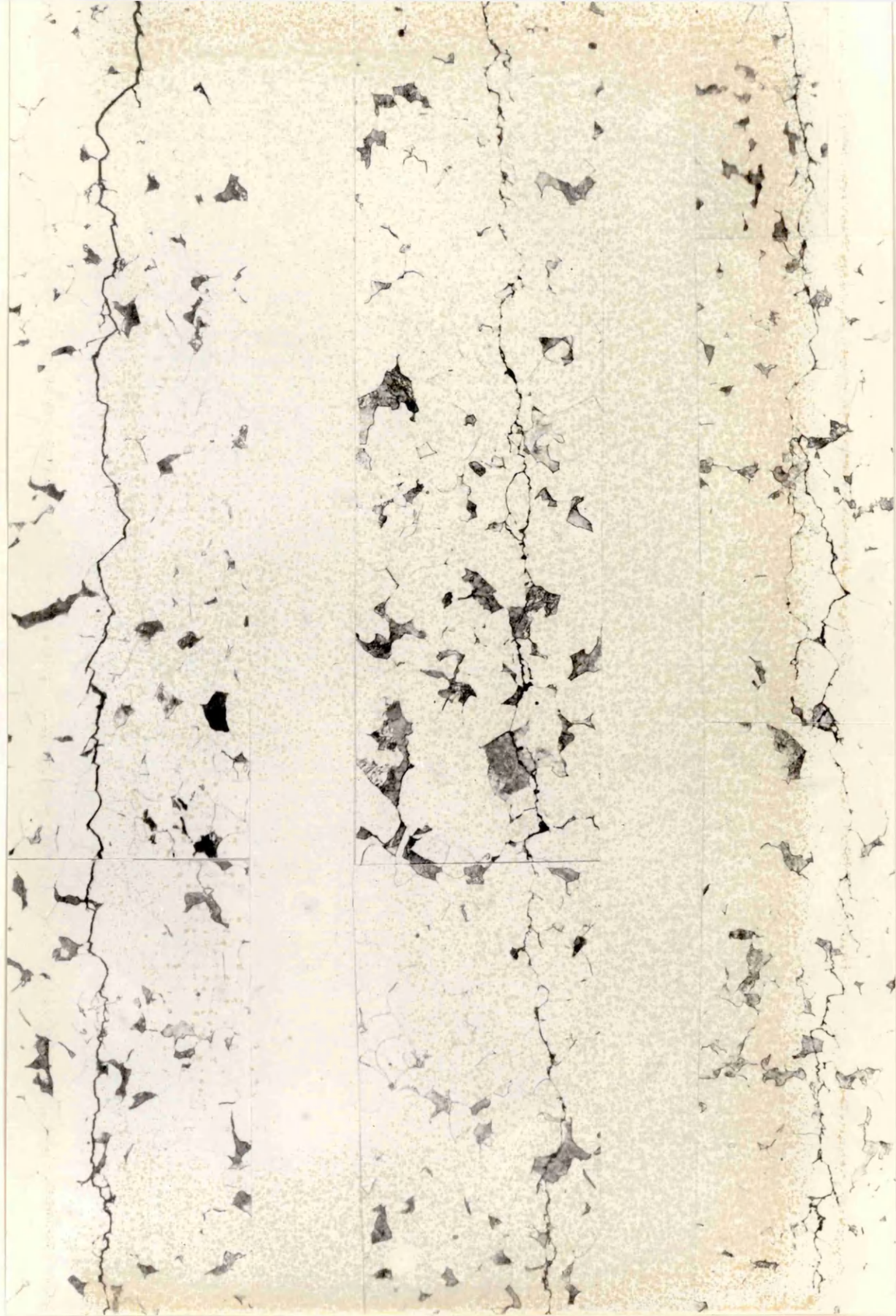


Fig. 44 Crack Propagation in 0.11% Carbon Steel. X 200

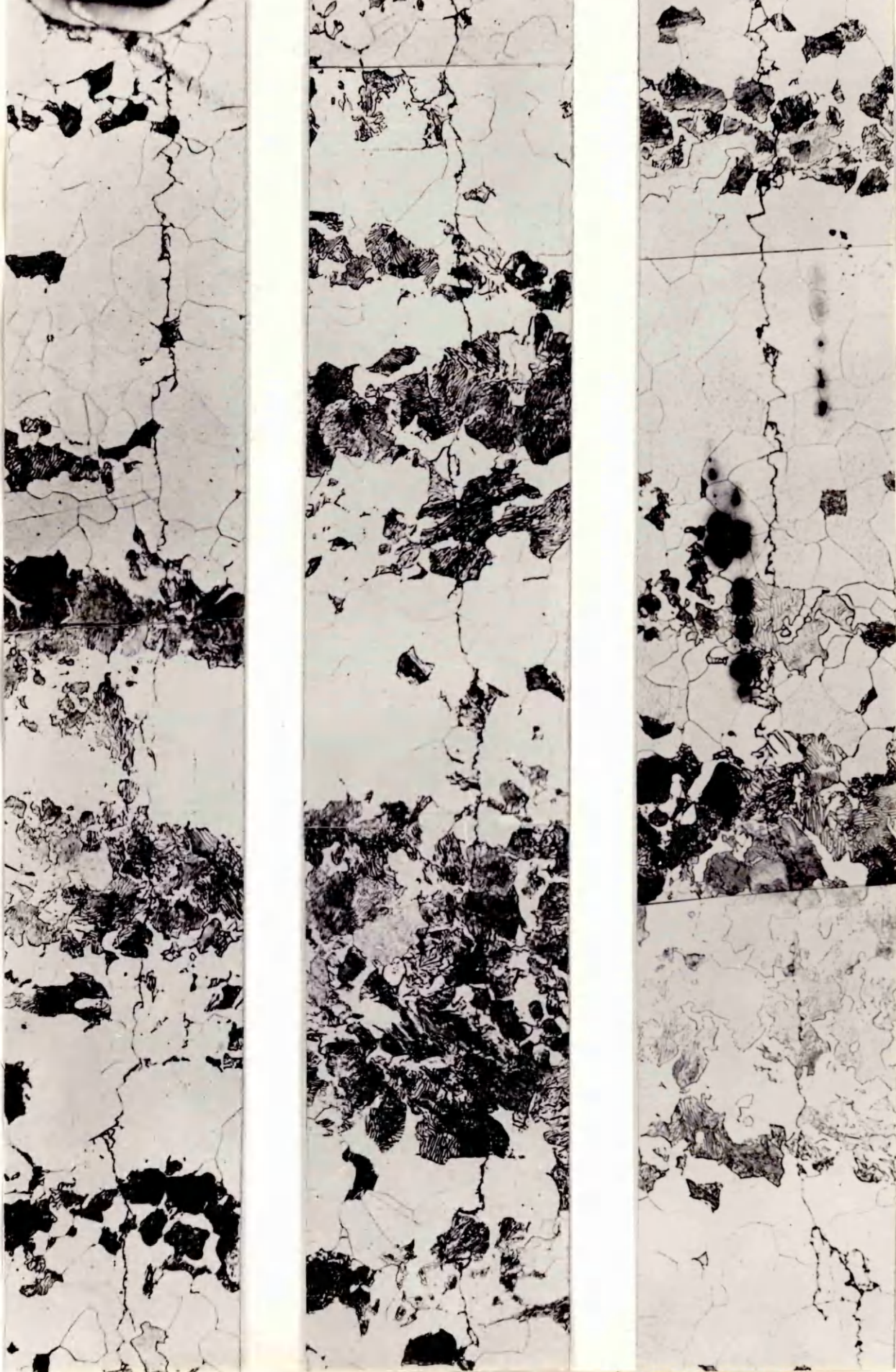


Fig. 45. Crack Propagation in 0.41% Carbon Steel X200



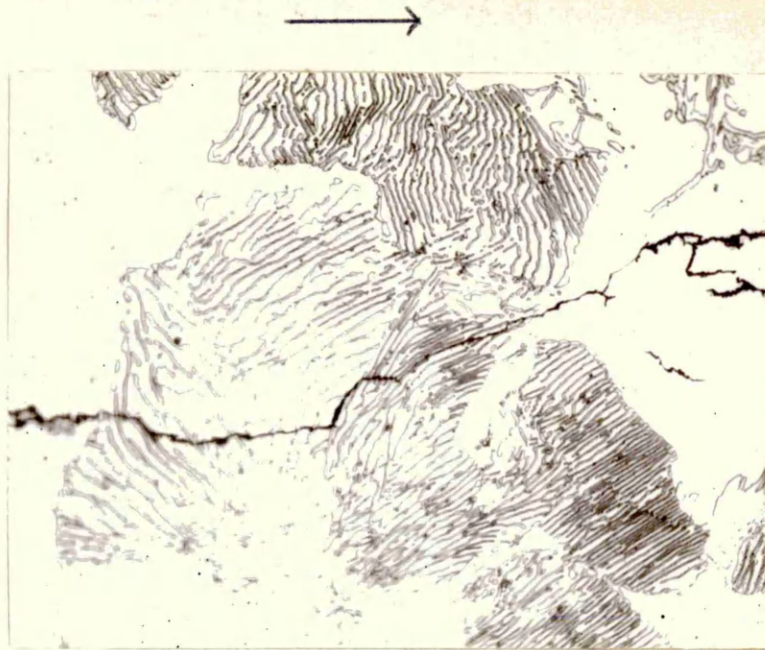


Fig. 46 x 1000
Effect of Orientation of Cementite Lamellae on the Mode of
Fatigue Crack Propagation in 0.41% Carbon Steel.

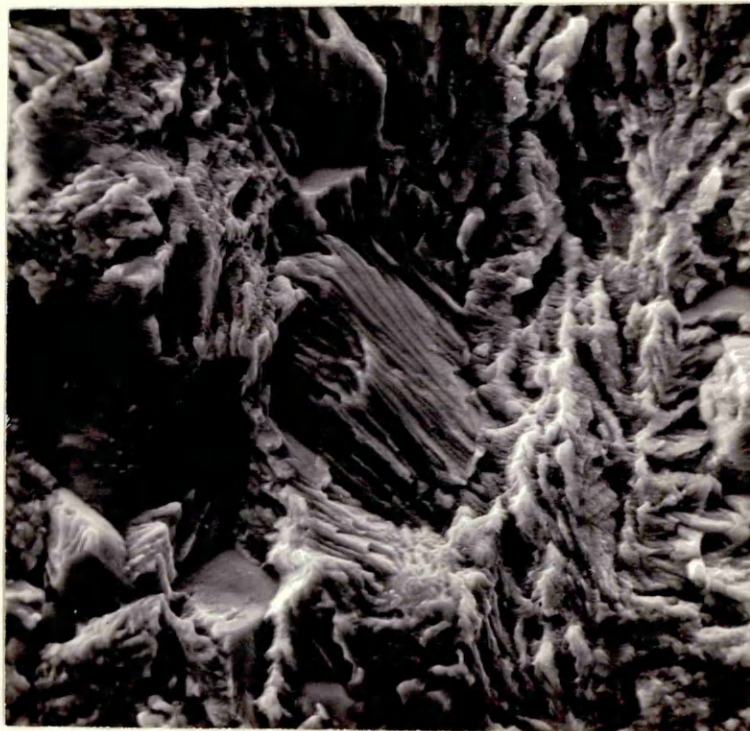


Fig. 47 x 1350
Fracture along a Ferrite-Pearlite Interface in 0.41% Carbon
Steel. Also shows propagation through a Pearlite Nodule.
Scanning Electron Micrograph.

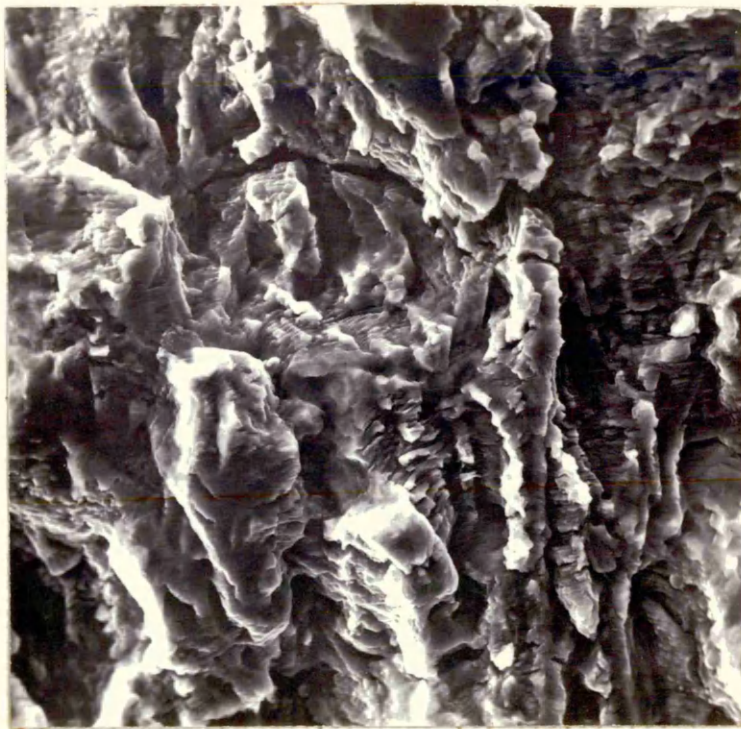


Fig 48 X1350
Later part of Stage II Crack Propagation in 0.11% Carbon Steel
showing Crack Branching.

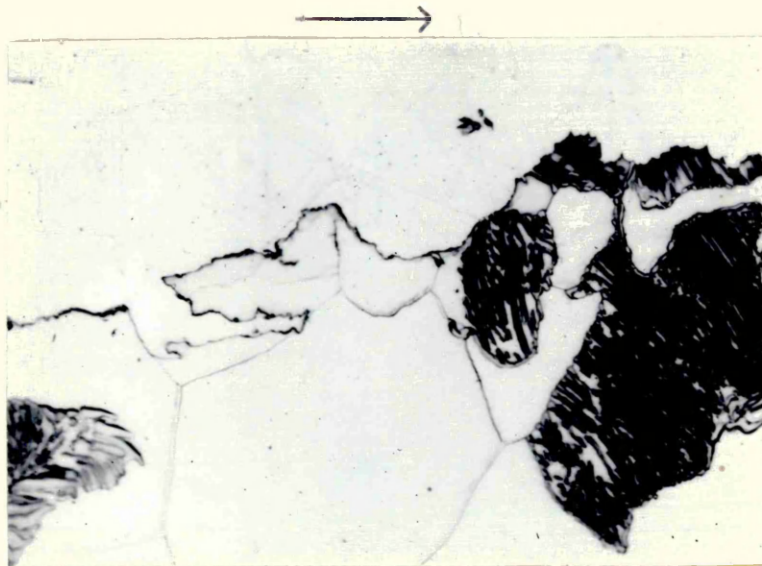
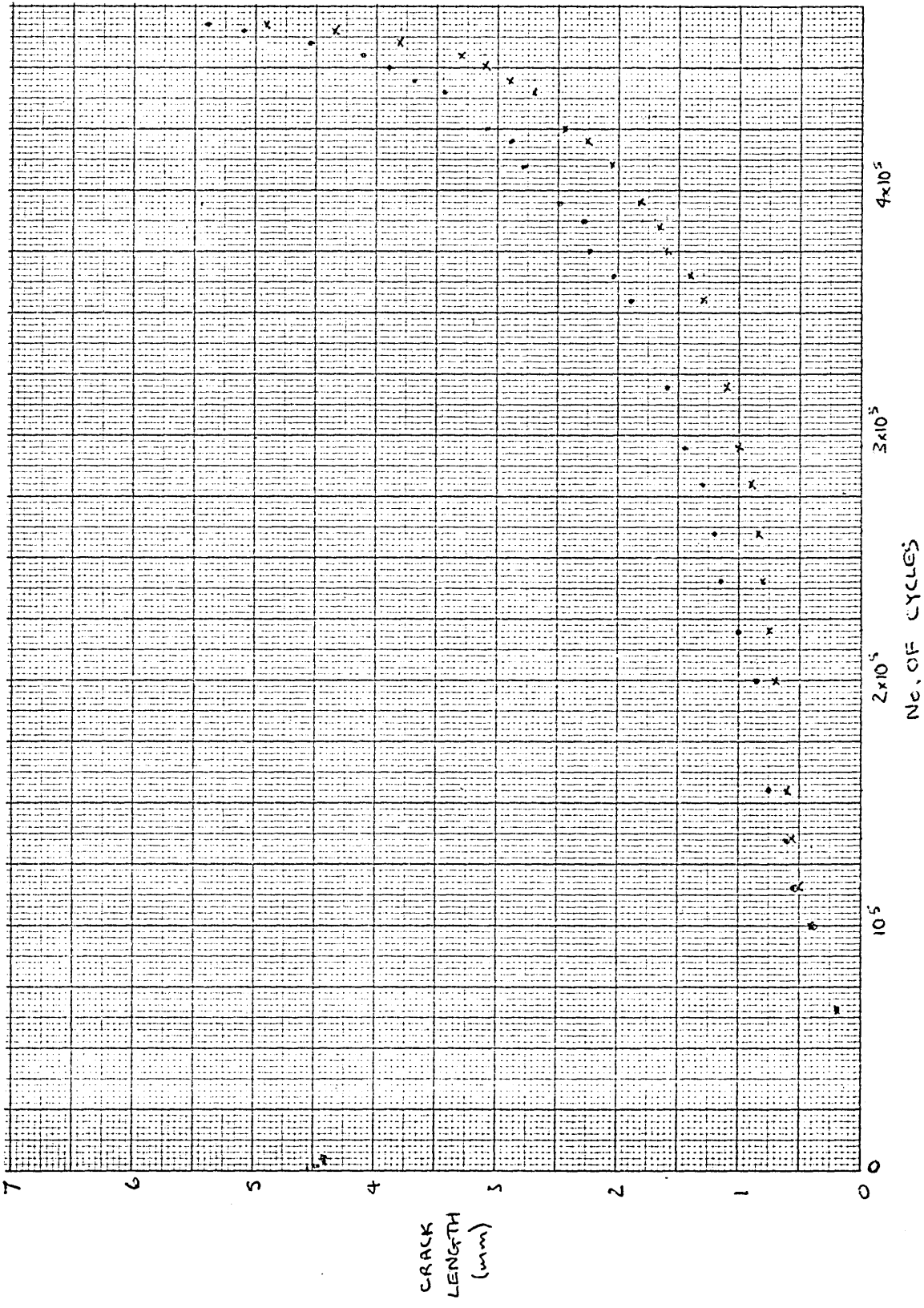


Fig 49 X1250
Branch Crack in 0.41% Carbon Steel. Later Stage II Crack
Propagation.

Fig A1/3. Specimen B5. Stress $4\frac{1}{2}$ tons/sq. in. (66 MN/m^2). Endurance 4.67×10^5 cycles



5. DISCUSSION

5.1 THE DEVELOPMENT OF SURFACE FATIGUE DAMAGE

Fatigue slip bands in the three carbon steels studied developed early in the tests and then tended to widen as cycling continued. This led to areas of damage being formed which contained one or more complete grains. The formation of these areas is in contrast to the situation in most FCC metals and alloys where discrete fatigue slip bands are formed. Scanning electron microscopy has shown that the topography of the fatigue slip bands is comparatively flat, i.e. the "notches" and "peaks" have very shallow contours. The height of the "peaks" is of the order of $1\frac{1}{2}\mu$, compared with 10μ for aluminium alloys. This is contrary to the impression gained from optical observation when the dark appearance of the areas of slip, which is caused by surface oxidation, tends to suggest a more severe type of damage. The fatigue slip lines themselves were wavy in appearance, this being due to the fact that cross slip in ferrite is very easy. There is also the possibility that $\{112\}$ and $\{123\}$ slip may sometimes operate, but it is thought that slip in ferrite at room temperature is predominantly of the $\{110\}$ type.

The tests carried out to investigate the surface spread of plasticity during fatigue showed that at high stress, the number of grains containing fatigue damage gradually increased until failure occurred, whereas at low stress there was virtually no surface spread of plasticity from grain to grain until failure occurred. It therefore seems unlikely that spread of plasticity from grain to grain as revealed by surface observation (as suggested by Oates and Wilson⁽⁵⁵⁾ for 0.11% carbon steel) can be the controlling factor for

fatigue failure in 0.41% carbon steel. Also this theory does not describe in detail the actual processes leading to fatigue failure. It is quite clear from previous work that in plain specimens, the majority of the fatigue life is spent in stage I crack propagation and it is therefore possible that the factor which decides whether fatigue failure will occur or not is the ability of a stage I crack to grow large enough to change over to a stage II crack. The surface spread of plasticity is an effect independent of this, but it may be controlled by similar factors.

The S-N curves showed a fatigue limit of 8.45 tons/sq.in. (131MN/m^2) for the 0.01% carbon steel and 10.35 tons/sq.in. (160MN/m^2) for the 0.11% carbon steel, and the fatigue ratios for these steels were virtually identical (0.43 and 0.44). It has been shown in the present work that crack initiation occurs in the ferrite and since the 0.11% carbon steel contained only 6% more pearlite than the 0.01% carbon steel (which contained none) one would not expect such a large difference as is observed in either fatigue limit - 1.9 tons/sq.in. (29MN/m^2) or U.T.S. - 3.1 tons/sq.in. (47MN/m^2), if the pearlite was equiaxed. However, the pearlite was elongated along ferrite grain boundaries and partly divorced and this would be more likely to impede plastic flow than if it were equiaxed. Hence the larger than expected difference in U.T.S. If the fatigue limit is controlled by the ability of a stage I crack to grow large enough to change over to a stage II crack, then it will be affected by second phases at grain boundaries and the percentage and morphology of the pearlite in the materials examined would account for the

difference in fatigue limits observed in the present work. One particularly attractive prediction of such a theory is that fatigue limit and U.T.S. are controlled by the same factors and therefore one would expect a correlation between the two. It is well known that this is in fact observed.

Slip intensification at grain boundaries has been briefly mentioned in the past (41,44) and has been shown to occur readily in the present work. This is an effect which appears to be peculiar to fatigue and may possibly be due to the boundaries acting as dislocation sources.

5.2 CRACK INITIATION

Although it has been shown by previous workers that fatigue cracks in plain carbon steel initiate from slip bands, the majority of the evidence has been obtained from optical microscopy, and electron microscopy of plastic replicas. In the former, it is easy to confuse cracks with dark oxide areas, and in the latter, what appear to be cracks may be just rumpling or cracking of the plastic film. In the present work, scanning electron microscopy has been used to provide direct evidence of the existence of cracks within the fatigue slip bands, and such cracks have also been observed in taper sections.

Grain boundary cracks have also been observed in all three materials but no evidence of main cracks initiating at grain boundaries was found. The intergranular cracking was generally seen at boundaries separating a grain containing heavy fatigue damage from one with relatively little damage. It is possible that there would be a large orientation difference between the grains in this case, and a crack

could form a means of stress relief. Grain boundary cracks were generally noted near to the main crack, and it is possible that these could have been formed by the stress concentration ahead of the advancing crack front.

It is thought that the reason for the non-propagation of these grain boundary cracks (if such cracks were formed early in the test, and not as the main crack was propagating as suggested above) could be in the fact that the mechanism of stage I crack propagation is thought to be an extension of the slip band crack initiation process. Whilst slip band cracks can easily propagate, grain boundary cracks would find this more difficult in a material not subject to grain boundary weakening. Also, although a grain boundary at the specimen surface might be suitably orientated for the applied stress to cause initiation, its orientation below the surface will, in general, change, so that further propagation of the crack will not occur.

5.3 CRACK PROPAGATION

Stage I crack propagation in all the plain specimens examined occupied an area of approximately one or two grains at the most before changeover to stage II occurred. The cracks seemed to be formed from a number of parallel slip band cracks in a single grain which tended to move on to one level as they extended, until they became one wide slip band crack. This is in contrast to what has previously been reported in other materials e.g. aluminium alloys and the high strength nickel alloy of Gell and Leverant (69), where the parallel lines in the direction of crack propagation extended throughout the stage I area. The reason for this difference in behaviour is presumably the ease of cross slip

in low and medium carbon steels, as compared with the other materials in which stage I crack propagation has previously been studied. The irregular appearance of the stage I fracture after the initial microcracks have moved on to one level is probably also due to the ease of cross-slip.

The data obtained from the crack propagation rate measurements showed an extremely large variation in crack growth rate at a given stress intensity range and it was not possible to relate this variation to an effect of nominal stress. The slight drift into tension which was mentioned in section 3.2.2 and occurred in the earlier tests had no measurable effect. The scatter in results obtained was larger for different specimens of the same material than for different materials. There are two possible reasons for this. Firstly, the experimental conditions were difficult to reproduce, because it was not easy to set the specimens up for axial loading and it was possible that some bending was also occurring. Secondly, the tests were carried out at zero mean stress, whereas the fracture mechanics analysis which has been used is strictly only applicable to pulsating tension tests. For these reasons it is not proposed to discuss these results any further.

It has been shown that stage II crack propagation in the materials studied occurs by a mechanism which produces striations on the fracture surface. The spacing between these striations remained remarkably constant at between $1-2 \times 10^{-4}$ mm, in contrast to what has in the past been observed on aluminium alloys. The crack growth rates were always smaller than the striation spacing e.g. in specimen B4

tested at 5.65 tons/sq.in. (87 MN/m^2), the crack growth rate at 1mm from the root of the notch was $1.0 \times 10^{-5} \text{ mm/cycle}$ and at 4.5mm this was $7.5 \times 10^{-5} \text{ mm/cycle}$. The striation spacing at both these points was $1.5 \times 10^{-4} \text{ mm}$, and it would have been possible to resolve striation spacings **an** order of magnitude smaller than this if they had been present. There are two possibilities to account for this phenomenon. Firstly, the whole crack may only propagate every n cycles, so that each striation represents n cycles of stress, where $n \approx 1.5$ to 10 in the present case. A more likely explanation is that, at any point in time, local parts of the crack front will be at rest, the amount of time any portion of the crack front spends at rest decreasing as the stress intensity range and hence the size of the plastic zone ahead of the crack tip increases.

Grain boundaries represent a possible source of delay to local crack propagation, and this was apparent early in most of the tests, since there was often a change in mode from transgranular to intergranular crack propagation or vice versa at grain boundaries. A possible explanation for the intergranular crack propagation which occurred in the earlier stages of all tests is as follows. Consider a propagating transgranular crack. Parts of this crack will easily propagate from grain to grain because of favourable orientations of the grains into which they are propagating. Others may be held back at grain boundaries, but eventually a high stress will be built up at these boundaries as neighbouring parts of the crack propagate, and intergranular failure may result. At high stress intensities, the probability of a crack being held up long enough for this to

occur will decrease, because of the increase in plastic zone size and intergranular fracture will not occur. The large proportion of grain boundary fracture present in the 0.01% carbon steel could have been a consequence of the high oxygen content of this material, which could cause grain boundary weakening by segregation. Also the 0.11% carbon steel had some grain boundary cementite which might also have led to some intergranular fracture. However, although these factors could contribute to the propensity of grain boundary cracking, they are obviously not the complete answer, as intergranular fracture still occurred in the 0.41% carbon steel. Furthermore it did not occur in any of the materials at high stress intensities, or in unidirectional deformation.

The actual crack extension mechanism, i.e. striation production was not studied in the present work. However, the photograph of the branch crack in Fig. 54 is very interesting, as the end of this crack has an appearance similar to that depicted in Fig. 2c, and tends to confirm the operation of the "plastic blunting process" as suggested by Laird (67). The frequent occurrence of these branch cracks throughout the tests as seen on scanning electron microscope observations of the fracture surface also lends support to this theory.

6. CONCLUSIONS

1. Surface fatigue damage in 0.01, 0.11 and 0.41% carbon steels occurred predominantly in the ferrite, and had a comparatively flat "hill and valley" appearance. The amount of surface damage evident at failure increased with increasing stress amplitude.
2. The spread of plasticity as revealed by surface observations did not appear to be the controlling factor in determining whether or not a plain specimen would fail.
3. All plain specimens of all three materials showed a certain amount of grain boundary slip intensification.
4. Both slip band cracks and intergranular cracks were observed on specimen surfaces of all three materials, but only the slip band cracks seemed to be responsible for failure.
5. Stage I crack propagation occurred by the linking up of a number of slip band cracks on parallel planes in a single grain and then by slip-plane growth in a wavy manner, this being attributed to the ease of cross-slip in the ferrite of low and medium carbon steels.
6. Stage II crack growth occurred by both transgranular and intergranular propagation. The amount of intergranular fracture increased with decreasing carbon content and decreasing distance from the notch root.
7. Transgranular stage II propagation in ferrite showed the characteristic fatigue striations as observed in other materials. However, the striation spacing could not be correlated with crack length and was relatively constant, varying from about 1 to 2×10^{-4} mm.

8. Branch cracks occurred at all stages of stage II crack propagation, becoming larger as the crack growth rate increased. The appearance of these tends to confirm Laird's plastic blunting process of crack propagation.

7. REFERENCES

- (1) W.A.Wood Fracture. Swampscott Conference
1958, Wiley 1959 p.412.
- (2) H.J.Gough Engineering 114, 291 (1922).
- (3) L.M.Clarebrough et al Proc.Roy.Soc. A242,160 (1957).
- (4) W.A.Backofen Fracture. Proc.Int.Conf.
Swampscott 1959. p435.
- (5) F.E.Fujita Acta.Met. 6,543 (1958).
- (6) D.H.Avery & Fracture of Solids. Maple Valley
W.A.Backofen Conf. Interscience 1963 p.339.
- (7) N.Thompson & Advances in Physics 7,72 (1958)
N.J.Wadsworth
- (8) A.S.Tetelman & Fracture of Structural Materials,
A.J.McEvily Wiley 1966.
- (9) J.R.Low Jr. Progress in Materials Science
12,1 (1963)
- (10) P.Lukás, M.Klesnil, Phys.Stat.Sol. 15,71 (1966)
J.Krejčí & P.Rys
- (11) W.J.Plumbridge & Metals and Materials 3,119
D.A.Ryder Reviews (1969).
- (12) J.A.Ewing & Phil.Trans.Roy.Soc. A200,241
J.C.W.Humphrey (1903).
- (13) H.J.Gough Proc. ASTM 33,3 (1933).
- (14) D.Kuhlmann-Wilsdorf Phil.Mag. 43,632 (1952)
et al
- (15) W.J.Craig Proc. ASTM 52,877 (1952).
- (16) P.J.E.Forsyth JIM 82, 449 (1953).
- (17) F.von Wever, M.Hempel Archiv. f.d. Eisenhüttenwesen
& A.Schrader 26,739 (1955).

- (18) E.Eisner Nature 188,1183 (1960).
- (19) N.Thompson, Phil.Mag. 1,113 (1956).
N.J.Wadsworth &
N.Louat
- (20) M.S.Hunter & Proc. ASTM 54,717 (1954).
W.G.Fricke
- (21) P.J.E.Forsyth Nature 171,172 (1953).
- (22) P.J.E.Forsyth & Nature 175,767 (1955).
C.A.Stubbington
- (23) W.A.Wood Phil.Mag. 3,692 (1958).
- (24) R.C.Boettner & Acta.Met. 13,937 (1965).
A.J.M.McEvily
- (25) P.J.E.Forsyth Proc.Roy.Soc. A242,198 (1957).
- (26) A.H.Cottrell & D.Hull Proc.Roy.Soc. A242,211 (1957).
- (27) D.Hull JIM 86,425 (1957).
- (28) W.A.Wood & R.L.Segall JIM 86,225 (1957).
- (29) D.H.Avery, G.A.Miller Acta.Met. 9,892 (1961).
& W.Backofen
- (30) D.M.Fegredo & JIM 87,1 (1958).
G.B.Greenhough
- (31) A.J.McEvily Jr. & Fracture of Solids, Interscience
E.S.Machlin 1963 p.450.
- (32) A.J.McEvily & Trans.Met.Soc. AIME 221,1086 (1961).
E.S.Machlin
- (33) T.H.Alden Acta Met. 11,791 (1963).
- (34) J.T.McGrath & Trans.Met.Soc. AIME, 227,645 (1963).
R.C.A.Thurston
- (35) G.A.Miller, D.H.Avery & Trans. Met. Soc. AIME 236,1667 (1966).
W.A. Backofen

- (36) W.A.Wood, Acta.Met. 11,643 (1963).
S.McK.Cousland &
K.R.Sargant
- (37) W.D.Dover & W.J.D.Jones Brit.J.Appl.Phys. 18,1257 (1967).
- (38) R.W.K.Honeycombe Proc.Roy.Soc. A242,189 (1957).
- (39) E.C.Elwood & R.Duckett Nature 173,497 (1934).
- (40) K.V.Snowden Phil.Mag. 3,1411 (1958).
- (41) D.I.Golland & Acta.Met. 15,1889 (1967)
P.L.James
- (42) D.W.Hoepfner & Trans.Met.Soc. AIME 230,1378 (1964).
F.H.Vitovec.
- (43) G.C.Smith Proc.Roy.Soc. A242,189 (1957).
- (44) D.S.Kemsley JIM 85,153 (1956-7).
- (45) D.S.Kemsley JIM 85,420 (1956-7).
- (46) R.C.Boettner, Phil.Mag. 10,95 (1964).
A.J.McEvily & Y.C.Liu
- (47) H.D.Williams & Phil.Mag. 13,312 (1966).
G.C.Smith
- (48) M.Hempel, Archiv.Eisen. 8,433 (1957).
A.Kochendorfer &
A.E.Hillnhagen
- (49) M.Hempel Fracture.Swampscott Conf. 1958,
Wiley 1959 p.376.
- (50) M.Hempel & Archiv.Eisen. 39,283 (1968).
A.E.Hillnhagen
- (51) G.F.Modlen & JISI 194,459 (1960)
G.C.Smith
- (52) W.A.Wood, W.H.Reimann Trans.Met.Soc. AIME 230,511 (1964)
K.R.Sargant

- (53) J. Holden Phil.Mag. 6,547 (1961).
- (54) W.H.Reimann JIM 93,406 (1965).
- (55) G.Oates & D.V.Wilson Acta Met. 12,21 (1964).
- (56) A.Ferro & Phil.Mag. 8,105 (1963).
G.Montalenti
- (57) A.H.Cottrell Symposium on Point Defects in
Metals and Alloys. Inst.Metals
(1956) p.32.
- (58) A.N.May Nature 185,303 (1960).
- (59) T.Broom & Phil.Mag. 8,1847 (1963).
J.M.Summerton
- (60) N.F.Mott Acta.Met. 6,195 (1958).
- (61) P.J.E.Forsyth Proc.Roy.Soc. A242,198 (1957).
- (62) C.A.Zapffe & Trans.ASM 18,958 (1951).
C.O.Worden
- (63) P.J.E.Forsyth Proc.Crack Propagation Symposium,
Cranfield, 1961 p.76.
- (64) C.A.Stubbington R.A.E. Report CPM4 (1963).
- (65) M.Gell & G.R.Leverant Acta.Met. 16,553 (1968).
- (66) P.J.E.Forsyth & Metallurgia 63,117 (1961).
D.A.Ryder
- (67) C.Laird "Fatigue Crack Propagation" ASTM
STP 415,131 (1967).
- (68) M.Shimura & J.Jap.Inst.Metals 32,559 (1968).
Y.Shinohara
- (69) H.I.Caplan & C.Laird Trans.Met.Soc. AIME 239,1017 (1967).
- (70) P.J.E.Forsyth Acta.Met. 11,703 (1963).
- (71) N.E.Frost Proc.Inst.Mech.Engrs. 173,811 (1959).

- (72) N.E.Frost & D.S.Dugdale J.Mech.Phys.Solids 6,92 (1958).
- (73) A.K.Head Phil.Mag. 44,925 (1953).
- (74) P.Paris & F.Erdogan Journal of Basic Engineering (ASME)
85,528 (1963).
- (75) G.R.Irwin J.App.Mech. 79,361 (1957).
- (76) P.Paris Ph.D.Thesis 1962.
- (77) B.Gross, J.E.Srawley & NASA Technical Note. D2603
W.F.Brown Jr. (Jan. 1965).
- (78) T.R.Gurney Metal Construction 1,91 (1969).
- (79) D.Broek Proc.Second Int.Conf.Fracture.
Brighton April 1969. Chapman & Hall
p. 754.
- (80) W.P.Rees, B.E.Hopkins JISI 169,157 (1951).
H.R.Tipler
- (81) H.R.Tipler & P.G.Forrest Inst.Mech.Engrs.Conf. on Fatigue,
London 510 (1956).

8. STATEMENT OF ADVANCED COURSES OF STUDY ATTENDED

Three advanced courses of study were attended during the period in which the research was being carried out. These were :

- (1) Statistical Methods (Sheffield Polytechnic)
- (2) Electron Microscopy (Sheffield Polytechnic)
- (3) The Relationship between Structure and Properties of Metals and Alloys (Sheffield University)

9. ACKNOWLEDGMENTS

Thanks are due to Dr. G.W.J. Waldron and Mr. P.E. Warin for supervising this work and for helpful discussions; to Miss Elaine Dodgson and Mr. Trevor Walker for help in the preparation of specimens; to Mrs Maureen Smith for typing the thesis and to the British Railways Board for enabling this work to be submitted for a further degree. I would also like to thank my wife for her patience and consideration during the trying period in which the project was being carried out.

Fig. A1/1. Specimen B1. Stress $5\frac{1}{2}$ tons/sq. in. (85 MN/m^2) Endurance: 1.71×10^5 cycles

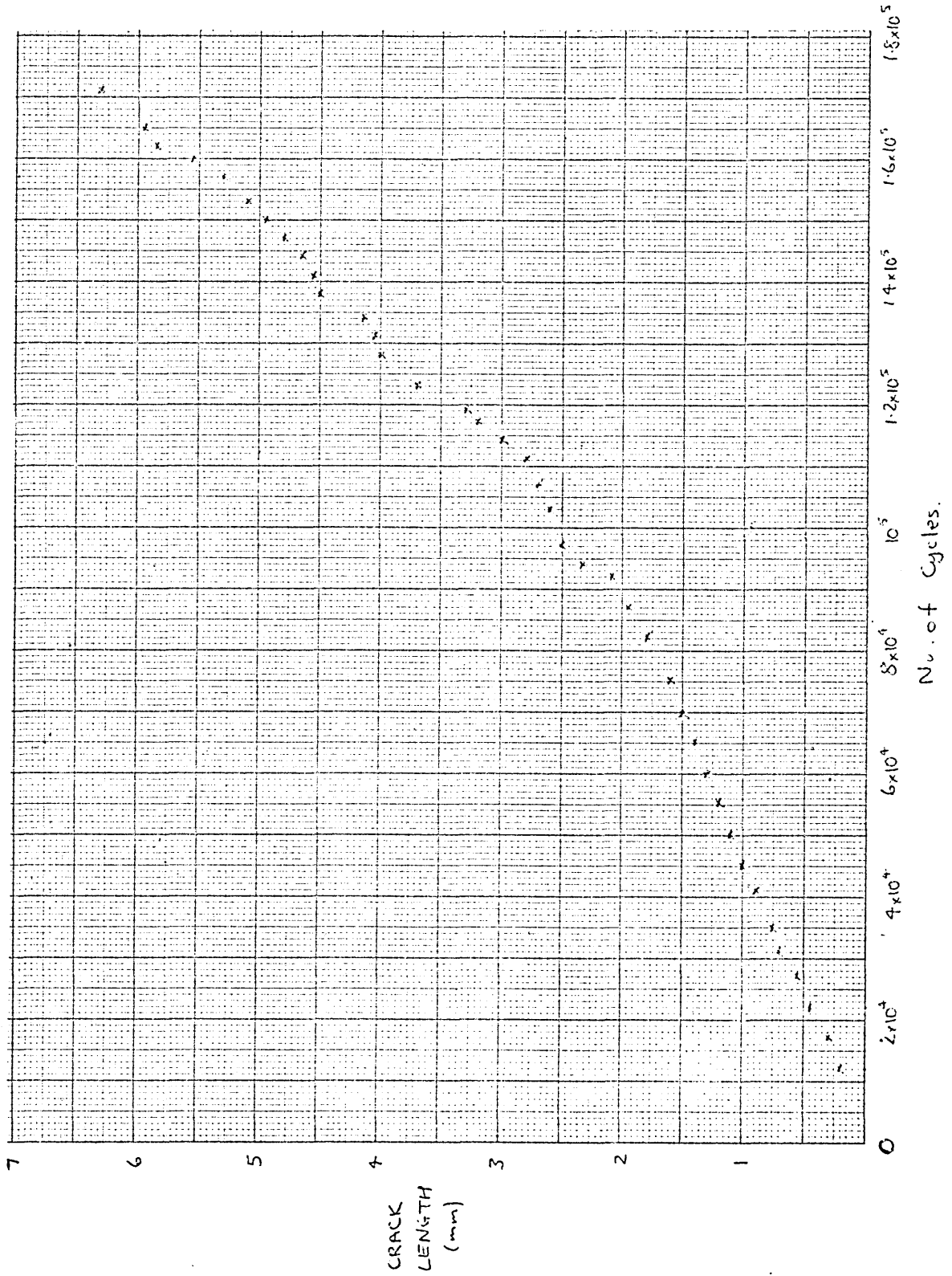


Fig A1/2. Specimen B4. Stress 6 tons/sq. in. (93MN/m²). Endurance: 6.53×10^6 cycles

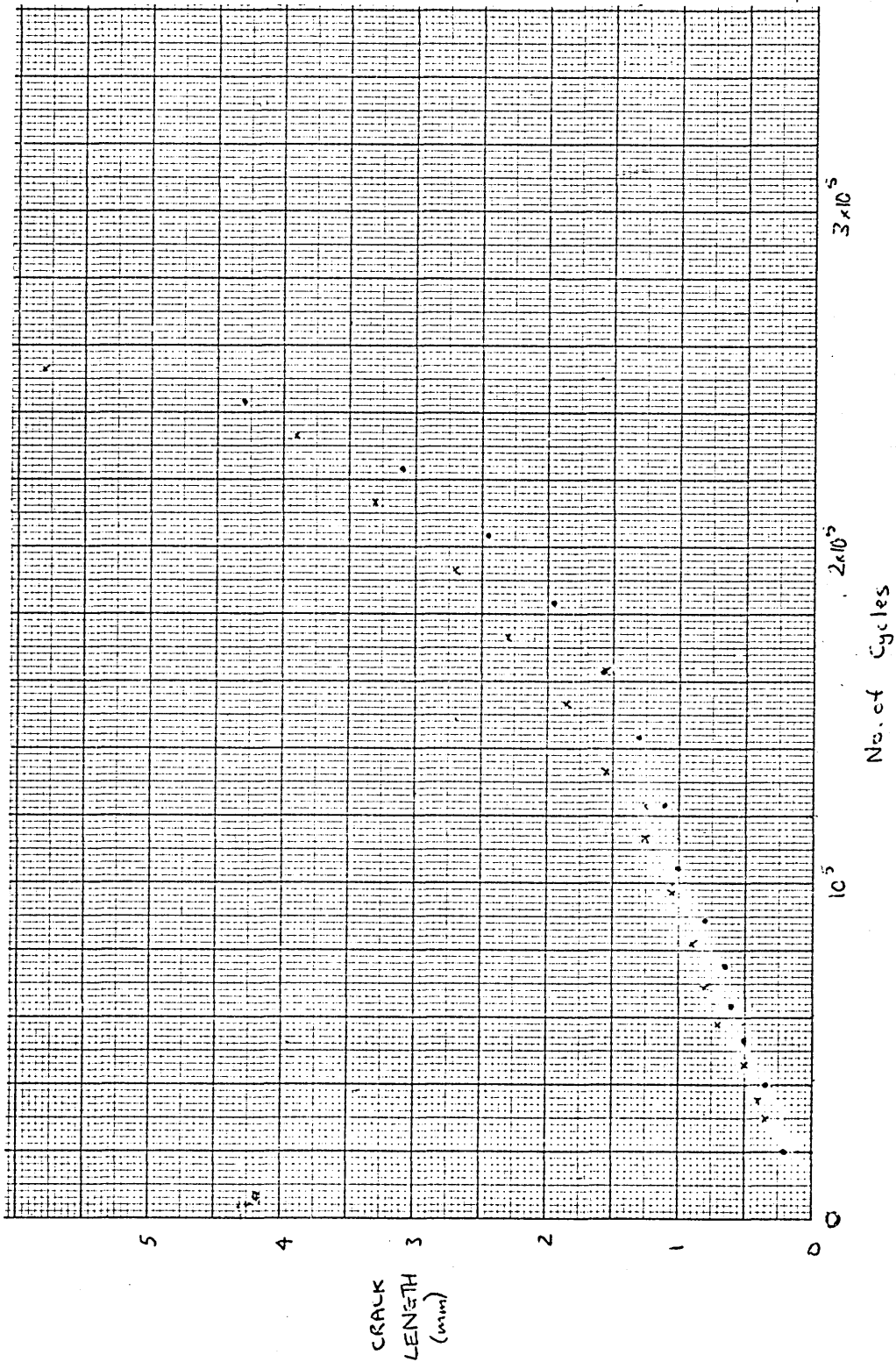


Fig A1/4. Specimen B6. Stress 5 tons/sq. in (77 MN/m^2). Endurance: 5.64×10^5 cycles.

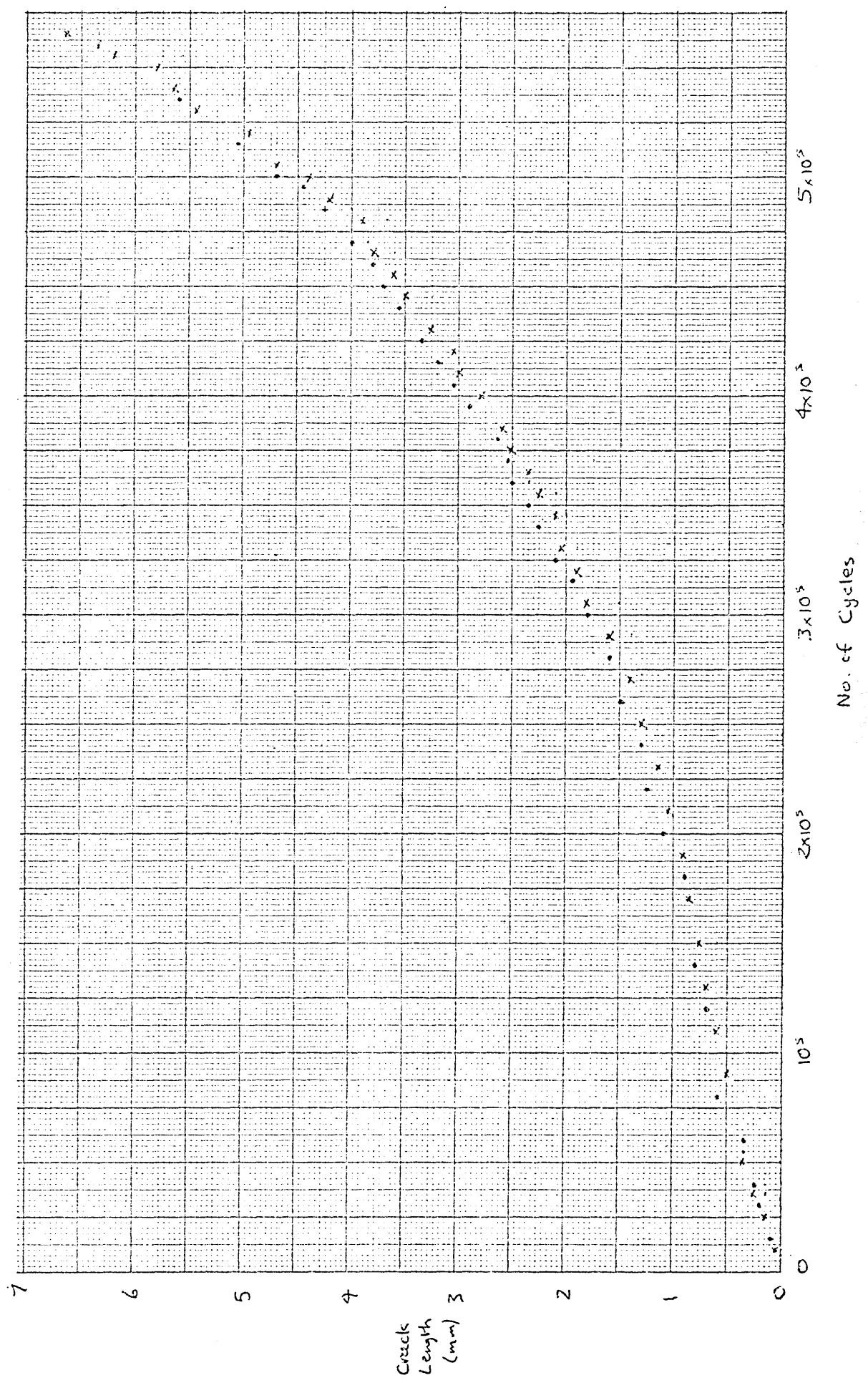


Fig A1/5. Specimen B60. Stress $4\frac{1}{2}$ tons/sq.in. (69 MN/m²). Endurance: 4.89×10^5 cycles.

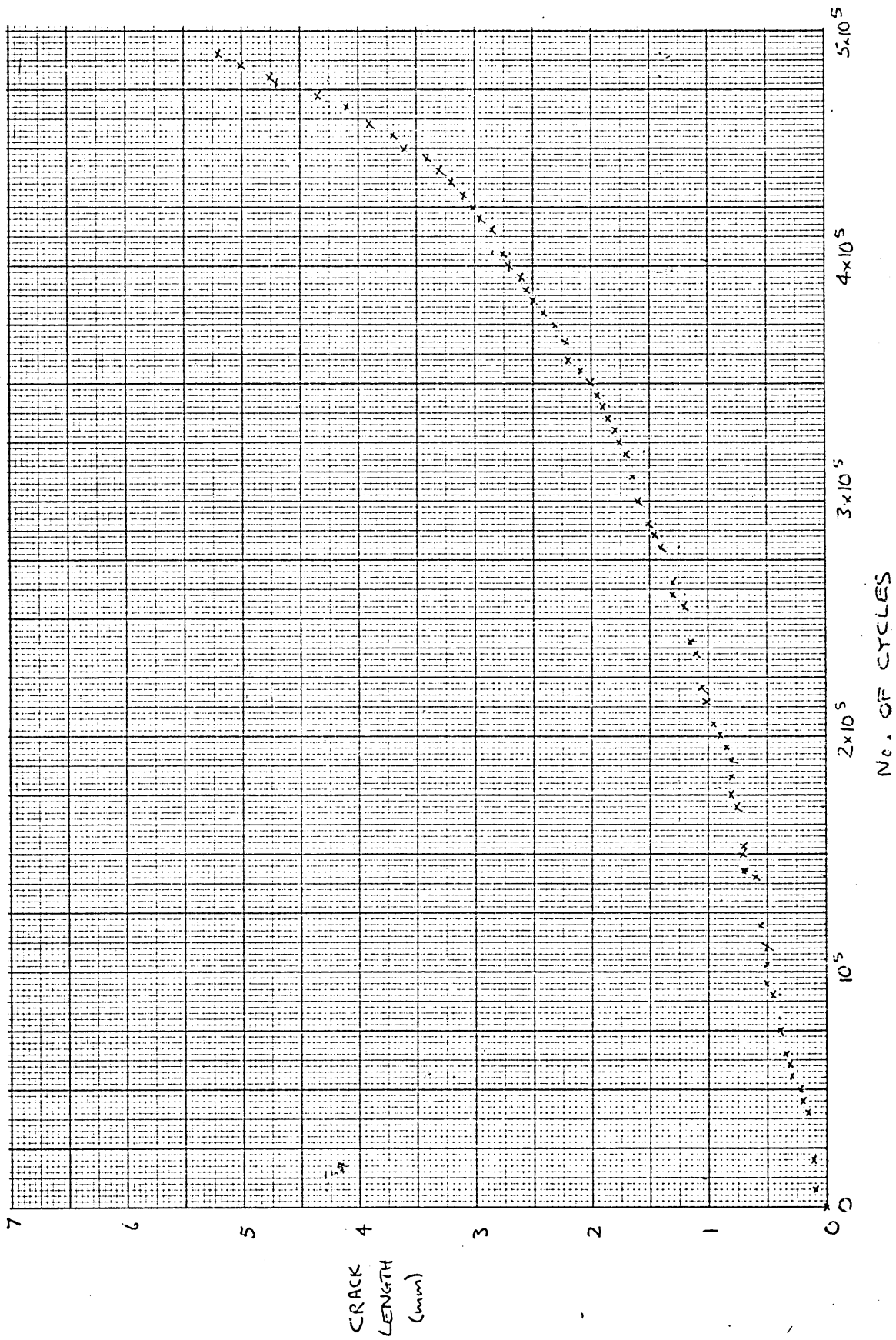


Fig A1/6. Specimen E1. Stress 4 tons/sq. in (61MN/m^2). Endurance: 7.05×10^5 cycles.

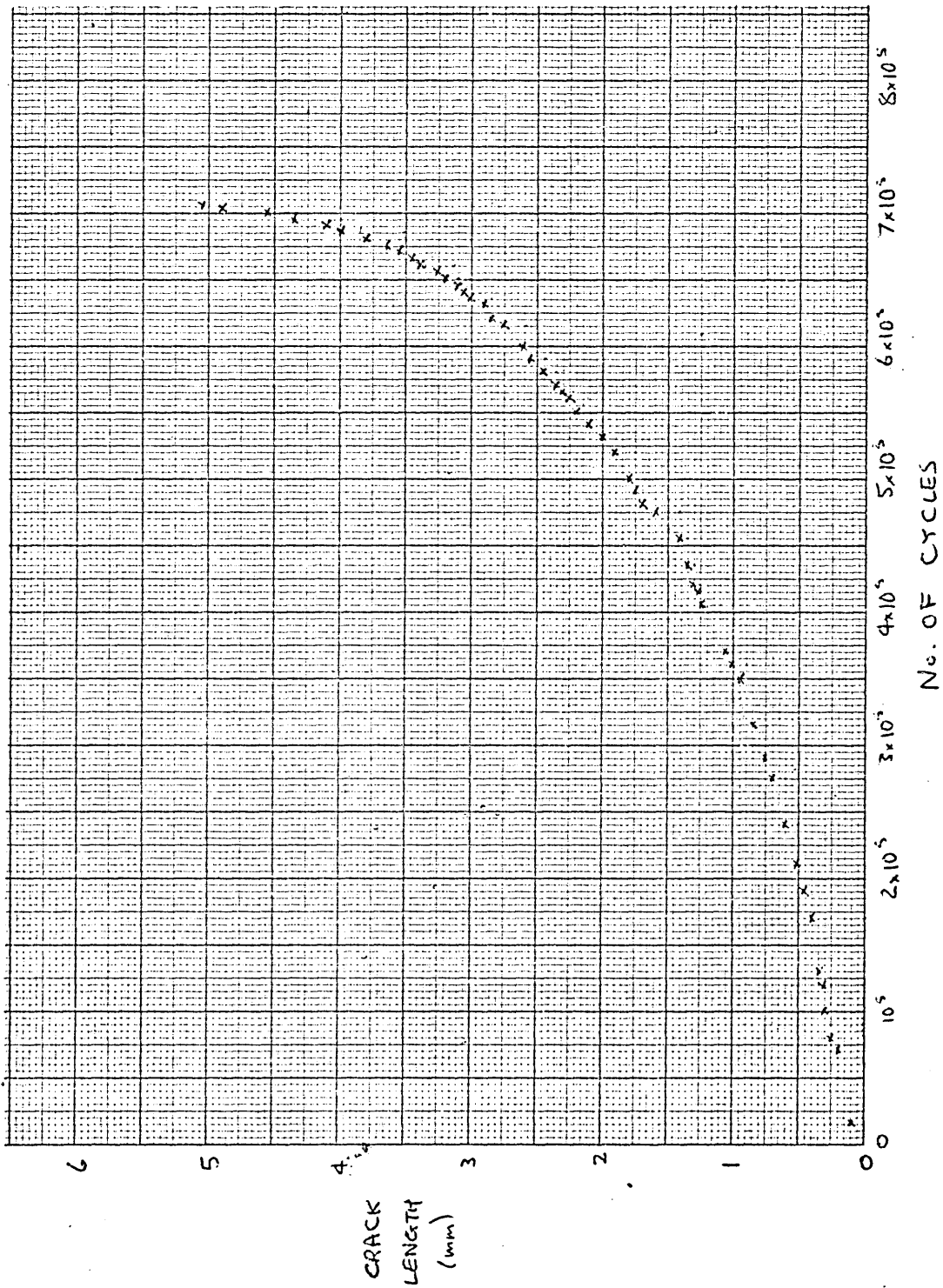


Fig. A1/7. Specimen E3. Stress 6 tons/sq. in. (93 MN/m²) Endurance 2.09 x 10⁵ cycles.

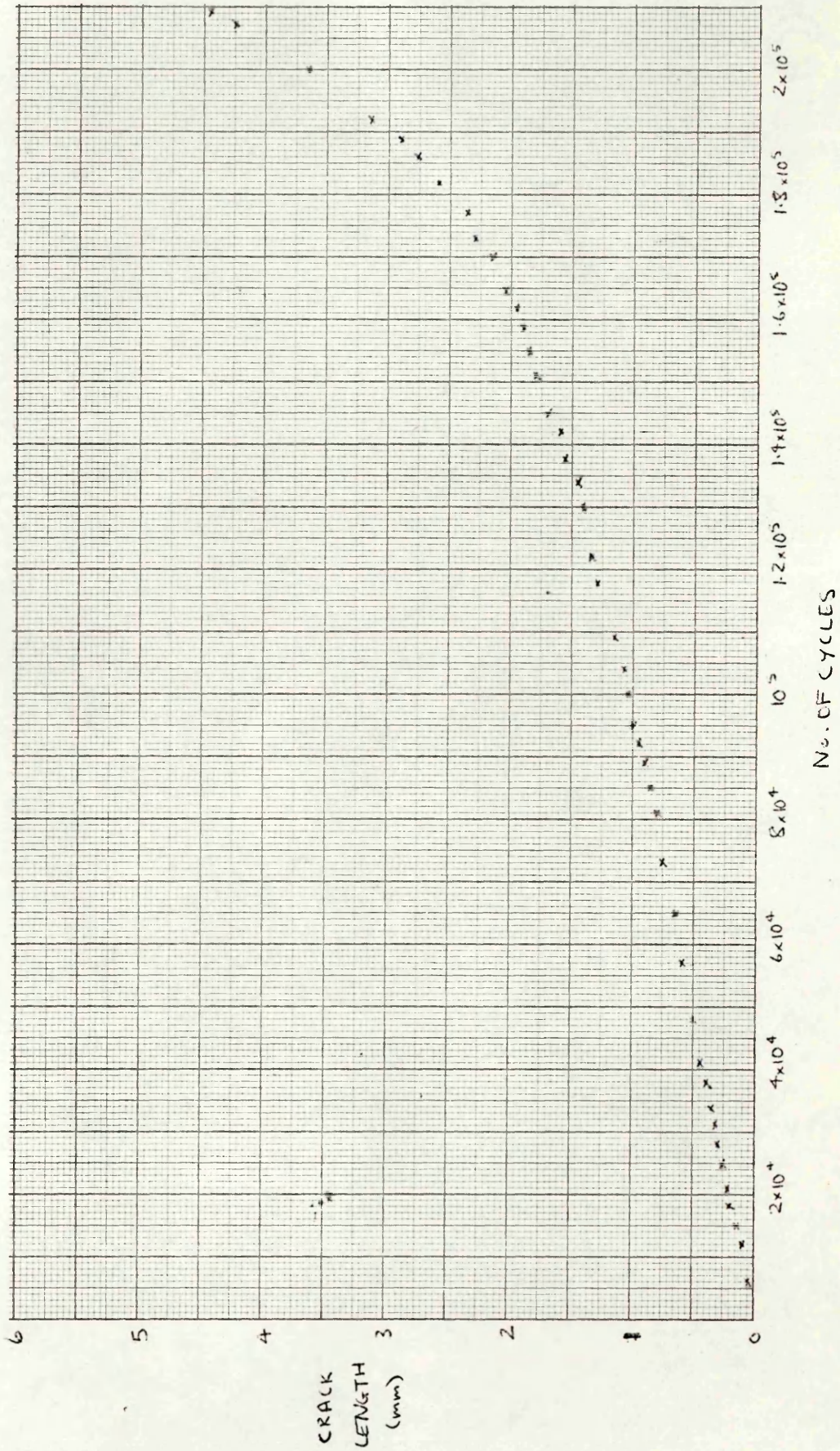


Fig A1/8. Specimen E5. Stress $4\frac{3}{4}$ tons/sq.in (73 MN/m^2). Endurance 3.45×10^5 cycles.

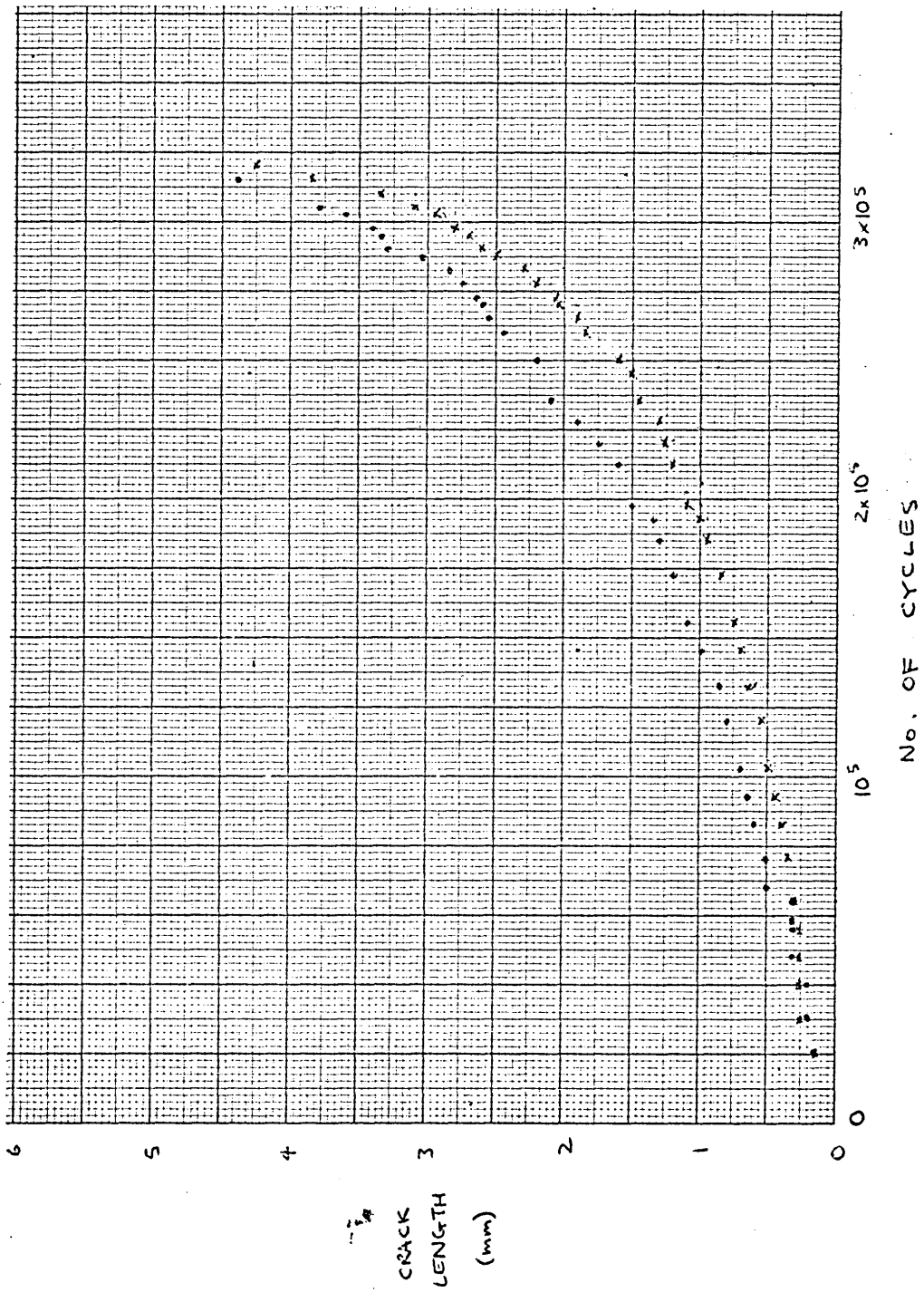
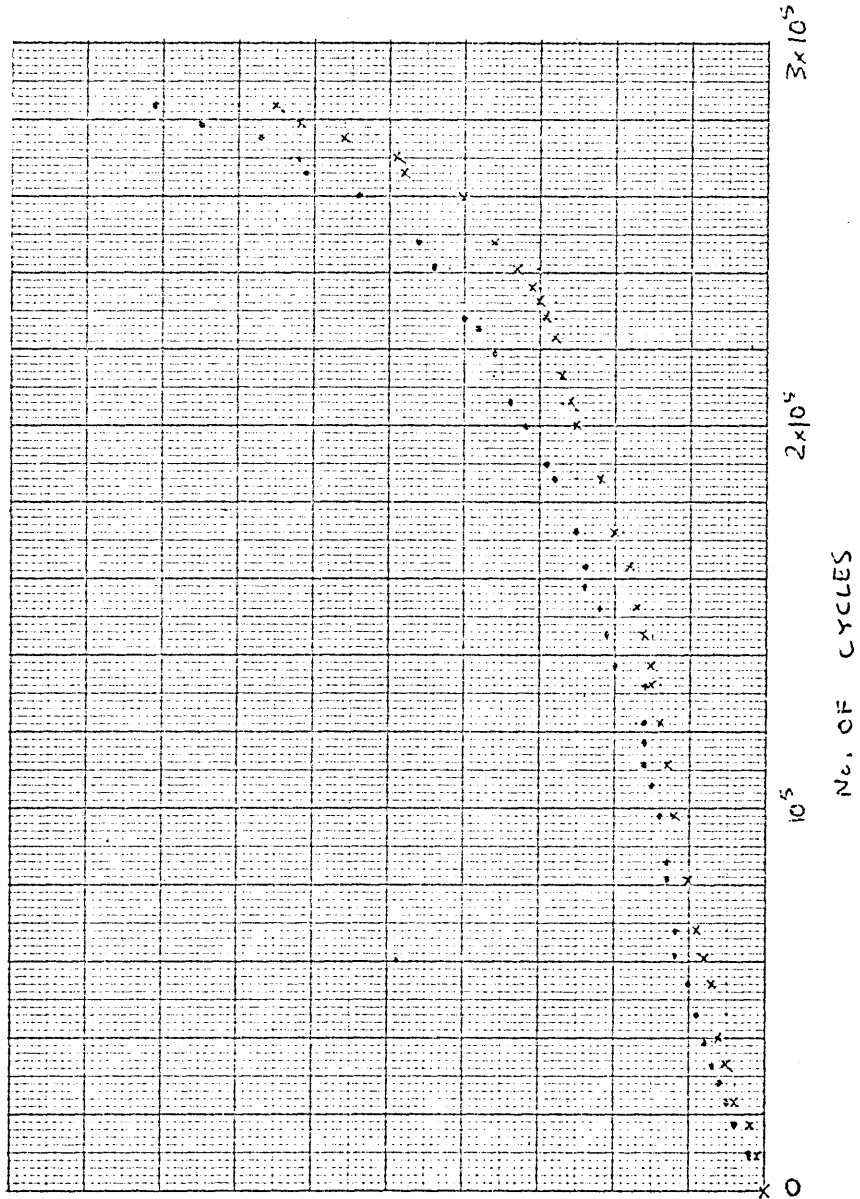


Fig A1/9. Specimen EG. Stress $5\frac{1}{2}$ tons/sq.in. (85 MN/m^2). Endurance 2.83×10^5 cycles.



CRACK
LENGTH

Fig. 11.10. Spectral density of stress fluctuations (0.27110/m) vs. number of cycles

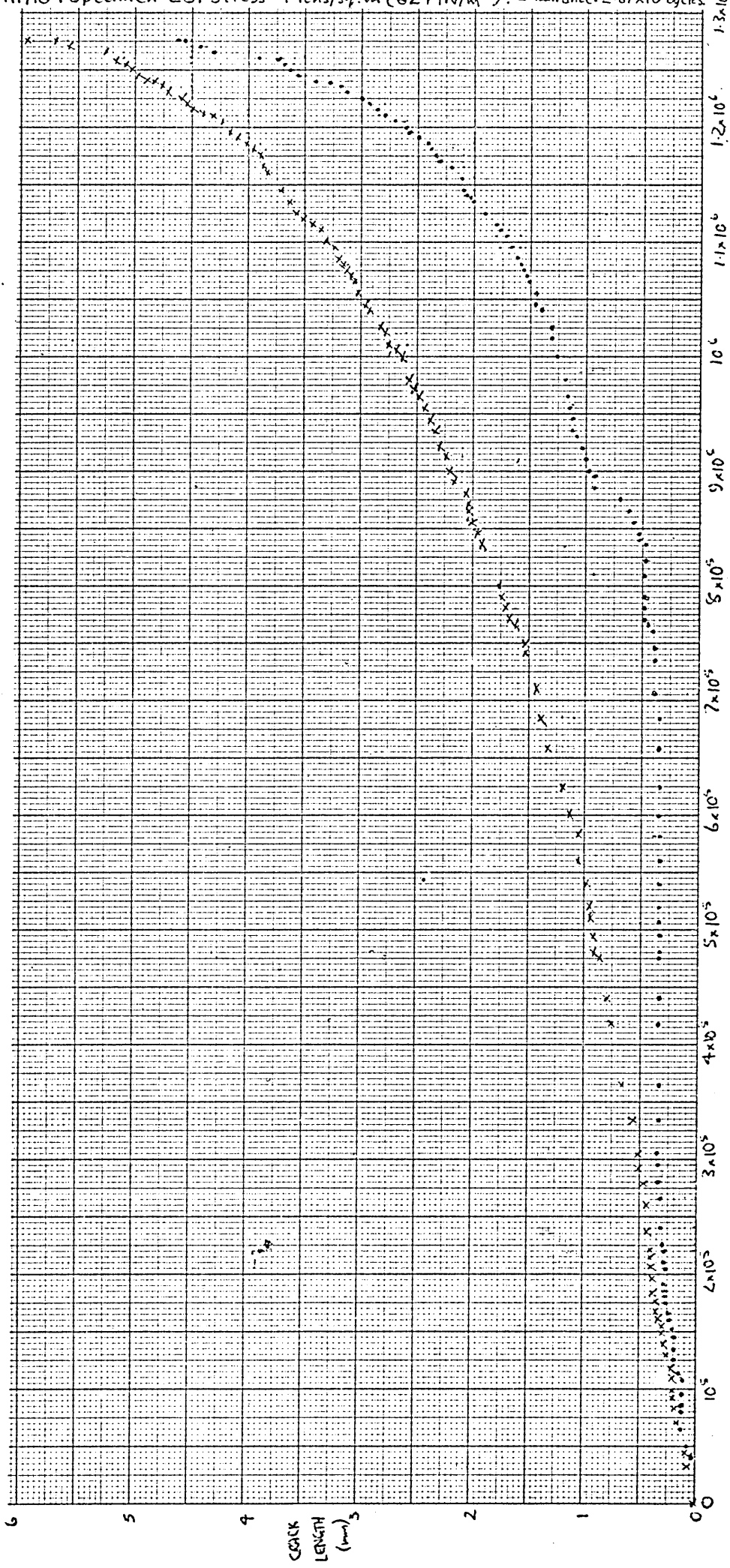


Fig A1/11. Specimen E10. Stress 5 tons/sq.in. (77 MN/m^2). Endurance: 4.86×10^5 cycles.

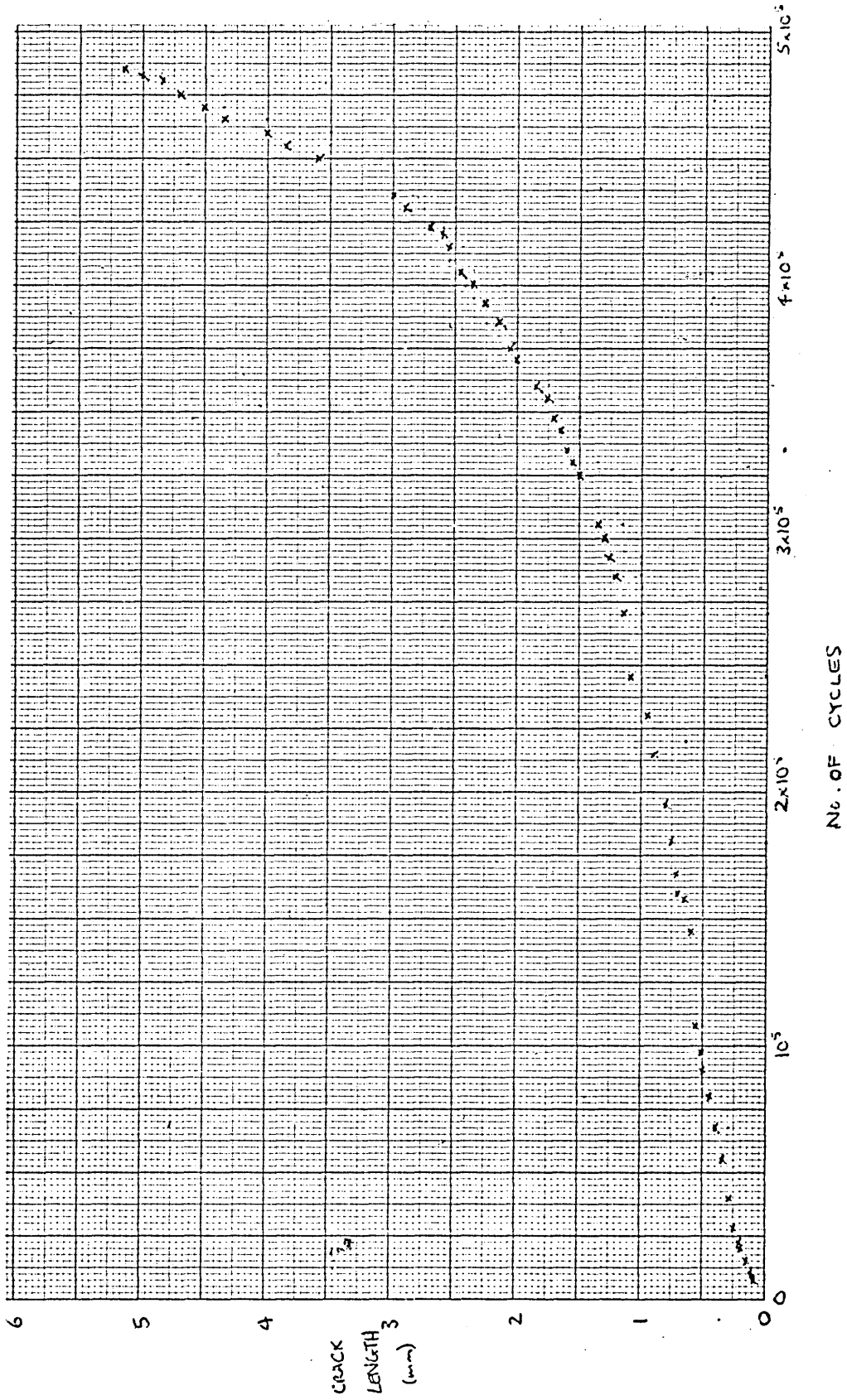


Fig A1/12. Specimen J5. Stress 6 tons/sq. in. (93 MN/m²). Endurance: 1.62 x 10⁵ cycles.

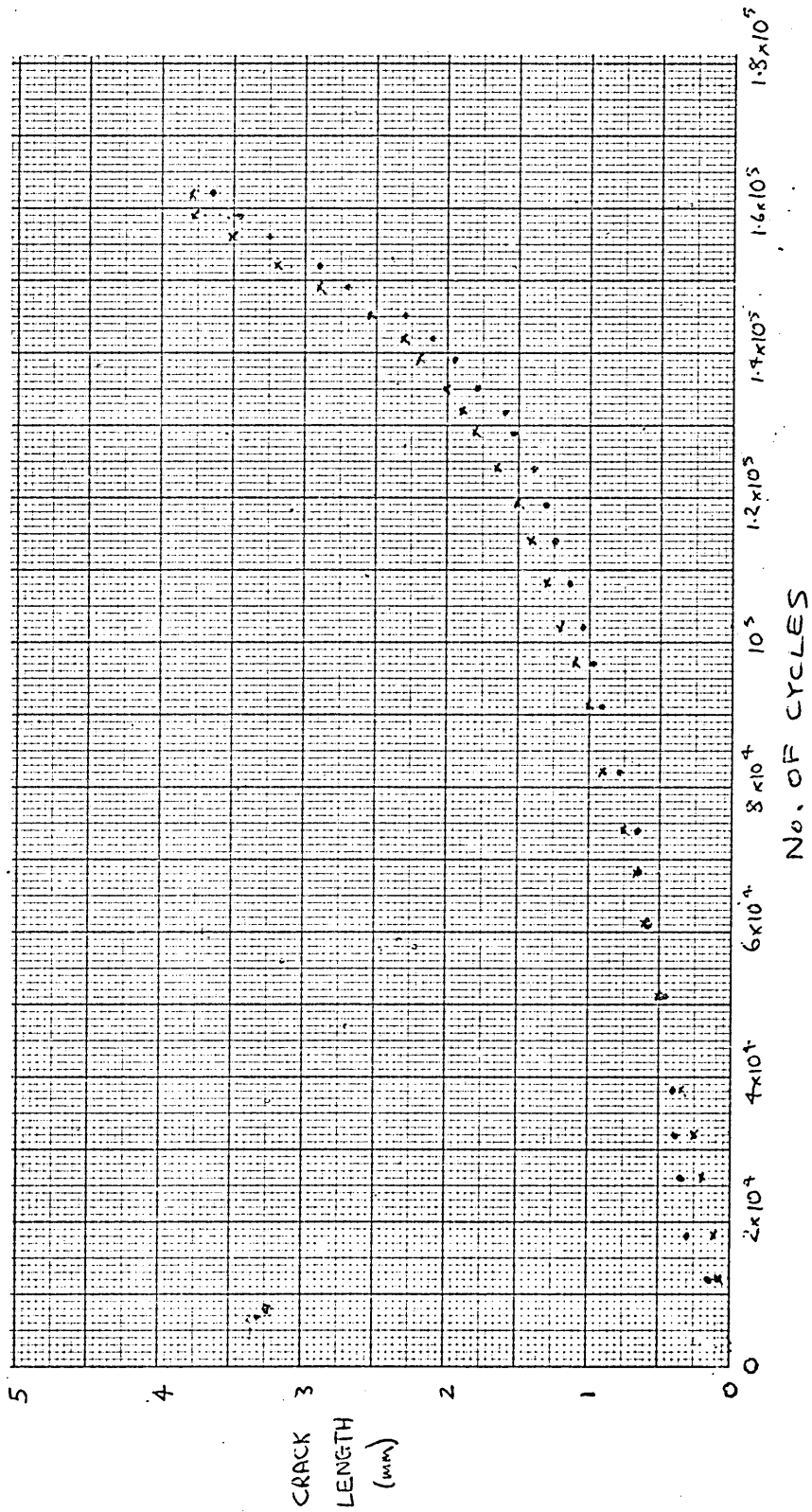
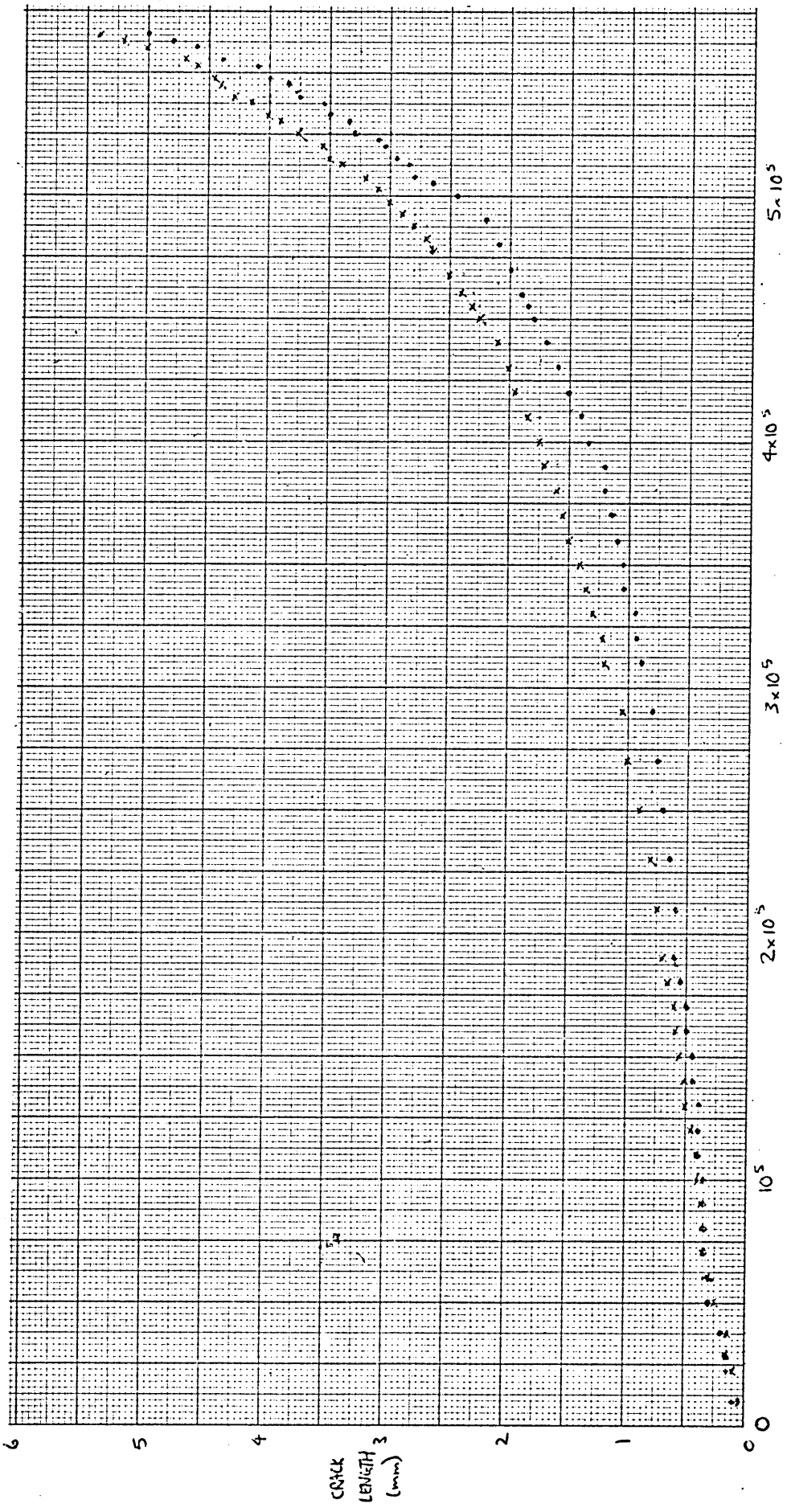


Fig A1/13. Specimen J6. Stress 5 tons/sq.in (77 MN/m²). Endurance 5.66x10⁵ cycles.



No. OF CYCLES

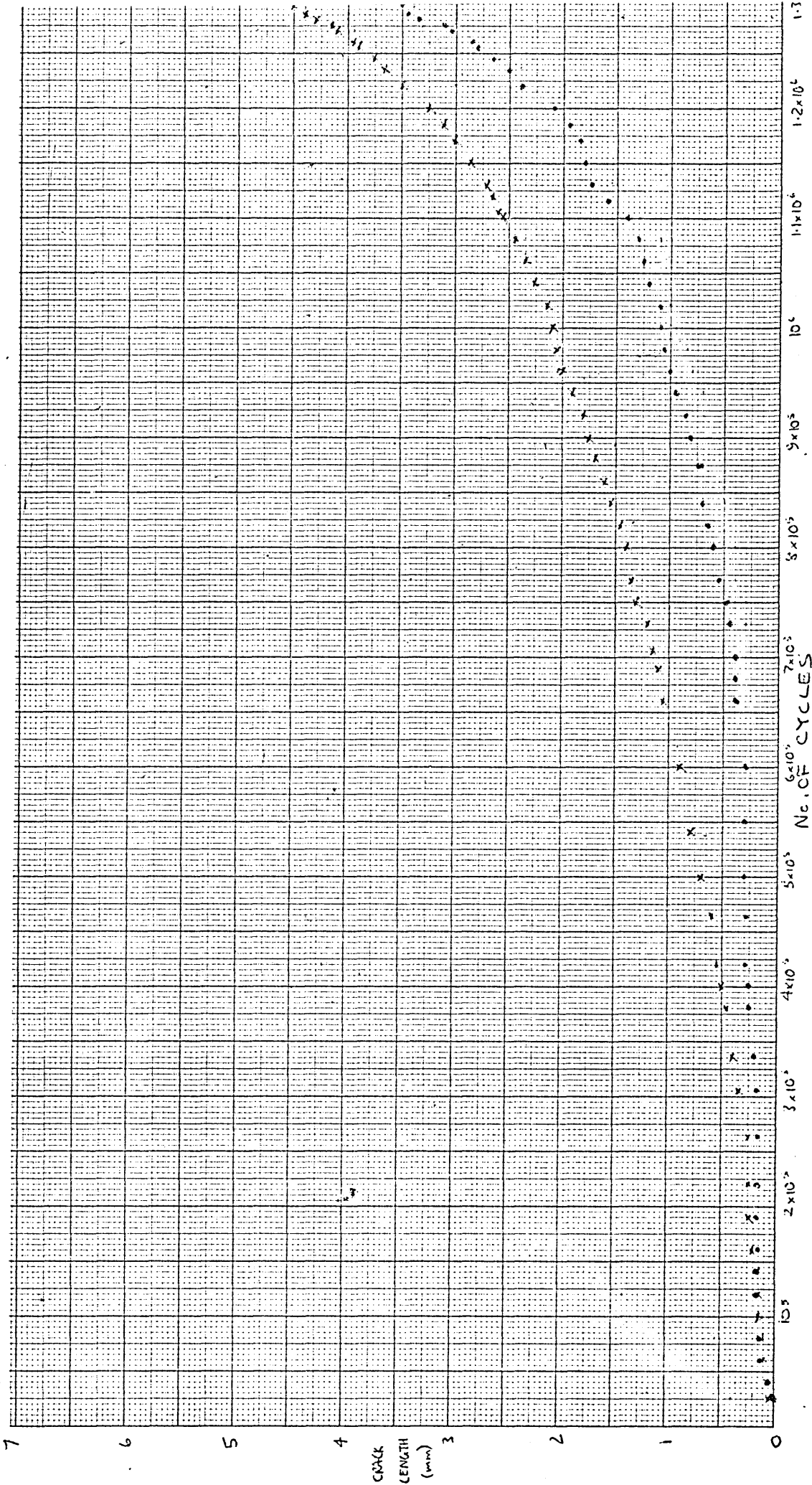
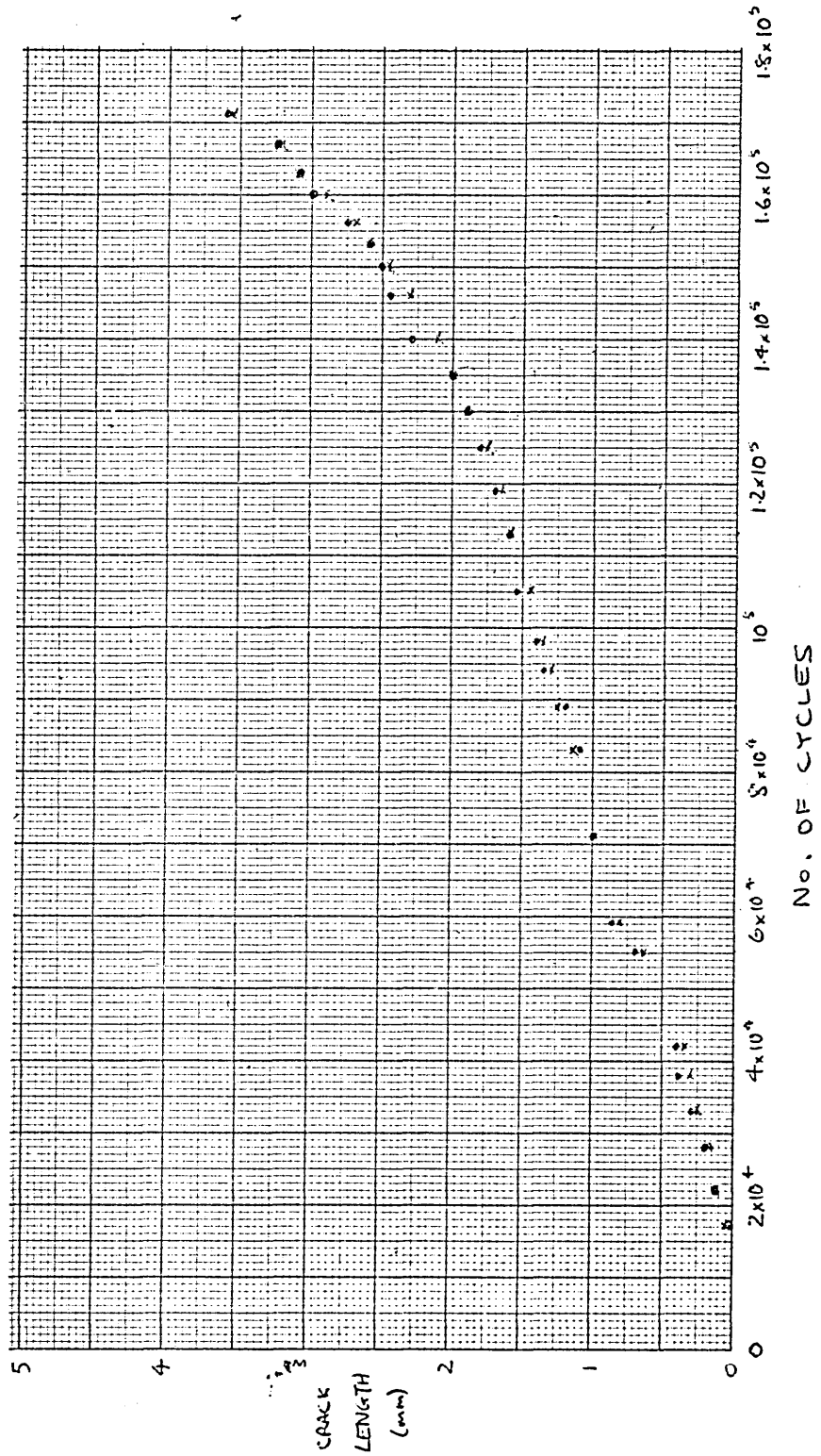


Fig. A1/15. Specimen J13. Stress 6 tens/sq.in. (93 MN/m²). Endurance 1.71x10⁵ cycles



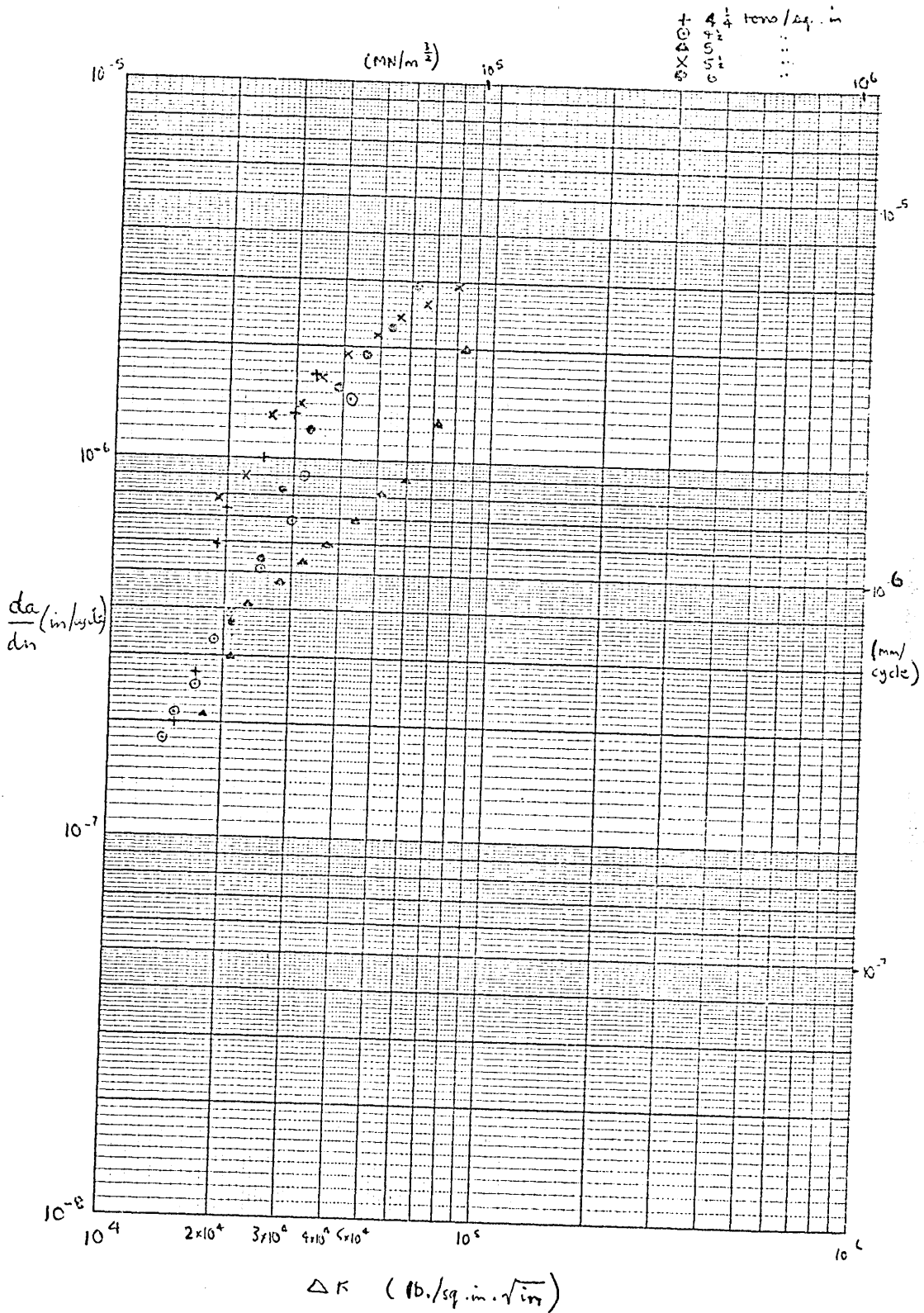


Fig. A2 RELATIONSHIP BETWEEN CRACK GROWTH RATE & STRESS INTENSITY
 RANGE FOR 0.01% CARBON STEEL,

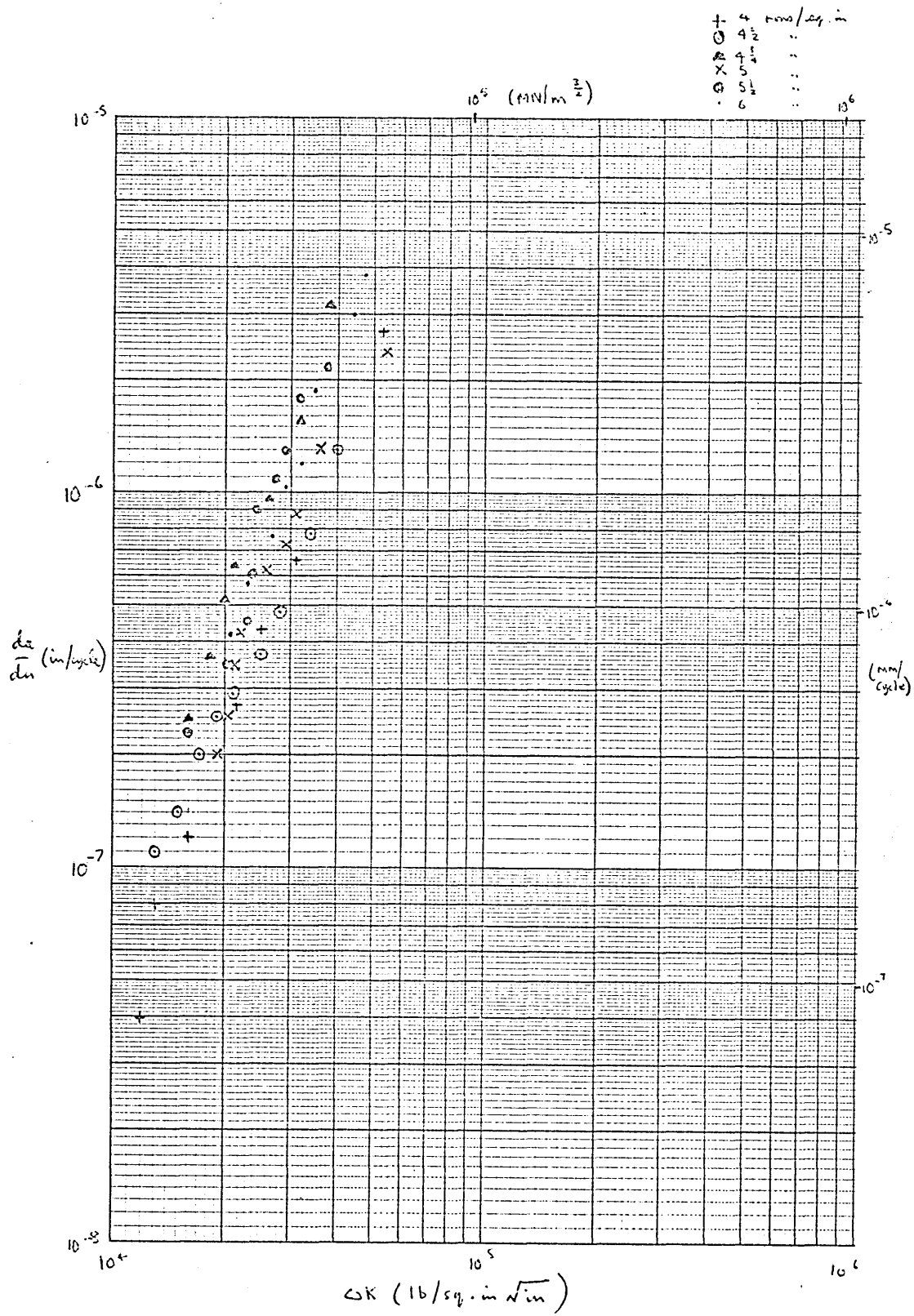


Fig. AB. RELATIONSHIP BETWEEN CRACK GROWTH RATE & STRESS INTENSITY RANGE FOR 0.11% CARBON STEEL.

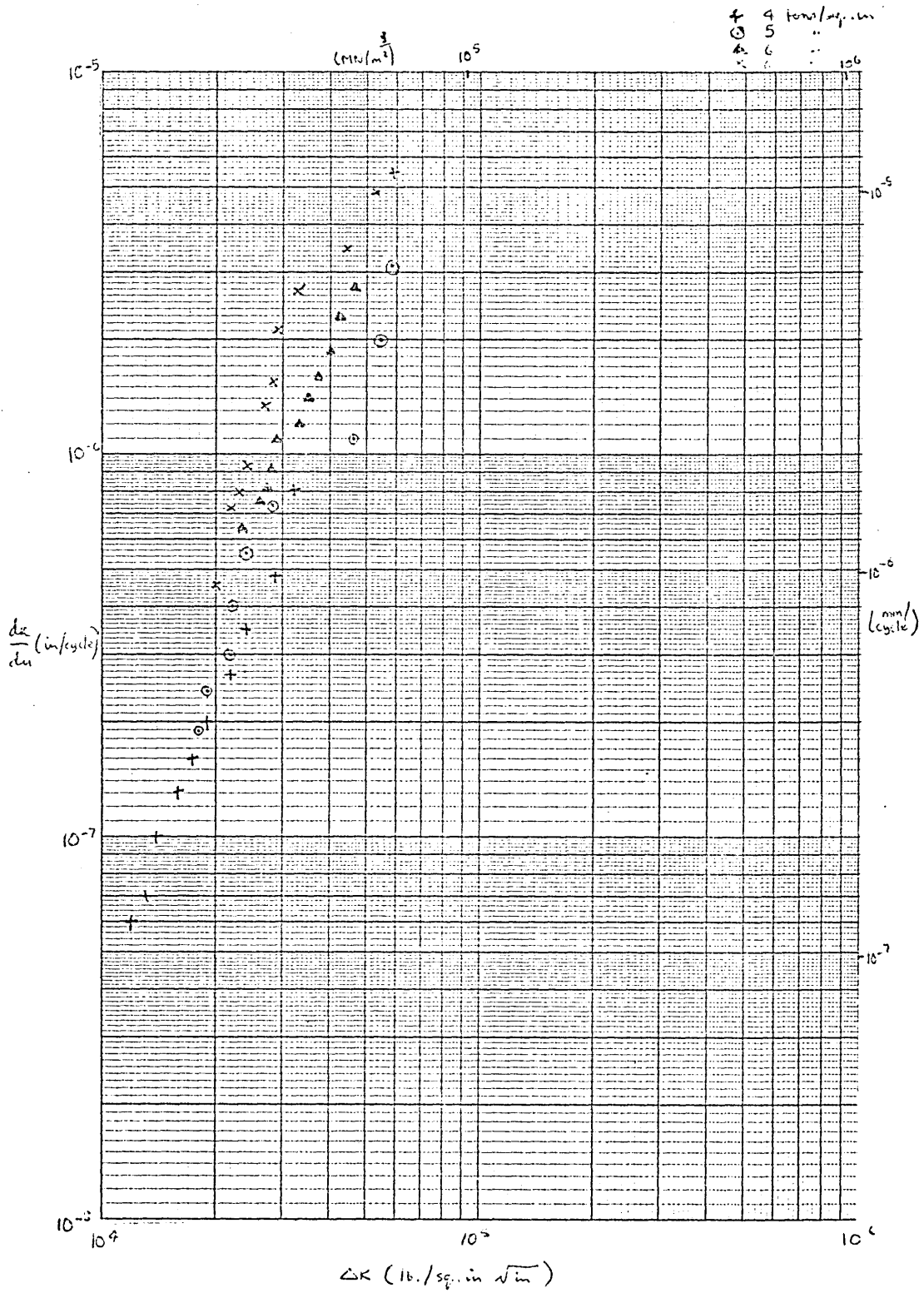


Fig. A4 RELATIONSHIP BETWEEN CRACK GROWTH RATE & STRESS INTENSITY
RANGE FOR 0.41% CARBON STEEL

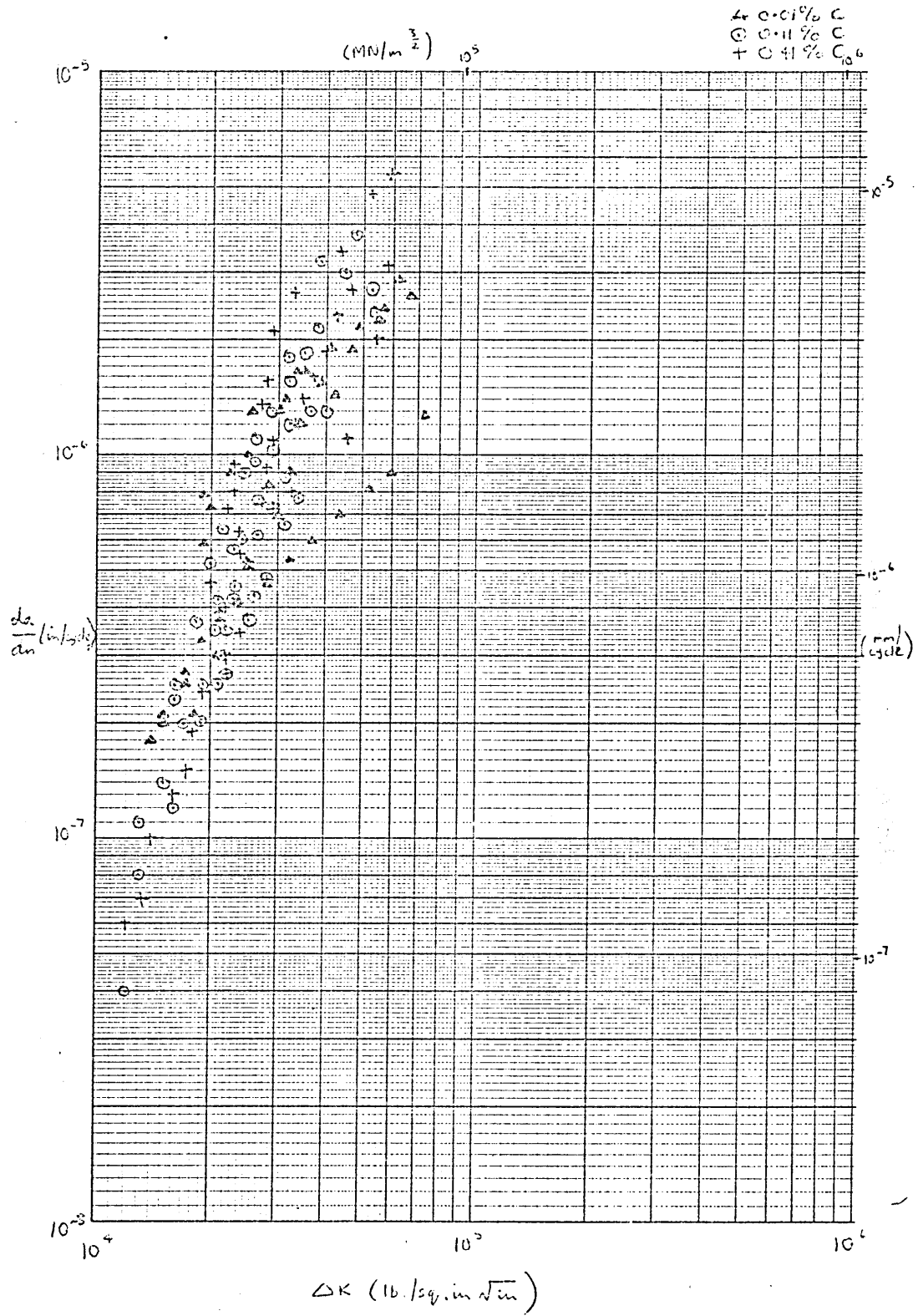


FIG. A5 RELATIONSHIP BETWEEN CRACK GROWTH RATE & STRESS INTENSITY RANGE FOR ALL THREE STEELS.

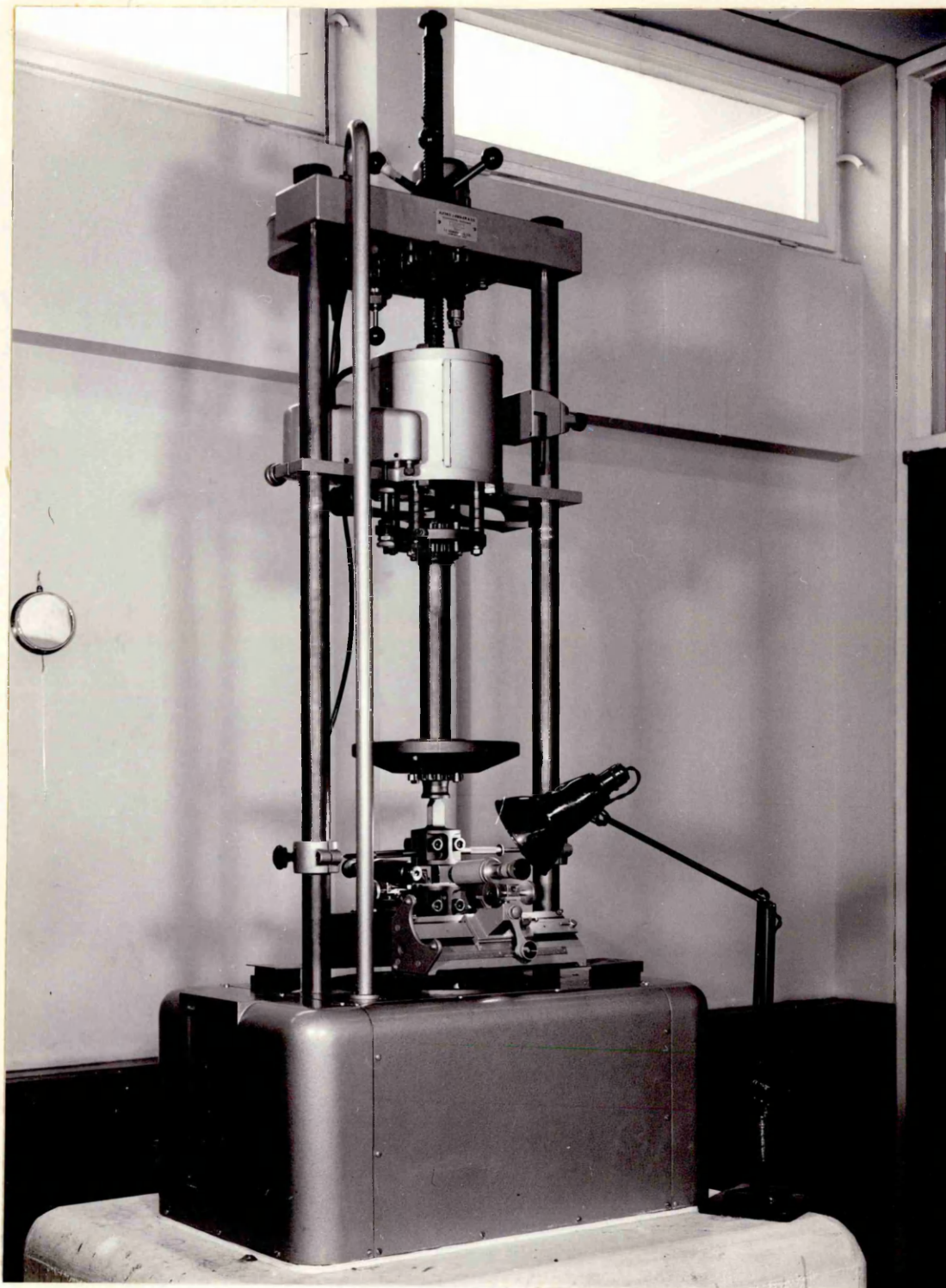


Fig. 7. Testing Arrangement Showing Amsler 2-ton Vibrophore.

7904057018



**Sheffield City Polytechnic
Eric Mensforth Library**

REFERENCE ONLY

This book must not be taken from the Library

PL/26

R5193

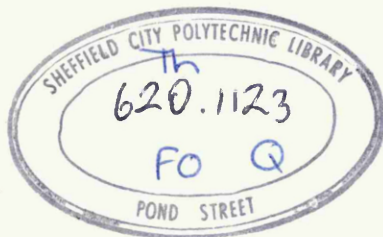
FATIGUE CRACK INITIATION AND PROPAGATION

IN PLAIN CARBON-MANGANESE STEELS

by

PETER FOX, A.C.T.(Sheff.), A.I.M.

A research project carried out for the
degree of Master of Philosophy of the
Council for National Academic Awards



7904057-01

"..... it may appear equally conclusive that a bar of iron or any other material so loaded, would, under the least change either by increasing or diminishing the load, however minute, ultimately tend to destruction. I am aware of the great difference of opinion which exists on this subject. It is one which I conceive to be worthy of investigation"

W. Fairbairn, Esq. Report of the Commissioners appointed to inquire into the Application of Iron to Railway Structures, 1848, p.403.

CONTENTS

| | | |
|----------|--|----|
| 1. | INTRODUCTION | 1 |
| 2. | REVIEW OF PREVIOUS LITERATURE | 3 |
| 2.1 | FATIGUE DAMAGE AND CRACK INITIATION | 3 |
| 2.1.1. | INITIAL PHYSICAL MECHANICAL & STRUCTURAL CHANGES. | 3 |
| 2.1.2. | OBSERVATIONS OF FATIGUE DAMAGE | 4 |
| 2.1.2.1. | Slip During Cyclic Loading | 4 |
| 2.1.2.2. | Persistent Slip Bands | 5 |
| 2.1.2.3. | Extrusions and Intrusions | 6 |
| 2.1.2.4. | Importance of cross-slip | 7 |
| 2.1.2.5. | Pore Formation | 9 |
| 2.1.2.6. | Effect of Grain Boundaries | 10 |
| 2.1.2.7. | Fatigue Crack Initiation in Iron and Carbon Steels. | 11 |
| 2.1.2.8. | Effect of Strain Ageing | 14 |
| 2.1.3. | MECHANISMS OF CRACK INITIATION | 15 |
| 2.1.3.1. | General | 15 |
| 2.1.3.2. | Mechanism of Cottrell and Hull | 15 |
| 2.1.3.3. | Random Walk Theory | 16 |
| 2.1.3.4. | Theories Involving Cross-slip | 16 |
| 2.2 | FATIGUE CRACK PROPAGATION | 17 |
| 2.2.1. | MICROSCOPIC OBSERVATIONS | 17 |
| 2.2.1.1. | Fractography | 17 |
| 2.2.1.2. | Modes of Fatigue Crack Propagation | 17 |
| 2.2.1.3. | Stage I Crack Propagation | 18 |
| 2.2.1.4. | Stage II Crack Propagation | 19 |
| 2.2.2. | MECHANISMS OF CRACK PROPAGATION | 21 |
| 2.2.2.1. | Stage I Crack Propagation | 21 |
| 2.2.2.2. | Stage II Crack Propagation | 22 |

| | | |
|----------|---|----|
| 2.2.3. | ANALYSIS OF CRACK PROPAGATION MEASUREMENTS | 24 |
| 2.2.3.1. | Early Work | 24 |
| 2.2.3.2. | Fracture Mechanics Approach | 26 |
| 3. | EXPERIMENTAL METHODS AND MATERIALS USED | 28 |
| 3.1 | EXPERIMENTAL MATERIALS | 28 |
| 3.1.1. | CHEMICAL COMPOSITION | 28 |
| 3.1.2. | PREPARATION | 28 |
| 3.1.3. | MICROSTRUCTURE | 29 |
| 3.1.4. | TENSILE PROPERTIES | 30 |
| 3.2 | FATIGUE TESTING | 30 |
| 3.2.1. | SPECIMENS | 30 |
| 3.2.2. | TESTING PROCEDURE | 31 |
| 3.2.3. | CRACK PROPAGATION MEASUREMENTS | 31 |
| 3.3 | EXAMINATION OF SPECIMENS | 32 |
| 4. | EXPERIMENTAL WORK | 34 |
| 4.1 | PRELIMINARY WORK ON PURE IRON | 34 |
| 4.2 | EXPERIMENTAL WORK ON CARBON-MANGANESE STEEL PLAIN SPECIMENS | 35 |
| 4.2.1. | TEST RESULTS | 35 |
| 4.2.2. | THE DEVELOPMENT OF SURFACE FATIGUE DAMAGE | 36 |
| 4.2.3. | THE SPREAD OF PLASTICITY DURING FATIGUE | 37 |
| 4.2.4. | SLIP INTENSIFICATION AT GRAIN BOUNDARIES | 39 |
| 4.2.5. | CRACK INITIATION | 40 |
| 4.2.6. | SURFACE CRACK PROPAGATION | 41 |
| 4.2.7. | INITIATION OF MAIN CRACKS AND STAGE I CRACK PROPAGATION | 41 |
| 4.3 | EXPERIMENTAL WORK ON CARBON-MANGANESE STEEL NOTCHED SPECIMENS | 43 |
| 4.3.1. | TEST RESULTS | 43 |
| 4.3.2. | STAGE II CRACK PROPAGATION | 45 |

| | | |
|----------|---|----|
| 4.3.2.1. | General | 45 |
| 4.3.2.2. | Intergranular Fracture | 45 |
| 4.3.2.3. | Effect of Pearlite | 46 |
| 4.3.2.4. | Branch Cracks | 47 |
| 5. | DISCUSSION | 48 |
| 5.1 | THE DEVELOPMENT OF SURFACE FATIGUE DAMAGE | 48 |
| 5.2 | CRACK INITIATION | 50 |
| 5.3 | CRACK PROPAGATION | 51 |
| 6. | CONCLUSIONS | 55 |
| 7. | REFERENCES | 57 |
| 8. | STATEMENT OF ADVANCED COURSES OF STUDY ATTENDED | 62 |
| 9. | ACKNOWLEDGMENTS | 63 |

1. INTRODUCTION

The term "fatigue" is used to denote those processes which occur in a material when it is subjected to fluctuating stresses, which may lead to failure at stress levels well below those required to cause failure in static tension. Fatigue in plain unnotched specimens of metals and alloys usually begins with changes in the mechanical properties of the bulk material, followed by the occurrence of surface damage. Cracks then form from this surface damage and propagate through the bulk of the material. Eventually the crack becomes large enough to be unstable, and final fracture occurs, which can be brittle or ductile depending upon the properties of the material under tensile loading.

Wood⁽¹⁾ has classified the stress-endurance diagram into three sections (Fig.1). These are the "H" or high stress fatigue range, the "F" or fatigue range and the "S" or pseudo-safe range. Wood considers the "F" range to be absent in body-centred cubic metals. The present work on crack initiation is restricted to the study of low stress fatigue, i.e. the F and S ranges.

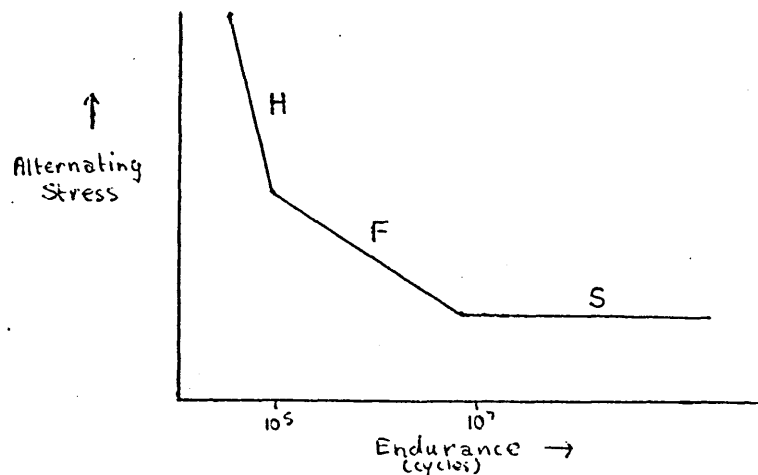


Fig.1 Schematic Representation of S-N diagram(after Wood⁽¹⁾).

Surface fatigue damage in face-centred cubic metals generally takes the form of wide slip bands from which cracks eventually develop. However, there is some conflict in the literature concerning fatigue crack initiation in iron and plain carbon steels, some workers observing persistent slip bands similar to those seen in FCC metals, whilst others have observed the formation of a cell structure with cracks originating in cell boundaries. Consequently, in the present work in order to resolve the question of initiation site three carbon steels have been studied, with carbon contents chosen to give no pearlite, a small percentage of pearlite and approximately 50% pearlite. These have been examined by optical microscopy, replica electron microscopy and scanning electron microscopy in an attempt to determine the type of fatigue damage which occurs, how cracks initiate, and the way in which microstructure affects this behaviour.

Fatigue crack propagation has in the past been studied by means of replica electron fractography. In the present work, scanning electron microscopy has been used. This enables fractures to be examined directly at magnifications ranging from x20 to x20,000, and therefore the fine fracture features can be related to the macroscopic fracture appearance. Also, artefacts due to replication technique are avoided. The majority of previous work has again been on non-ferrous materials, and in the present work, three carbon steels of similar compositions to the three used for crack initiation studies have been used to determine crack propagation rate data by direct microscopical observation, and to correlate this with the fractographic features.

2. REVIEW OF PREVIOUS LITERATURE

2.1. FATIGUE DAMAGE AND CRACK INITIATION

2.1.1. INITIAL PHYSICAL, MECHANICAL AND STRUCTURAL CHANGES

The first stage in the fatigue process consists of an initial rapid change in physical and mechanical properties, followed by a slowing down and then saturation⁽²⁾. Many workers have observed the change in mechanical properties with number of cycles, and methods used include the measurement of the peak stress required to produce a fixed strain amplitude or the strain resulting from a fixed stress amplitude, and the variation in the stress-strain curve or the indentation hardness. It has been found that whereas annealed metals show an initial increase in hardness, cold worked metals often show an initial decrease. In annealed pure metals, the saturation level of hardening generally occurs within 0.1-10% of the fatigue life, but alloys of low stacking fault energy may saturate much later in the test.

During the initial hardening stage, there is also an increase in electrical resistivity, which appears to be partly due to an increase in point defect concentration as well as to an increase in dislocation density, since some of the increase will anneal out at temperatures where only point defects are sufficiently mobile⁽³⁾.

It has been suggested by Backofen⁽⁴⁾ that the same mechanism is responsible both for work softening and the absence of hardening at saturation in fatigue. He suggests that a balance is eventually created between dislocation generation and annihilation, and that cross slip of screw

dislocations is an important feature of the mechanism. Edge dislocation annihilation could also be occurring by a process of internal void formation as suggested by Fujita⁽⁵⁾.

Avery & Backofen have shown that if a fatigue test is interrupted during the initial fatigue hardening stage, and annealing carried out, any damage present is removed and the fatigue life is prolonged, suggesting that no permanent damage (such as cracks or voids) exists⁽⁶⁾.

More detailed reviews of fatigue hardening are given in references 7, 8 & 9.

Thin foil electron microscopy has been used by many workers to determine the dislocation arrangements which produce the effects referred to above. At high strain amplitudes, a cell structure similar to that accompanying unidirectional deformation is produced. At low strain amplitudes, small dislocation loops and dipoles are formed. The dislocation distribution in the surface layer has been correlated with the shape of the persistent slip bands in copper by Lukás et al⁽¹⁰⁾. The persistent slip bands consist of zones of alternately high and low dislocation density, the high density zones linking together at a particular depth below the surface. The low density zones in between act as "channels in which dislocation motion is easy and extrusions occur on the surface of these zones". An extensive review⁸ of this subject appears in reference 11.

2.1.2. OBSERVATIONS OF FATIGUE DAMAGE

2.1.2.1. Slip during cyclic loading

Ewing and Humfrey carried out surface observations on Swedish iron, and found that slip lines appeared in certain

grains after a few cycles of stress⁽¹²⁾. As cycling continued, these lines became far more distinct and later broadened into wide bands with rather hazily defined edges. Eventually cracks appeared along the broadened slip bands. These were proved to be cracks by repolishing the surface. The density of bands was higher at higher stress levels, and cracks appeared earlier the higher the stress level. Gough showed that slip in fatigue occurs on the same slip systems as under static loading for various metals⁽¹³⁾. These were aluminium and silver (F.C.C. $\{111\} \langle 110 \rangle$), zinc (C.P.H. $\{0001\} \langle 10\bar{1}0 \rangle$) and iron (B.C.C. $\{110\}$, $\{112\}$ and $\{123\} \langle 111 \rangle$). He also showed that the same critical resolved shear stress law was followed, and that there was a stress below which slip could be observed without cracking occurring.

It has been shown by electron microscopy that the slip bands formed in F.C.C. metals in unidirectional deformation consist of parallel straight lines of varying heights⁽¹⁴⁾. The slip bands formed under cyclic loading, however are much less regular in appearance and appear to be curved⁽¹⁵⁻¹⁷⁾.

Plastic deformation is an essential process in fatigue failure. This has been confirmed by Eisner⁽¹⁸⁾ who carried out tests on copper whiskers and found that fatigue failure did not occur until plastic flow had occurred.

2.1.2.2. Persistent Slip Bands

Thompson et al carried out repolishing experiments during the fatigue of annealed copper, and found that many of the surface slip bands could be removed in this way⁽¹⁹⁾. A few persisted, however, and these were therefore named

"persistent slip bands". These were present after about 5% of the specimen life, and fatigue cracks grew from them. It was, therefore, suggested that the persistent slip bands were in fact incipient cracks, and that the majority of the test was spent propagating these cracks. If the specimens were repeatedly electropolished, the persistent slip bands were eventually removed. No new slip bands were ever discovered in this process showing that they only formed on the surface of the specimen, despite the uniform stress throughout its volume. If electropolishing was carried out long enough to remove the persistent slip bands and the specimen was refatigued, new slip bands formed in the same positions, showing that slip was still active on the same planes.

It has been shown that cracks in fatigue slip bands form as early as 1% of the total fatigue life, the rest of the time being spent propagating these cracks⁽²⁰⁾. In copper and α -brass, persistent slip bands can be revealed by etching after electropolishing⁽¹⁾.

2.1.2.3. Extrusions and Intrusions

Forsyth carried out surface observations on fatigued partially age hardened Al-4%Cu, and observed ribbons of material exuded from the slip bands⁽²¹⁾. He referred to these as "extrusions" and noted that they were of the order of $10\ \mu$ high and very thin. They had a metallic lustre and were sometimes continuous along the length of the slip band, although they were usually broken up into smaller lengths. Extrusion was almost negligible at -25°C and because of this and the fact that extrusions had not been

observed in pure aluminium, it was thought that the phenomenon was caused by localised overageing.

Forsyth and Stubbington showed that extrusions could occur in aluminium if it had previously been cold rolled⁽²²⁾. It was thought that this could be due to local softening of the work hardened material. However, extrusions have since been observed in many materials including annealed pure copper⁽¹⁹⁾, α -brass⁽²³⁾, iron⁽¹⁷⁾ and silicon iron⁽²⁴⁾.

The reverse process to extrusion formation, namely, the production of intrusions has also been shown to occur^(25,26). Hull found that extrusions and intrusions could be observed in copper at less than 1% of the fatigue life at temperatures as low as 4.2°K⁽²⁷⁾. It was, therefore, unlikely that thermally activated processes were necessary for the production of intrusions, and a mechanism involving cross-slip was proposed⁽²⁶⁾ (see section 2.1.3.2.). It has been demonstrated by Wever et al and Wood and Segall⁽²⁸⁾ that intrusions can grow into cracks.

2.1.2.4. Importance of Cross-Slip

The effect of cross-slip on the formation of extrusions has been demonstrated by Avery, Miller and Backofen⁽²⁹⁾ who fatigued two single crystals of high purity copper. The orientations of these crystals were such that the Schmid resolved shear stress factors for the primary slip system were nearly alike, but those for the cross-slip system were different, one being³10 times the other. Both crystals were fatigued beyond saturation, and the extrusions produced on the surface were removed by electropolishing. After an additional 50 cycles, the crystal with the higher Schmid

factor on the cross-slip system showed much higher extrusions than the other crystal when examined by a taper sectioning technique. Also, the height of the extrusions was greater than could be accounted for by a mechanism involving steady extrusion development.

It has also been shown that fatigue failure is extremely difficult to produce in materials which have a high resistance to cross-slip, e.g. zinc single crystals fatigued at -196°C ⁽³⁰⁾, lithium fluoride⁽³¹⁾ and magnesium oxide⁽³²⁾. Alden⁽³³⁾ has compared dynamic recovery in zinc and cadmium at low temperatures and found that cadmium easily saturates at about 200lb/sq.in., whereas the fatigue hardening curve for zinc is essentially linear up to 3000lb/sq.in. Both metals are CPH and have a primary slip system of (0001) $[\bar{1}\bar{2}10]$, but cadmium cross slips on (10 $\bar{1}$ 1) $[\bar{1}\bar{2}10]$ whereas zinc does not. However, it is possible to produce fatigue failure in zinc at low temperature (see section 2.1.3.3.).

It seems, therefore, that the ability to cross-slip is extremely important in allowing saturation, and hence fatigue failure to occur, since it has been mentioned previously that fatigue cracks do not form in fatigue slip bands until saturation has occurred. The fact that cross-slip can be important in the development of a surface notch peak topography also lends support to the view that cross-slip plays an essential part in the fatigue failure mechanism of most metals.

The effect of reducing stacking fault energy, and hence inhibiting cross-slip has been demonstrated by McGrath

and Thurston⁽³⁴⁾ who compared Cu, Cu-15%Zn and Cu-35%Zn fatigued at the same stress level. They found that slip bands became thinner and fatigue life increased greatly as the concentration of zinc (and the resistance to cross-slip) was increased. However, when zinc is added to copper, mechanical properties, e.g. yield stress and U.T.S. are also altered. Later work⁽³⁵⁾ has compared Cu-Al and Cu-Ni alloys. Aluminium and nickel additions have similar effects on the mechanical properties of copper but aluminium produces a greater reduction in stacking fault energy, and was shown to produce the better fatigue properties.

2.1.2.5. Pore Formation

Wood, Cousland and Sargant⁽³⁶⁾ used a taper sectioning technique on copper and 70/30 brass, and observed pore formation on slip planes. Later during the tests, these pores linked up to form fissures which were the embryo fatigue cracks. In another paper⁽¹⁾ blocks of metal were seen to be loosened from the surface. Intrusions and extrusions were considered to be side effects which could not account for the primary source of damage, even though slip band cracks often seemed to be associated with surface extrusions.

Dover and Jones⁽³⁷⁾ used a technique of successive sectioning to build up a three-dimensional picture of the features near the surface in fatigued copper. The major conclusion of their work was that as successive surface layers were polished away, no new pores or cracks appeared below the surface. It was considered that the "pores" observed by Wood et al were in fact intrusions, which appeared to be pores because of Wood's taper sectioning

technique. Irregular microcracks were seen linking up the slip band cracks below the surface. The slip band cracks had an irregular crack front, and split up into a series of tubular holes before disappearing.

2.1.2.6. Effect of Grain Boundaries

Predominantly grain boundary fatigue cracking has usually been considered to occur at high temperatures, but a number of workers have reported such cracking at lower temperatures. Lead and tin fail by grain boundary fracture when fatigued at room temperature⁽³⁸⁻⁴⁰⁾, but these are low melting point metals, and this can be classed as high temperature fracture. Snowden⁽⁴⁰⁾ has observed extrusions at grain boundaries in lead fatigued at room temperature in vacuo. These were of two types, whisker-like extrusions up to 50μ long with a diameter of approximately 1μ , and more continuous extrusions which were much smaller. Some boundaries showed localised slip patterns which were parallel to slip traces in other parts of the same grain, on one or both sides of the boundaries.

Golland and James⁽⁴¹⁾ have also observed grain boundary exudation in iron with a high oxygen content. They observed slip intensification near grain boundaries, and the whole of the fatigue fracture was intergranular. They attributed this to grain boundary embrittlement due to the high oxygen content of the material.

Grain boundary fatigue cracking has, however, been observed at room temperature in metals with high melting points in which there is no obvious grain boundary embrittlement. Hoepfner and Vitovec⁽⁴²⁾ tested tricrystals

of 99.988% copper with grain boundaries orientated at various angles to the stress axis. The fractures were part intergranular and part transgranular. They showed that the probability of initiation of grain boundary cracks increases with decreasing angular misorientation of neighbouring grains.

Smith⁽⁴³⁾ has shown that the tendency for grain boundary fatigue cracking is a function of temperature. In high purity aluminium, grain boundary cracking was most marked at 300°C, but was still visible at -73°C. It was absent at -180°C.

Local concentration of slip bands at grain boundaries has been observed in copper⁽⁴⁴⁾. Valleys occur in high stress specimens at grain boundaries, and it has been shown that intergranular fracture is favoured by high stress⁽⁴⁵⁾. Cracking also frequently occurs at twin boundaries in copper which are parallel to slip planes, and it has been proposed that the twin boundaries and grain boundaries act as dislocation sources, resulting in increased plastic deformation adjacent to them⁽⁴⁶⁾.

Grain boundary crack initiation has also been observed in β -brass, which has an ordered body-centred-cubic structure at room temperature⁽⁴⁷⁾. This has been attributed to the high elastic anisotropy of the material ($E_{111}/E_{100} = 8.94$) which would result in a high stress concentration at grain boundaries.

2.1.2.7. Fatigue Crack Initiation in Iron and Carbon Steels

In contrast to the large amount of work done in the past on fatigue crack initiation in F.C.C. materials, comparatively little work has been carried out on ferrous materials. The most exhaustive treatment is that of Hempel

and his co-workers⁽⁴⁸⁻⁵⁰⁾. They showed that in an 0.09% carbon steel, slip bands begin to occur in the first 1% of the life. The number and extent of the slip bands increase as the test progresses, and slip bands occur both above and below the fatigue limit, but are completely absent at a stress amplitude which is 22% below the fatigue limit. Repolishing after fatigue shows that many of the slip bands contain fine microcracks. Persistent slip bands in mild steel which develop into cracks have also been observed by Modlen and Smith⁽⁵¹⁾.

Electron microscopy of plastic replicas shows that the slip bands have a pitted surface showing numerous fine dark lines and some crevice-like grooves and splits. Hempel et al propose that these fissures join together to produce microcracks which can then propagate.

Single crystal work on Armco iron shows that fatigue slip bands are either straight or wavy, depending on whether their orientation is such that single or multiple slip occurs. The wavy course of the slip bands produced in specimens oriented for multiple slip appears to result from an accumulation of several slip lamellae which "arch out from the ferrite to different extents".

Tests on bi- and tri-crystals showed that when a grain boundary is favourably orientated at right angles to the direction of the bending stress, slip bands are concentrated into a narrow zone alongside the grain boundary. The fatigue failure starts from this boundary, which is heavily deformed because of the anisotropic behaviour of the adjoining crystals.

Wood et al⁽⁵²⁾ studied the microstructural changes

produced in pure iron and Armco iron subjected to alternating torsion at amplitudes above and below the knee of the S-N curve to identify the basic mechanisms of fatigue and to find why they should give rise to a sharp S-N knee in contrast to the smooth S-N curve shown by face centred cubic metals.

Above the knee of the S-N curve they found that an unusually pronounced cell structure appeared in the grains. They suggested that this was due to internal disorientation or rumpling of the grains. This rumpling was accompanied by so much local distortion as to be almost of the nature of a structural fault, and the cell boundaries were zones of very high dislocation density. Eventually pores appeared at these cell boundaries, which then multiplied into boundary microcracks. These microcracks then became cross-linked with other cell boundary cracks to give macroscopic crack formations. These observations are similar to those of Holden⁽⁵³⁾.

Below the knee of the S-N curve they found dense "clouds" of short faint slip markings. A "cloud" would start in one region of a grain and eventually spread over the grain in a dense mass too fine to resolve optically. Pores formed from these slip bands, but these were so dispersed as to preclude their linking up to form microcracks, although odd cracks were noticed at grain boundaries.

Reimann⁽⁵⁴⁾ considered that the apparent discrepancies between Wood's work and that of Hempel was due to the initial condition of the test specimens. He therefore carried out tests on Armco iron in alternating torsion on

specimens that had been subjected to preliminary cycling at high strain amplitudes and compared these with specimens subjected to low strain amplitude cycling only. It was found that specimens with preliminary large amplitude cycling showed slip in concentrated zones similar to Hempel's observations.

2.1.2.8. Effect of Strain Ageing

It has been shown that strain ageing plays an important part in determining the fatigue limit in carbon steels^(7,55). Two types of strain ageing are thought to be responsible for the effect. Oates and Wilson⁽⁵⁵⁾ have shown that a fatigue limit exists in fine grained annealed low carbon steel which is considerably reduced by pre-straining just above the yield point. Thus initial dislocation locking or "static strain ageing" is probably a prime cause of the fatigue limit in steels where the fatigue limit is at or below the yield point. Coarse grained mild steel, on the other hand, has a fatigue limit above its yield point. Pre-straining this before fatigue led to the fatigue limit being raised, this being consistent with a "dynamic strain ageing" mechanism, i.e. strain ageing during fatigue.

It was stated in section 2.1.2.1. that fatigue slip bands can still be seen below the fatigue limit, thus leading to the conclusion that the fatigue limit does not depend on micro-yielding behaviour. It has been proposed, however, that the spread of plasticity across grain boundaries rather than the initiation of plasticity is the limiting factor⁽⁵⁶⁾. Above the fatigue limit, fatigue slip bands gradually grow in width during a test, so that the

possibility of a dislocation source in an adjacent grain coming within the range of a high stress concentration will increase with time. The fatigue limit is the critical stress for this spread of plasticity to occur.

2.1.3. MECHANISMS OF CRACK INITIATION

2.1.3.1. General

The first theories of fatigue assumed that each cycle of stress work hardened the material by a small increment, until eventually a critical stress was exceeded and the material fractured. There is no evidence for either progressive work hardening, or such a critical fracture stress. More recently, it has been suggested that condensation of vacancies in a slip band could form voids which would nucleate a crack⁽⁵⁷⁾. These could be produced either by the non-conservative motion of a jogged screw dislocation or by dislocation pile ups of opposite sign on adjacent slip planes joining together to form a crack⁽⁵⁾. None of these proposals involves the nucleation of cracks at free surfaces, which are almost universally accepted to be the sites of fatigue crack initiation except in special circumstances. The only work in which this view is not accepted is that of Wood and his co-workers, in which crack initiation is said to be due to the accumulation of sub-surface "pores".

2.1.3.2. Mechanism of Cottrell and Hull⁽²⁶⁾

This involves slip on two intersecting slip systems. During the tensile half-cycle, a dislocation source S_1 produces a slip step on the surface. At a slightly higher stress in the same half cycle, source S_2 on an intersecting slip plane produces a second step. During the compression

half-cycle, the source S_1 produces a step of opposite sign which is in a different but parallel plane to the first slip step produced by this source, and an intrusion is formed. Similarly, S_2 produces an extrusion. If this mechanism were to occur, similar numbers of intrusions and extrusions would be observed, and the extrusions would be in a different slip band to the intrusions. These predictions are not always found to be true.

2.1.3.3. Random Walk Theory

May⁽⁵⁸⁾ has proposed that a notch-peak topography can develop by a process of random reversed slip, in metals where cross-slip is difficult. If slip occurs at random in each direction, and the distribution of slip at each half-cycle is independent of slip in previous cycles, the surface will be roughened. This roughening will concentrate the stress in the valleys, so that once valleys are formed, they will deepen. This mechanism could occur equally well in metals where cross slip is easy or difficult, and probably accounts for the fact mentioned earlier that fatigue can still occur in metals which do not cross-slip, e.g. zinc at low temperature⁽⁵⁹⁾.

2.1.3.4. Theories involving cross slip

Mott⁽⁶⁰⁾ has proposed that extrusions could form by the cyclic movement of a screw dislocation round a closed circuit, involving movement from the primary plane on to the cross-slip plane, returning via parallel primary and cross-slip planes. In the original mechanism, a pre-existing sub surface cavity was assumed to be present and it was proposed that this could form by the Fujita mechanism⁽⁵⁾.

This theory does not account for intrusion production, and requires a large number of cycles to produce one extrusion. However, extrusions have been observed in the first few cycles of fatigue testing⁽⁴⁾, and cavities beneath extrusions have not been observed in transparent crystals⁽⁶¹⁾.

McEvily and Machlin⁽³¹⁾ proposed that if two screw dislocations were to cross-slip simultaneously, material injected into the grain by intrusion could replace that lost underneath the extrusion. A number of other dislocation mechanisms involving cross-slip have been suggested, none of which is entirely satisfactory. Any successful mechanism must involve cross-slip and explain rapid intrusion - extrusion formation, the production of unequal numbers of extrusions and intrusions, and the appearance of intrusions and extrusions in the same slip band.

2.2. FATIGUE CRACK PROPAGATION

2.2.1. MICROSCOPIC OBSERVATIONS

2.2.1.1. Fractography

"Fractography" is a term coined by Zapffe and Worden⁽⁶²⁾ for the microscopical study of fracture surfaces. Originally optical microscopy was employed, but the majority of work has been carried out by electron microscopy, because of the superior resolution and depth of focus of this technique. Carbon replicas (both single stage and two stage) have been mainly employed for this work. Recently, the scanning electron microscope has become available but this instrument has only just begun to be employed for fractography.

2.2.1.2. Modes of Fatigue Crack Propagation

Forsyth⁽⁶³⁾ has distinguished two types of crack growth, which he calls Stage I and Stage II. Stage I growth is a

continuation of the crack initiation process, and occurs on slip planes orientated near to 45° to the direction of maximum tensile stress. This is also known as "shear mode crack growth". Stage II crack growth occurs after Stage I, and occurs at right angles to the direction of maximum tensile stress. Stage I crack growth is favoured by low stresses and slip on a single system, whereas Stage II growth is favoured by higher stresses and duplex slip.

2.2.1.3. Stage I Crack Propagation

Stage I crack propagation occurs on slip planes orientated near to the directions of maximum shear stress. Forsyth has suggested that the changeover from crack initiation to Stage I propagation is arbitrary and difficult to define and, therefore, he makes no distinction between these two stages. Stage I growth is favoured by low stresses, and in plain fatigue specimens may occupy the majority of the time of the test. Since the rate of crack propagation in Stage I is very small, normally only a small proportion of the fracture surface is taken up by this mode of propagation. Under certain circumstances, however, the whole of the final fracture may take place in Stage I. This has been shown to occur under corrosion fatigue conditions in aluminium alloys (64), and in a high strength nickel "superalloy" (65), where fatigue occurs at stresses well below the yield stress. Usually, the transition from Stage I to Stage II occurs at a grain boundary, but it can also occur within a grain. This was seen by Forsyth in Al-7.5%Zn - 2.5%Mg, and the changeover was not associated with any obvious metallurgical feature.

Stage I fracture surfaces in aluminium alloys often

show parallel lamellae running along the direction of crack growth. Flat and relatively featureless facets have also been observed, but this work was done by optical microscopy, and any fine detail would probably not have been resolved⁽⁶⁴⁾. Gell and Leverant⁽⁶⁵⁾ have also observed parallel lamellae running along the direction of crack growth in a high strength nickel alloy. They maintained that these were surface steps on highly reflective fracture facets. These facets were shown to be $\{111\}$ planes, and the cracks propagated in $\langle 110 \rangle$ directions. Replica electron microscopy showed a series of parallel narrow straight markings that make angles of approximately 60° to the steps. These markings correspond to traces of $\{111\}$ planes in the fracture facet and were attributed to slip occurring during the relaxation of the stress field at the crack front after the crack had passed.

2.2.1.4. Stage II Crack Propagation

This occurs at 90° to the maximum tensile stress and is of major engineering interest. In notched specimens, the time spent in Stage I is extremely small, and in the majority of engineering components failing by fatigue almost the whole of the fatigue process is spent in Stage II. The major feature of Stage II fracture surfaces is the existence of striations running perpendicular to the direction of crack propagation^(62,63). These striations occur on small plateaux, separated from one another by ridges. Forsyth and Ryder showed by programme loading experiments that each striation was produced by one cycle of stress⁽⁶⁶⁾. They also showed that the striation spacing increased as the stress increased. Two types of striations were distinguished in the work of Forsyth and his co-workers: ductile striations, in which the

spacing between the striations is narrow and there is no evidence of cleavage, and brittle striations in which cleavage fracture is thought to play an important part. These brittle striations show characteristic river markings running in the direction of crack propagation. This is discussed in section 2.2.2.2.

In high strain fatigue fine striations have been noted which run between and roughly parallel to the striations discussed above. It has been suggested that these are slip lines formed during plastic flow at the crack tip, and evidence has been presented to support this view⁽⁶⁷⁾.

There is little mention in the literature of the effect of grain boundaries and grain orientation on the direction of Stage II crack propagation. In most cases, it seems to be assumed that Stage II cracks propagate at 90° to the applied tensile stress, independently of grain orientation. Williams and Smith have, however, distinguished two types of Stage II crack propagation in β -brass⁽⁴⁷⁾. The initial mode of Stage II growth was described as "crystallographic". This was because the crack appeared to propagate along crystallographic planes, which were inclined at not more than 20° to the macroscopic crack propagation direction. River patterns similar to those observed on cleavage fracture were seen, and the plane of propagation changed direction at grain boundaries. Etch pitting showed that the fracture planes were either $\{100\}$ or $\{110\}$ planes, and x-ray diffraction showed that the surfaces were within 10° of the $\{110\}$ planes. Striations could be resolved towards the end of the "crystallographic" zone. When the rate of crack propagation increased

to $0.5 - 1\mu$ per cycle, the mode of crack propagation became "non-crystallographic" and the plane of fracture was normal to the applied tensile stress. The crack did not change direction at grain boundaries. It has recently been shown that α -titanium behaves in a similar manner⁽⁶⁸⁾.

2.2.2. MECHANISMS OF CRACK PROPAGATION

2.2.2.1. Stage I Crack Propagation

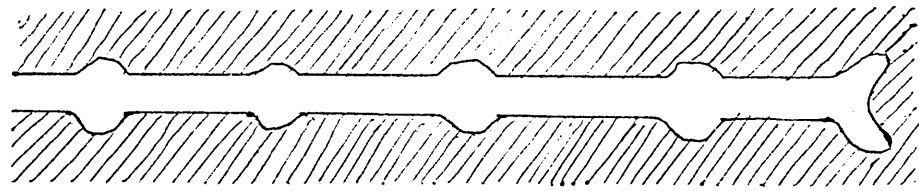
The majority of workers have considered Stage I crack propagation to occur by the same process as crack initiation. Any of the proposed initiation mechanisms could, therefore, be cited to account for this process. Kaplan and Laird have suggested two mechanisms by which Stage I crack propagation could occur⁽⁶⁹⁾. The first is a modification of Laird's "plastic blunting process" (see section 2.2.2.2.) in which slip occurs on one slip band only. The second is based on an unslipping process. During the tensile half-cycles shear occurs, and the distance from the specimen surface to the crack tip on one side of the crack increases. During the compression half-cycle, the original crack geometry is recovered, except that the crack has grown by a small increment.

Laird's evidence for the occurrence of the plastic blunting process in Stage I crack propagation⁽⁶⁷⁾ is that Williams and Smith observed striations towards the end of the "crystallographic" mode of crack growth in β -brass. However, this "crystallographic" crack propagation was in fact a type of Stage II propagation, and therefore, no real evidence of the occurrence of this process in Stage I propagation has yet been presented.

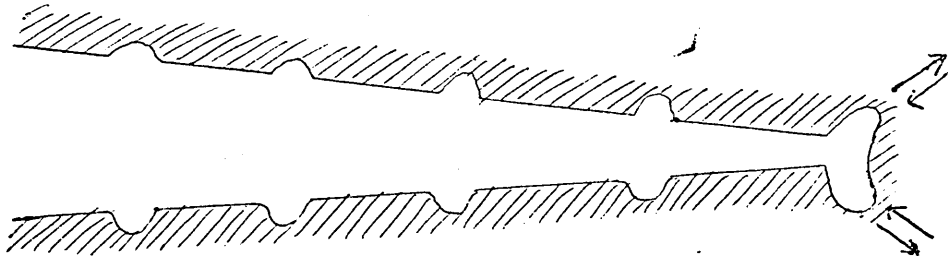
2.2.2.2. Stage II Crack Propagation

According to Forsyth⁽⁷⁰⁾ there are two mechanisms of Stage II crack propagation, depending on whether "ductile" or "brittle" striations are produced. For a ductile striation, the mechanism is as follows : at low stresses in the tensile half-cycle screw dislocations operate on a plane running lengthwise along the crack root, and the crack is extended by an unslipping process. As the stress rises, cross-slip occurs and rapid blunting of the crack tip occurs because slip operates on many parallel planes. For brittle striations, cleavage occurs along a (100) plane until crack tip blunting takes place by dislocation cross slip to accommodate the curvature of the crack front. A slight crack extension then occurs at 45° , but this is very insignificant compared to the large amount of cleavage fracture which takes place. Forsyth's mechanisms do not clearly account for the effect of stress reversal, except that he suggests the compression half-cycle will result in resharpenering of the crack tip, and a reversal of the residual stresses present there.

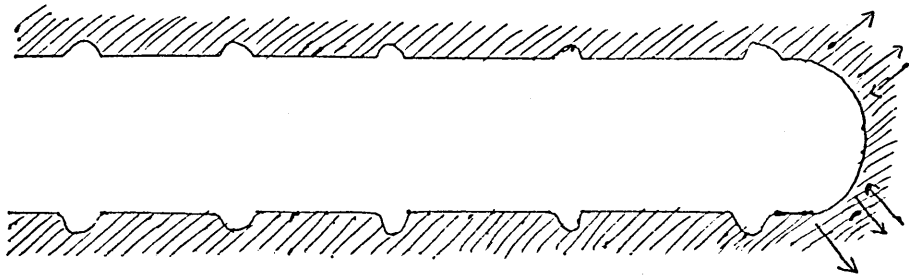
The most detailed treatment of Stage II crack propagation has been given by Laird, who has proposed a mechanism for fatigue crack propagation known as the "plastic blunting process"⁽⁶⁷⁾. This is shown schematically in Fig. 2. At zero load, the crack has the appearance shown in Fig. 2a. As the tensile load is applied, slip is concentrated in zones along planes at 45° to the direction of crack propagation (Fig. 2b). At the maximum tensile load, the crack tip blunts to the configuration shown in Fig. 2c. When compression occurs, the crack faces move together and



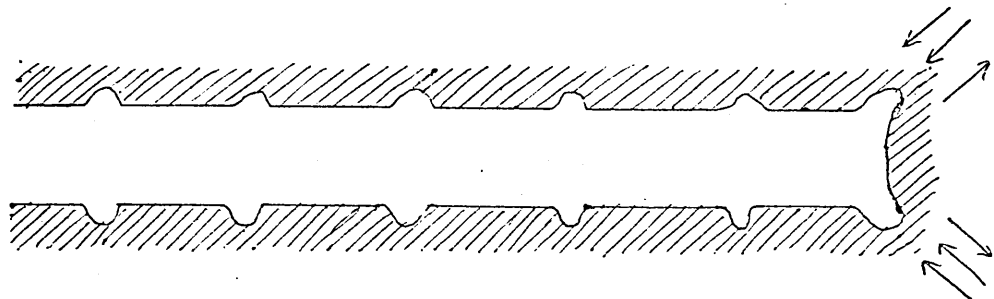
(a) zero load



(b) small tensile load



(c) maximum tensile load



(d) small compressive load

Fig. 2. The Plastic Blunting Process of Fatigue Crack Propagation (after Laird⁽⁶⁷⁾)

the new blunted crack tip surface created in tension is forced into the plane of the crack by buckling (Fig. 2d). At the maximum compressive load, the configuration shown in Fig. 2a reappears, and the cycle is then repeated.

Laird states that it is unlikely that cleavage plays a part in fatigue crack propagation, since the conditions under which cleavage striations have been observed do not produce cleavage fracture in unidirectional deformation. Also, when FCC metals fail by cleavage, (111) is the cleavage plane, and not (100). If crack propagation is by the plastic blunting mechanism, and slip occurs on (111) planes of an FCC metal, then the resultant plane of crack propagation would be (100).

Laird considers that the ridges which separate the plateaux on which the striations appear are caused by asymmetry of the residual notch left at a closed crack tip in compression. Along some lengths of the crack front, the part of the notch below the overall crack plane will be the more prominent, whereas the opposite will occur along the rest of the crack front. Plastic relaxation in the tension half-cycle will be concentrated in the most prominent of the two parts of the notch, and this will cause the crack plane to diverge onto different levels with a shear step in between.

The plastic blunting process predicts that peaks on one side of the crack should match up with peaks on the other side of the crack, and troughs should match up with troughs. This morphology has in fact commonly been noted. However, the opposite case, namely peaks matching up with troughs has also been reported, but in this case small cracks are

often seen undercutting the ridges on the fracture surface. This type of striation is formed when the orientation of the crystal with respect to the stress axis at the crack tip is such that the two parts of the notch remaining at the crack tip during the compression half-cycle are asymmetrical. During the tension half-cycle, the most advanced notch will propagate, and the other notch appears as an undercutting crack.

2.2.3. ANALYSIS OF CRACK PROPAGATION MEASUREMENTS

2.2.3.1. Early Work

Frost and his co-workers studied the behaviour of fatigue cracks by both mechanical and physical methods with the object of determining :

- (a) the critical alternating stress required to propagate a crack of given length, and
- (b) the laws governing the rate of growth of a growing crack.

For a wide variety of materials, Frost⁽⁷¹⁾ showed experimentally that :

$$\sigma^3 a = C \dots\dots\dots (1)$$

where σ = nominal alternating stress

a = crack length

C = a constant which varies from material to material.

If $\sigma^3 a > c$, the crack would grow, whereas if $\sigma^3 a < c$, the crack would remain dormant. If the stress concentration factor at the root of a notch was high, a crack would be initiated, but would not propagate.

It was also shown⁽⁷²⁾ that the rate of growth of a

propagating crack was given by :

$$\frac{da}{dN} = ka \dots\dots\dots (2)$$

where $\frac{da}{dN}$ = rate of crack growth

k = a constant

Also $k = A\sigma^3$

Hence $\frac{da}{dN} = A\sigma^3 a \dots\dots\dots (3)$

The constant A varies from material to material and bears no relationship to the static mechanical properties or plain fatigue strengths of the materials. For some materials the constant depends on mean stress.

The above relationship holds only when crack growth is continuous. Frost noticed experimentally that, even on a macroscopic scale, this is not the case, and while the crack length is small, it is possible for the rate of growth to decrease, sometimes to zero, for quite prolonged periods before continuing to grow again at the expected rate.

Other crack propagation laws have been formulated by a number of workers, e.g. Head's law : (73)

$$\frac{da}{dN} = \frac{C_1 \sigma^3 a^{\frac{3}{2}}}{(\sigma_y - \sigma) w_0^{\frac{1}{2}}} \dots\dots\dots (4)$$

where C_1 depends on the static mechanical properties of the material.

σ_y = the yield strength of the material.

w_0 = size of plastic zone near crack tip
(assumed to be constant)

Paris and Erdogan (74) have shown that if one plots the same crack propagation data on various axes, e.g. $\frac{1}{a^2} v.N$ for Head's law (integrating equation 4 gives $-\frac{2}{a^2} = DN+C$ where D&C are constants), or $\log a v.N$ for Frost's law,

straight lines can be drawn through portions of the data, but the slopes of these lines vary greatly with applied stress. According to the early method of verifying crack propagation laws, i.e. plotting data from single test specimens, the laws all accounted for observed data! It has since been suggested that to verify adequately a crack propagation law, a clear trend should be established using data from several specimens at different stresses plotted on the same graph.

2.2.3.2. Fracture Mechanics Approach

Irwin⁽⁷⁵⁾ suggested that the effect of the external load and the geometrical configuration on the intensity of the total stress field around a crack tip could be expressed as a "stress intensity factor", K . It was reasoned by Paris⁽⁷⁶⁾, that this factor should also control the rate of fatigue crack propagation, i.e. :

$$\frac{da}{dN} = f(\Delta K)$$

where K is the stress intensity range.

Many workers have proposed a simple power law, i.e. :

$$\frac{da}{dN} = A.(\Delta K)^n$$

where A and n are constants.

Since $\log \frac{da}{dN} = n \log \Delta K + \log A$.

then a plot of $\log \frac{da}{dN}$ v. $\log \Delta K$ should give a straight line of slope n . It has been shown that a straight line is indeed obtained by this method, even when data from tests at a number of stress levels are plotted on a single graph.

The stress intensity factor for a crack growing in a single edge notched specimen tested in tension is

$$K = \frac{Y.P. \sqrt{a}}{BW}$$

where P = applied force

B = breadth of specimen

W = width of specimen

a = crack length

where Y can either be determined experimentally or calculated from the relation of Gross et al⁽⁷⁷⁾

$$Y = 1.99 - 0.41\left(\frac{a}{W}\right) + 18.70\left(\frac{a}{W}\right)^2 - 38.48\left(\frac{a}{W}\right)^3 + 53.85\left(\frac{a}{W}\right)^4$$

Pulsating tension tests carried out on various carbon - manganese steels⁽⁷⁸⁾ showed that the rate of fatigue crack propagation was proportional to some function of the stress intensity range, but that the relationship consisted of two branches. For the upper branch, it was found that :

$$\frac{da}{dN} = c(\Delta K)^m$$

where c and m were functions of the yield stress

The lower branch of the $\log \frac{da}{dN}$ v. $\log \Delta K$ plot had a steeper gradient, and the position of the change in slope was stress dependant. No change in mechanism was noted at this position.

Broek⁽⁷⁹⁾ working on aluminium-zinc and aluminium-copper alloys showed a departure from linearity of the $\log da/dN$ v. $\log \Delta K$ curve at both low and high stress intensities, giving an S-shaped curve. He considered that at high stress intensities static tearing was taking place, and at low stress intensities the crack was "still in the initiation stage".

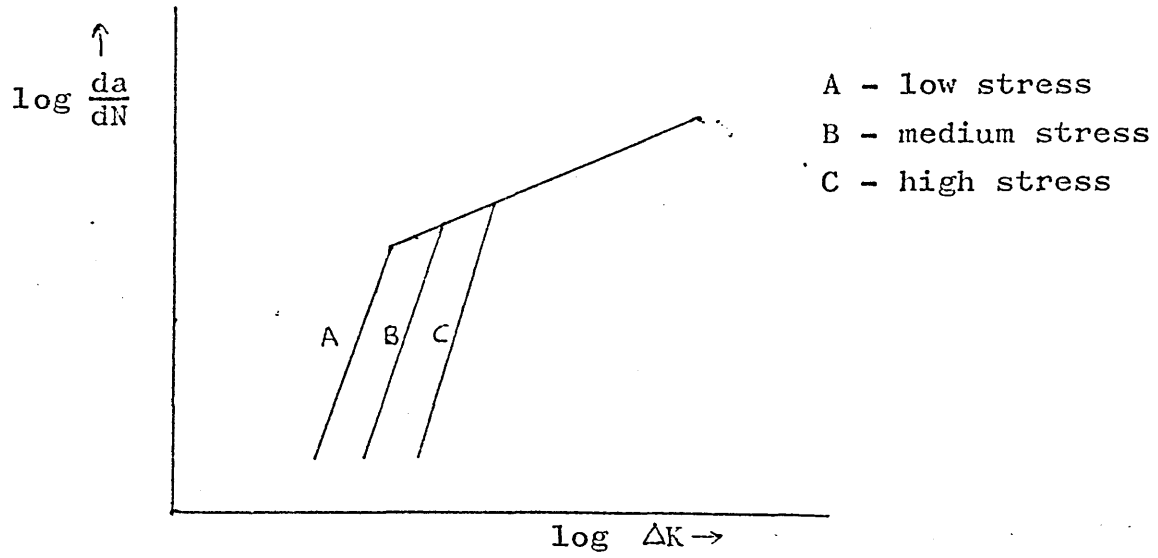


Fig. 3. Diagrammatic Representation of Results of Crack Propagation Measurements on Carbon-Manganese Steels (after Gurney (78)).

3. EXPERIMENTAL METHOD & MATERIALS USED

3.1 EXPERIMENTAL MATERIALS

3.1.1. CHEMICAL COMPOSITION

The materials used in the investigation consisted of a "pure" iron, and steels containing 0.01, 0.1 and 0.4% carbon (nominal). The compositions are shown in table I.

TABLE I. COMPOSITIONS OF EXPERIMENTAL MATERIALS

| MATERIAL | C | Si | Mn | S | P | Ni | Cr | Mo | Cu | O | N |
|----------|------|------|------|------|------|------|------|------|------|------|-------|
| A | .008 | .005 | .005 | .007 | .003 | .008 | .005 | .002 | .007 | .029 | - |
| B | .01 | <.01 | .42 | .022 | .032 | .10 | .018 | .030 | .09 | .012 | .004 |
| E | .11 | <.01 | .39 | .018 | .007 | .11 | .012 | .028 | .06 | .008 | .004 |
| F | .41 | <.01 | .40 | .018 | .008 | .11 | .015 | .025 | .07 | .003 | .003 |
| G | .011 | .012 | .51 | .016 | .025 | .12 | .02 | .02 | .10 | .009 | .003 |
| H | .125 | <.01 | .42 | .018 | .008 | .11 | .017 | .025 | .06 | .007 | .0035 |
| J | .40 | <.05 | .34 | .016 | .006 | .09 | <.03 | <.03 | .08 | .006 | .003 |

3.1.2. PREPARATION

Materials A, B, E, F, G and H were supplied by the British Iron and Steel Research Association, and were vacuum melted and rolled into strip of cross-section 3" x $\frac{3}{8}$ " (76 x 9.5mm). Material J was vacuum melted by G.I. Willan and Co. Ltd., and rolled into strip of cross section 3" x 1" (76 x 25mm) by BISRA.

After the fatigue specimens had been machined (section 3.2.1.) they were annealed for 30 minutes in a vacuum furnace. The furnace could be moved on rollers whilst the work tube remained stationary, to give a mean cooling rate of 33°C per minute from 900 to 600°C. The annealing temperatures are shown in Table II. The 0.41%C steels (F&J) were used without further heat treatment. The 0.01 and 0.11%C materials

(B, E, G and H) were subjected to a sub-critical anneal of 33½ hours at 200°C, in order to precipitate carbon from solution.

TABLE II. ANNEALING TEMPERATURES

| <u>MATERIAL</u> | <u>A</u> | <u>B</u> | <u>E</u> | <u>F</u> | <u>G</u> | <u>H</u> | <u>J</u> |
|-------------------------|----------|----------|----------|----------|----------|----------|----------|
| <u>TEMPERATURE (°C)</u> | 940 | 930 | 900 | 830 | 930 | 900 | 830 |

3.1.3. MICROSTRUCTURE

Fig. 4 shows photomicrographs of the materials used.

The iron (material 'A') consisted of ferrite grains, with numerous inclusions, which were probably iron oxide, both within the grains and at grain boundaries.

The 0.01% carbon steels ("B" & "G") consisted of ferrite grains, with small amounts of grain boundary cementite. There was also a cementite precipitate within the grains.

The 0.11 and 0.41% carbon steels consisted of ferrite and coarse pearlite. A certain amount of pearlite "banding" was present. It is extremely difficult to remove this by heat treatment, and it was decided to accept these materials in this form.

Table III shows the grain sizes and percentages of pearlite for the seven materials. The grain sizes were determined by lineal analysis, and the pearlite percentages by using a Metals Research "Quantimet" quantitative television microscope.

TABLE III. GRAIN SIZES AND PEARLITE PERCENTAGES

| <u>MATERIAL</u> | <u>FERRITE GRAIN SIZE (mm)</u> | <u>PERCENT PEARLITE</u> |
|-----------------|--------------------------------|-------------------------|
| A | .092 | - |
| B | .042 | - |
| E | .024 | 6 |
| F | .017 | 38 |
| G | .061 | - |
| H | .020 | 7 |
| J | .019 | 37 |

3.1.4. TENSILE PROPERTIES

Tensile tests were carried out in an Instron Universal Testing Machine using small specimens with a gauge length of 1" (25.4mm) and a cross-sectional area of .0625sq.in. (40.3mm²). The results are shown below :-

TABLE IV TENSILE PROPERTIES

| MATERIAL | YIELD STRESS tsi (MN/m ²) | | U.T.S. tsi (MN/m ²) | ELONGATION % | REDUCTION IN AREA % |
|----------|--|-------|------------------------------------|-----------------|---------------------------|
| B | 9.7 | (148) | 19.2 (297) | 75 | 80 |
| E | 14.6 | (225) | 22.1 (341) | 60 | 65 |
| F | 14.4 | (222) | 30.9 (477) | 40 | 45 |
| G | 10.4 | (161) | 19.8 (306) | 65 | 60 |
| H | 13.5 | (208) | 23.5 (363) | 55 | 50 |
| J | 14.7 | (227) | 29.9 (462) | 45 | 33 |

The yield stresses of materials F and J (0.41%C) were low when compared with the lower carbon materials. This is discussed in section 4.2.1.

The fracture surfaces of the tensile specimens were examined on the scanning electron microscope. All consisted entirely of ductile fracture. Equiaxed dimples were observed in all specimens (Fig. 5) and no intergranular failure was observed.

3.2. FATIGUE TESTING

3.2.1. SPECIMENS

Two types of specimen were used in the experiments, a plain one for crack initiation work, and a notched one for crack propagation work. The dimensions of these are shown in Fig. 6. The specimens were machined and rough ground

before heat treatment (see section 3.1.2.). After heat treatment all specimens were ground on successive grades of wet silicon carbide paper down to 600 grit. The specimens for initiation work were then electropolished in a bath of the following composition :

| | |
|-------------------------------------|-------|
| Glacial Acetic Acid 99.5 wt. % min. | 133ml |
| CrO ₃ | 25g |
| H ₂ O | 7ml |

Only the gauge length and the parts immediately beyond it were polished, the rest of the specimen being blanked off with "Lacomit". The electropolishing was carried out at a temperature of 20°C and at 20.5 volts. The time of polishing was half an hour, about .01mm being removed from the specimen surface. The test pieces for propagation work were not electropolished, but were finally mechanically polished with 6 micron and 1 micron diamond compound.

3.2.2. TESTING PROCEDURE

All fatigue tests were carried out in alternating tension and compression at zero mean stress on a 2 ton Amsler "Vibrophone". The frequency of testing was 185 cycles per second. During the test, the mean stress tended to show a slight drift into tension of about 0.25 t.s.i. (3.8MN/m²) but in the later propagation tests, an automatic mean load maintainer became available, so that zero mean stress could then be maintained through the test. This slight drift into tension is not thought to have significantly affected the results.

3.2.3. CRACK PROPAGATION MEASUREMENTS

Direct measurements of the progress of the propagating cracks in the notched specimens were made using two Vickers

travelling microscopes, one on each side of the specimen under test (Figs. 7 & 8). On the early work, only one set of measurements was taken, but since sloping crack fronts were sometimes obtained, it was thought desirable to record crack propagation on both surfaces. The interval between successive readings was determined by the observed rate of crack propagation, but was generally of the order of 5000 cycles.

3.3. EXAMINATION OF SPECIMENS

Observations of fatigue damage and crack initiation on the surfaces of the plain specimens were first made using the optical microscope. Replica electron microscopy was also carried out using two stage cellulose acetate - carbon replicas. Cellulose acetate sheet, .002" (.05mm) thick, was softened in acetone and applied to the specimen surface. When this had dried, it was stripped off, and then shadowed with platinum - carbon in a vacuum evaporating unit, at an angle of 30° to the specimen surface. Carbon was then evaporated on to this, and the cellulose acetate dissolved away in acetone. Considerable difficulty was experienced at this stage due to the expansion of the cellulose acetate causing the carbon film to break up. The two stage method was used so that the specimen surfaces could be preserved.

A "Stereoscan" scanning electron microscope became available later and this was also used for surface observations.

Taper sections were prepared for optical examination. The specimens were first nickel plated to preserve the specimen surface topography, and sections were prepared at an angle of $11\frac{1}{2}^{\circ}$ to the surface. This gave a taper

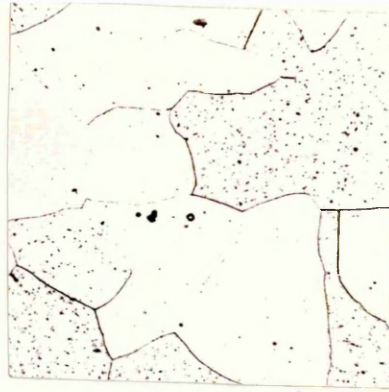
magnification of 5x. This magnification was chosen because it was thought that it would be high enough to give a clear picture of the phenomena occurring on the surface of the specimen, but would not be so high as to cause errors of interpretation to be made.

The fracture surfaces of the crack propagation specimens were examined by the naked eye, and by means of the scanning electron microscope. This information was supplemented by observation of cross-sections through the cracked specimens.

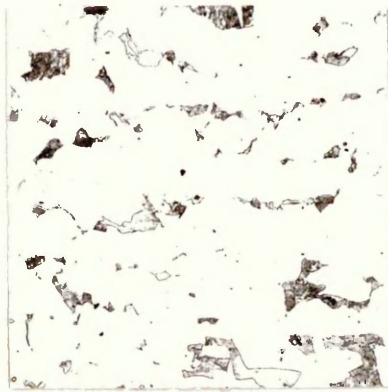
Note : arrows on photographs indicate the stress axis in the case of plain specimens, and the direction of crack propagation in the case of notched specimens.



0.01%C Material B



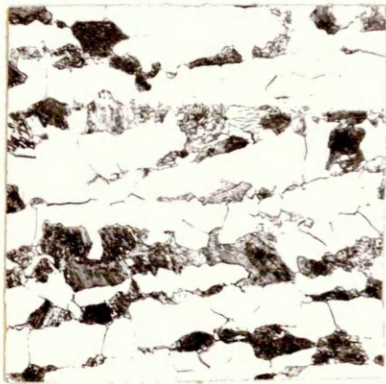
0.01%C Material G.



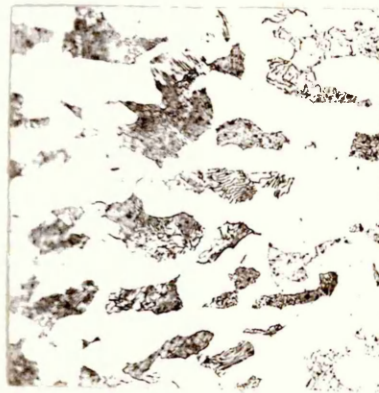
0.11%C Material E.



0.11%C Material H.

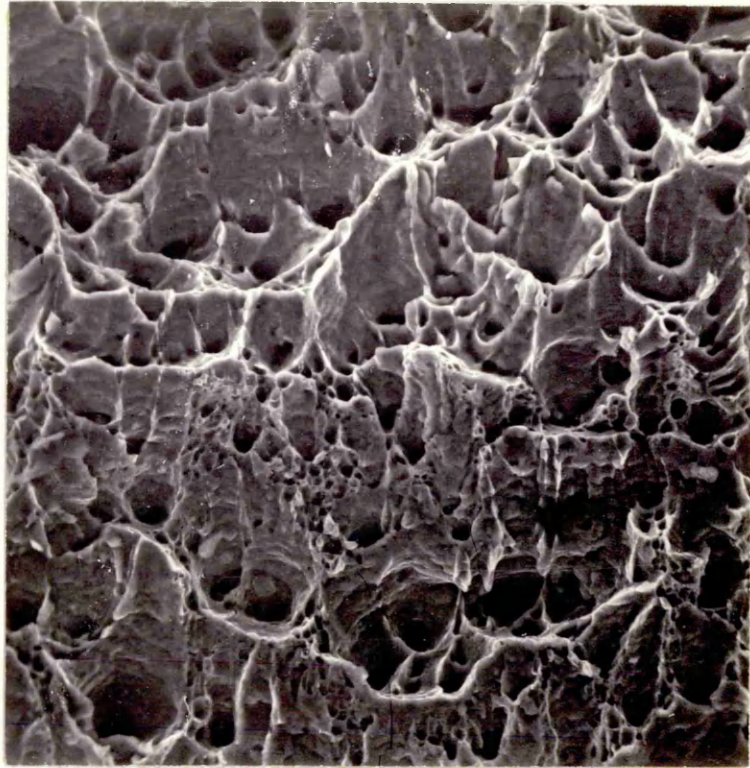


0.41%C Material J.



0.41%C Material F.

Fig. 4. Microstructure of Experimental Materials. X200



X 650

Fig. 5. Scanning Electron Micrograph of Fracture Surface of Tensile Specimen 0.01% Carbon Steel.

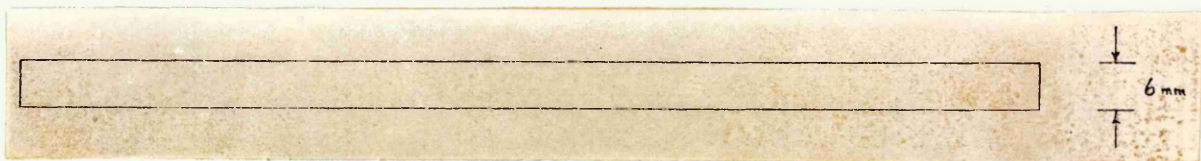
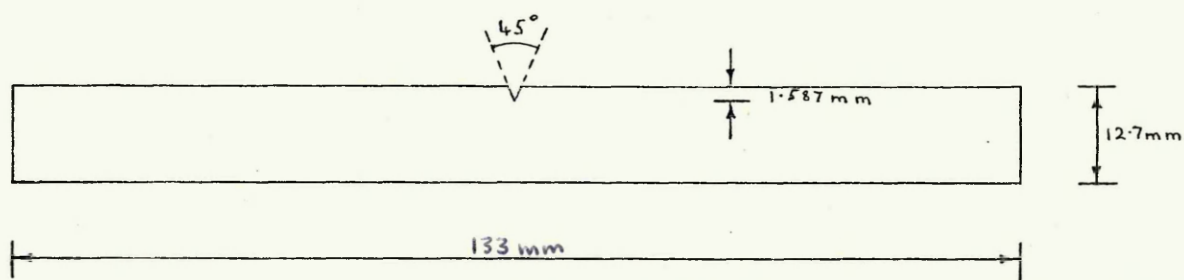
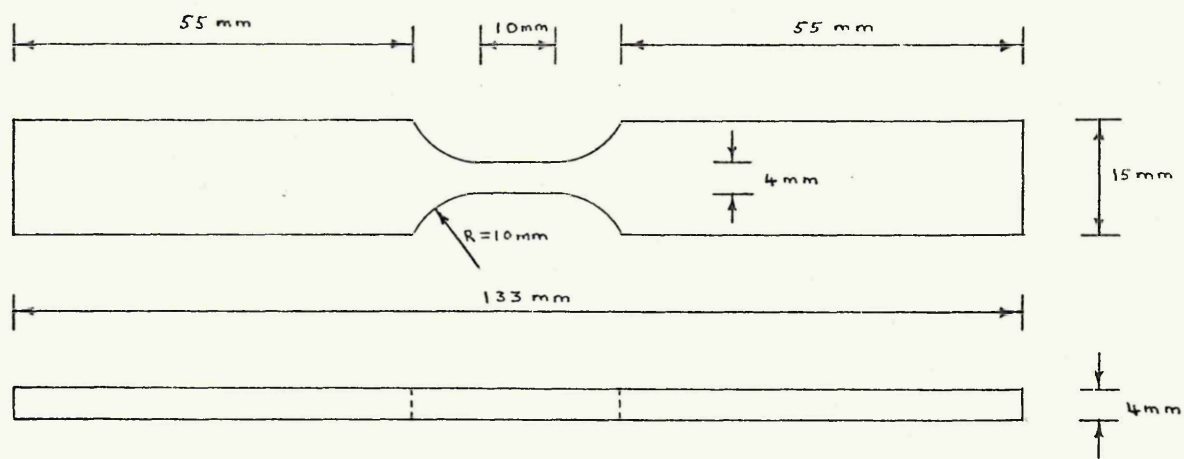


Fig. 6. Dimensions of Test Specimens.

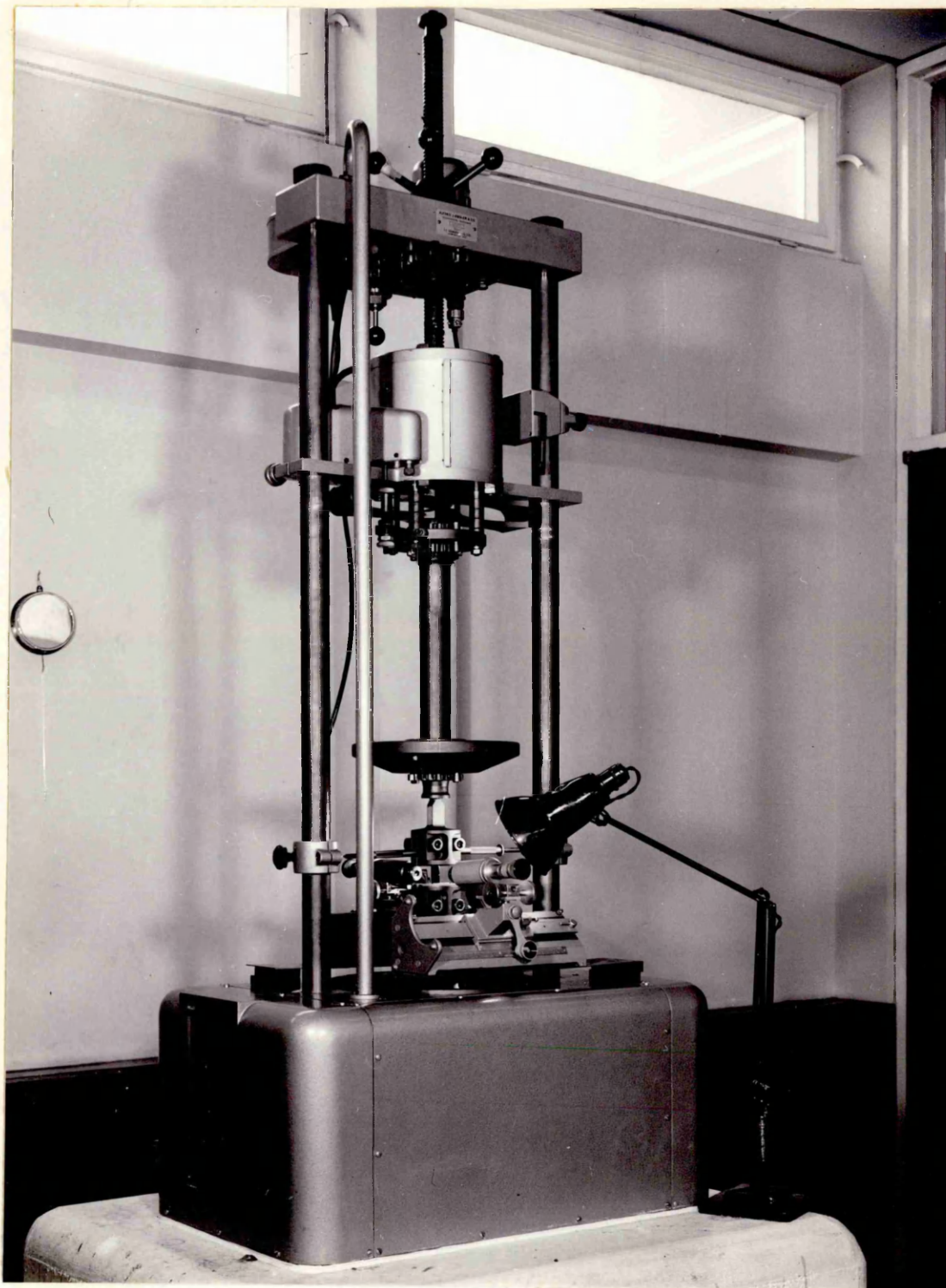


Fig. 7. Testing Arrangement Showing Amsler 2-ton Vibrophore.

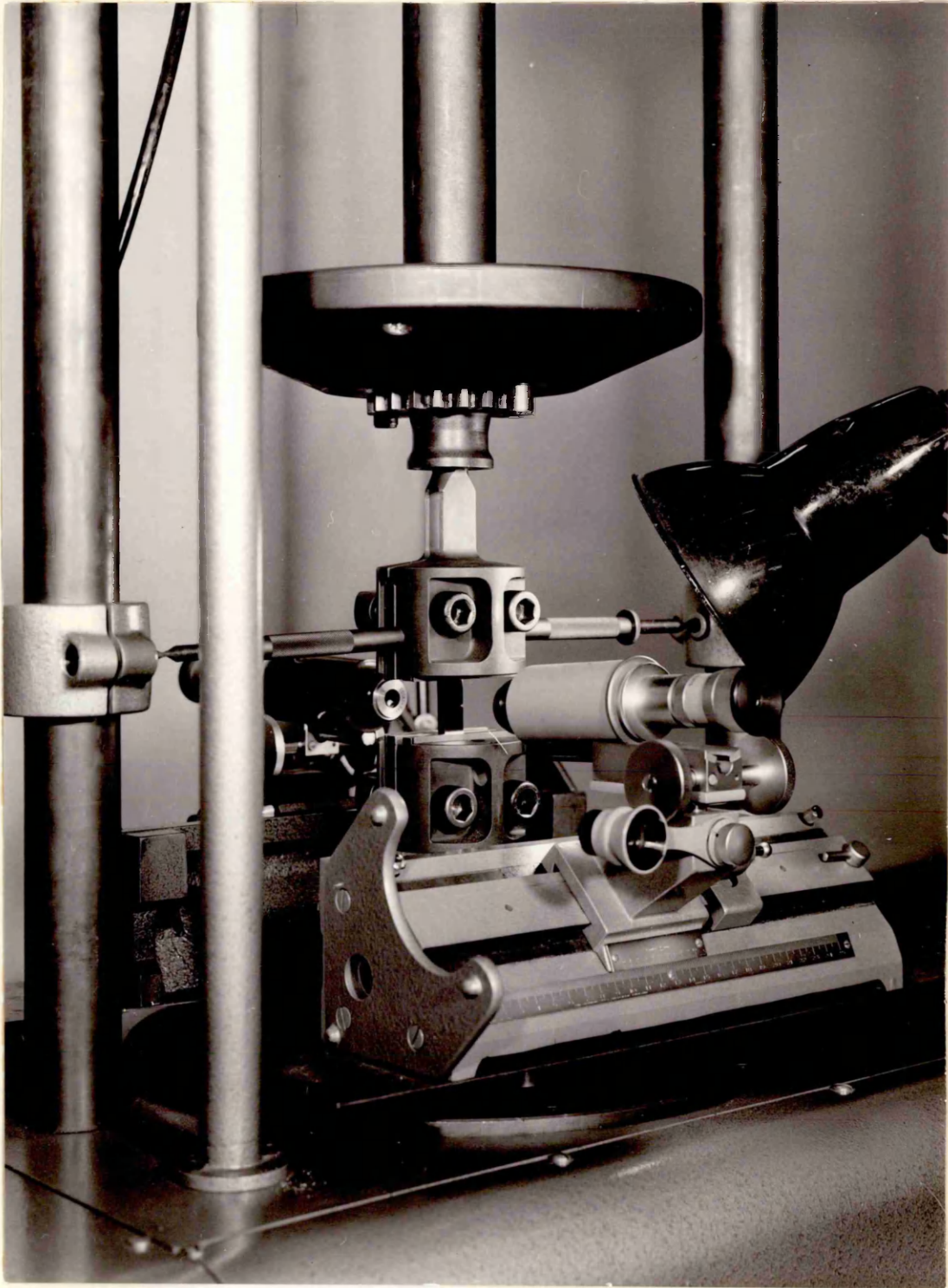


Fig. 8. Close-up of 2-ton Vibrophore Showing Notched Specimen and Travelling Microscopes.



4. EXPERIMENTAL WORK

4.1 PRELIMINARY WORK ON "PURE" IRON

Originally, it was intended to study the fatigue of pure iron, and then to proceed to the study of the plain carbon steels, in order to determine the effect of increasing amounts of pearlite on the fatigue process.

Tests were carried out in the as-rolled state, and after annealing at 940°C. In both cases, wavy slip bands which were very dark in appearance were noted, and crack propagation was intergranular. The appearance of the fatigue slip bands at low magnification, and the intergranular nature of the crack propagation is shown in Fig. 9. Fig. 10 is a higher magnification photograph and shows the diffuse appearance of the fatigue slip bands.

Rees, Hopkins & Tipler have shown that pure iron containing oxygen suffers from grain boundary embrittlement (80). It has also been shown by Tipler and Forrest that fatigue cracks in grain boundary embrittled iron are intergranular (81). The oxygen content of the pure iron used in this investigation was very high (.029%) and it was thought that this was probably the cause of the intergranular crack propagation. Because of the difficulty of obtaining a pure iron of lower oxygen content, it was decided not to continue the work on pure iron and to concentrate on the plain carbon steels. Work on intergranular cracking in iron has since been reported by Golland and James (41) and has confirmed the above results.

4.2 EXPERIMENTAL WORK ON CARBON-MANGANESE STEEL PLAIN SPECIMENS

4.2.1. TEST RESULTS

Semi-stress range - number of cycles to failure (S-N) curves for all uninterrupted fatigue tests carried out on the three materials used for the testing of plain specimens (F, G and H) are shown in Fig. 11. These curves were produced so that (a) estimates of percentage of life to failure could be made for specimens not taken to failure and (b) the approximate positions of the fatigue limits were known. The fatigue limits and fatigue ratios (fatigue limit/U.T.S.) for the three materials are as follows :

| MATERIAL | FATIGUE LIMIT TONS/SQ.IN. | (MN/m ²) | FATIGUE RATIO |
|------------|------------------------------|----------------------|---------------|
| F (0.41%C) | 10.6 | (164) | 0.34 |
| G (0.01%C) | 8.45 | (131) | 0.43 |
| H (0.11%C) | 10.35 | (160) | 0.44 |

It can be seen that there is a discrepancy in the fatigue ratio, as far as material "F" is concerned. Material "F" also has a low yield stress for its carbon content when compared with materials G and H. It is considered that the reason for this was the difference in heat treatments mentioned in section 3.1.2. A low temperature heat treatment causes carbide precipitation and will promote dislocation locking, which will in turn increase the yield stress. Oates and Wilson⁽⁵³⁾ have shown that this initial dislocation locking raises the fatigue limit of low carbon steels which have fatigue limits below the yield stress,

thus explaining the effect observed in this work.

4.2.2. THE DEVELOPMENT OF SURFACE FATIGUE DAMAGE

Examination of the polished surfaces of the fatigued specimens showed that the general surface appearance consisted of dark irregularly shaped areas of fatigue deformation separated by damage - free areas. The areas of fatigue deformation often bore no relation to grain shape. Although they often stopped at grain boundaries, they also sometimes crossed grain boundaries. This type of deformation occurred on all specimens examined. There did not appear to be any marked difference in the type of fatigue damage formed in the three materials. The proportion of the surface on which fatigue damage occurred increased with increasing stress amplitude. This is shown in Fig. 12, which compares three specimens of 0.11% carbon steel fatigued to failure at different stress levels. Fig. 13 shows parts of the same areas of fatigue damage at higher magnification.

The darkening of the surface slip bands is thought to be due to a thin film of oxide on the surface. The oxide showed interference colours in the early stages of the tests, changing to a dark appearance as the test progressed. It is thought that this is due to oxidation of the active newly generated surfaces in the slip bands.

Examination of carbon replicas taken from the surface of fatigued 0.41% carbon steel specimens showed that the fatigue damage consisted of wavy slip bands, which were rather shallow and which did not appear to exhibit the very sharp notch-peak topography which is characteristic of many FCC metals. The type of surface damage observed is shown in

figs. 14 and 15. The surface in these regions of fatigue damage was of a rather undulating character.

Scanning electron microscopy of specimen surfaces confirmed the replica observations as far as the type of surface fatigue damage was concerned (Fig. 16). Fig. 16A also shows a grain boundary crack (section 4.2.4.).

Fatigue damage almost invariably occurred in the ferrite grains. Very occasionally, a small amount of damage could be seen in the ferrite of the pearlite, but this was rather exceptional. Examination of taper sections confirmed this. Fig. 17 shows a surface notch-peak topography in a ferrite grain, with the surfaces of the adjacent pearlite colonies remaining quite flat.

The taper sectioning showed clearly the phenomena occurring in the surface slip bands. To demonstrate the effect of stress amplitude, three specimens of the 0.11% carbon steel tested at different stresses were examined (Fig. 18). The specimen tested below the fatigue limit showed only short extrusions and intrusions. In contrast, the two specimens tested above the fatigue limit showed much larger notches and peaks in those grains where damage was being produced. The maximum height of these peaks was of the order of $1\frac{1}{2}\mu$.

4.2.3. THE SPREAD OF PLASTICITY DURING FATIGUE

Oates and Wilson⁽⁵⁵⁾ proposed that the spread of plasticity was the controlling factor in deciding whether a plain fatigue specimen would fail or not. If appreciable numbers of fatigue damage clusters beyond a certain size (extending over several grains) were not formed, the specimen

would not fail. To investigate the validity of this concept for a material with a greater pearlite content than Oates and Wilson's 0.1% carbon steel, two 0.41% carbon steel specimens were examined at regular intervals during fatigue testing, and counts were made of the proportion and size of areas of fatigue damage. The results are shown in Figs. 19 and 20, which show the variation in the number of surface grains containing fatigue damage with endurance. Different curves are shown for single grains, clusters of 2 or 3 grains, clusters containing 4 or more grains and the total number of damaged grains. It can be seen from the graphs that in the higher stress specimen (F12), the total number of damaged grains gradually increased as the test progressed, until at approximately 50% of the life 30% of all grains contained surface damage. At 11% of the life (10^5 cycles), the majority of the fatigue damage consisted of clusters of fewer than 4 grains. Above 11% of the life, the size and number of fatigue damage clusters gradually increased, until at 50% of the life the majority of these clusters contained 4 or more grains. At failure, about 40% of all grains contained surface damage. The lower stress specimen (F16) showed an initial amount of fatigue damage at 7% of the life, which had not apparently changed after 85% of the life. There was then a sudden increase and the specimen failed. Examination of the failed specimen showed that the area adjacent to the fracture contained a large number of grains containing fatigue damage, but the rest of the specimen showed no increase in the number or size of fatigue damage areas.

4.2.4. SLIP INTENSIFICATION AT GRAIN BOUNDARIES

In all specimens, a certain amount of slip intensification was noted at grain boundaries. Fig. 21 shows an example of this effect at various percentages of the life of a 0.01% C steel specimen. At 2% of the life, the appearance was certainly that of a crack with a small amount of slip in each adjacent grain. At 10% of the life, however, the slip bands at right angles to the grain boundary were more apparent, and grain boundary extrusions were visible. These had a metallic appearance. At failure, both the intensity of slip and the size of the extrusions had increased.

In observations using the optical microscope, grain boundary slip intensification was easily confused with grain boundary cracking, especially at low percentage lives. To resolve this phenomenon, an area which showed this black grain boundary appearance on the optical microscope was observed on the Stereoscan. This is shown in Fig. 22, which compares optical and stereoscan photographs of the same area of a 0.11% carbon steel specimen which had been fatigued for 10% of its expected life. Although a crack appears to be present under the optical microscope, the Stereoscan clearly shows this to be an area of intense slip. Deformation has occurred adjacent to the boundary in both grains, so that there is a depression in the left-hand grain, and a peak in the right-hand grain.

Grain boundary slip intensification is also shown in Fig. 25, section 4.2.5. In this case a "cliff edge" has been formed at the grain boundary.

Taper sectioning clearly showed that enhanced slip at

grain boundaries could lead to the formation of intrusion-extrusion pairs. This effect is shown in Fig. 23.

4.2.5. CRACK INITIATION

Two types of cracks could be distinguished on the surface of failed specimens, namely slip band cracks and grain boundary cracks.

It was very difficult to distinguish slip band cracks under the optical microscope, owing to the dark surface oxide film which covered most of the fatigue damage regions. Thin black lines could be observed in these areas (Fig. 24) but it was not possible to say whether these were cracks or not. However, examination of areas of fatigue damage under the scanning electron microscope showed clearly that slip band cracking did occur (Figs. 25 and 26). Slip band cracks were also observed in taper sections (Fig. 27).

Certain specimens tested above the fatigue limit showed grain boundary cracks. One of these is shown in Fig. 28. However, as mentioned earlier, it was quite possible that this could just have been another case of grain boundary slip intensification. However, when this specimen was repolished, although it was difficult to find the area depicted in Fig. 28 again, a clear case of grain boundary cracking was revealed (Fig. 29). These cracks were often seen near to the main crack, and it is possible that these might have been a consequence of the high stress in the region around the advancing crack front. A grain boundary crack in a taper section is shown in Fig. 30.

Fig. 31 shows a scanning electron micrograph of a grain boundary crack which was seen in an area near to the main crack. The crack separates a grain in which much surface

fatigue damage has occurred from one in which there has been little damage. This is similar to Fig. 16A.

4.2.6. SURFACE CRACK PROPAGATION

Examination of the surface fatigue cracks showed that propagation occurred in a mixed transgranular - intergranular manner. When transgranular propagation occurred, the microscopic direction of crack propagation was irregular, and not straight as in a cleavage crack. Grain boundary propagation occurred when the boundary was suitably orientated with respect to the stress axis.

On virtually all the specimens examined, only one large crack was present at failure and this usually initiated at one of the specimen corners. However, on one side of one of the 0.01% carbon steel specimens, a large secondary crack was present, the appearance of which is shown in Fig. 32. It would seem that the feature in the centre consisted of two slip band cracks. This specimen was repolished and etched to show up the shape of the crack in relation to the grain structure. It can be seen that these two cracks have occurred on parallel planes in a single grain. Forking of the main crack had occurred at both ends. In Fig. 32B it can be seen that the direction of forking at the left-hand side is away from the slip band cracks. Observation earlier in the repolishing process also showed that this was also the case on the right-hand side of these cracks. It is, therefore, reasonable to assume that this crack originated at these slip band cracks.

4.2.7. INITIATION OF MAIN CRACKS & STAGE I PROPAGATION

In order to determine whether the fatigue cracks which

led to final failure were initiated at slip bands or grain boundaries, certain specimens of all three materials were broken open, and the fracture surfaces examined to determine the point of origin. Stereoscan examination was then carried out at this point. None of these specimens had fractures which had obviously initiated at a grain boundary. Fig. 33 shows the corner of a specimen at which a fracture originated. A distinct stage I fatigue zone can be seen at this point. Fig. 34 shows this origin from a different angle, and Fig. 35 shows this at higher magnification. It is rather difficult to decide whether the edge at "A" in Fig. 35 is a grain boundary. The edge at "B" is, however, definitely transgranular. On Fig. 36, which is a series of photographs taken at the same angle as Fig. 32 but at higher magnifications, line markings can be seen radiating away from the edge which corresponds to "B" in Fig. 35. It has been mentioned earlier (section 2.2.1.3.) that these lines run parallel to the direction of local crack propagation. Thus edge "B" is the likely crack initiation zone.

The general appearance of the stage I fracture near to the surface consisted of parallel slip band cracks. These seemed to converge onto one level at about one third of the way down the stage I area. Stage I fracture was not planar as has previously been reported for aluminium alloys⁽⁶³⁾, but appeared most irregular at high magnifications (Fig. 36).

Another Stage I fracture, this time in a 0.41% carbon steel is shown in Fig. 37. On this occasion, fracture did not start from a corner, but from the centre of one face of the specimen. Again, the lines parallel to the direction of

crack propagation could be seen at the specimen surface, but these tended to become less evident further away from the surface. The wavy nature of the propagating crack is clearly evident, and in the later stages the whole of the crack front appeared to change direction periodically.

4.3. EXPERIMENTAL WORK ON CARBON-MANGANESE STEEL NOTCHED SPECIMENS

4.3.1. TEST RESULTS

Endurance data from the crack propagation tests is shown in Table V (S-N diagrams have not been drawn, because the number of tests carried out on each material is not considered sufficient for these to be useful). "Endurance" denotes the number of cycles after which the test was stopped. Tests were stopped when the crack growth rate became too fast to follow accurately.

At the same time, the load could not be maintained without greatly increasing the power input to the machine.

The measured results for crack length v. number of cycles for all the specimens except B2, J1 and J2 are shown graphically in the appendix, Fig. A1. Specimens B3, J1 and J2 developed cracks in the area below the notch root, but these did not propagate.

Values of the slope, $\frac{da}{dN}$ of these curves at various points were obtained graphically and plotted against the calculated stress intensity range at such points, ΔK , on log-log graph paper. The results are shown in the appendix, Figs. A2-A4 for each material, and a composite plot for all three materials is shown in Fig. A5. There was considerable scatter in these results, the scatter in the results for individual materials being so large as to mask any possible effect of material on

the relationship. The slopes of the curves varied from approximately $\frac{1}{2}$ to $\frac{1}{3}$, giving a relationship of the form $\frac{da}{dn} \propto \Delta K^n$ where $n = 2$ to 3 .

TABLE V ENDURANCE OF CRACK PROPAGATION SPECIMENS

| SPECIMEN | STRESS | | ENDURANCE (cycles) |
|---------------|----------|----------------------|--------------------|
| | (t.s.i.) | (MN/m ²) | |
| <u>0.01%C</u> | | | |
| B1 | 5.15 | (80) | 1.3×10^5 |
| B2 | 3.80 | (59) | 1.6×10^7 |
| B4 | 5.65 | (87) | 2.3×10^5 |
| B5 | 4.00 | (62) | 4.7×10^5 |
| B6 | 4.70 | (73) | 4.8×10^5 |
| B10 | 4.25 | (66) | 4.6×10^5 |
| <u>0.11%C</u> | | | |
| E1 | 4.25 | (66) | 7.1×10^5 |
| E3 | 5.65 | (87) | 2.0×10^5 |
| E5 | 4.50 | (69) | 3.5×10^5 |
| E6 | 5.15 | (80) | 2.8×10^5 |
| E8 | 3.80 | (59) | 2.6×10^6 |
| E10 | 4.70 | (73) | 4.9×10^5 |
| <u>0.41%C</u> | | | |
| J1 | 3.30 | (51) | 1.4×10^7 |
| J2 | 2.83 | (44) | 1.9×10^7 |
| J5 | 5.65 | (87) | 1.6×10^5 |
| J6 | 4.70 | (73) | 5.7×10^5 |
| J7 | 3.80 | (59) | 1.3×10^6 |
| J13 | 5.65 | (87) | 1.7×10^5 |

4.3.2. STAGE II CRACK PROPAGATION

4.3.2.1. General

Observation of fracture surfaces on the scanning electron microscope showed that in the earlier part of Stage II crack propagation in all three materials, both transgranular and intergranular propagation occurred (Fig. 38). In the later stages, however, wholly transgranular propagation occurred (Fig. 39). The transgranular areas consisted of plateaux with edges running parallel to the local direction of crack propagation (Fig. 40). Characteristic fatigue striations which ran perpendicular to the local direction of crack propagation could be seen on top of the plateaux, and in the valleys between the plateaux. The plateaux sometimes tended to run together, to form one wider plateaux. Sometimes the opposite would occur, i.e. one plateaux would split into a number of narrower plateaux. Examination of stereo pairs showed that what appeared on one photograph to be plateaux were, in fact, hills and valleys which presented a curved appearance (Fig. 41). The spacing between fatigue striations was remarkably constant throughout the Stage II region, being of the order of $1 - 2 \times 10^{-4}$ mm for all three materials. On a number of specimens, fretting had occurred on the fracture surface producing rub marks and debris (Fig. 42). There was no problem in distinguishing between rub marks and striations.

4.3.2.2. Intergranular Fracture

The intergranular fractures were relatively featureless, apart from markings which resembled the slip lines seen on the surface of ferritic steels which have been subjected to unidirectional deformation (Fig. 43). Counts were carried

out of percentage intergranular fracture v. crack length for one specimen of each of the three steels. The results are shown below :-

| | <u>% INTERGRANULAR FRACTURE AT (mm)</u> | | | | | | | |
|--------|---|-----|-----|-----|-----|-----|-----|-----|
| | 0.5 | 1.0 | 1.5 | 2.0 | 2.5 | 3.0 | 3.5 | 4.0 |
| 0.01%C | 20 | 40 | 65 | 40 | 35 | 18 | 0.5 | 0 |
| 0.11%C | 10 | 12 | 18 | 14 | 6 | 1 | 0 | 0 |
| 0.41%C | 4 | 7 | 9 | 3 | 0 | 0 | 0 | 0 |

The 0.01 and 0.11% carbon steels showed more intergranular fracture than the 0.41% carbon steel. The percentage intergranular fracture showed an initial increase, and then decreased until a point occurred when the fracture became wholly transgranular. This effect occurred at all nominal stress levels in all three materials. During the first part of the stage II fracture, i.e. the part which contained the intergranular fracture the crack propagation path seemed to be structure sensitive, sometimes changing direction at grain boundaries. The latter part of the stage II fracture was structure insensitive, i.e. no clear indication of grain boundaries could be observed on the fracture surface, unless etching was resorted to.

4.3.2.3. Effect of Pearlite

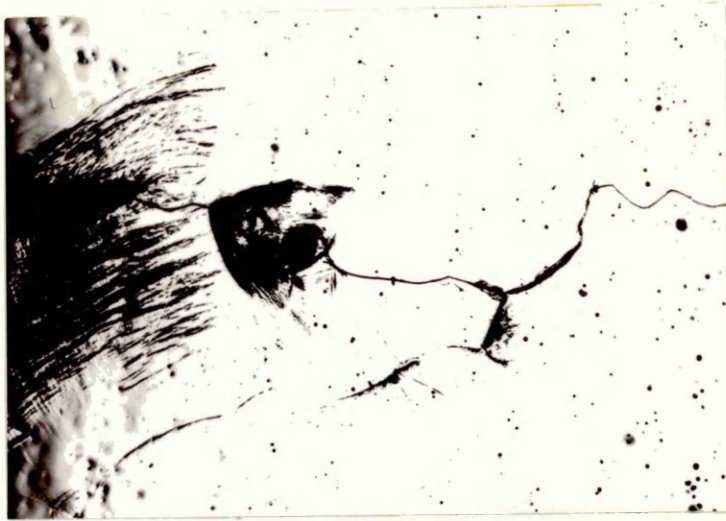
The effect of pearlite on the local direction of crack propagation was studied in both the 0.11 and 0.41% carbon steels by observation of cross-sections through the fracture (Figs. 44 and 45). Although, occasionally a crack would run down the interface between a pearlite colony and a ferrite grain, the crack usually cut through the pearlite colony. The actual mode of crack propagation through the pearlite

depended on the orientation of the cementite lamellae (Fig. 46). If this was approximately parallel to the direction of crack propagation, the crack propagated along the ferrite-cementite interface. If the orientation of the cementite was perpendicular to the crack propagation direction, the crack cut through both the ferrite and cementite as though no structure change was present. Some colonies showed a combination of these effects which gave rise to a step-like pattern. There was no tendency for the crack to avoid the pearlite colonies.

The appearance of both a fracture along a ferrite-pearlite interface and a fracture through a pearlite colony is shown in Fig. 47. This shows the fracture surface of a 0.41% carbon steel. Observation of stereo pairs showed that the crack had propagated along the ferrite-pearlite interface (A), and had then turned to propagate through the pearlite (B).

4.3.2.4. Branch Cracks

Direct observation of propagating cracks showed that a large amount of crack branching occurred in the later stages of crack propagation. This could be plainly seen on the scanning electron microscope (Fig. 48). Cross sections through the fractures, however, indicated that this crack branching also occurred early in the process, but that, as would be expected, the branch cracks were much larger and wider in the latter stages of Stage II crack propagation. An example of one of these cracks is shown in Fig. 49.



X 50

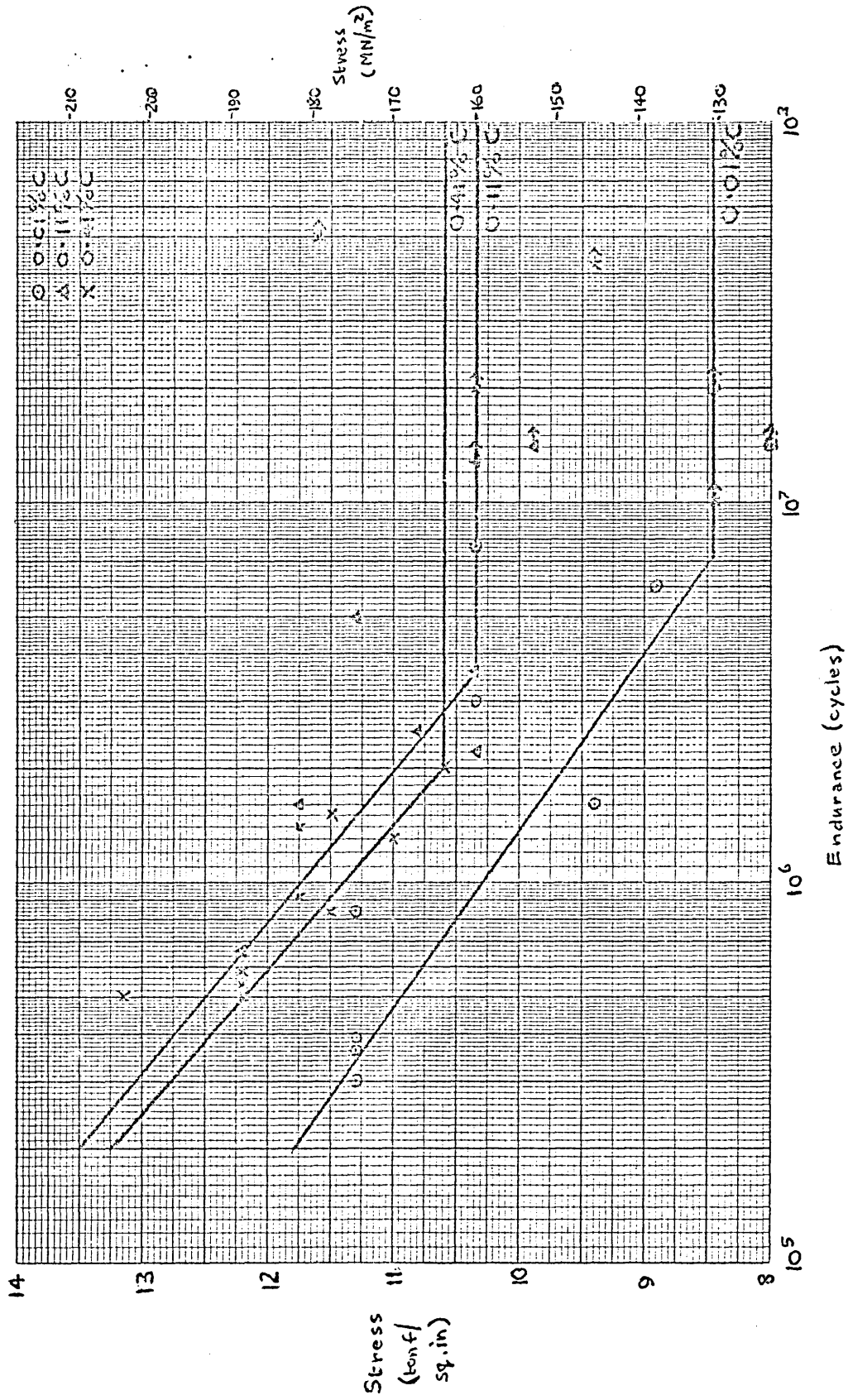
Fig. 9. Surface Damage and Intergranular Crack Propagation in Iron.



X200

Fig. 10. Surface Damage in Iron.

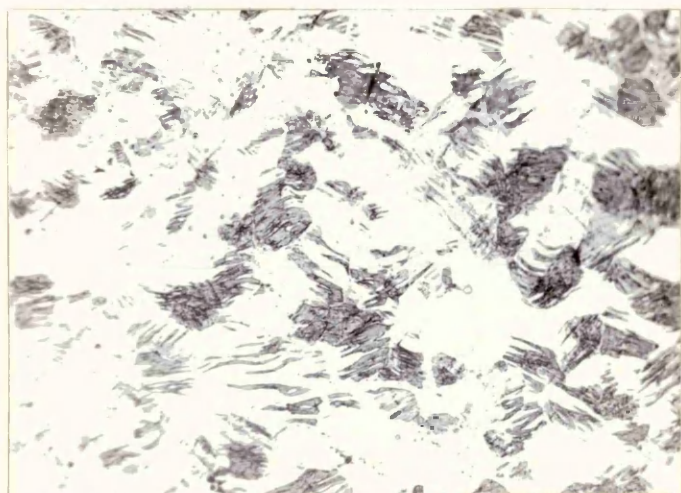
Fig. 11. S-N Curves for Plain specimens of 0.01, 0.11 & 0.41% Carbon Steels





Stress: 10.35 tons/sq.in.
(160 MN/m²)
Unbroken.

Stress: 10.8 tons/sq.in.
(167 MN/m²)
Endurance: 2.6 x 10⁶ cycles.



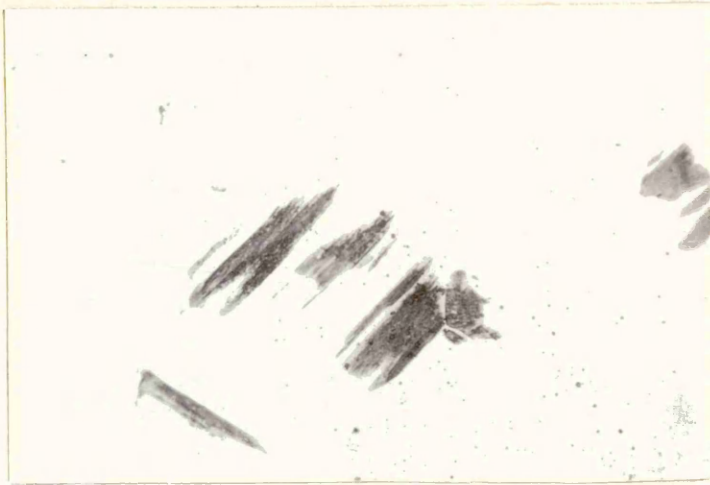
Stress: 11.75 tons/sq.in.
(181 MN/m²)
Endurance: 1.16 x 10⁶ cycles.

Fig. 12

x 200

Effect of Stress Amplitude on the Appearance of Surface Fatigue Damage in 0.11% Carbon Steel.

Stress: 10.35 tons/sq.in.
(160 MN/m²)
Unbroken.



Stress: 10.8 tons/sq.in.
(167 MN/m²)
Endurance: 2.6 x 10⁶ cycles.

Stress: 11.75 tons/sq.in.
(181 MN/m²)
Endurance: 1.16 x 10⁶ cycles.

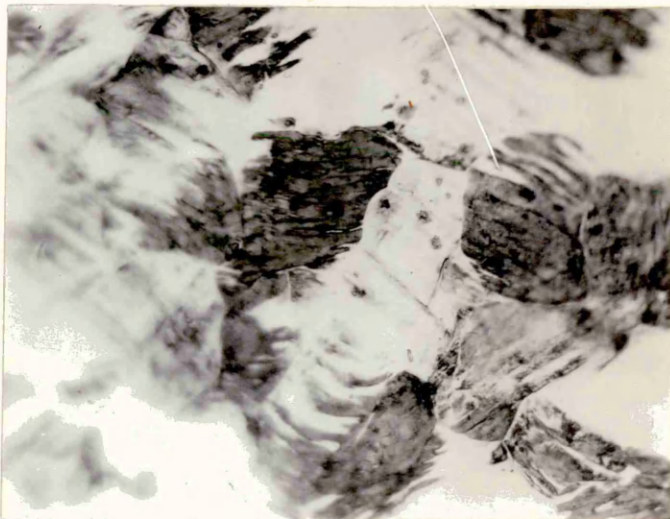


Fig. 13.

x 500

Effect of Stress Amplitude on the Appearance of Surface Fatigue
Damage in 0.11% Carbon Steel.



Fig. 1. Surface of a specimen
after 100 cycles
at a stress level of 0.11.

Fig. 2. Surface of a specimen
after 1000 cycles
at a stress level of 0.11.

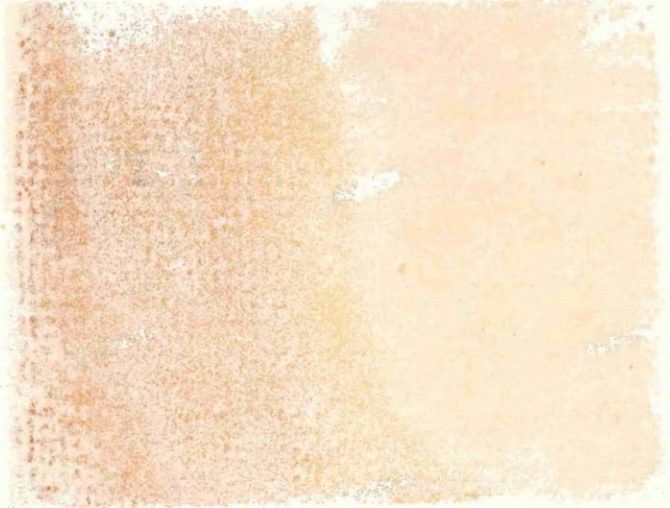
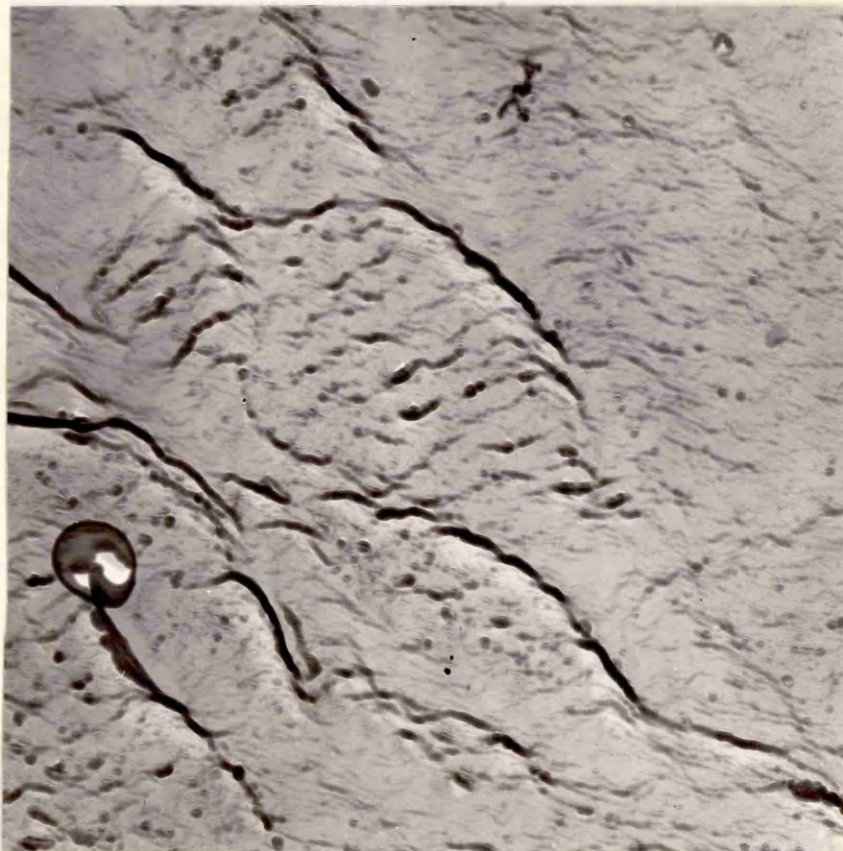


Fig. 3. Surface of a specimen
after 10,000 cycles
at a stress level of 0.11.

Effect of Stress Amplitude on the Appearance of Surface Fatigue
Cracks in 0.11 Carbon Steel.



x 2000



x 21000

Fig. 14.
Surface damage in a 0.41% Carbon Steel Specimen.
Stress 12.2 tons/sq.in (188 MN/m^2) Endurance
 5×10^5 cycles (Electron Micrographs of two stage
platinum - carbon shadowed carbon replica).

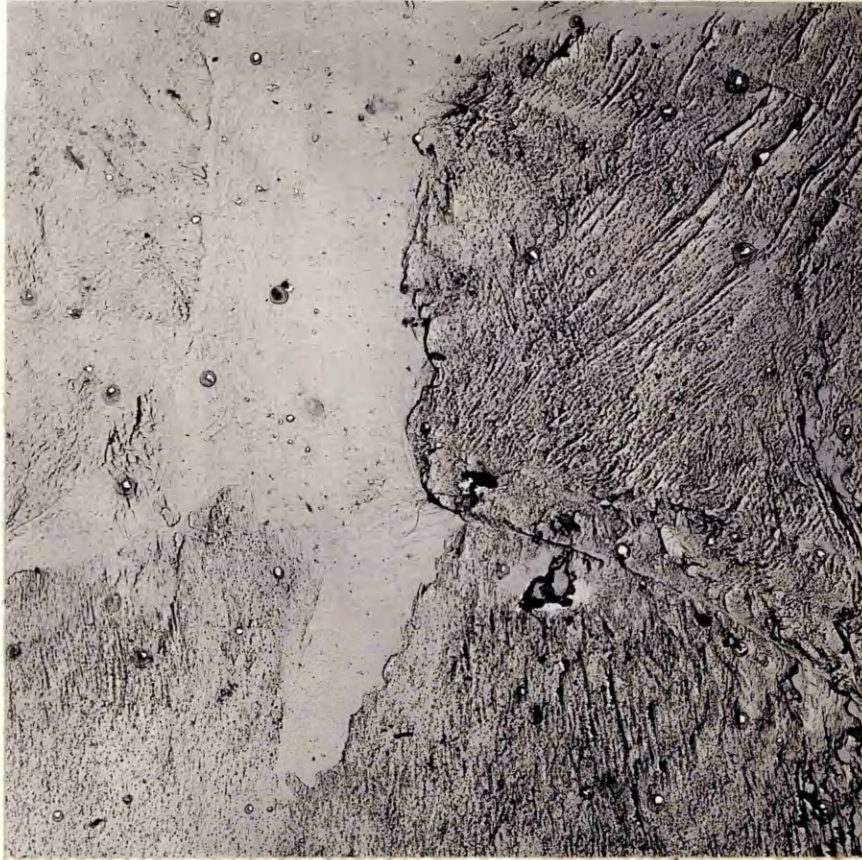
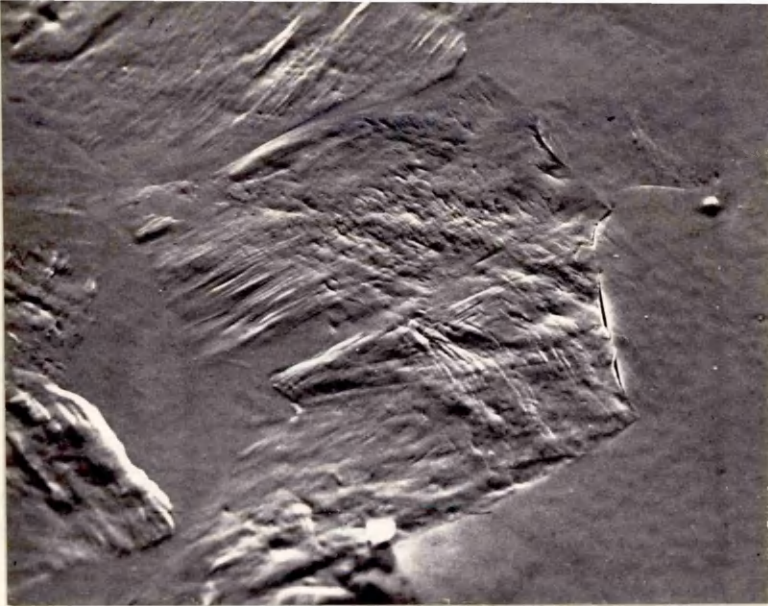


Fig. 15.

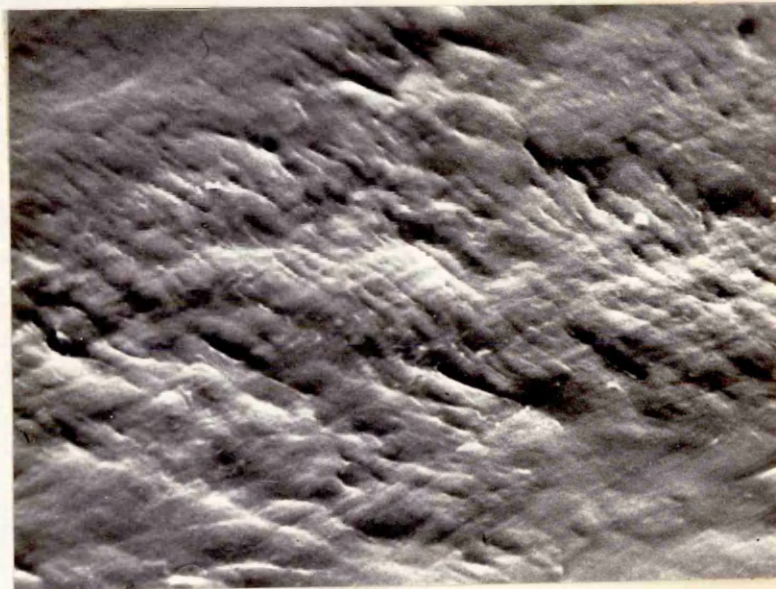
x 2000

Surface Damage on a specimen of 0.41% Carbon Steel, Stress 11.5 tons/sq.in. (177 MN/m^2). Endurance 7.33×10^5 cycles. (Electron micrograph. Two stage platinum-carbon shadowed carbon replica).

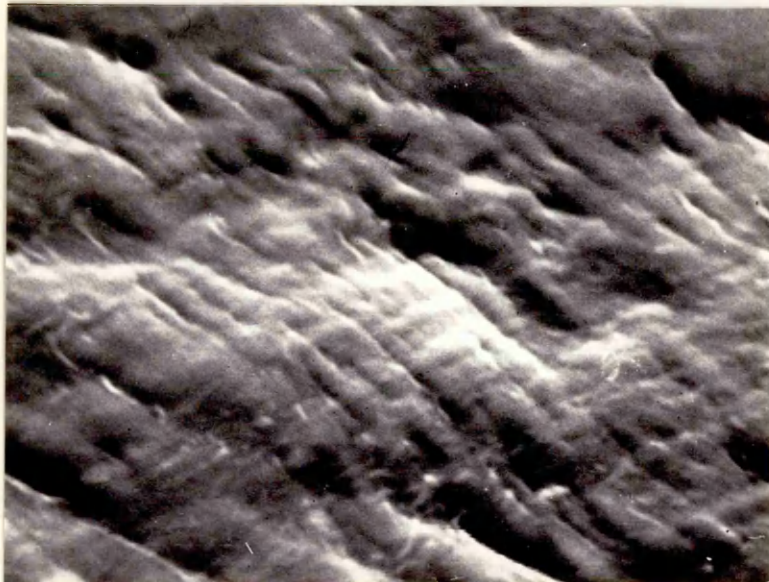


A.
x1150

A.



B.
x 5600



C.
x 11500

Fig. 16
Scanning Electron Micrographs of 0.41% Carbon Steel Specimen
Surface. Stress: 11.75 tons/sq.in (181 MN/m^2) Endurance:
 1.4×10^6 cycles.

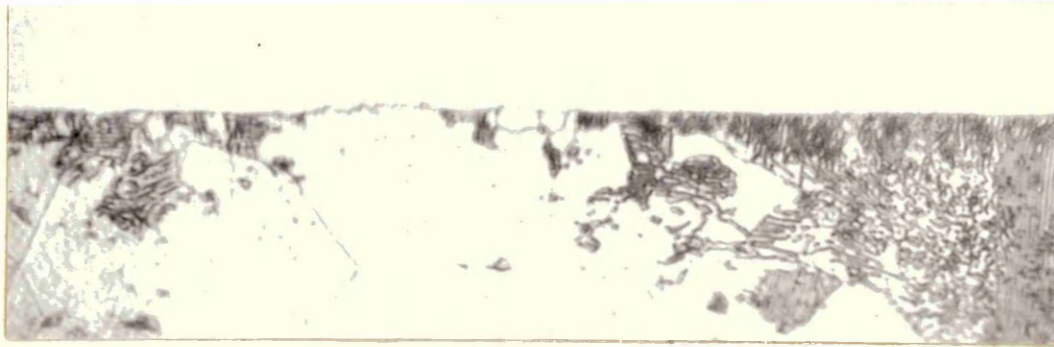
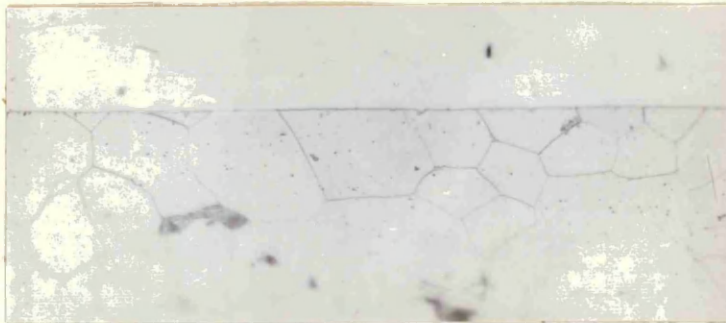
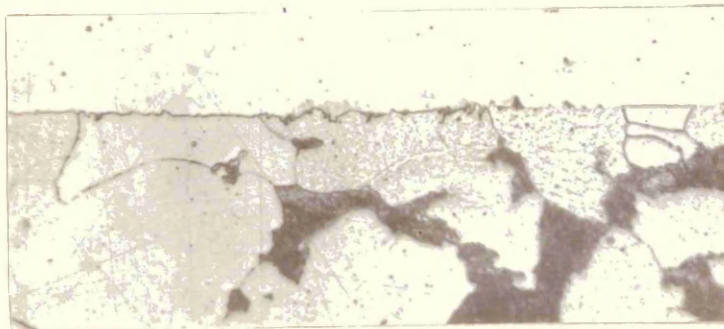
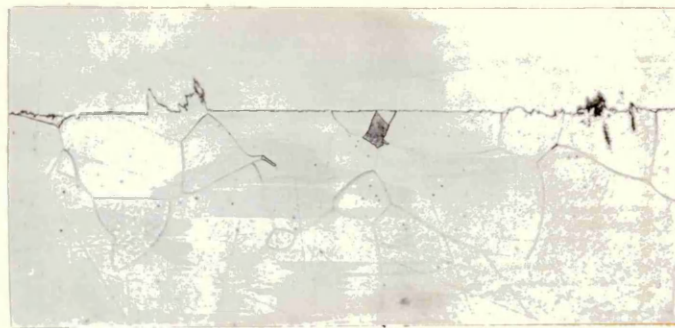


Fig. 17 x 1000
 Effect of Pearlite on the Development of Surface Fatigue
 Damage, 0.41% Carbon Steel. Stress: 11.75 tons/sq.in.
 (181 MN/m²) Endurance: 14 x 10⁶ cycles. Taper section.



Stress: 10.35 tons/sq.
 in. (160 MN/m²)
 Unbroken.

Stress: 10.8 tons/sq.in.
 (167 MN/m²)
 Endurance 2.6 x 10⁶ cycles.



Stress: 11.75 tons/sq.in.
 (181 MN/m²)
 Endurance 1.16 x 10⁶ cycles.

Fig. 18 x 500
 Effect of Stress Amplitude on Surface Fatigue Damage, 0.11%
 Carbon Steel. Taper Section.

Fig. 19. Variation in number of Grains containing fatigue damage with endurance. Specimen F12. Stress 12 tons/sq.in. (185 MN/m²) Endurance 9 x 10⁵ cycles.

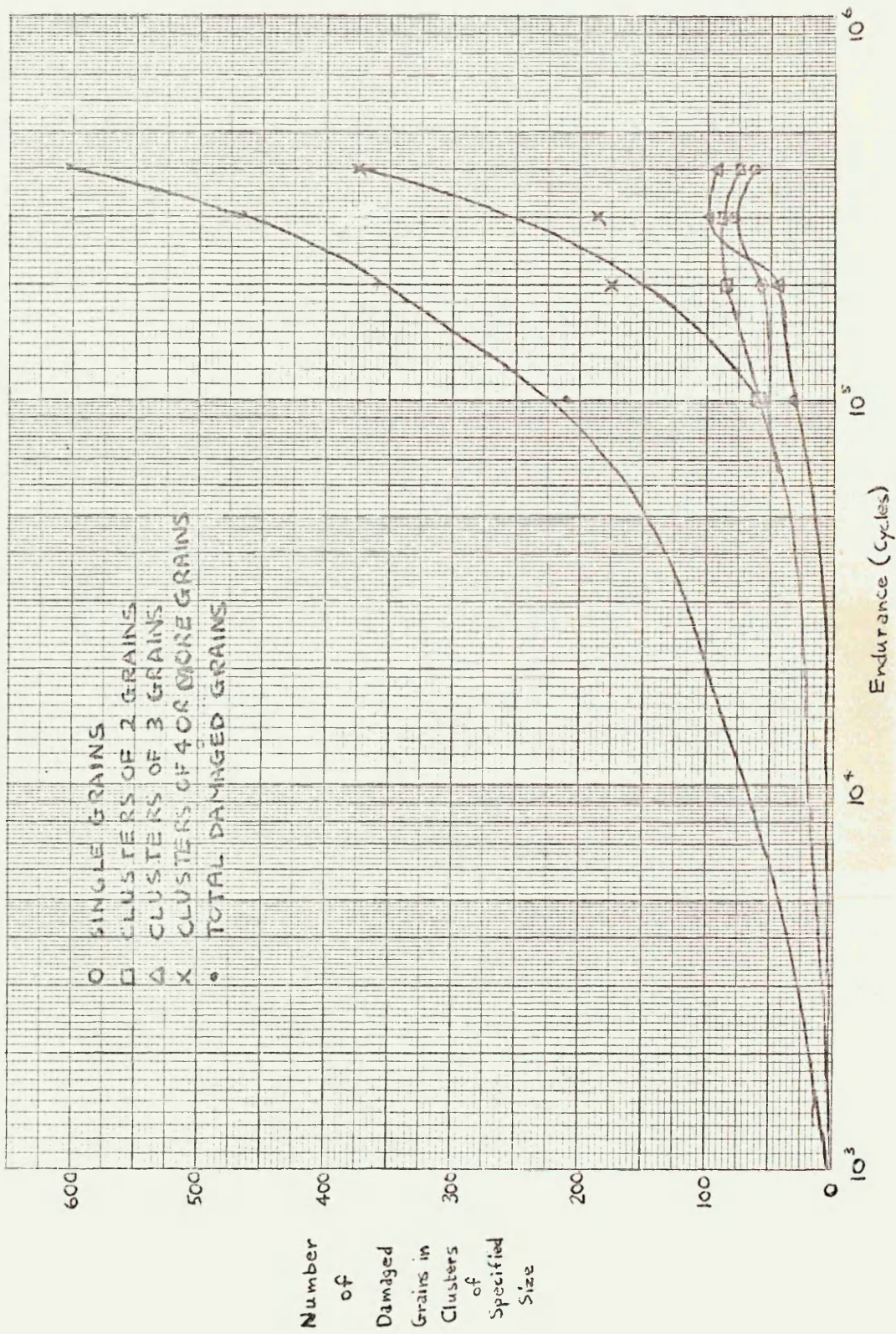
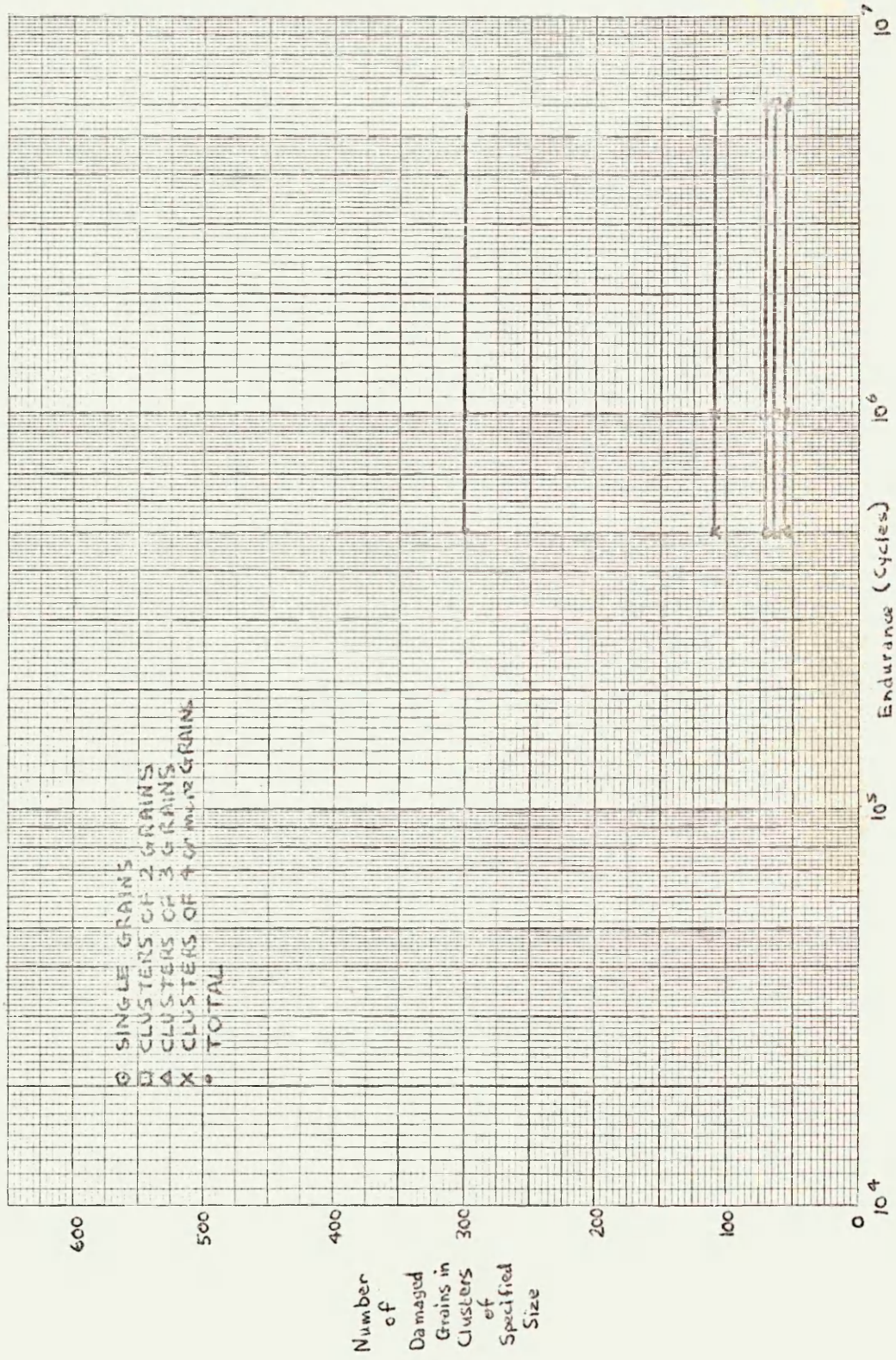


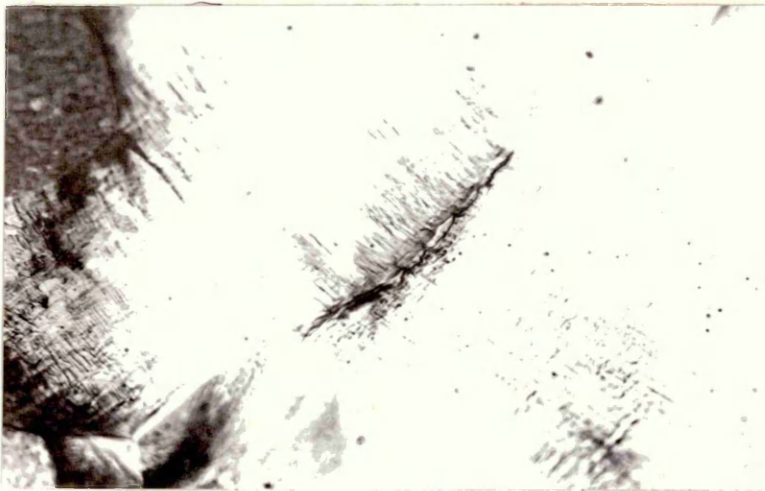
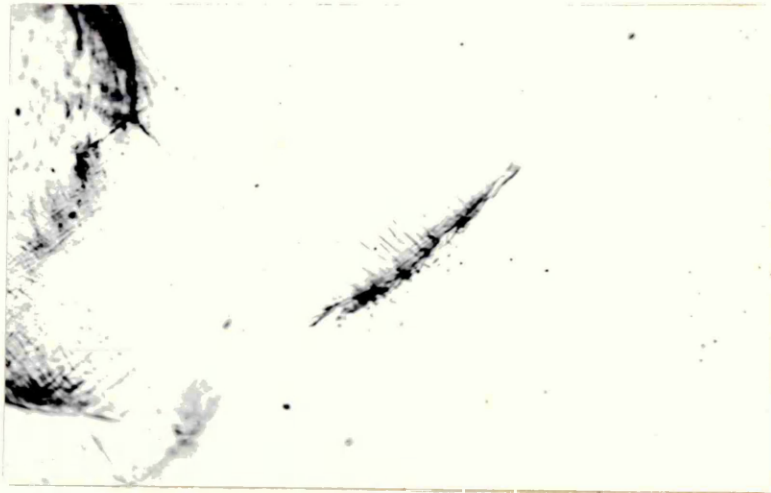
Fig. 20. Variation in Number of Grains Containing fatigue damage with endurance. Specimen F16. Stress 10.5 tons/sq.in. (162 MN/m²) Endurance 7 x 10⁶ cycles.





A. 2% of Life

B. 10% of Life



C. At Failure

Fig. 21

x 500

Slip Intensification at a Grain Boundary in 0.01% Carbon Steel. Stress: 11.3 tons/sq.in (175 MN/m^2). Endurance: 8.4×10^5 cycles.



A. Optical Micrograph X1000



B. Scanning Electron Micrograph
X2300



C. Scanning Electron Micrograph X5750

Fig. 22. Comparison of Optical and Scanning Electron Micrographs of Grain Boundary Slip Intensification in a 0.11% Carbon Steel. Stress: 10.35 tons/sq.in. (160 MN/m^2). Removed after 1.04×10^5 cycles.

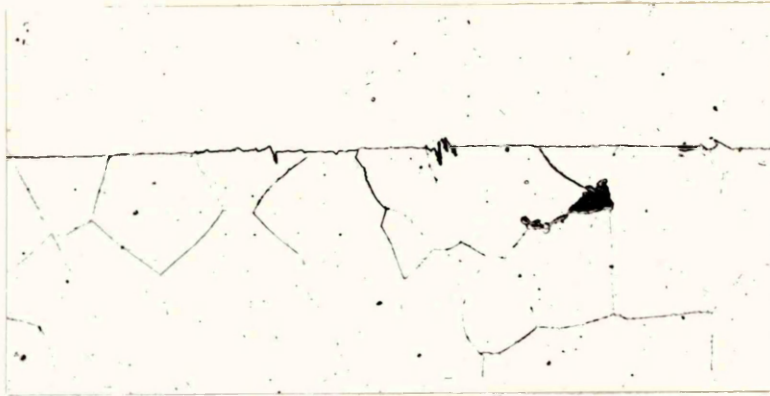


Fig. 23

X 500

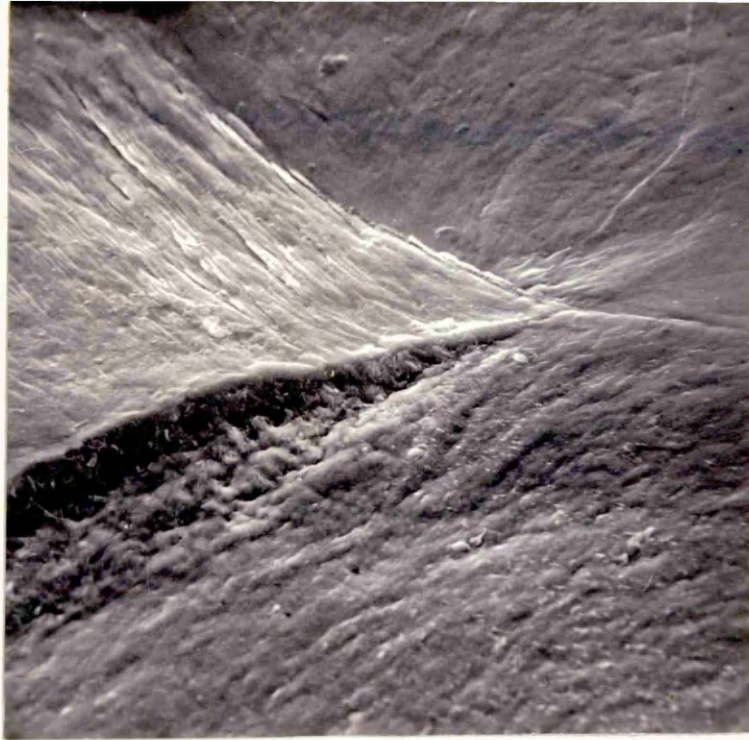
Formation of Intrusion-Extrusion Pairs near a Grain Boundary in 0.11% Carbon Steel Taper Section. Stress = 11.75 tons/sq. in. (181 MN/m^2). Endurance : 1.16×10^6 cycles.



Fig. 24

X 1000

Fatigue Damage on a 0.41% Carbon Steel Specimen Showing Dark Lines which could be Slip-band Cracks. Stress : 11 tons/sq. in. (170 MN/m^2). Endurance : 1.3×10^6 cycles.



A X 2000

B X 5000

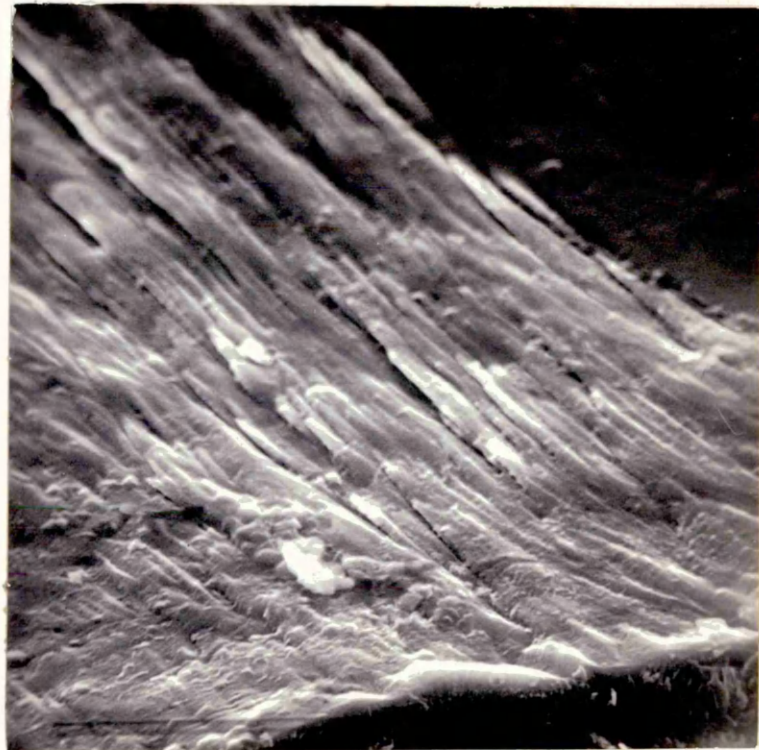
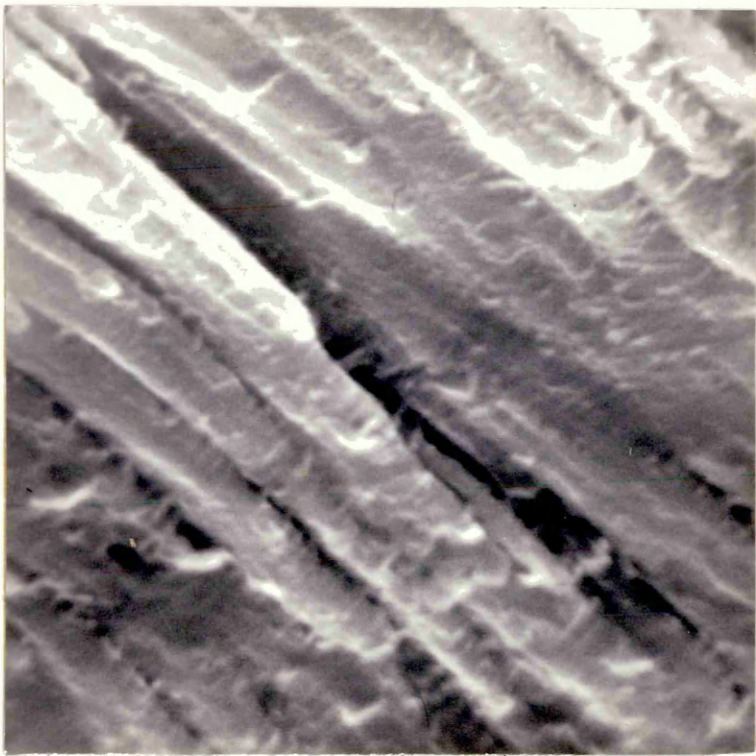


Fig. 25

Scanning Electron Micrographs of an 0.01% Carbon Steel Specimen Surface showing Slip Band Cracking. Fig. 25A also shows a ridge at the grain boundary separating a grain in which much slip has occurred from one in which little slip has occurred. Stress 11.3 tons/sq. in. (175 MN/m^2). Endurance 3×10^5 cycles.

C. X 10000



D X 20000

Fig. 25 cont.

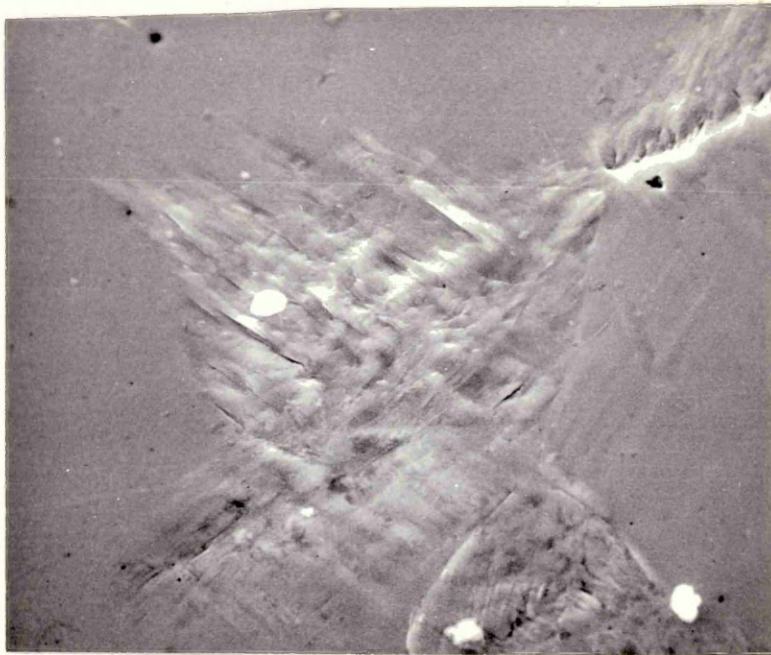


Fig. 26

x 1500

Slip Band Cracking in 0.01% Carbon Steel, Stress: 8.45 tons/sq.in. (130 MN/m^2). Endurance: 1.11×10^6 .



Fig. 27

X1500

Slip Band Cracking in 0.11% Carbon Steel. Taper Section. Stress: 11.75 tons/sq.in. (181 MN/m^2). Endurance 1.16×10^6 cycles.

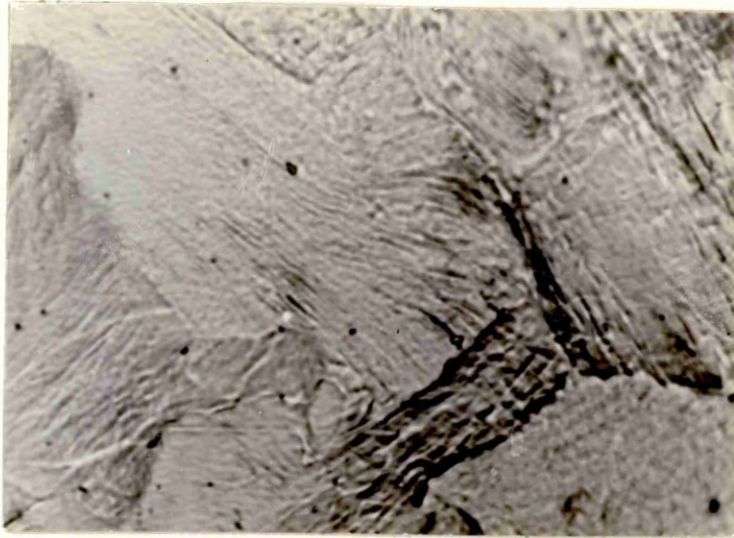


Fig. 28

x 2000

Grain Boundary Crack in 0.41% Carbon Steel. Stress: 11.5
tons/sq. in. (1.78 MN/m^2) Endurance: 1.5×10^6 .

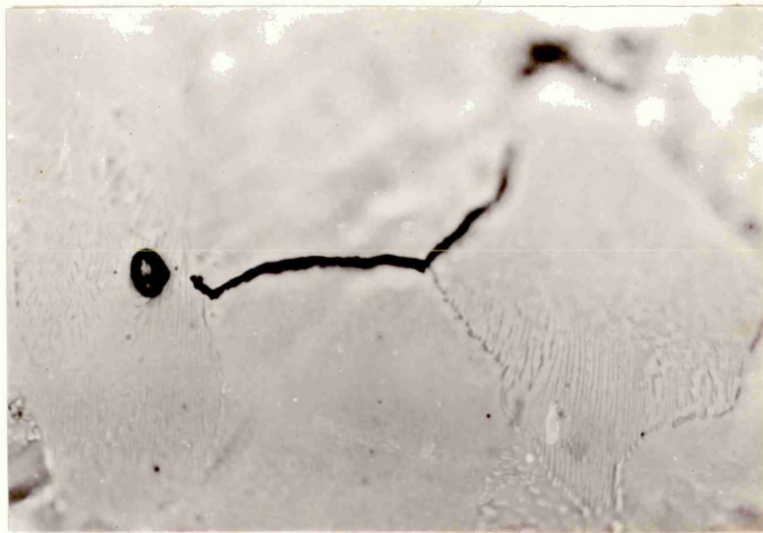


Fig. 29

x 1000

Same Specimen as Fig. 28 above, electropolished after fatigue,
showing Grain Boundary Crack.

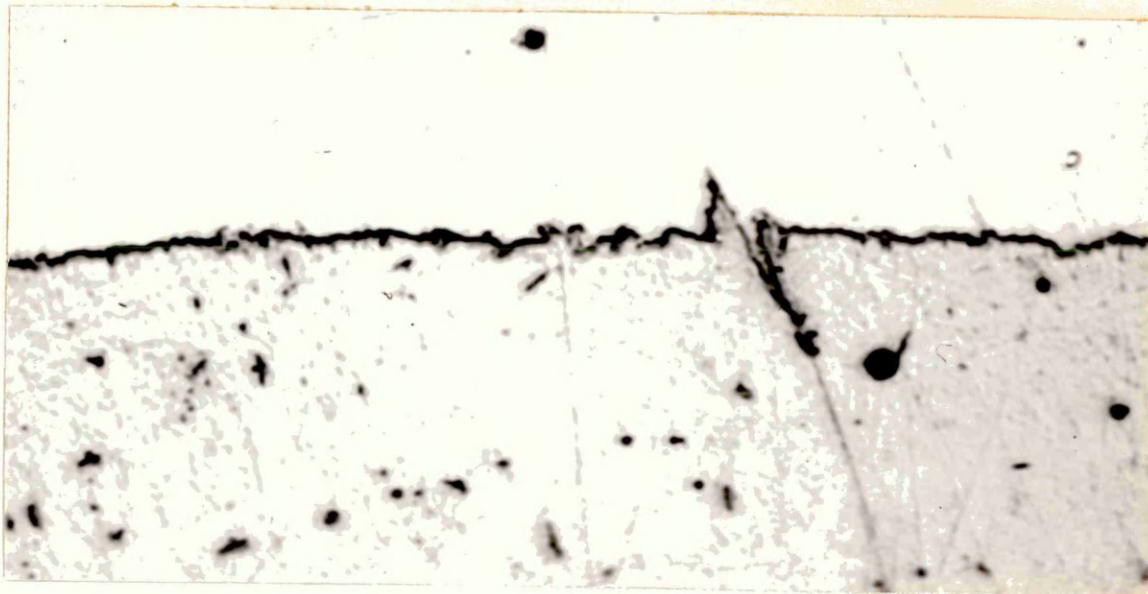


Fig. 30

x 2000

Grain Boundary Crack with Associated Extrusion in 0.01% Carbon Steel Taper Section. Stress: 11.3 tons/sq. in. (175 MN/m^2)
Endurance: 3.6×10^5 cycles.

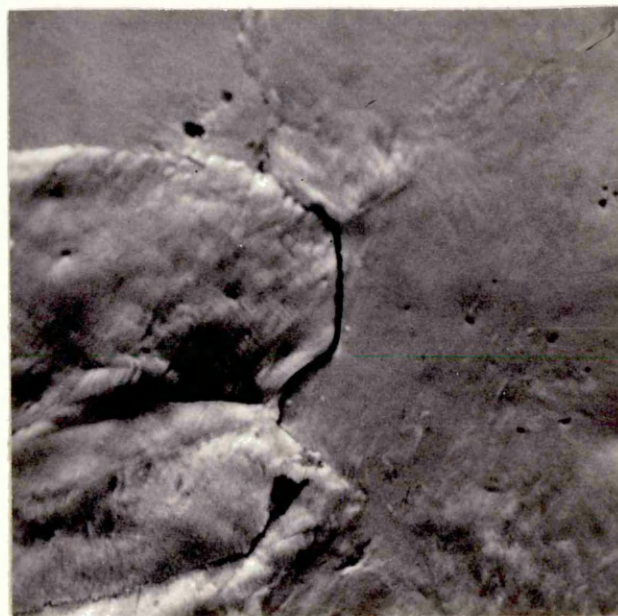


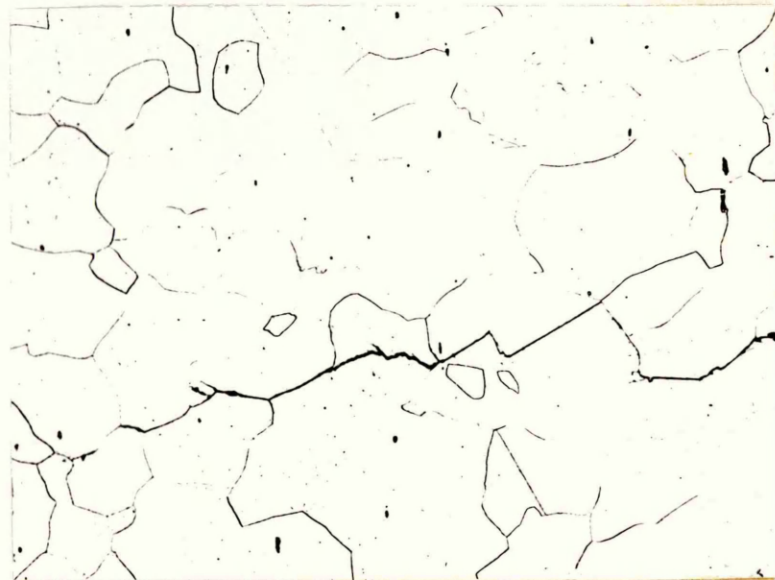
Fig. 31

x 3000

Scanning Electron Micrograph of 0.41% Carbon Steel Specimen showing Grain Boundary Microcrack. Stress: 10.6 tons/sq. in. (164 MN/m^2). Endurance: 5×10^5 cycles.



A. As fatigued



B. Repolished and Etched

Fig. 32

x160

Secondary Crack in a 0.01% Carbon Steel Specimen. Stress: 10.35 tons/sq.in (160 MN/m^2). Endurance: 3×10^6 cycles.



A. x 50

B. Diagrammatic Representation

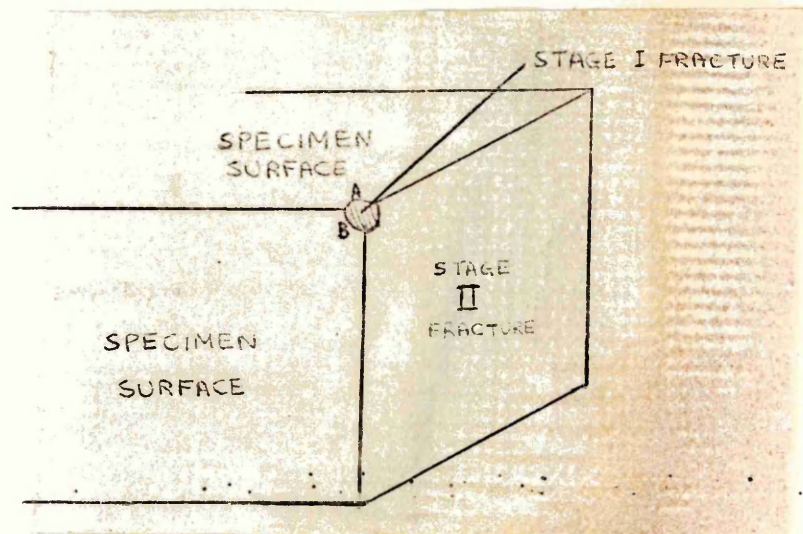


Fig. 33. Scanning Electron Micrograph of 0.01% Carbon Steel Specimen, showing Area of Stage **I** Crack Propagation. Stress: 11.3 tons/sq.in (175 MN/m^2). Endurance: 3×10^5 cycles

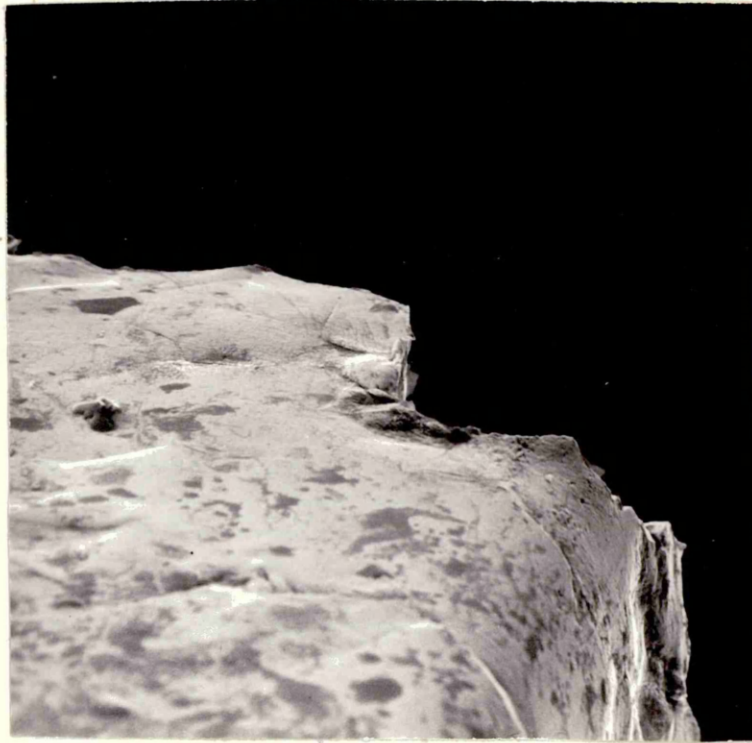


Fig. 34

x220

View of surface of specimen shown in Fig. 32 from an angle of 30° to the specimen surface showing the edge of the Stage I fracture.

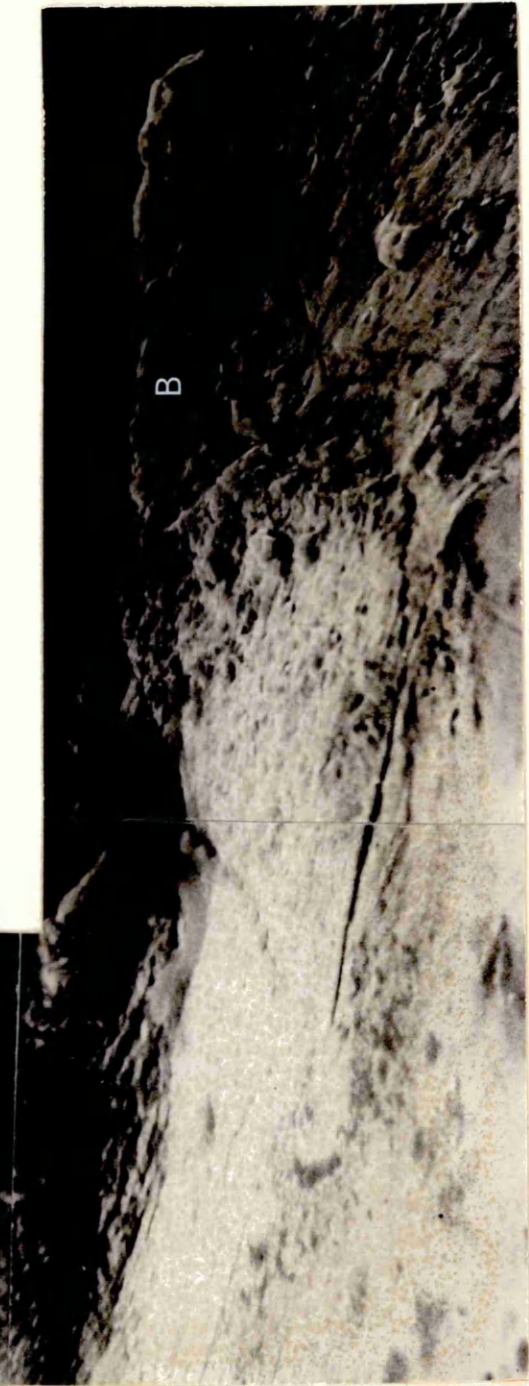
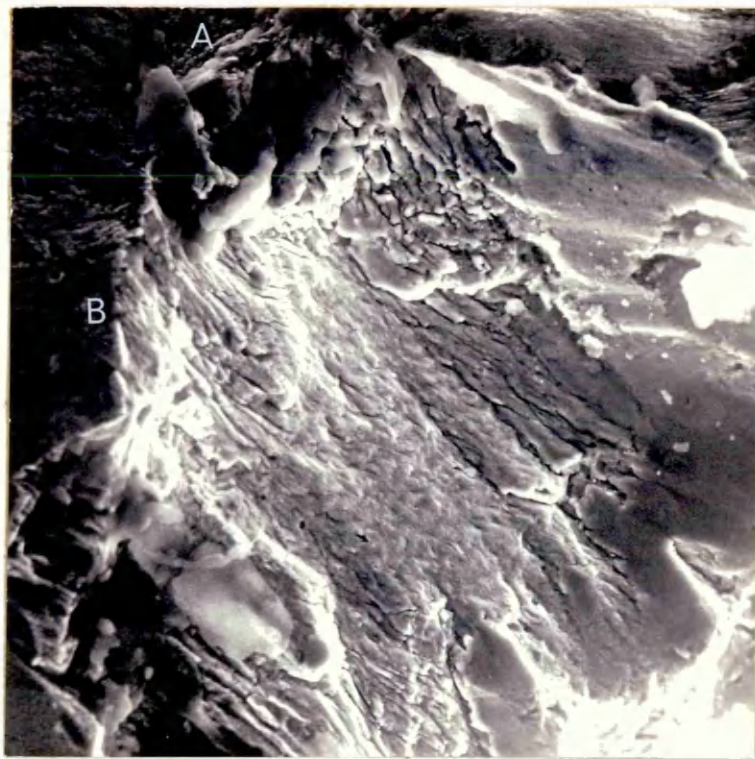
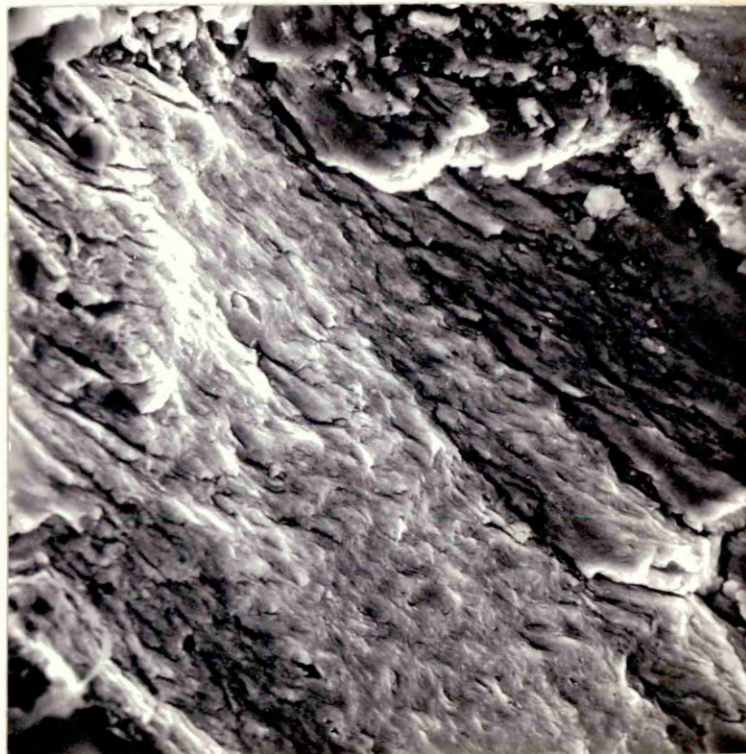


Fig. 35 High Magnification view of the edge of the Stage I fracture taken from the same angle as Fig. 34

x1100



A x 500

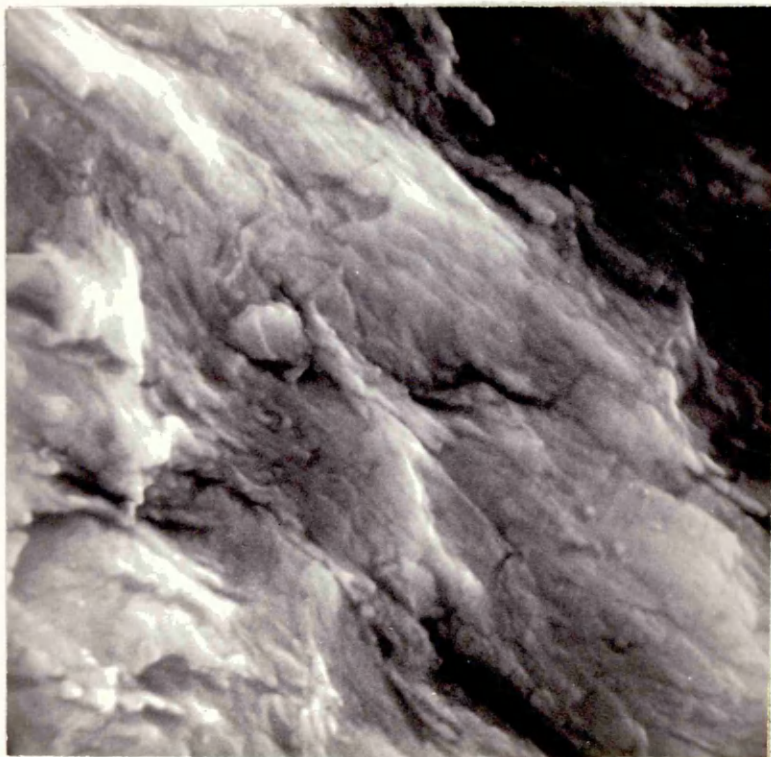
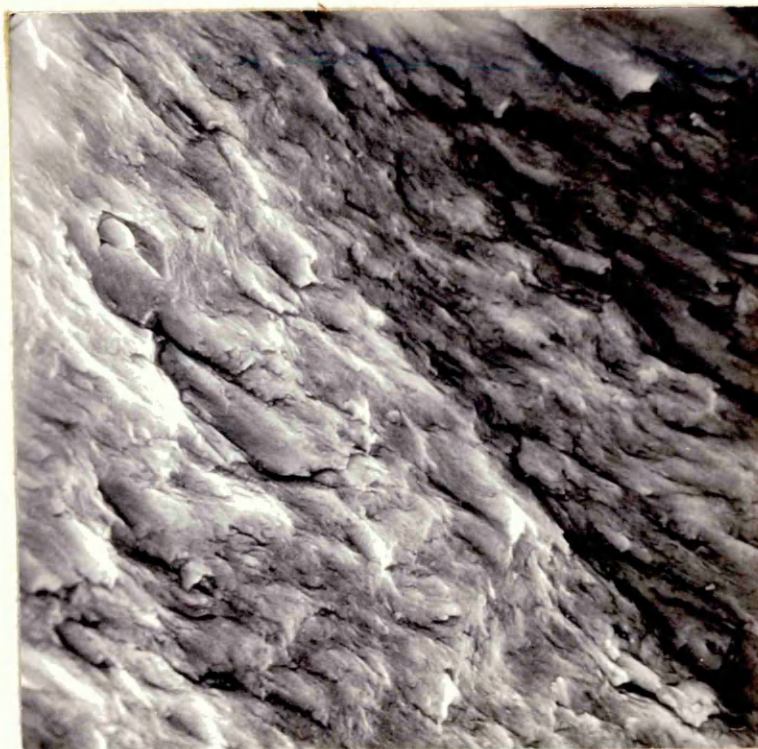


B x 1000

Fig. 36

Series of photographs of Stage I fracture in 0.01% Carbon Steel (same specimen as Figs. 32-35. Scanning Electron Micrographs.)

C X 2000



D X 10000

Fig 36 Cont.



A X 600



B X 2400

Fig. 37

Stage I Crack Propagation in 0.41% Carbon Steel. Scanning
Electron Micrographs. Stress: 9.85 tons/sq. in. (152 MN/m^2)
Endurance : 4.7×10^6 cycles.



Fig. 37 (Cont.)

C X 6000



X 130

Fig. 38
Early form of Stage II fracture in 0.01% Carbon Steel showing mixed transgranular and intergranular propagation 1 mm from root of notch. Scanning electron micrograph.



X 130

Fig. 39
Later form of Stage II fracture in 0.01% Carbon Steel showing Wholly Transgranular Crack Propagation. $3\frac{1}{2}$ mm from root of notch. Scanning Electron Micrograph.

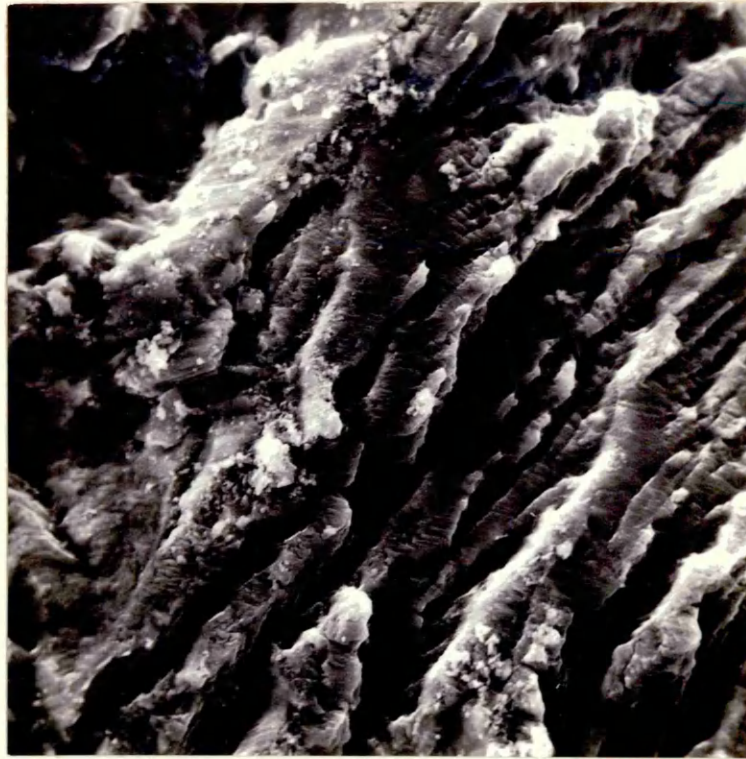


Fig. 40

X 2400

Stage II fracture surface of 0.01% Carbon Steel Specimen showing hills and valleys on which the Characteristic Fatigue Striations can be observed. Scanning electron micrograph.

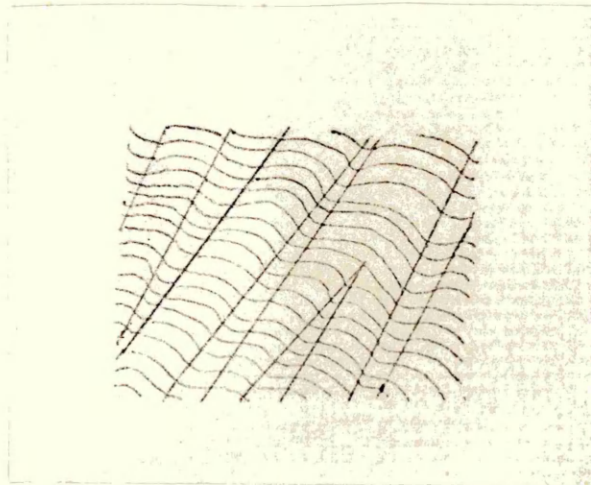


Fig. 41

Diagrammatic Representation of Fatigue Striations on Hills and Valleys on a Stage II Fatigue Fracture Surface.



Fig. 42

X 2350

Fretting on Stage II fracture surface producing rub marks and debris. Scanning Electron Micrograph.

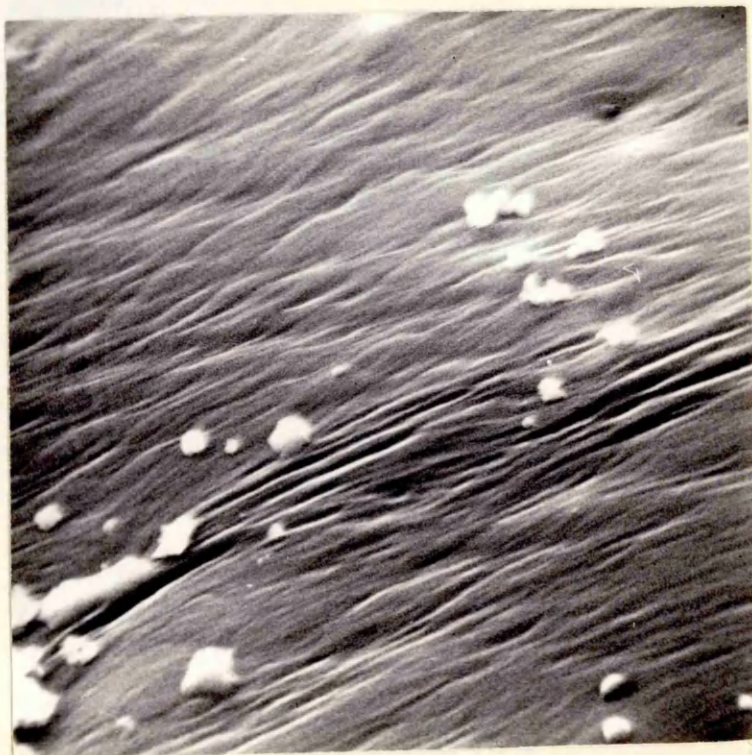
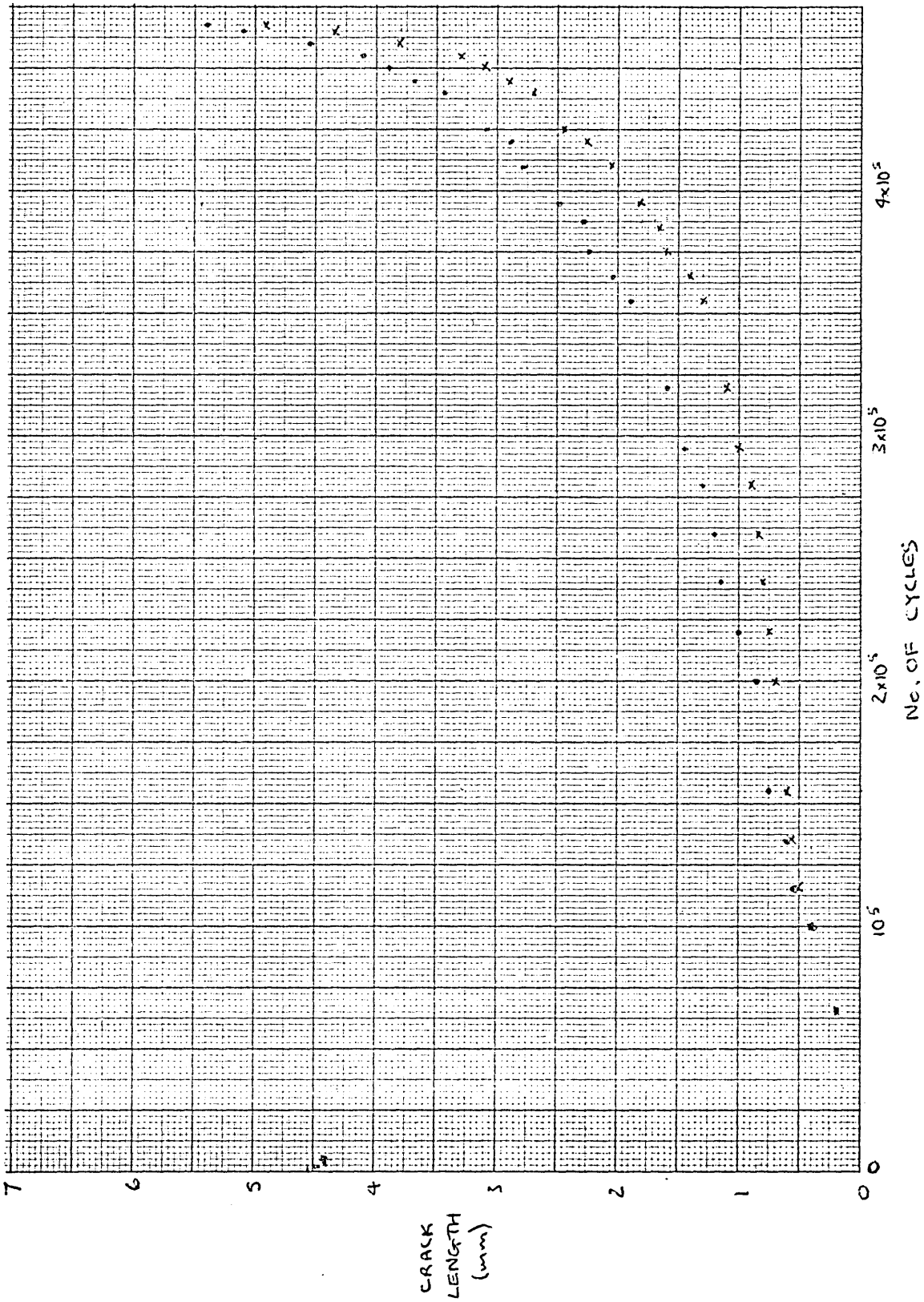


Fig. 43

X 12000

Intergranular Stage II Fatigue Surface in 0.01% Carbon Steel, showing slip lines.

Fig A1/3. Specimen B5. Stress $4\frac{1}{2}$ tons/sq. in. (66 MN/m^2). Endurance 4.67×10^5 cycles



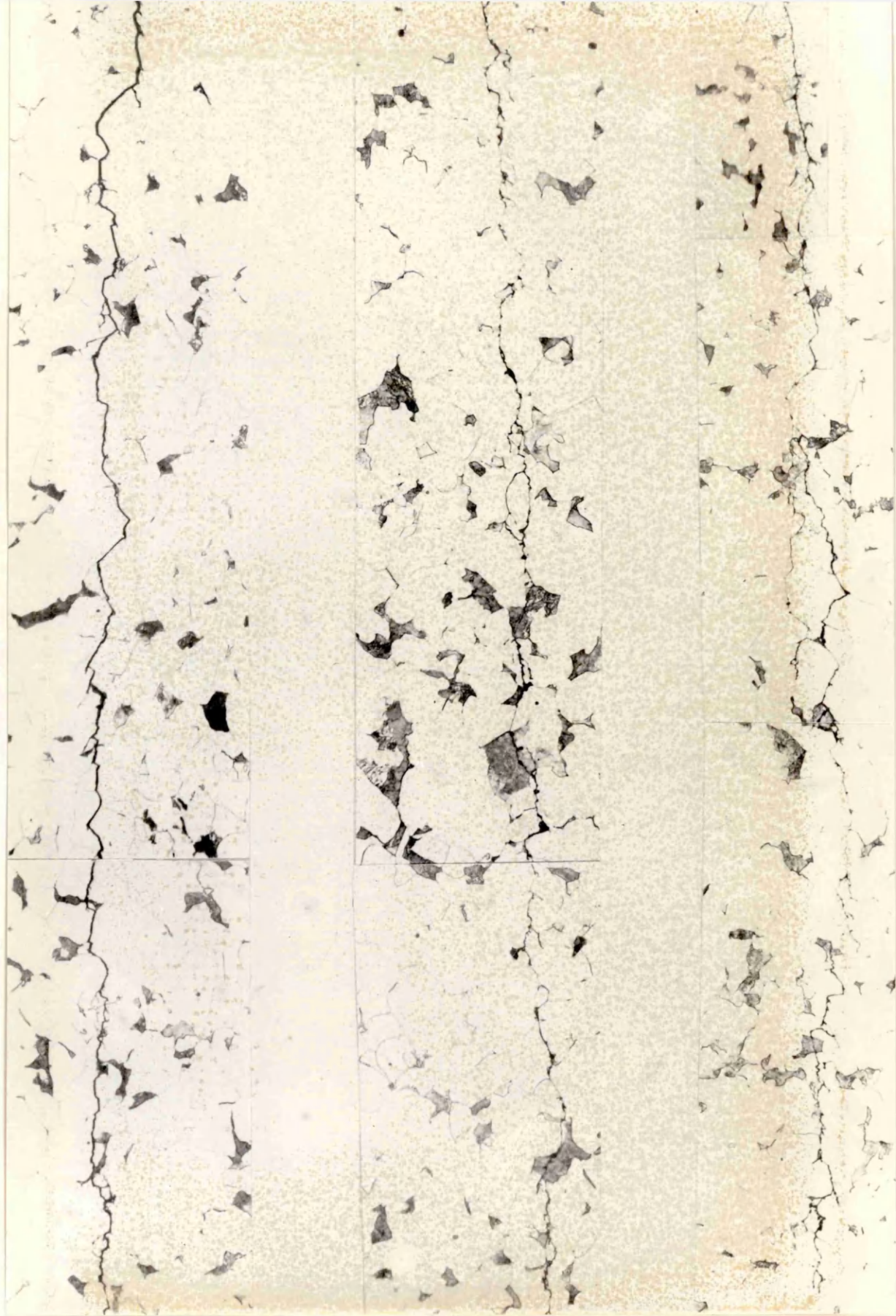


Fig. 44 Crack Propagation in 0.11% Carbon Steel. X 200

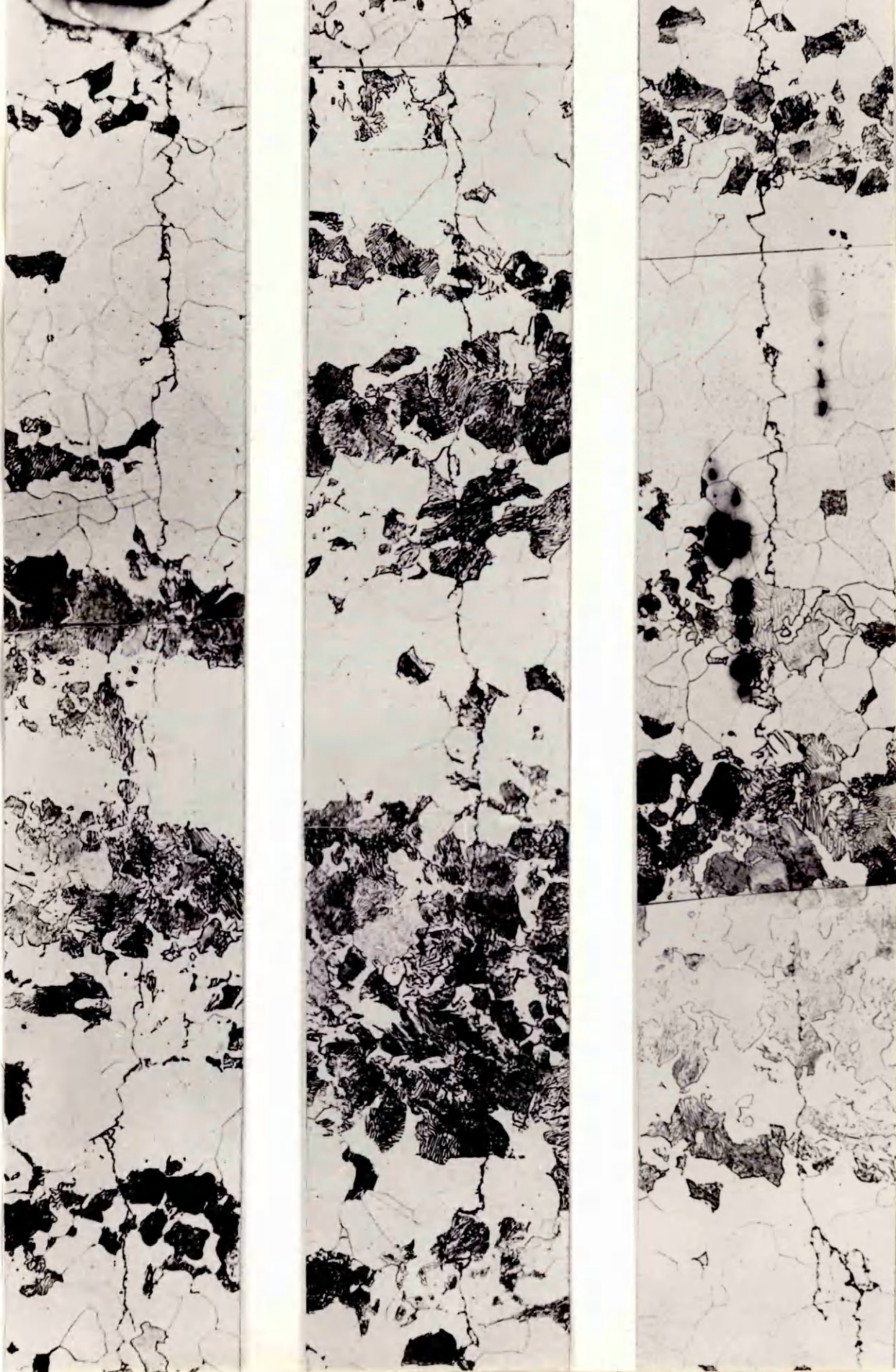


Fig. 45. Crack Propagation in 0.41% Carbon Steel X200





Fig. 46 x 1000
Effect of Orientation of Cementite Lamellae on the Mode of
Fatigue Crack Propagation in 0.41% Carbon Steel.

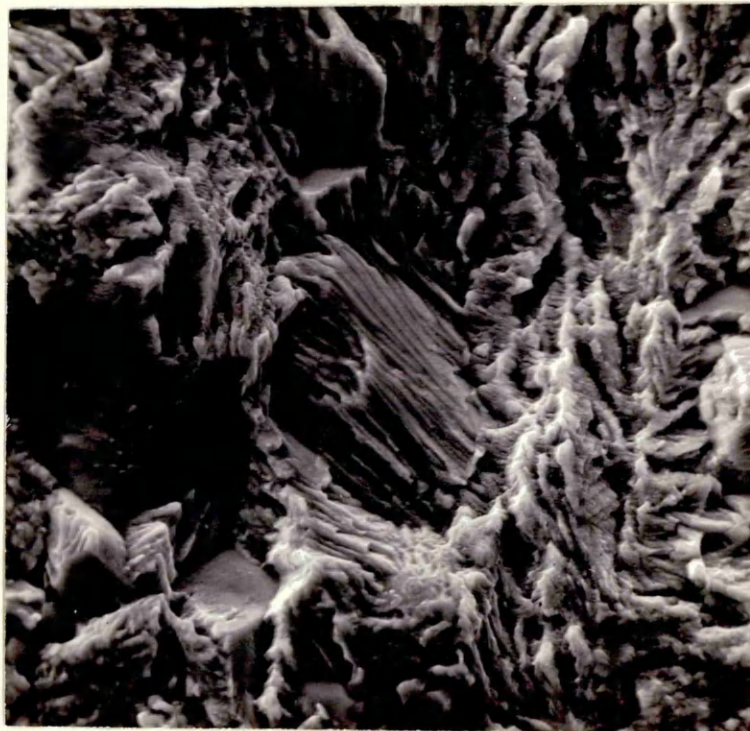


Fig. 47 x 1350
Fracture along a Ferrite-Pearlite Interface in 0.41% Carbon
Steel. Also shows propagation through a Pearlite Nodule.
Scanning Electron Micrograph.

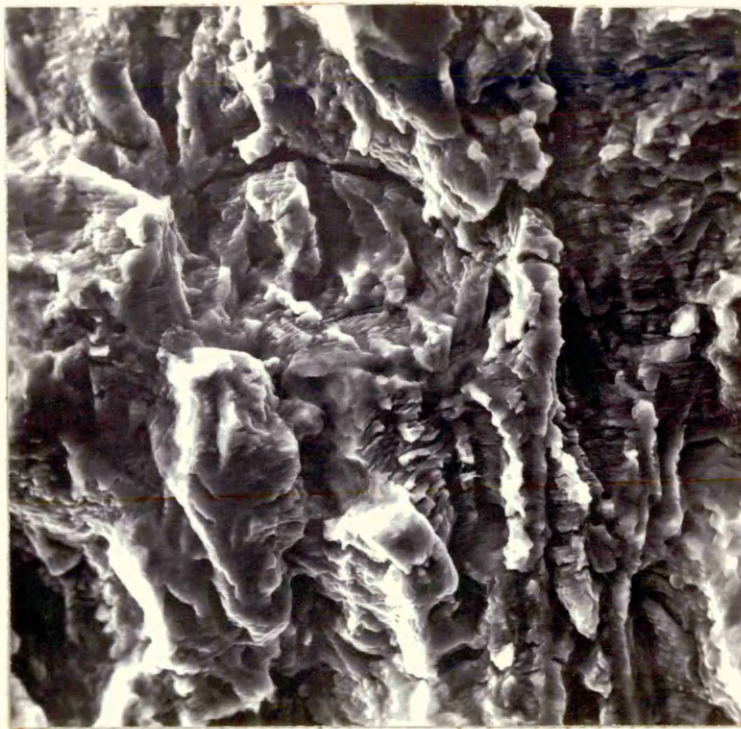


Fig 48 X1350
Later part of Stage II Crack Propagation in 0.11% Carbon Steel
showing Crack Branching.

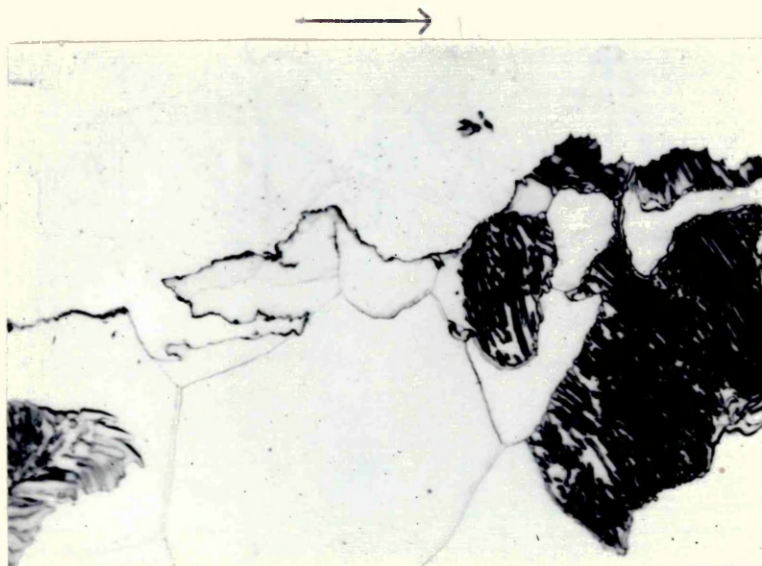
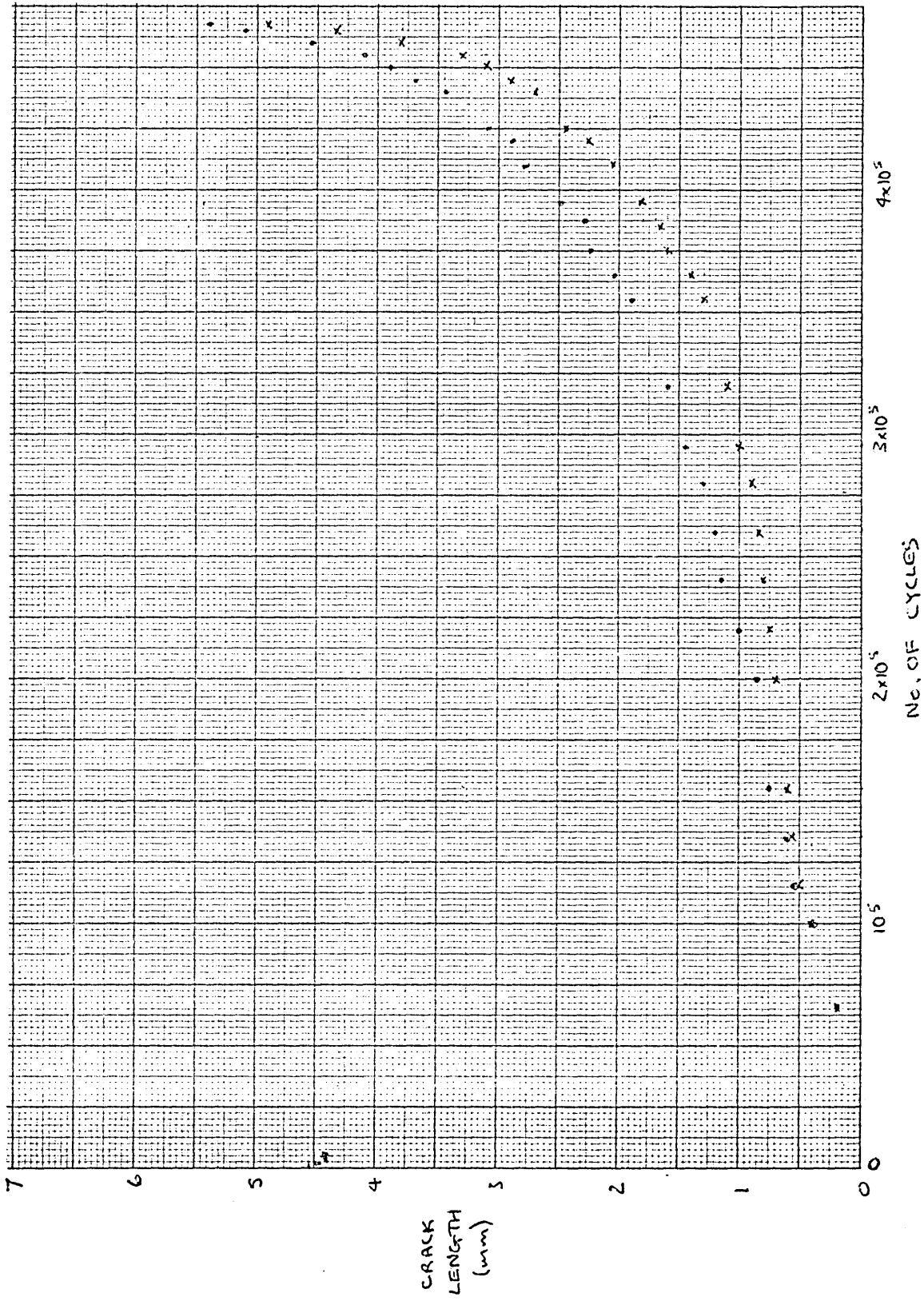


Fig 49 X1250
Branch Crack in 0.41% Carbon Steel. Later Stage II Crack
Propagation.

Fig A1/3. Specimen B5. Stress $4\frac{1}{2}$ tons/sq. in. (66 MN/m^2). Endurance 4.67×10^5 cycles



5. DISCUSSION

5.1 THE DEVELOPMENT OF SURFACE FATIGUE DAMAGE

Fatigue slip bands in the three carbon steels studied developed early in the tests and then tended to widen as cycling continued. This led to areas of damage being formed which contained one or more complete grains. The formation of these areas is in contrast to the situation in most FCC metals and alloys where discrete fatigue slip bands are formed. Scanning electron microscopy has shown that the topography of the fatigue slip bands is comparatively flat, i.e. the "notches" and "peaks" have very shallow contours. The height of the "peaks" is of the order of $1\frac{1}{2}\mu$, compared with 10μ for aluminium alloys. This is contrary to the impression gained from optical observation when the dark appearance of the areas of slip, which is caused by surface oxidation, tends to suggest a more severe type of damage. The fatigue slip lines themselves were wavy in appearance, this being due to the fact that cross slip in ferrite is very easy. There is also the possibility that $\{112\}$ and $\{123\}$ slip may sometimes operate, but it is thought that slip in ferrite at room temperature is predominantly of the $\{110\}$ type.

The tests carried out to investigate the surface spread of plasticity during fatigue showed that at high stress, the number of grains containing fatigue damage gradually increased until failure occurred, whereas at low stress there was virtually no surface spread of plasticity from grain to grain until failure occurred. It therefore seems unlikely that spread of plasticity from grain to grain as revealed by surface observation (as suggested by Oates and Wilson⁽⁵⁵⁾ for 0.11% carbon steel) can be the controlling factor for

fatigue failure in 0.41% carbon steel. Also this theory does not describe in detail the actual processes leading to fatigue failure. It is quite clear from previous work that in plain specimens, the majority of the fatigue life is spent in stage I crack propagation and it is therefore possible that the factor which decides whether fatigue failure will occur or not is the ability of a stage I crack to grow large enough to change over to a stage II crack. The surface spread of plasticity is an effect independent of this, but it may be controlled by similar factors.

The S-N curves showed a fatigue limit of 8.45 tons/sq.in. (131MN/m^2) for the 0.01% carbon steel and 10.35 tons/sq.in. (160MN/m^2) for the 0.11% carbon steel, and the fatigue ratios for these steels were virtually identical (0.43 and 0.44). It has been shown in the present work that crack initiation occurs in the ferrite and since the 0.11% carbon steel contained only 6% more pearlite than the 0.01% carbon steel (which contained none) one would not expect such a large difference as is observed in either fatigue limit - 1.9 tons/sq.in. (29MN/m^2) or U.T.S. - 3.1 tons/sq.in. (47MN/m^2), if the pearlite was equiaxed. However, the pearlite was elongated along ferrite grain boundaries and partly divorced and this would be more likely to impede plastic flow than if it were equiaxed. Hence the larger than expected difference in U.T.S. If the fatigue limit is controlled by the ability of a stage I crack to grow large enough to change over to a stage II crack, then it will be affected by second phases at grain boundaries and the percentage and morphology of the pearlite in the materials examined would account for the

difference in fatigue limits observed in the present work. One particularly attractive prediction of such a theory is that fatigue limit and U.T.S. are controlled by the same factors and therefore one would expect a correlation between the two. It is well known that this is in fact observed.

Slip intensification at grain boundaries has been briefly mentioned in the past (41,44) and has been shown to occur readily in the present work. This is an effect which appears to be peculiar to fatigue and may possibly be due to the boundaries acting as dislocation sources.

5.2 CRACK INITIATION

Although it has been shown by previous workers that fatigue cracks in plain carbon steel initiate from slip bands, the majority of the evidence has been obtained from optical microscopy, and electron microscopy of plastic replicas. In the former, it is easy to confuse cracks with dark oxide areas, and in the latter, what appear to be cracks may be just rumpling or cracking of the plastic film. In the present work, scanning electron microscopy has been used to provide direct evidence of the existence of cracks within the fatigue slip bands, and such cracks have also been observed in taper sections.

Grain boundary cracks have also been observed in all three materials but no evidence of main cracks initiating at grain boundaries was found. The intergranular cracking was generally seen at boundaries separating a grain containing heavy fatigue damage from one with relatively little damage. It is possible that there would be a large orientation difference between the grains in this case, and a crack

could form a means of stress relief. Grain boundary cracks were generally noted near to the main crack, and it is possible that these could have been formed by the stress concentration ahead of the advancing crack front.

It is thought that the reason for the non-propagation of these grain boundary cracks (if such cracks were formed early in the test, and not as the main crack was propagating as suggested above) could be in the fact that the mechanism of stage I crack propagation is thought to be an extension of the slip band crack initiation process. Whilst slip band cracks can easily propagate, grain boundary cracks would find this more difficult in a material not subject to grain boundary weakening. Also, although a grain boundary at the specimen surface might be suitably orientated for the applied stress to cause initiation, its orientation below the surface will, in general, change, so that further propagation of the crack will not occur.

5.3 CRACK PROPAGATION

Stage I crack propagation in all the plain specimens examined occupied an area of approximately one or two grains at the most before changeover to stage II occurred. The cracks seemed to be formed from a number of parallel slip band cracks in a single grain which tended to move on to one level as they extended, until they became one wide slip band crack. This is in contrast to what has previously been reported in other materials e.g. aluminium alloys and the high strength nickel alloy of Gell and Leverant (69), where the parallel lines in the direction of crack propagation extended throughout the stage I area. The reason for this difference in behaviour is presumably the ease of cross slip

in low and medium carbon steels, as compared with the other materials in which stage I crack propagation has previously been studied. The irregular appearance of the stage I fracture after the initial microcracks have moved on to one level is probably also due to the ease of cross-slip.

The data obtained from the crack propagation rate measurements showed an extremely large variation in crack growth rate at a given stress intensity range and it was not possible to relate this variation to an effect of nominal stress. The slight drift into tension which was mentioned in section 3.2.2 and occurred in the earlier tests had no measurable effect. The scatter in results obtained was larger for different specimens of the same material than for different materials. There are two possible reasons for this. Firstly, the experimental conditions were difficult to reproduce, because it was not easy to set the specimens up for axial loading and it was possible that some bending was also occurring. Secondly, the tests were carried out at zero mean stress, whereas the fracture mechanics analysis which has been used is strictly only applicable to pulsating tension tests. For these reasons it is not proposed to discuss these results any further.

It has been shown that stage II crack propagation in the materials studied occurs by a mechanism which produces striations on the fracture surface. The spacing between these striations remained remarkably constant at between $1-2 \times 10^{-4}$ mm, in contrast to what has in the past been observed on aluminium alloys. The crack growth rates were always smaller than the striation spacing e.g. in specimen B4

tested at 5.65 tons/sq.in. (87 MN/m^2), the crack growth rate at 1mm from the root of the notch was $1.0 \times 10^{-5} \text{ mm/cycle}$ and at 4.5mm this was $7.5 \times 10^{-5} \text{ mm/cycle}$. The striation spacing at both these points was $1.5 \times 10^{-4} \text{ mm}$, and it would have been possible to resolve striation spacings **an** order of magnitude smaller than this if they had been present. There are two possibilities to account for this phenomenon. Firstly, the whole crack may only propagate every n cycles, so that each striation represents n cycles of stress, where $n \approx 1.5$ to 10 in the present case. A more likely explanation is that, at any point in time, local parts of the crack front will be at rest, the amount of time any portion of the crack front spends at rest decreasing as the stress intensity range and hence the size of the plastic zone ahead of the crack tip increases.

Grain boundaries represent a possible source of delay to local crack propagation, and this was apparent early in most of the tests, since there was often a change in mode from transgranular to intergranular crack propagation or vice versa at grain boundaries. A possible explanation for the intergranular crack propagation which occurred in the earlier stages of all tests is as follows. Consider a propagating transgranular crack. Parts of this crack will easily propagate from grain to grain because of favourable orientations of the grains into which they are propagating. Others may be held back at grain boundaries, but eventually a high stress will be built up at these boundaries as neighbouring parts of the crack propagate, and intergranular failure may result. At high stress intensities, the probability of a crack being held up long enough for this to

occur will decrease, because of the increase in plastic zone size and intergranular fracture will not occur. The large proportion of grain boundary fracture present in the 0.01% carbon steel could have been a consequence of the high oxygen content of this material, which could cause grain boundary weakening by segregation. Also the 0.11% carbon steel had some grain boundary cementite which might also have led to some intergranular fracture. However, although these factors could contribute to the propensity of grain boundary cracking, they are obviously not the complete answer, as intergranular fracture still occurred in the 0.41% carbon steel. Furthermore it did not occur in any of the materials at high stress intensities, or in unidirectional deformation.

The actual crack extension mechanism, i.e. striation production was not studied in the present work. However, the photograph of the branch crack in Fig. 54 is very interesting, as the end of this crack has an appearance similar to that depicted in Fig. 2c, and tends to confirm the operation of the "plastic blunting process" as suggested by Laird (67). The frequent occurrence of these branch cracks throughout the tests as seen on scanning electron microscope observations of the fracture surface also lends support to this theory.

6. CONCLUSIONS

1. Surface fatigue damage in 0.01, 0.11 and 0.41% carbon steels occurred predominantly in the ferrite, and had a comparatively flat "hill and valley" appearance. The amount of surface damage evident at failure increased with increasing stress amplitude.
2. The spread of plasticity as revealed by surface observations did not appear to be the controlling factor in determining whether or not a plain specimen would fail.
3. All plain specimens of all three materials showed a certain amount of grain boundary slip intensification.
4. Both slip band cracks and intergranular cracks were observed on specimen surfaces of all three materials, but only the slip band cracks seemed to be responsible for failure.
5. Stage I crack propagation occurred by the linking up of a number of slip band cracks on parallel planes in a single grain and then by slip-plane growth in a wavy manner, this being attributed to the ease of cross-slip in the ferrite of low and medium carbon steels.
6. Stage II crack growth occurred by both transgranular and intergranular propagation. The amount of intergranular fracture increased with decreasing carbon content and decreasing distance from the notch root.
7. Transgranular stage II propagation in ferrite showed the characteristic fatigue striations as observed in other materials. However, the striation spacing could not be correlated with crack length and was relatively constant, varying from about 1 to 2×10^{-4} mm.

8. Branch cracks occurred at all stages of stage II crack propagation, becoming larger as the crack growth rate increased. The appearance of these tends to confirm Laird's plastic blunting process of crack propagation.

7. REFERENCES

- (1) W.A.Wood Fracture. Swampscott Conference
1958, Wiley 1959 p.412.
- (2) H.J.Gough Engineering 114, 291 (1922).
- (3) L.M.Clarebrough et al Proc.Roy.Soc. A242,160 (1957).
- (4) W.A.Backofen Fracture. Proc.Int.Conf.
Swampscott 1959. p435.
- (5) F.E.Fujita Acta.Met. 6,543 (1958).
- (6) D.H.Avery & Fracture of Solids. Maple Valley
W.A.Backofen Conf. Interscience 1963 p.339.
- (7) N.Thompson & Advances in Physics 7,72 (1958)
N.J.Wadsworth
- (8) A.S.Tetelman & Fracture of Structural Materials,
A.J.McEvily Wiley 1966.
- (9) J.R.Low Jr. Progress in Materials Science
12,1 (1963)
- (10) P.Lukás, M.Klesnil, Phys.Stat.Sol. 15,71 (1966)
J.Krejčí & P.Rys
- (11) W.J.Plumbridge & Metals and Materials 3,119
D.A.Ryder Reviews (1969).
- (12) J.A.Ewing & Phil.Trans.Roy.Soc. A200,241
J.C.W.Humphrey (1903).
- (13) H.J.Gough Proc. ASTM 33,3 (1933).
- (14) D.Kuhlmann-Wilsdorf Phil.Mag. 43,632 (1952)
et al
- (15) W.J.Craig Proc. ASTM 52,877 (1952).
- (16) P.J.E.Forsyth JIM 82, 449 (1953).
- (17) F.von Wever, M.Hempel Archiv. f.d. Eisenhüttenwesen
& A.Schrader 26,739 (1955).

- (18) E.Eisner Nature 188,1183 (1960).
- (19) N.Thompson, Phil.Mag. 1,113 (1956).
N.J.Wadsworth &
N.Louat
- (20) M.S.Hunter & Proc. ASTM 54,717 (1954).
W.G.Fricke
- (21) P.J.E.Forsyth Nature 171,172 (1953).
- (22) P.J.E.Forsyth & Nature 175,767 (1955).
C.A.Stubbington
- (23) W.A.Wood Phil.Mag. 3,692 (1958).
- (24) R.C.Boettner & Acta.Met. 13,937 (1965).
A.J.M.McEvily
- (25) P.J.E.Forsyth Proc.Roy.Soc. A242,198 (1957).
- (26) A.H.Cottrell & D.Hull Proc.Roy.Soc. A242,211 (1957).
- (27) D.Hull JIM 86,425 (1957).
- (28) W.A.Wood & R.L.Segall JIM 86,225 (1957).
- (29) D.H.Avery, G.A.Miller Acta.Met. 9,892 (1961).
& W.Backofen
- (30) D.M.Fegredo & JIM 87,1 (1958).
G.B.Greenhough
- (31) A.J.McEvily Jr. & Fracture of Solids, Interscience
E.S.Machlin 1963 p.450.
- (32) A.J.McEvily & Trans.Met.Soc. AIME 221,1086 (1961).
E.S.Machlin
- (33) T.H.Alden Acta Met. 11,791 (1963).
- (34) J.T.McGrath & Trans.Met.Soc. AIME, 227,645 (1963).
R.C.A.Thurston
- (35) G.A.Miller, D.H.Avery & Trans.Met.Soc. AIME 236,1667 (1966).
W.A.Backofen

- (36) W.A.Wood, Acta.Met. 11,643 (1963).
S.McK.Cousland &
K.R.Sargant
- (37) W.D.Dover & W.J.D.Jones Brit.J.Appl.Phys. 18,1257 (1967).
- (38) R.W.K.Honeycombe Proc.Roy.Soc. A242,189 (1957).
- (39) E.C.Elwood & R.Duckett Nature 173,497 (1934).
- (40) K.V.Snowden Phil.Mag. 3,1411 (1958).
- (41) D.I.Golland & Acta.Met. 15,1889 (1967)
P.L.James
- (42) D.W.Hoepfner & Trans.Met.Soc. AIME 230,1378 (1964).
F.H.Vitovec.
- (43) G.C.Smith Proc.Roy.Soc. A242,189 (1957).
- (44) D.S.Kemsley JIM 85,153 (1956-7).
- (45) D.S.Kemsley JIM 85,420 (1956-7).
- (46) R.C.Boettner, Phil.Mag. 10,95 (1964).
A.J.McEvily & Y.C.Liu
- (47) H.D.Williams & Phil.Mag. 13,312 (1966).
G.C.Smith
- (48) M.Hempel, Archiv.Eisen. 8,433 (1957).
A.Kochendorfer &
A.E.Hillnhagen
- (49) M.Hempel Fracture.Swampscott Conf. 1958,
Wiley 1959 p.376.
- (50) M.Hempel & Archiv.Eisen. 39,283 (1968).
A.E.Hillnhagen
- (51) G.F.Modlen & JISI 194,459 (1960)
G.C.Smith
- (52) W.A.Wood, W.H.Reimann Trans.Met.Soc. AIME 230,511 (1964)
K.R.Sargant

- (53) J. Holden Phil. Mag. 6, 547 (1961).
- (54) W. H. Reimann JIM 93, 406 (1965).
- (55) G. Oates & D. V. Wilson Acta Met. 12, 21 (1964).
- (56) A. Ferro & Phil. Mag. 8, 105 (1963).
G. Montalenti
- (57) A. H. Cottrell Symposium on Point Defects in
Metals and Alloys. Inst. Metals
(1956) p. 32.
- (58) A. N. May Nature 185, 303 (1960).
- (59) T. Broom & Phil. Mag. 8, 1847 (1963).
J. M. Summerton
- (60) N. F. Mott Acta. Met. 6, 195 (1958).
- (61) P. J. E. Forsyth Proc. Roy. Soc. A242, 198 (1957).
- (62) C. A. Zapffe & Trans. ASM 18, 958 (1951).
C. O. Worden
- (63) P. J. E. Forsyth Proc. Crack Propagation Symposium,
Cranfield, 1961 p. 76.
- (64) C. A. Stubbington R. A. E. Report CPM4 (1963).
- (65) M. Gell & G. R. Leverant Acta. Met. 16, 553 (1968).
- (66) P. J. E. Forsyth & Metallurgia 63, 117 (1961).
D. A. Ryder
- (67) C. Laird "Fatigue Crack Propagation" ASTM
STP 415, 131 (1967).
- (68) M. Shimura & J. Jap. Inst. Metals 32, 559 (1968).
Y. Shinohara
- (69) H. I. Caplan & C. Laird Trans. Met. Soc. AIME 239, 1017 (1967).
- (70) P. J. E. Forsyth Acta. Met. 11, 703 (1963).
- (71) N. E. Frost Proc. Inst. Mech. Engrs. 173, 811 (1959).

- (72) N.E.Frost & D.S.Dugdale J.Mech.Phys.Solids 6,92 (1958).
- (73) A.K.Head Phil.Mag. 44,925 (1953).
- (74) P.Paris & F.Erdogan Journal of Basic Engineering (ASME)
85,528 (1963).
- (75) G.R.Irwin J.App.Mech. 79,361 (1957).
- (76) P.Paris Ph.D.Thesis 1962.
- (77) B.Gross, J.E.Srawley & NASA Technical Note. D2603
W.F.Brown Jr. (Jan. 1965).
- (78) T.R.Gurney Metal Construction 1,91 (1969).
- (79) D.Broek Proc.Second Int.Conf.Fracture.
Brighton April 1969. Chapman & Hall
p. 754.
- (80) W.P.Rees, B.E.Hopkins JISI 169,157 (1951).
H.R.Tipler
- (81) H.R.Tipler & P.G.Forrest Inst.Mech.Engrs.Conf. on Fatigue,
London 510 (1956).

8. STATEMENT OF ADVANCED COURSES OF STUDY ATTENDED

Three advanced courses of study were attended during the period in which the research was being carried out. These were :

- (1) Statistical Methods (Sheffield Polytechnic)
- (2) Electron Microscopy (Sheffield Polytechnic)
- (3) The Relationship between Structure and Properties of Metals and Alloys (Sheffield University)

9. ACKNOWLEDGMENTS

Thanks are due to Dr. G.W.J. Waldron and Mr. P.E. Warin for supervising this work and for helpful discussions; to Miss Elaine Dodgson and Mr. Trevor Walker for help in the preparation of specimens; to Mrs Maureen Smith for typing the thesis and to the British Railways Board for enabling this work to be submitted for a further degree. I would also like to thank my wife for her patience and consideration during the trying period in which the project was being carried out.

Fig. A1/1. Specimen B1. Stress $5\frac{1}{2}$ tons/sq. in. (85 MN/m^2) Endurance: 1.71×10^5 cycles

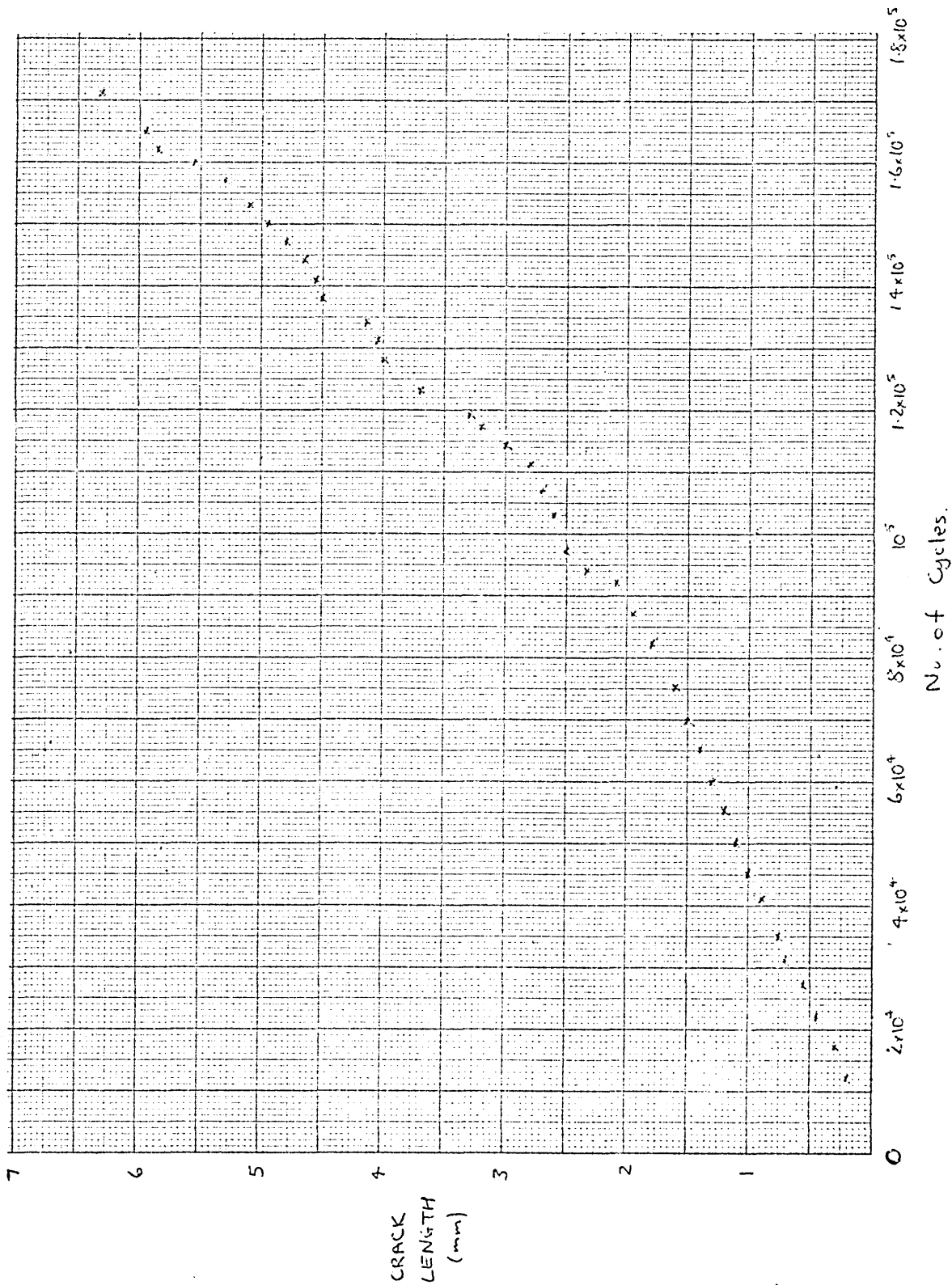


Fig A1/2. Specimen B4. Stress 6 tons/sq. in. (93MN/m²). Endurance: 6.53×10^6 cycles

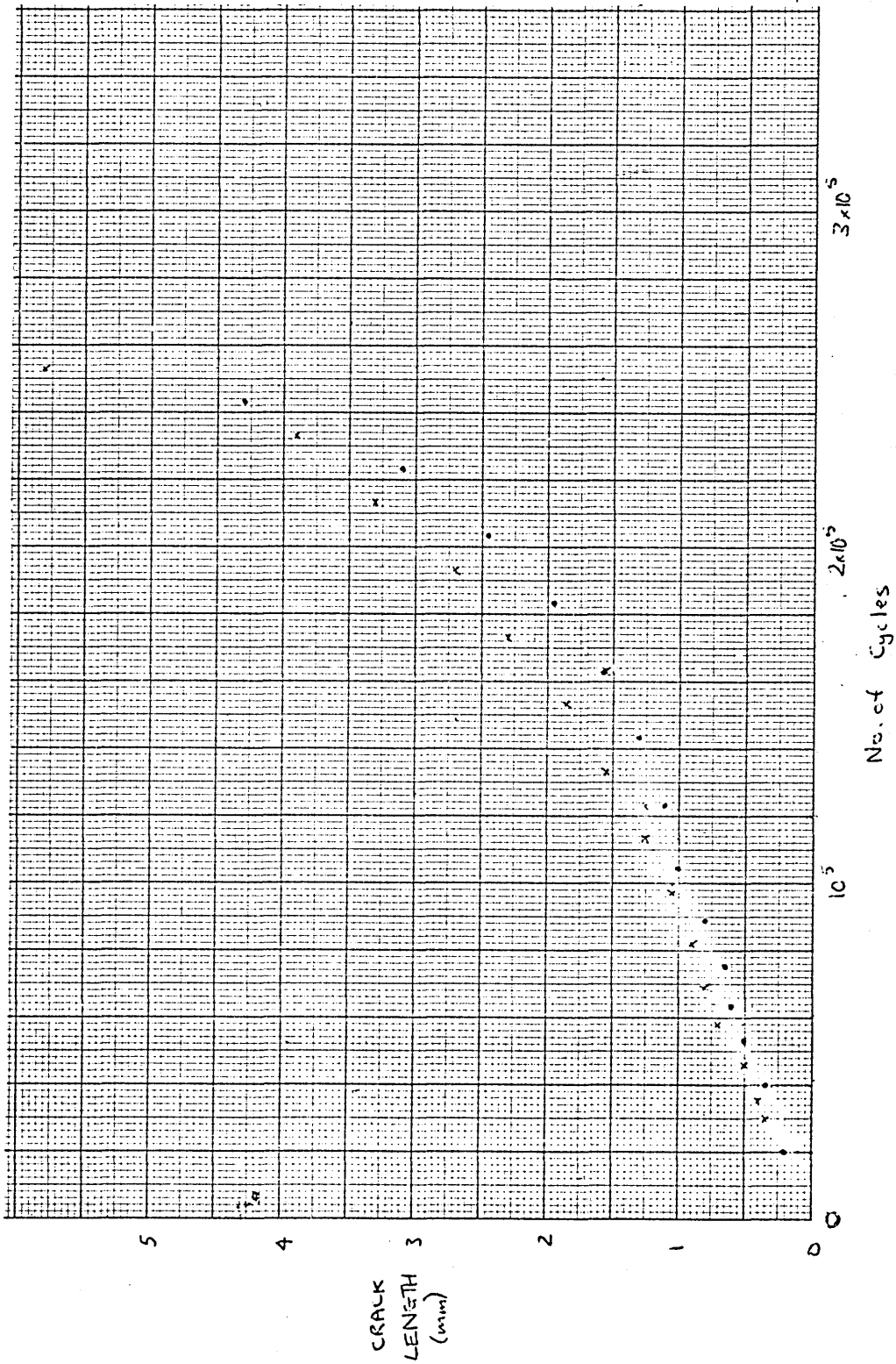


Fig A1/4. Specimen B6. Stress 5 tons/sq. in (77 MN/m^2). Endurance: 5.64×10^5 cycles.

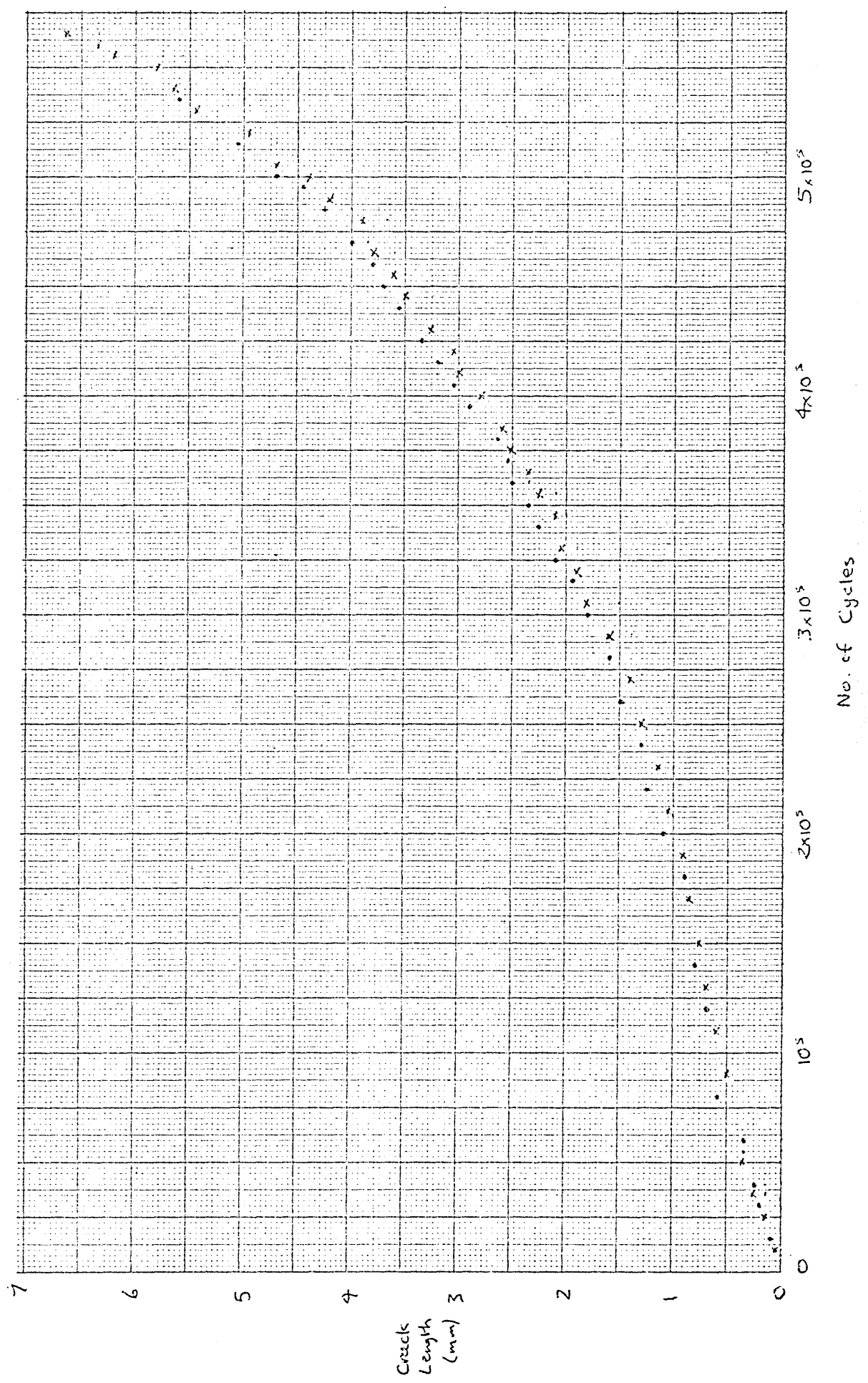


Fig A1/5. Specimen B60. Stress $4\frac{1}{2}$ tons/sq.in. (69 MN/m²). Endurance: 4.89×10^5 cycles.

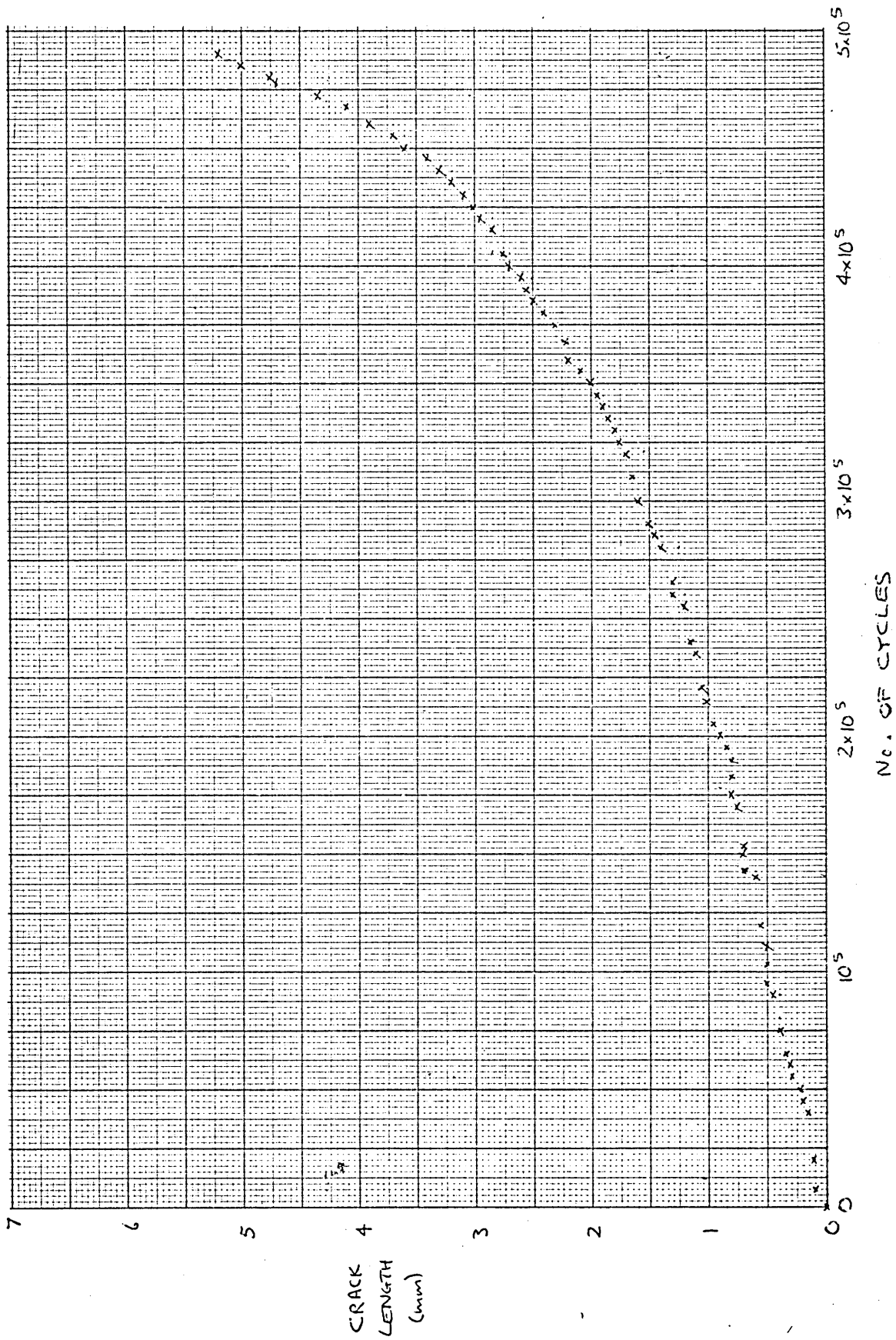


Fig A1/6. Specimen E1. Stress 4 tons/sq. in (61MN/m^2). Endurance: 7.05×10^5 cycles.

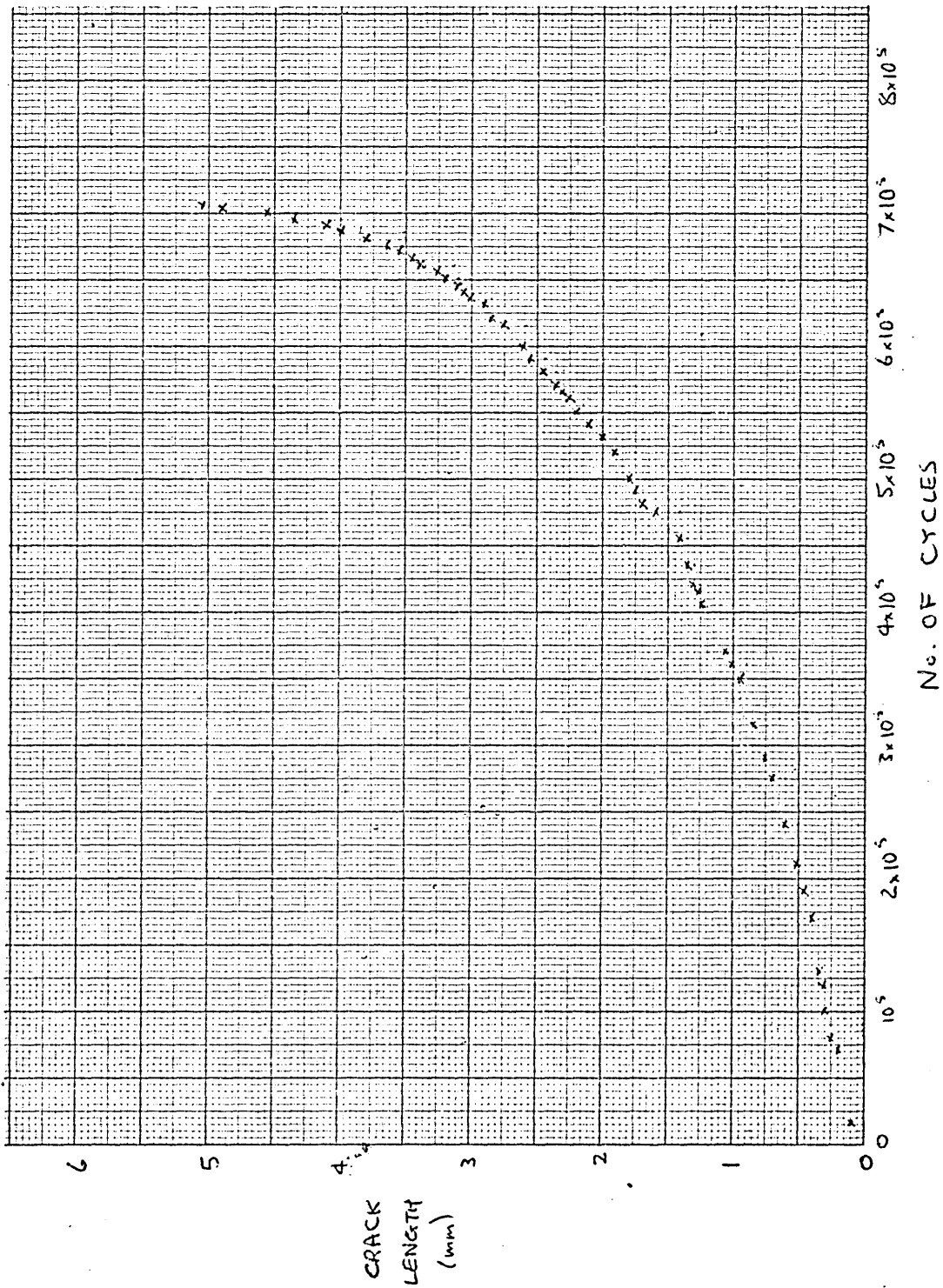


Fig. A1/7. Specimen E3. Stress 6 tons/sq. in. (93 MN/m²) Endurance 2.09 x 10⁵ cycles.

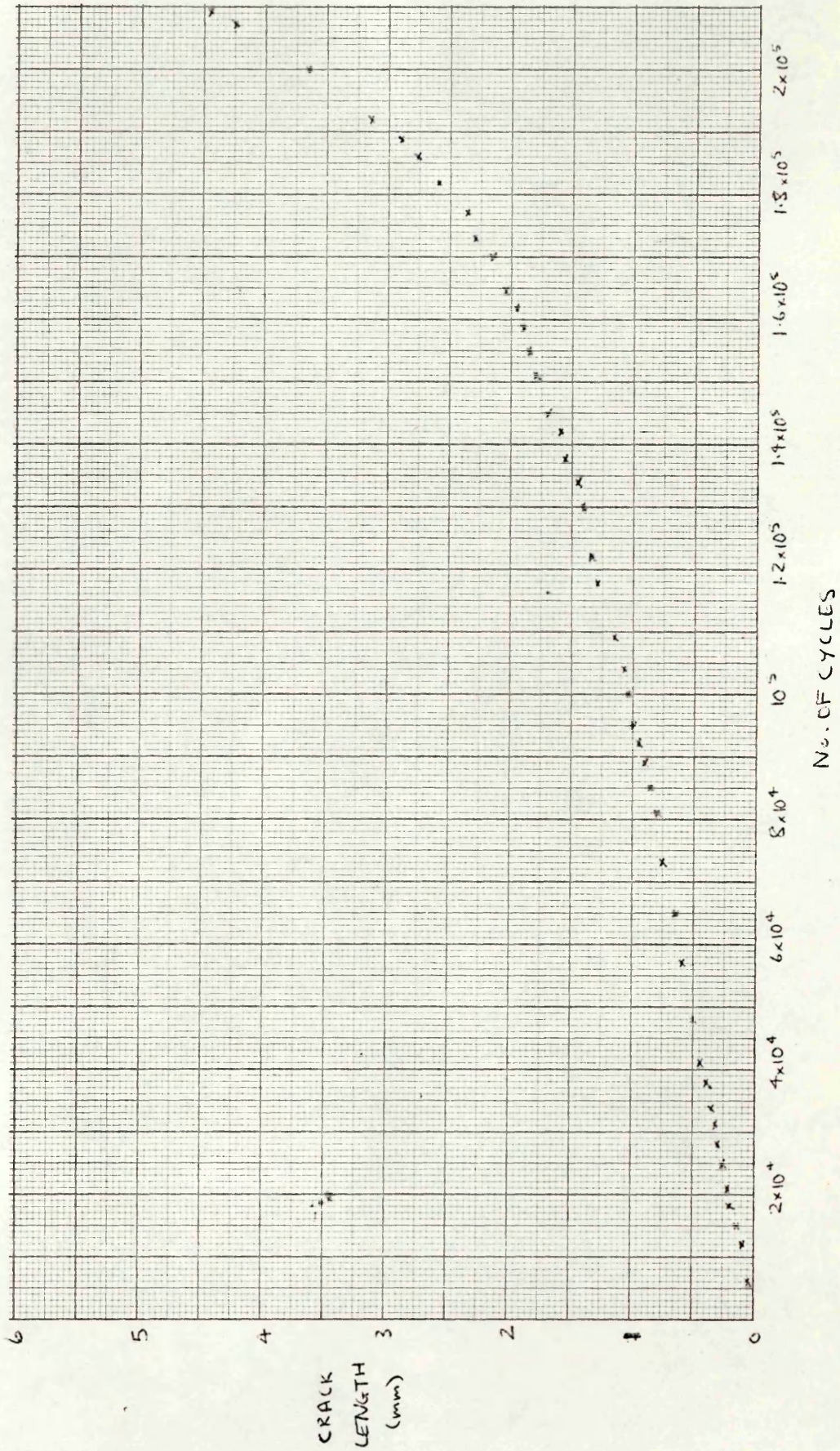


Fig A1/8. Specimen E5. Stress $4\frac{3}{4}$ tons/sq.in (73 MN/m^2). Endurance 3.45×10^5 cycles.

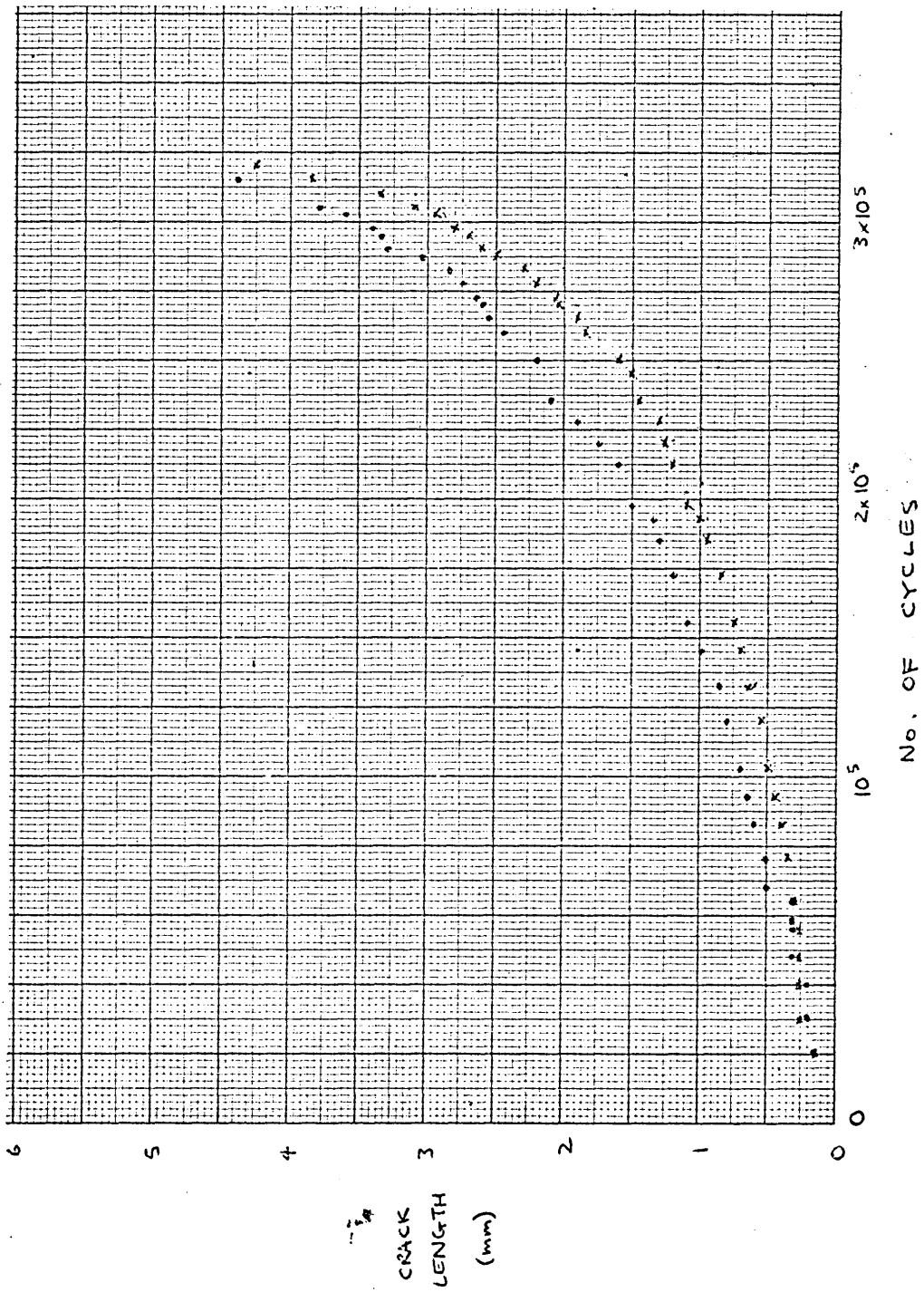
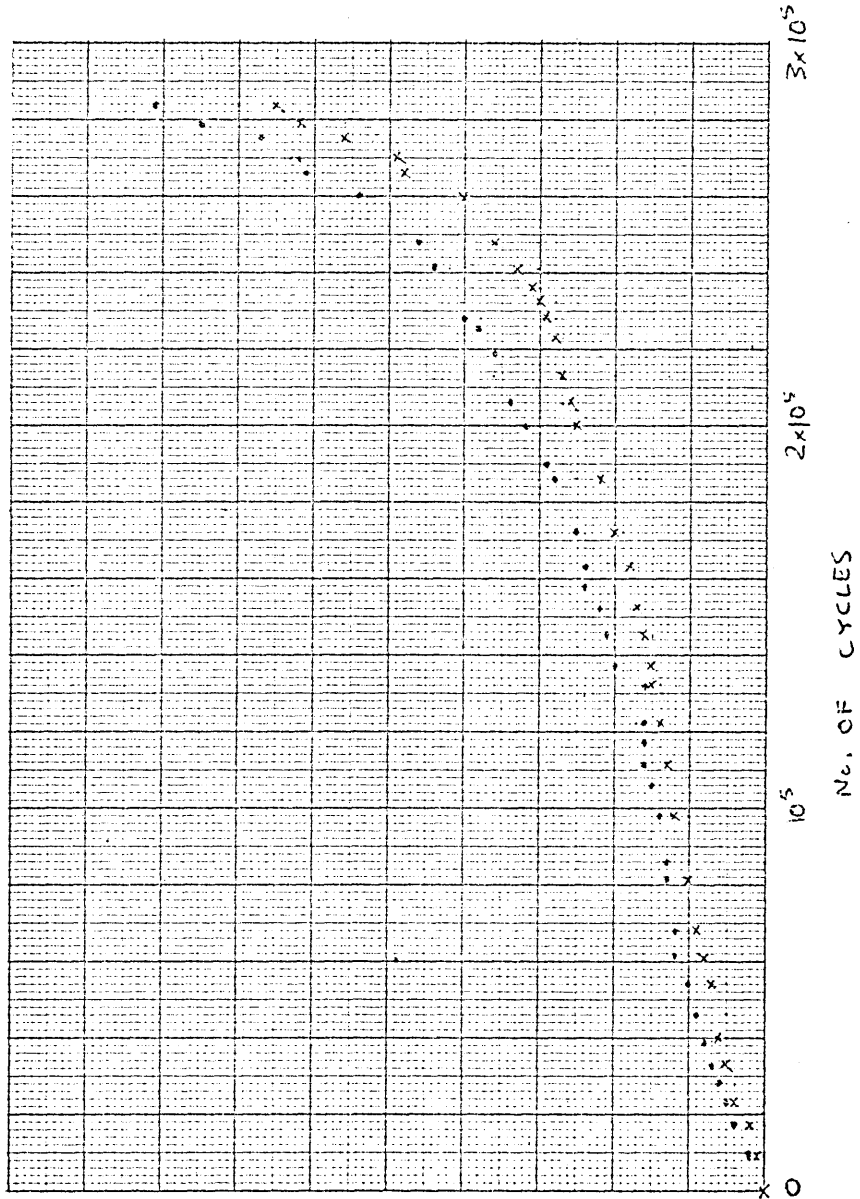


Fig A1/9. Specimen EG. Stress $5\frac{1}{2}$ tons/sq.in. (85 MN/m^2). Endurance 2.83×10^5 cycles.



CRACK
LENGTH

Fig. 11.10. Spectral density of stress fluctuations (0.27110/m) vs. number of cycles

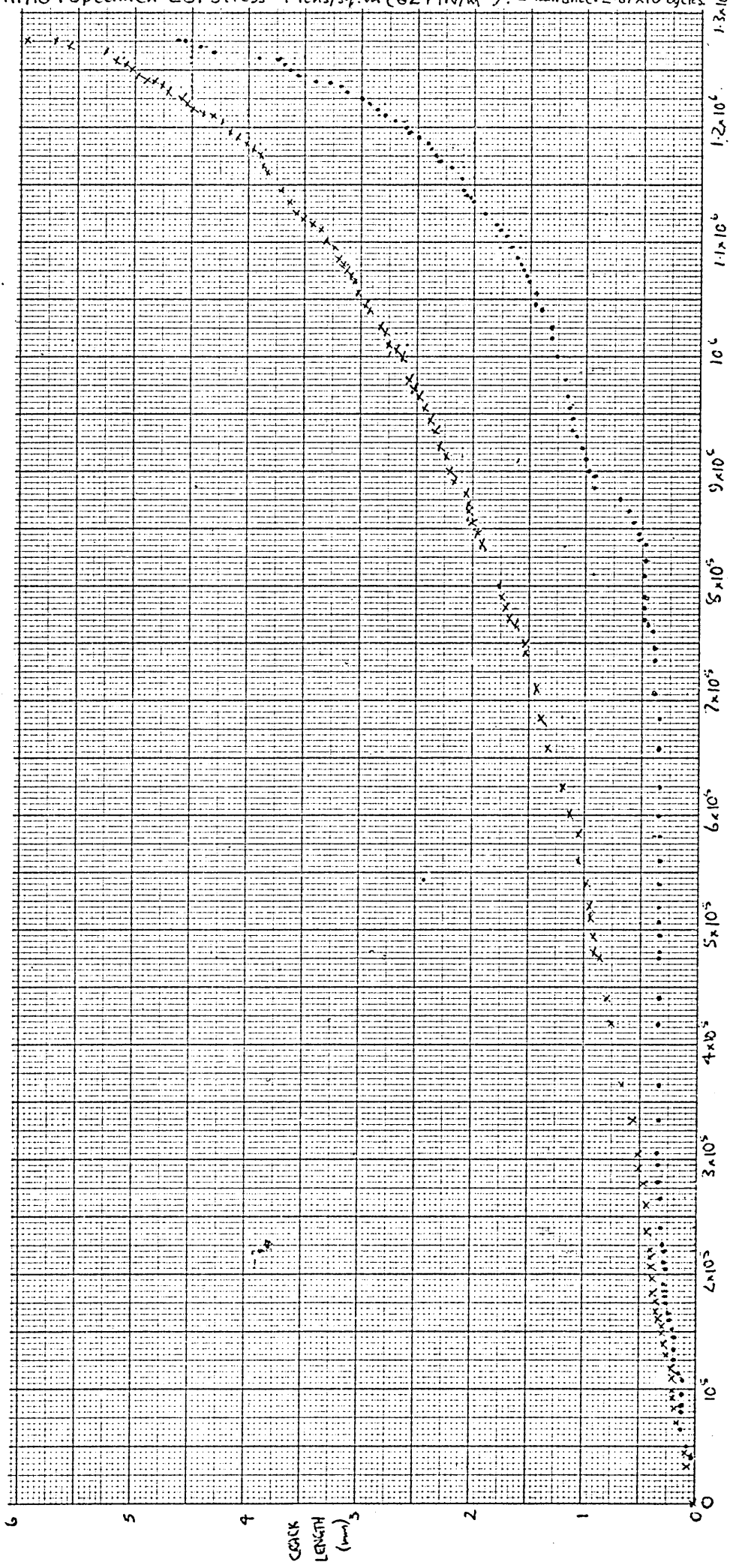


Fig A1/11. Specimen E10. Stress 5 tons/sq.in. (77 MN/m^2). Endurance: 4.86×10^5 cycles.

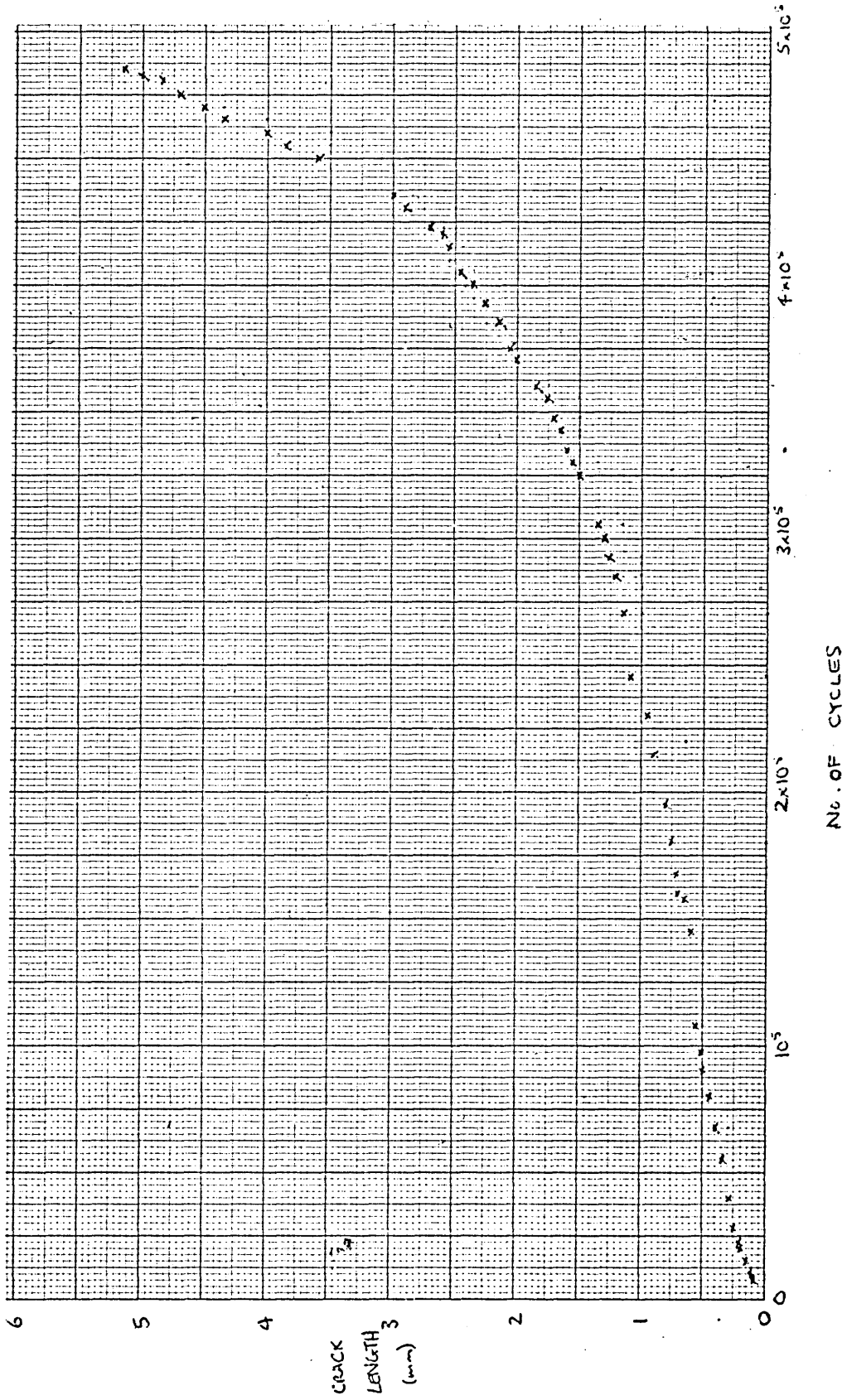


Fig A1/12. Specimen J5. Stress 6 tons/sq. in. (93 MN/m²). Endurance: 1.62 x 10⁵ cycles.

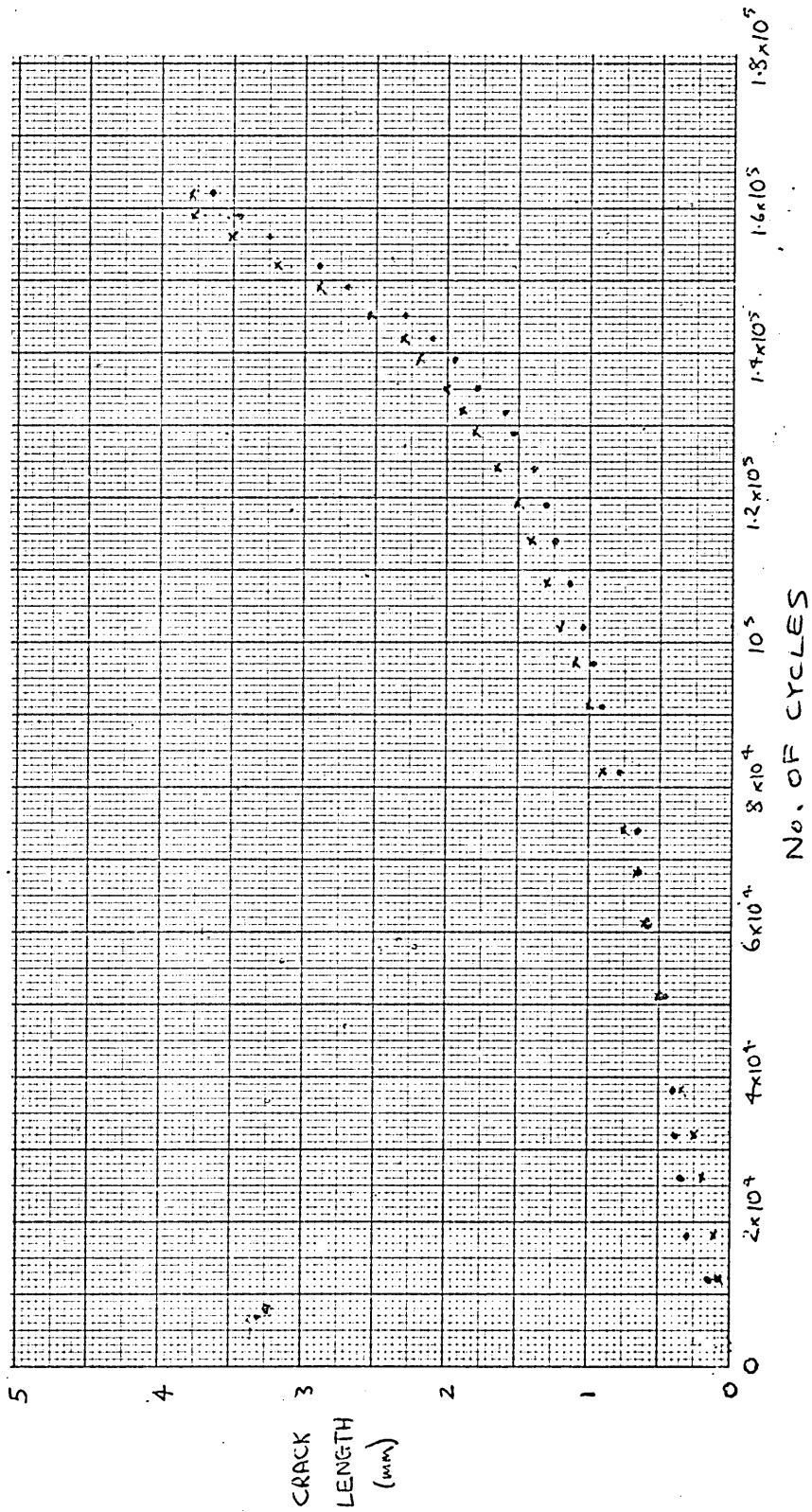
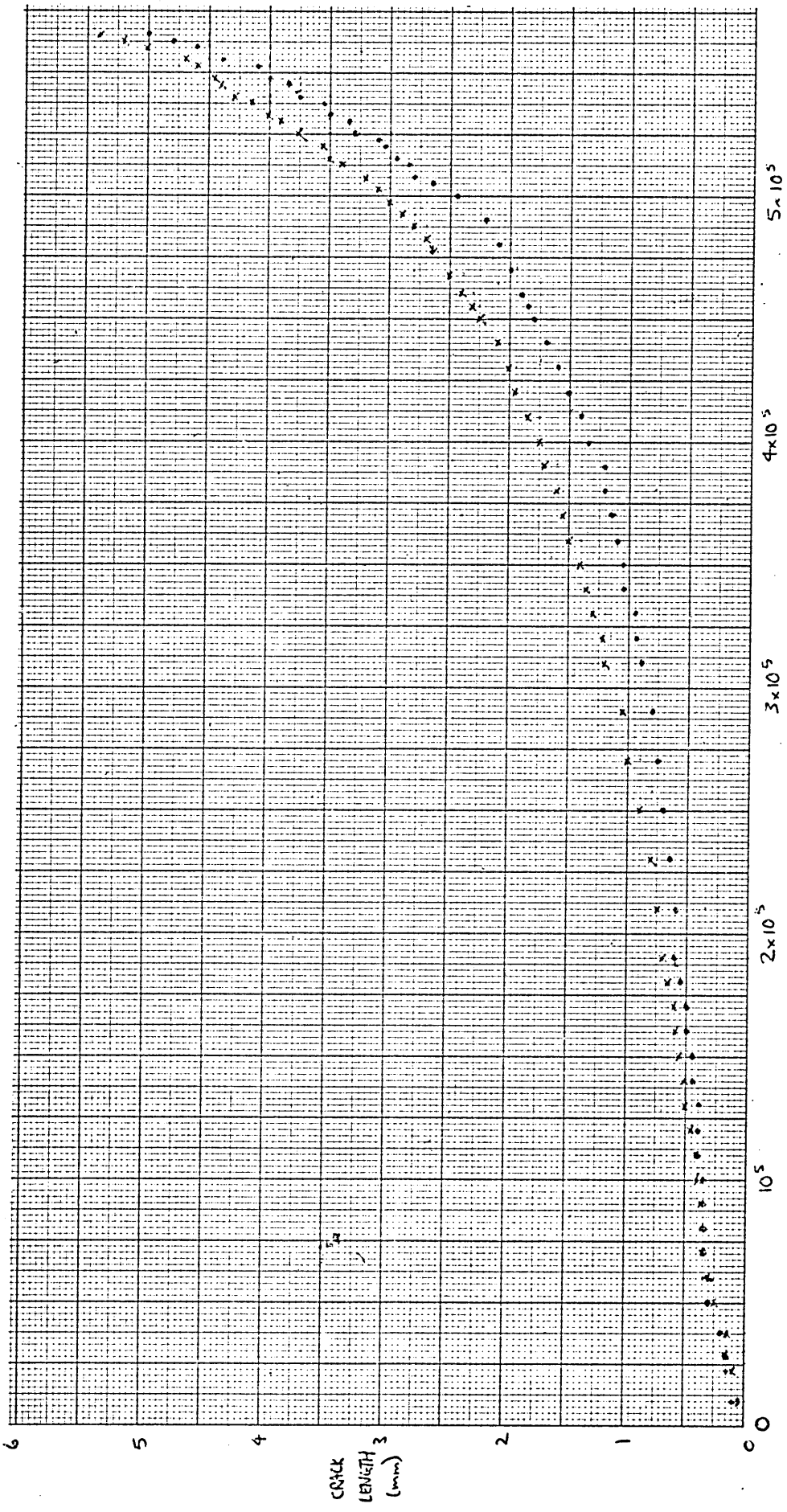


Fig A1/13. Specimen J6. Stress 5 tons/sq. in (77 MN/m²). Endurance 5.66x10⁵ cycles.



No. OF CYCLES

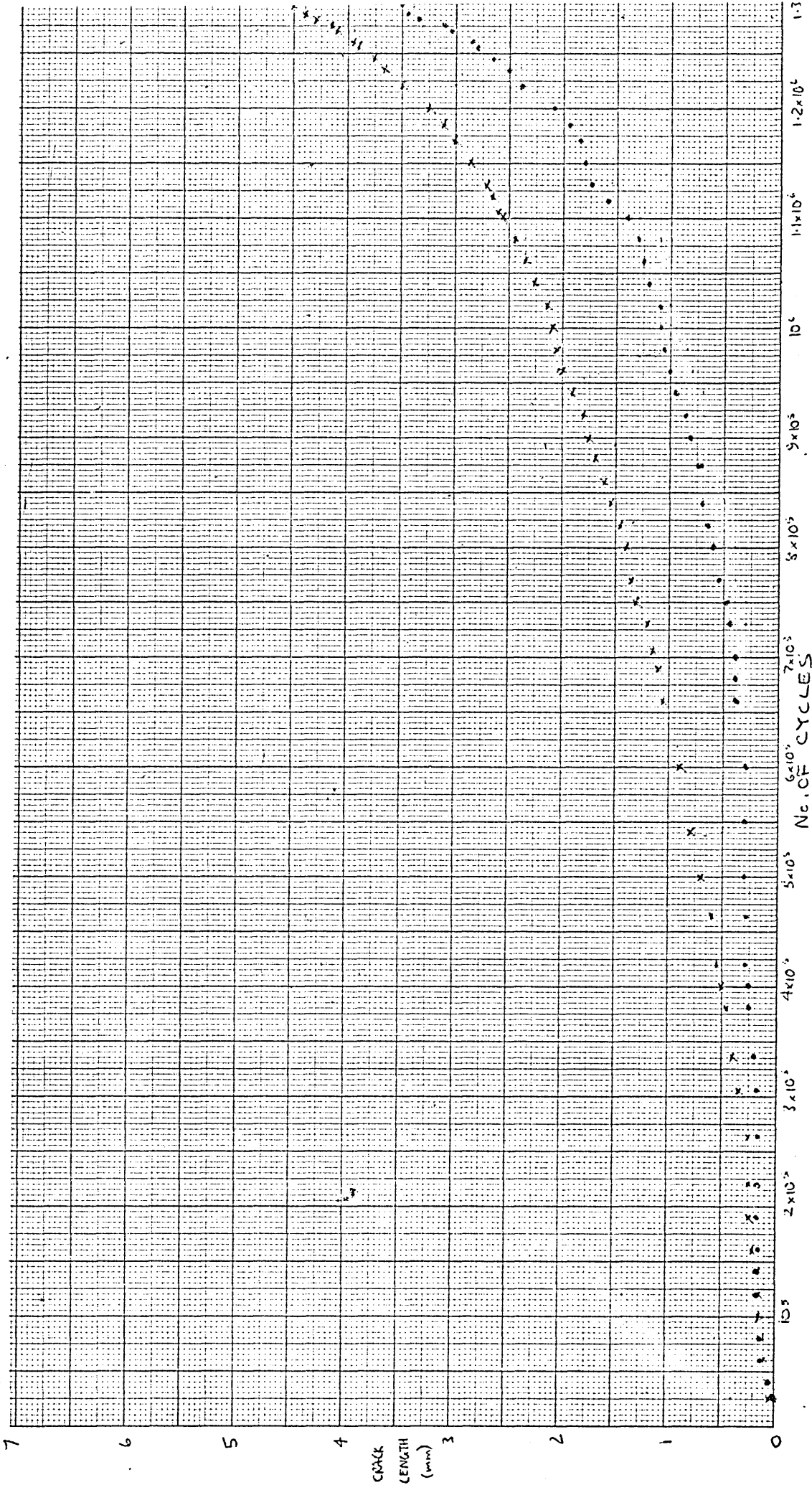
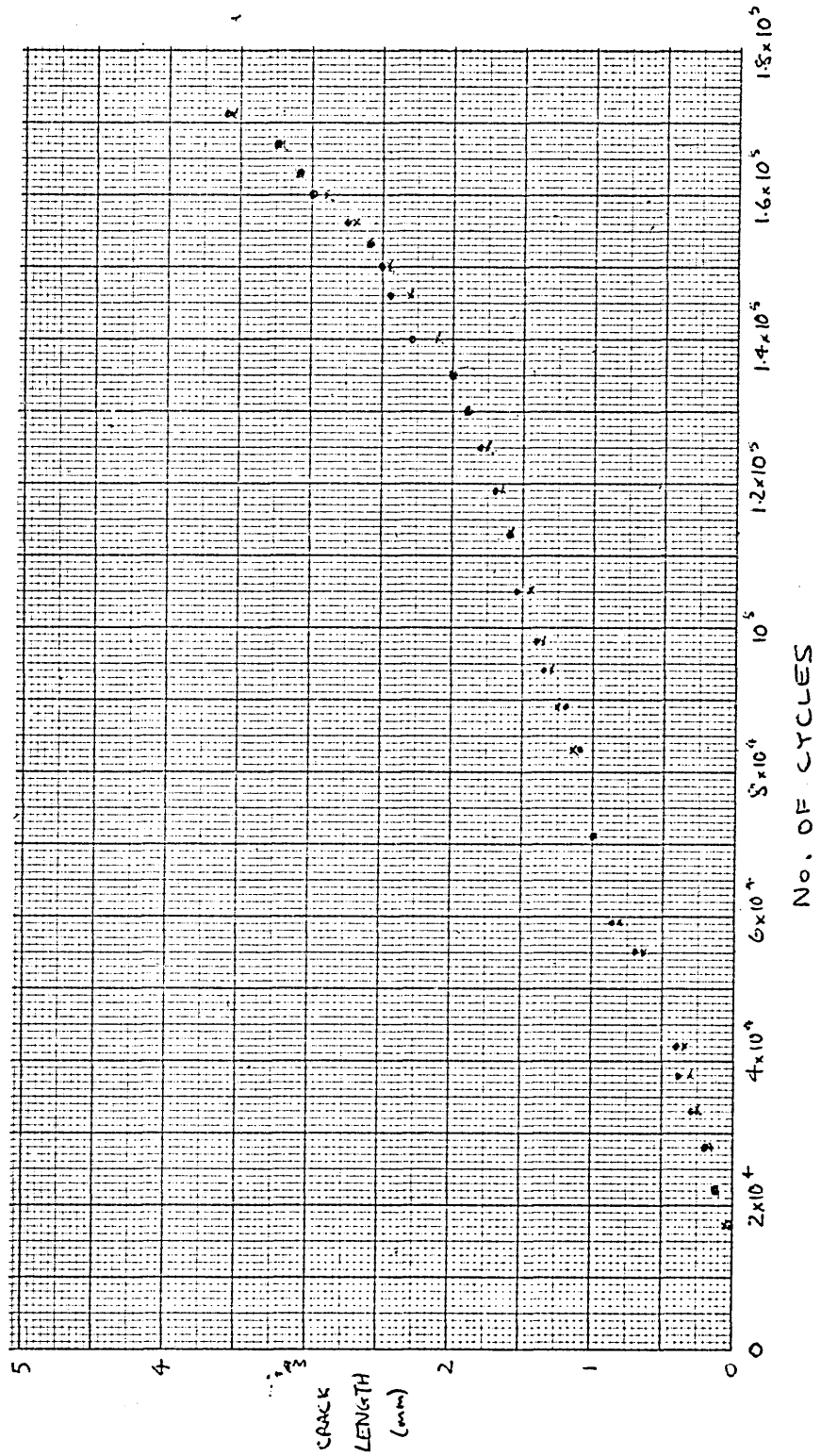


Fig. A1/15. Specimen J13. Stress 6 tens/sq.in. (93 MN/m²). Endurance 1.71x10⁵ cycles



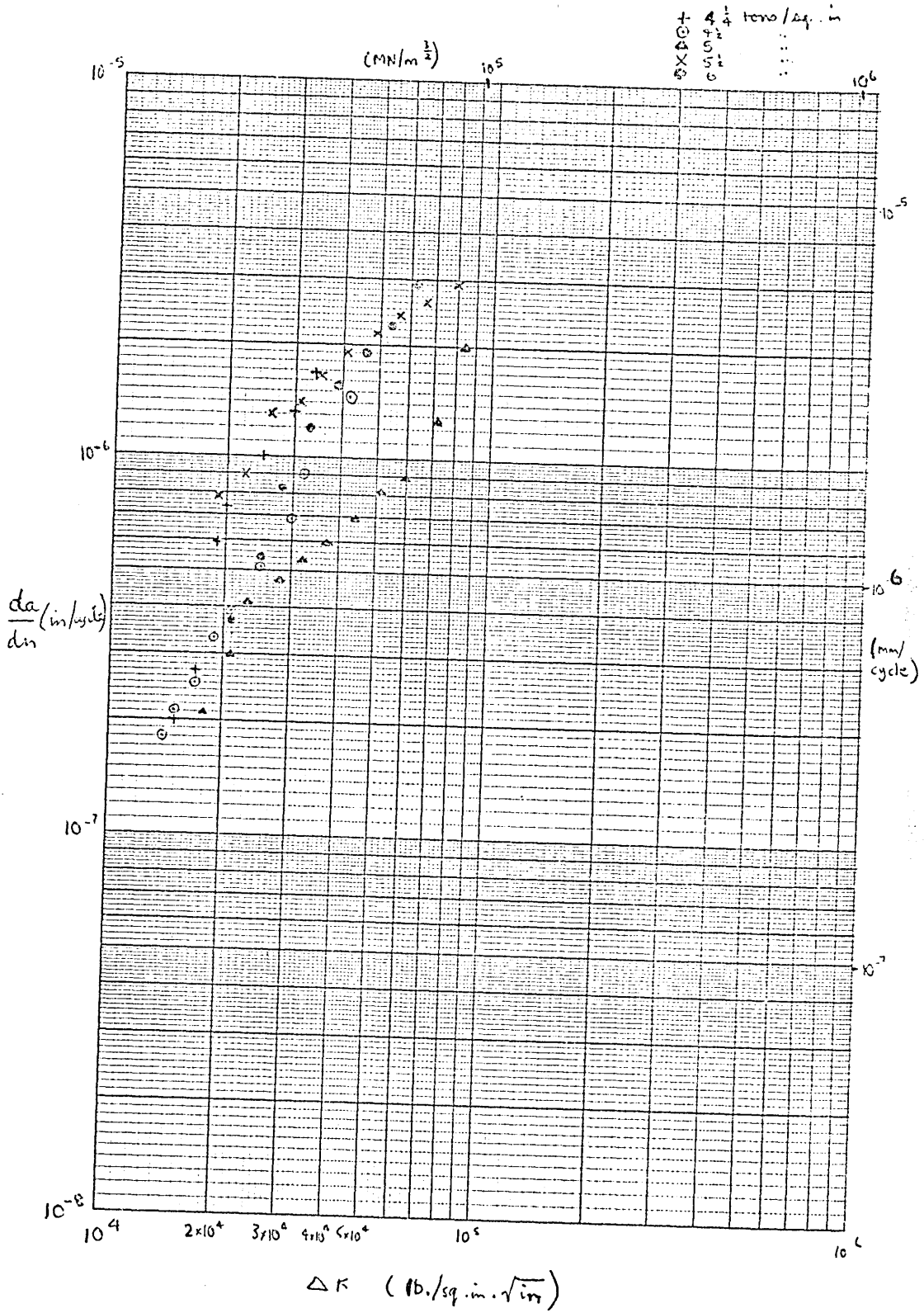


Fig. A2 RELATIONSHIP BETWEEN CRACK GROWTH RATE & STRESS INTENSITY
 RANGE FOR 0.01% CARBON STEEL,

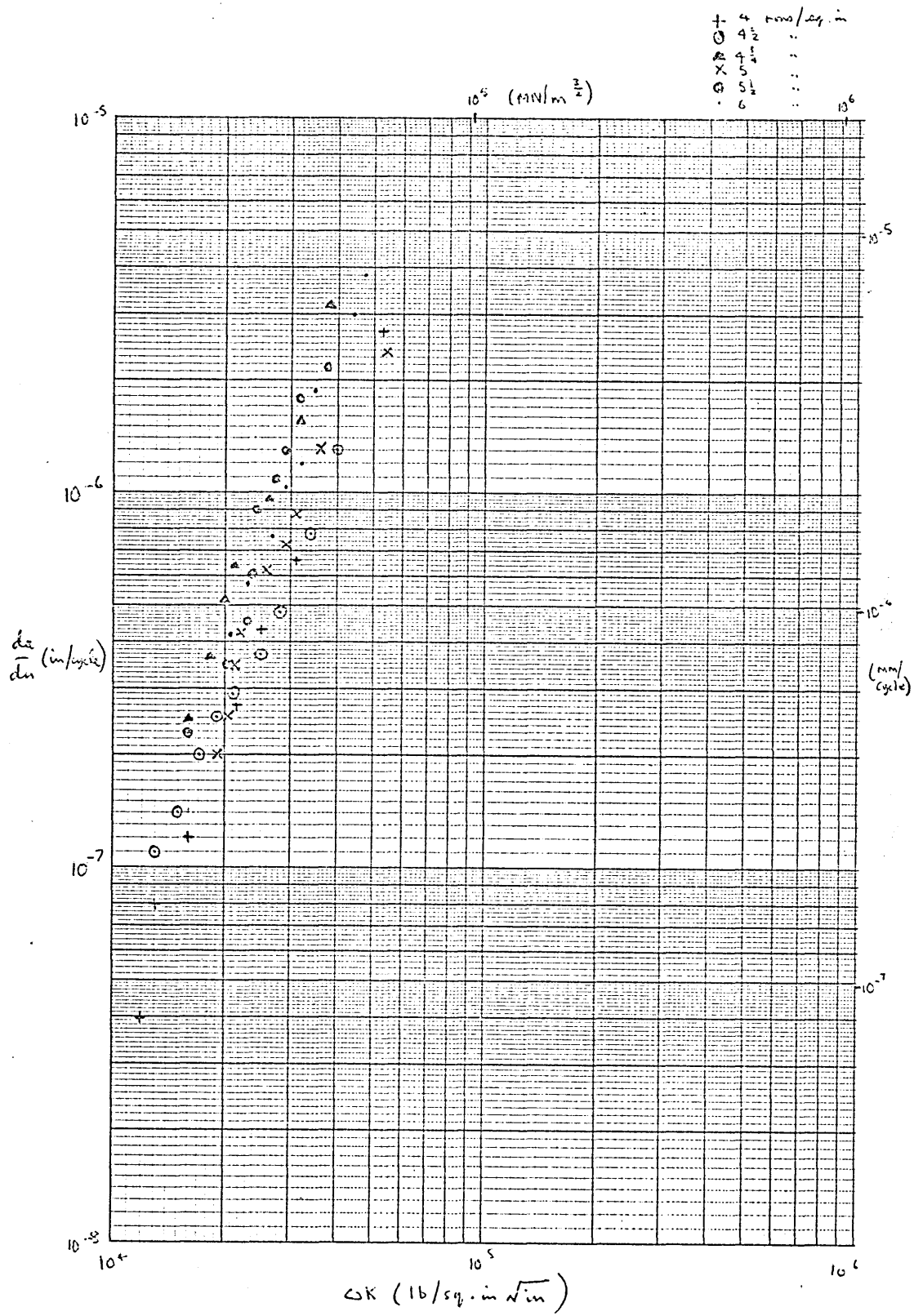


Fig. AB. RELATIONSHIP BETWEEN CRACK GROWTH RATE & STRESS INTENSITY RANGE FOR 0.11% CARBON STEEL.

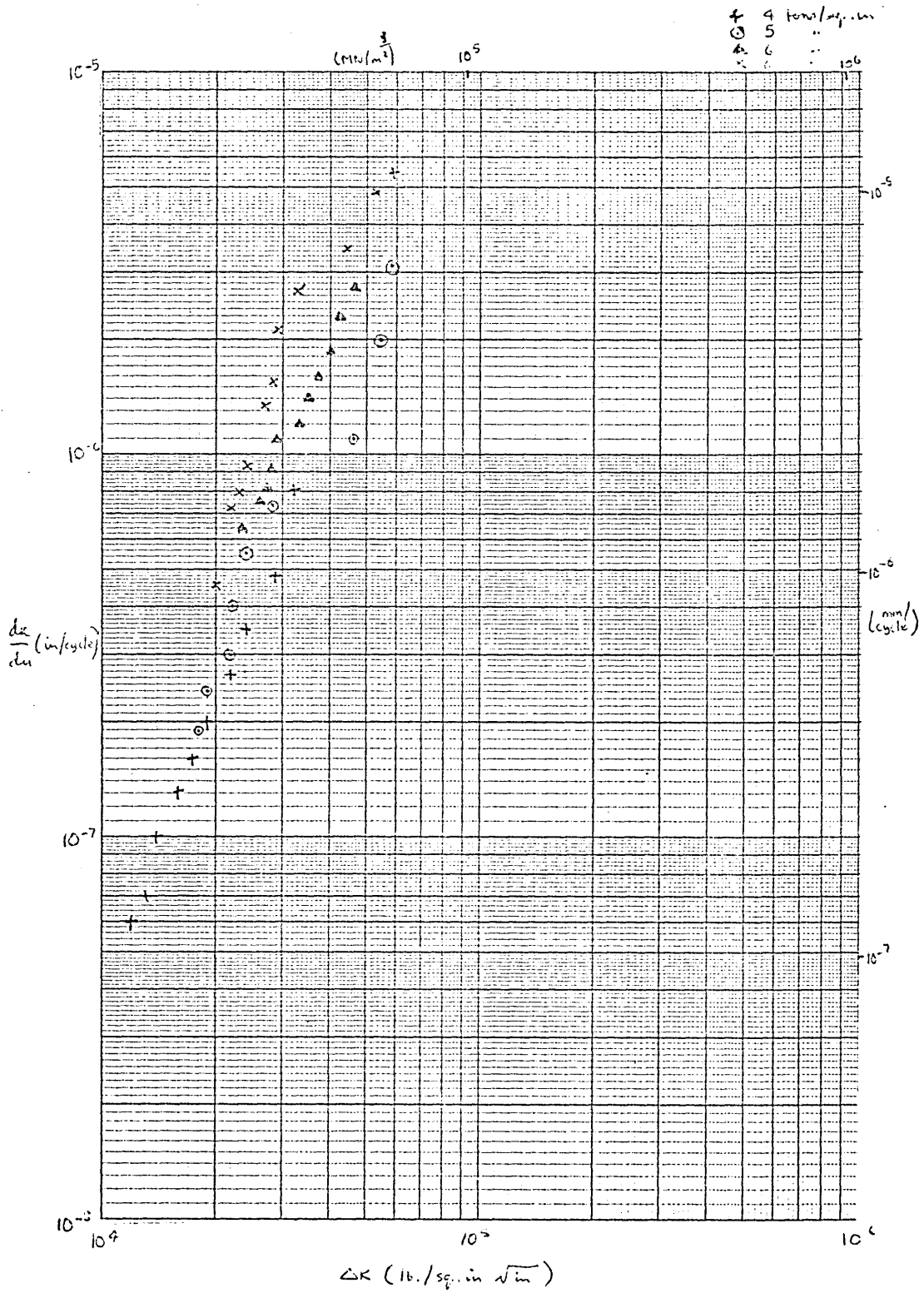


Fig. A4 RELATIONSHIP BETWEEN CRACK GROWTH RATE & STRESS INTENSITY
RANGE FOR 0.41% CARBON STEEL

